NASA-CR-202203

Final Technical Report

NASA Grant Number NAGW-903

Principal Investigator:	Dr. William M. Jackson
Title of Research:	"Photodissociation Cross Sections for the Production of C_2 from C_2H Using Laser Induced Hg Photosensitization and Tunable Ultraviolet and Visible Lasers"
Period Covered by Report:	December 1, 1985 - November 30, 1995
Grantee Institution:	University of California at Davis Davis, California 95616
Continuation Information:	This research is being continued under NASA Grant Number NAGW-5083.

The NASA Technical Officer for this grant is Dr. Jay Bergstralh, NASA Headquarters, Office of Space Science, Code SL, Washington, DC 20546-0001.

$X^2\Sigma^+_g$ and the $a^3\Pi_u$ were produced since these states do not correlate to the electronic states of C_2H which are initially excited. This lead us to the conclusion that non-adiabatic transitions must be occurring as the molecule dissociates. Cometary observations near the nucleus of a comet should reflect the initial distribution of the $X^2\Sigma^+_g$ if they are produced by the photolysis of C_2H.

Recent observations of Comet Hyakutake may have confirmed this proposition.

Papers Published

1. 1986, W. M. Jackson, and M. G. Prisant. A comparison of the high resolution IUE observations of CS emission in comets Halley and Giacobini-Zinner, p. 545-551. In European Space Agency SP-250, Proceedings of the 20th European Space Laboratory Symposium, Heidelberg, West Germany.

2. 1987, M. G. Prisant and W. M. Jackson. A Rotational State Population Analysis of the High-Resolution IUE Observation of CS Emission in Comet P/Halley. Astron. Astrophys. 187, 489-496.

3. 1986, P. D Feldman., M. C. Festou, M. F. A'Hearn, C. Arpigny, T. S. Butterworth, C. B. Cosmovici, A. C. Banks, R. Gilmozzi, W. M. Jackson, L. A. McFadden, T. Patriarchi, D. G. Schleicher, G. T. Tozzi, M. K. Wallace, H. A. Weaver and T. N. Woods. IUE observations of comet Halley: Evolution of the UV spectrum between September 1985 and July 1986, p. 325-328. In European Space Agency SP-250, Proceedings of the 20th European Space Laboratory Symposium, Heidelberg, West Germany.

4. 1987, M. G. Prisant and W. M. Jackson. A Rotational State Population Analysis of the High-Resolution IUE Observation of CS Emission in Comet P/Halley. Astron. Astrophys. 187, 489-496.

5. 1989, R.S. Urdahl, Y. Bao, and W.M. Jackson. Laboratory Studies of Photo-dissociation Processes Relevant to the Formation of Cometary Radicals. NASA Conference Publication 3077, Proceedings of the 1st International Conference on Laboratory Research for Planetary Atmospheres, Bowie State University, Maryland, p.266.

6. 1990, J. B. Halpern, L. Petway, R. Lu, W. M. Jackson and V. R. McCrary. The Photochemistry of Cyano- and Dicyanoacetylene at 193 nm. J. Phys. Chem. 94: 1869-1873, 1990.

7. 1991 Yihan Bao, R.S. Urdahl, and W.M. Jackson. Detection of $C_2(B'\,^1\Sigma_{g+})$ in the multiphoton dissociation of acetylene at 193 nm. J. Chem. Phys.94: 808-809

8. 1991, R.S. Urdahl, Yihan Bao, and W.M. Jackson. An Experimental Determination of the

Heat of Formation of C_2 and the C–H Bond Dissociation Energy in C_2H. Chem. Phys.Letts. 178: 425-428.

9. 1991 William M. Jackson. Recent Laboratory Photochemical Studies and Their Relationship to the Photochemical Formation of Cometary Radicals. Kluwer Academic Publishers, Comets in the Post-Halley Era, 1:313-332.

10. 1991, W.M. Jackson, Yihan Bao and R.S. Urdahl. Implications of C_2H Photochemistry on the Modeling of C_2 Distributions in Comets. J. Geophys. Research., 96:17,569.

11. 1992 W. M. Jackson, Y. Bao, R. S. Urdahl, X. Song, J. Gosine and Chi Lu, Cometary implications of recent laboratory experiments on the photochemistry of the C_2H and C_3H_2 Radicals, Asteroids,Comets, Meteors 1991, Lunar and Planetary Institute, Houston, 253-256.

12. 1995 V. R. Morris, Ke-Li Han, and W. M. Jackson, Time-Resolved IR Chemiluminescene from reactive collisions between hydrogen atoms and SO_2, J. Phys. Chem. , 99:10086-10091.

13. 1995 V. M. Blunt, H. Lin, O. Sorkhabi, and W. M. Jackson, Revised Molecular Constants for the D $^1\Sigma_u^+$ State of C_2, J. of Molec. Spect., 174: 274-276.

14. 1996 W. M. Jackson, V. Blunt, H. Lin, M. Green, G. Olivera, W. H. Fink, Y. Bao, R. S. Urdahl, F. Mohammad, and M. Zahedi, Astrophysics and Space Science, 236:29-47.

Final Report
NASA 903

The principle goal of our research was to understand the formation of free radicals in comets. To do this we compared laboratory results with cometary observations in attempt to make sure that the cometary observations agree with what is known about the photochemistry of the proposed parent molecule. Initially we concentrated on the CS emission in an effort to show that the parent of this molecule was CS_2. From the cometary observations we knew that the parent of CS had a very short photochemical lifetime. Two possible parents of the CS radical were COS and CS_2. Of the two possible parents the CS_2 molecules has the shortest photochemical lifetime which is consistent with the cometary observations. We also analyzed the rotational profile of the high resolution cometary spectra to determine if it retained any memory of its formation. The proposition was that the CS radical is produced with such a short scale length it might show a rotational distribution that reflects the original distribution the radical is formed with. The laboratory work shows CS radicals are vibrationally and rotationally excited when they are produced photochemically. If the CS radicals are excited by a solar photon before they can be quenched then there is a chance that the cometary distribution might reflect this. Rotational analysis of the cometary spectrum showed that it could not be fit with one Boltzmann temperature and that the rotational profile required at least two different rotational distributions. This work shows that although collisions and radiation tend to cool the CS radicals in the inner coma, the radicals do retain some memory of the initial populations.

We then started to look into the problem of C_2 formation in comets. Some time ago we had postulated that the following mechanism could explain the origin of C_2 in comets.

$$C_2H_2 + h\nu \rightarrow C_2H + H \qquad (1)$$

$$C_2H + h\nu \rightarrow C_2 + H \qquad (2)$$

Thus in comets it takes two solar photons to produce the C_2 radical. We set out to to see if we could measure all of the nascent distributions of the C_2 products in the hope that they would be a characteristic signature of the formation process. It is difficult to exactly simulate the conditions in comets in the laboratory. Rather than do this we wanted to understand the photochemistry of the intermediate since the C_2 in comets will be characteristic of this photochemistry. The C_2H radical should be in it's lowest vibrational and rotational state in comets because it has a permanent dipole and it will radiatively relax to this state. Laboratory studies are further complicated because the C_2H is unstable and it must be produced while the study is going on. The photochemistry of acetylene at 193 nm was used to produce the C_2H which were then photolyzed by light from the same laser. Vibrationally hot C_2H radicals are produced in the laboratory and absorption of the second 193 nm photon allows us to scan several excited electronic levels that will be photochemically active in comets.

Using this method we were able to show that C_2 in the following electronic states are produced $X^2\Sigma^+_g$, $A^1\Pi_u$, $a^3\Pi_u$, $B^1\Delta_g$, and the $B'^1\Sigma^+_g$. We were rather surprised to find that the

Plasma & Gas

December 1986

#69

20th ESLAB SYMPOSIUM on the EXPLORATION OF HALLEY'S COMET

Proceedings of the International Symposium
Heidelberg, Germany
27 – 31 October 1986

Organised jointly by

- Space Science Department of ESA, ESTEC, Noordwijk, The Netherlands
- Max-Planck-Institut für Kernphysik, Heidelberg, W. Germany

Sponsored by

- Inter-Agency Consultative Group (IACG)
- International Halley Watch (IHW)

Co-sponsored by

- Committee on Space Research (COSPAR)
- International Astronomical Union (IAU)

european space agency / agence spatiale européenne
8-10, rue Mario-Nikis, 75738 PARIS 15, France

A Comparison of the High Resolution IUE observations of CS emission in Comets Halley and Giacobini-Zinner

William M. Jackson[1*], and M. G. Prisant[2]

[1]Chemistry Department, University of California, Davis, Ca. 95616

[2]Chemistry Department, University of California, Berkeley, Ca. 94720

Abstract

The high resolution spectra of comets Giacobini-Zinner and Halley have been measured in the region of the CS emission. Both spectra have essentially the same shape, but the Halley spectrum has a better signal to noise ratio. Attempts have been made to obtain the rotational distribution of the radical in these comets by using an inversion program and spectral simulation. Both procedures suggest that the rotational distribution is dominated by CS radicals with J" ≤ 5. Despite this it appears that another distribution with higher J"'s is needed to explain the shape of the rotational distribution. Arguments are presented which suggest that this second distribution is due to a balance between collisions and radiation in the inner coma.

Introduction

The CS molecule occupies a unique position in comets. It is the only molecule, which is consistently observed in the spectra of comets that has a short scale length in the coma [1,2,3,4]. Because of this we have speculated that it's spectral signature can be a monitor of the local conditions in this region of the coma. The scale length has been shown to be about 600 km [4] which is still in a region where collisions could affect the rotational populations of the CS radicals. To evaluate this idea a model is needed which would allow one to match the observed high resolution spectra with theoretical profiles. Earlier a very simple model was used that assumed the rotational distribution of the CS radical could be described by a Boltzmann distribution [3]. This amounts to assuming that the CS rotational distribution is a thermometer for the collision region. Subsequently more theoretical analysis and laboratory work [5] has suggested that a more sophisticated model is needed. In particular a model is required that could extract the rotational distribution from the observed spectra, which could then be compared with the expected distributions based upon a molecular model. Recently Prisant and Zare [6] have described an inversion procedure that can be used to obtain the rotational distribution from an observed spectra. In this paper this method will be adapted to analyze high resolution spectra obtained in IUE observations of Comets Giacobini-Zinner during the ICE encounter and Halley's comet on December 25 and 26, 1985. Various simulation procedures have also been used and will be compared with the inversion procedure. The extracted rotational distributions are then discussed in terms of what should be expected from a molecular model.

Observations

Bogess [7] has previously described the IUE instrumentation and only the observational details and the results will be given in this section. The CS portion of the high resolution spectra which was obtained with the LWP camera during observations of comets Giacobini-Zinner and Halley are shown in Figs. 1 and 2, respectively. The wavelength scale is from the IUE guest observer tape and has not been corrected for the relative motion of the comet and the telescope. A 390 min exposure was used for the Giacobini-Zinner (LWP 6694) spectrum, obtained on 30 August 1985, while a 720 min exposure was used for the Halley spectrum (LWP 7383) observed on the 25 and 26 of December, 1985. The data is presented as is, with no smoothing and the signal to noise ratio is estimated to be 12/1 for Giacobini-Zinner and 33/1 for Halley. The noise was estimated from the negative excursion peaks in the spectra in the region where there should not be any CS rotational lines. The CS spectra was observed in two different orders in both spectra but in this paper only the order that occurs near the center of the camera will be discussed. The IUE instrumental bandwidth is quoted to be 0.2 A for a point source and 0.8 A for an extended source. This is varied in the analysis because the images of these comets completely fill the slit. The true resolution is somewhere between these values.

Theory

The high resolution emission spectrum of both comets obtained from IUE should contain information about the local condition in the inner coma. The production scale lengths of CS had previously been shown to be less than [3,4] 1000 km. Thus this species is formed in the inner coma and may be a probe of this region. The rotational distribution of the CS radical in this region could possibly monitor the local conditions of the inner coma. To determine whether this is the case it is necessary to see if the observed spectra can be fitted with models that require collisions.

There are several approaches that can be taken to match the observed spectra with a model spectra. Earlier work [3] had calculated the high resolution spectra assuming that the rotational distribution could be fitted with a Boltzmann distribution of rotational levels. In the present work that approach will be used as well as the inversion method [6] which has been developed for inverting the distribution from the observed spectra.

*Guest observer with the International Ultraviolet Explorer Satellite observatory

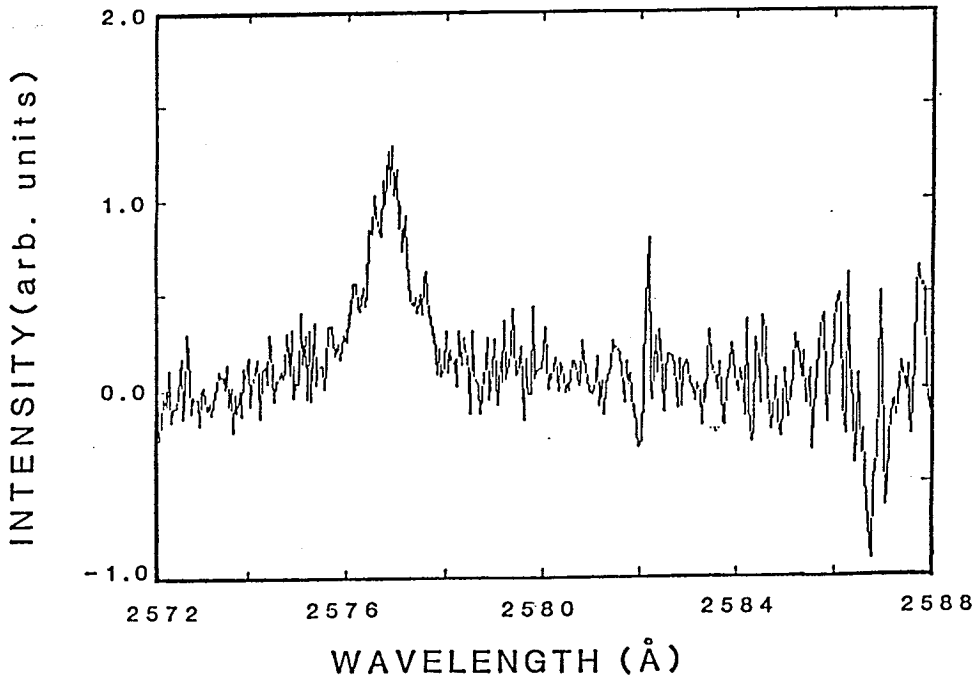

Fig. 1 The CS region of the LWP6694 Giacobini-Zinner spectrum. This is a 390 min exposure and the data is as it is provided to the guest observer on tape. It was extracted from the tape image using ANA software supplied by Gibor Basir.

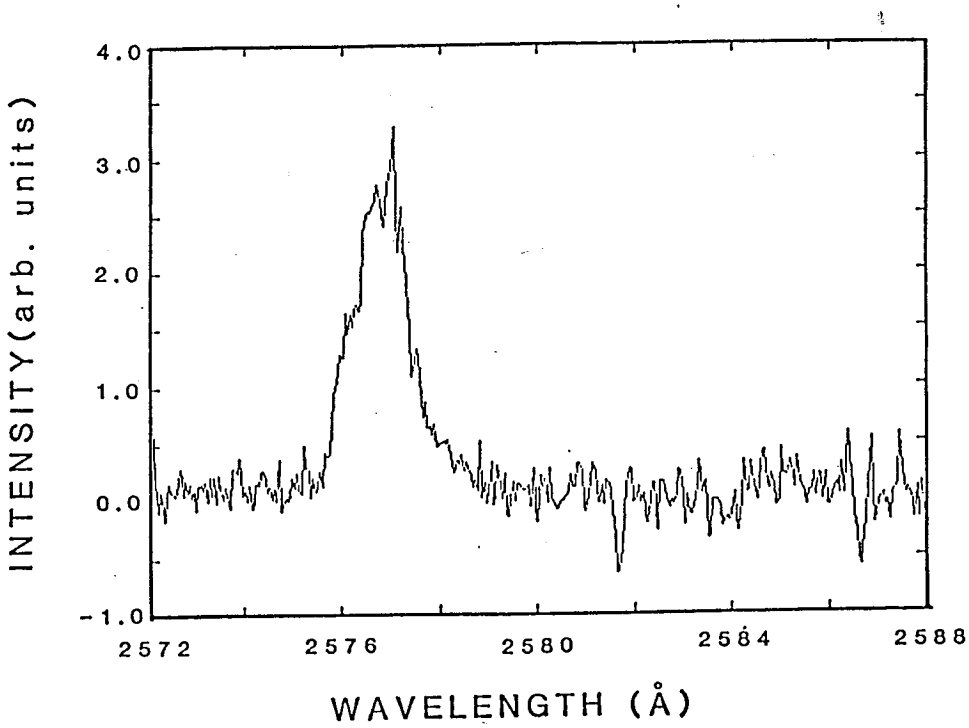

Fig. 2 The same spectral region for comet Halley, but this is a 720 min exposure. The data were taken on 12/25 and 12/26, 1985.

In the analysis it will be assumed that the CS radical is produced by photodissociation of CS_2. Ample evidence has been presented that suggest that this is the most likely source of CS [4]. Photodissociation of CS_2 is known to lead to the production of highly vibrationally and rotationally excited CS radicals [5]. The radicals appear to be formed with internal energy up to the thermodynamic limit, so that at 193 nm they can be formed with up to 12 quanta of vibrational energy and with substantial amounts of rotational energy. Once the radicals are formed in the cometary environment it is unlikely that they will survive in these highly excited vibrational levels. The natural radiative lifetime for a CS radical radiating in the infrared region via the following process,

$$CS(v'') \longrightarrow CS(v''-1) + h\upsilon \qquad (1)$$

is of the order of a few milliseconds. This is much smaller than the solar excitation rate and the collision rate, so that it is unlikely that vibrationally excited radicals will survive long enough to be electronically excited and detected. Similar considerations for the highly excited rotational levels lead to the same conclusion for the upper rotational levels, with large spacings. The exact number of rotational levels that will have to be considered will depend upon radiative relaxation time and the collision time between the CS radical and the gas in the coma.

With the above considerations in mind a model can be developed to try to match the observed high resolution spectra. The overall process can be described by the following series of reactions,

$$CS(X^1\Sigma,v'',J'') + h\upsilon \longrightarrow CS(A^1\Pi,v',J') \qquad (2)$$

$$CS(A^1\Pi,v',J') \longrightarrow CS(X^1\Sigma,v'',J'') + h\upsilon \qquad (3)$$

First, label all of the initial levels of $CS(X^1\Sigma)$ with the index i, the intermediate levels of $CS(A^1\Pi)$ with the index j, and the final levels of $CS(X^1\Sigma)$ with the index k. The levels i are the populated levels in the coma, the levels j are the levels that are optically populated by absorption of solar radiation, and the levels k are the levels that are optically coupled by emission from j. It is this latter emission that is measured by the IUE telescope.

The emission intensity, $I_{jk}(\lambda_l)$, from a given j level to a k level at wavelength λ_l is proportional to,

$$I_{jk}(\lambda_l) = \Sigma_{jk} N_j S_{jk} \upsilon^3_{jk} \phi(\lambda_{jk}-\lambda_l) \qquad (4)$$

where, $\phi(\lambda_{jk}-\lambda_l)$ is the instrument function of the telescope, υ_{jk} is the frequency of the transition between the j and the k levels, S_{jk} is the natural line strength, λ_{jk} is the Doppler shifted transition wavelength, and N_j is the population of the intermediate level j. The natural line strength is given by,

$$S_{jk} = q^2_{v'v''}\mu^2_{jk}S_{jk} \qquad (5)$$

in which $q_{v'v''}$ is the Franck-Condon factor, μ is the transition dipole, and S is the rotational line strength. The sum in the intensity function is over all optically coupled levels in emission and absorption.

The population of the intermediate level j can be determined from the following relationship,

$$N_j = \Sigma_i N_i S_i \upsilon_{ij} O(\upsilon_{ij}) \qquad (6)$$

where, $O(\upsilon_{ij})$ is the intensity of the solar radiation at the Doppler shifted absorption frequency υ_{ij} and all of the other symbols are the same. The equation for the emitted light intensity I_l can now be rewritten as,

$$I_l = \Sigma_i N_i (\Sigma_{jk} S_{ij} \upsilon_{ij} \upsilon^3_{jk} O(\upsilon_{ij}) \phi(\lambda_{jk}-\lambda_l)) \qquad (7)$$

The light intensity at a given line is linearly dependent upon the population of the initial states responsible for that line. If the instrument function is such that all of the lines are resolved then the population of the initial rotational levels are completely defined. In fact since there are three branches, the P,Q, and R branches, we have more equations than unknowns.

The above equation can be written in matrix form as follows,

$$\mathbf{I} = \mathbf{M}\,\mathbf{N} \qquad (8)$$

In this equation the I is a L dimensional column vector with L being the number of points measured in the spectrum, and N is an I dimensional column vector with I being the number of ground state rovibrational levels.

The rotational levels can be further parameterized, in terms of J_{max} where J_{max} is defined by $E_{max} = BJ''_{max}\ (J''_{max} + 1)$. Let us define a new variable X, where,

$$X = -1 + (2J/J_{max}) \qquad (9)$$

The population for a given X, P(X), can be expanded in a Legendre Series, so that

$$N(X) = \Sigma_q P_q(X) a_q \qquad (10)$$

where, $$a_q = \langle P_q | P \rangle = \int_{-1}^{+1} P_q P d_l X \qquad (11)$$

with $$\langle P_p | P_q \rangle = \delta_{pq} \qquad (12)$$

The a_q are the moments of the distribution.

therefore,

$$I_l = \Sigma_q a_q \Sigma_i P_q(X_i) \Sigma_{jk} S_{ij} S_{jk} \upsilon_{ij} \upsilon^3_{jk} O(\upsilon_{ij}) \phi(\lambda_{jk}-\lambda_l) \qquad (13)$$

since,

$$\mathbf{I}_l = q\mathbf{M} \qquad (14)$$

so,

$$\mathcal{M}_{lq} = \Sigma_{ijk} P_q(X_i) S_{ij} S_{jk} \upsilon_{ij} \upsilon^3_{jk} O(\upsilon_{ij}) \phi(\lambda_{jk}-\lambda_l) \qquad (15)$$

and,

$$q = \{A_q\} \qquad (16)$$

The a_q are the moments of the distribution and may be independently extracted from the least-square's analysis of the spectrum [8].

Results and Discussion

A careful comparison of Figs. 1 and 2 suggest that the two spectra were identical except for the signal to noise ratio. Because of this, it was decided to only analyze the Halley comet spectra since it has a much better signal to noise ratio.

A synthetic spectra was first derived assuming various Boltzmann temperatures. Some of the results of this simulation procedure are shown in Fig. 3, along with the Halley comet spectra for comparison. The 29 K spectrum has the right width but it has two distinct peaks corresponding to the R branch and the overlapping P and Q branches. The resolution of the IUE instrument is not high enough to resolve these latter two branches. The 7 K spectrum has the right shape, but it is too narrow to match the spectrum that is observed. Increasing the temperature does not improve the match because the two peaks remain and eventually become too wide.

A simulated spectra was them computed using a uniform distribution, such that, $P(J''_i) = P(J''_k)$ for all J''_i and $J''_k < J''_{max}$, and is equal to zero outside of this range. These results are shown in Fig. 4, which show that the shape is better fitted with a distribution that only employs levels with low J. The spectra calculated from distributions with higher J's have too many peaks and eventually become too wide.

Fig. 5 shows, a better shape can be obtained by employing a rotational distribution function that monotonically decreases from J" = 0 to J" = 5, with a slope of one. The width of the simulated spectrum, however, is still too narrow.

Several bimodal distributions have been tried. The best fit that we have been able to obtain thus far with a bimodal distribution is given in Fig. 6. This calculated spectrum is wider than the spectra obtained with a single distribution and has the correct shape. It is still, however, not as wide as the observed spectrum.

Several spectral inversions were attempted using the theory that was described earlier. All of them gave results similar to those shown in Fig. 6, which looks very much like some of the results obtained by direct simulation. In this case it has the undesirable properties that both the width and shape are in poor agreement with the observed spectrum.

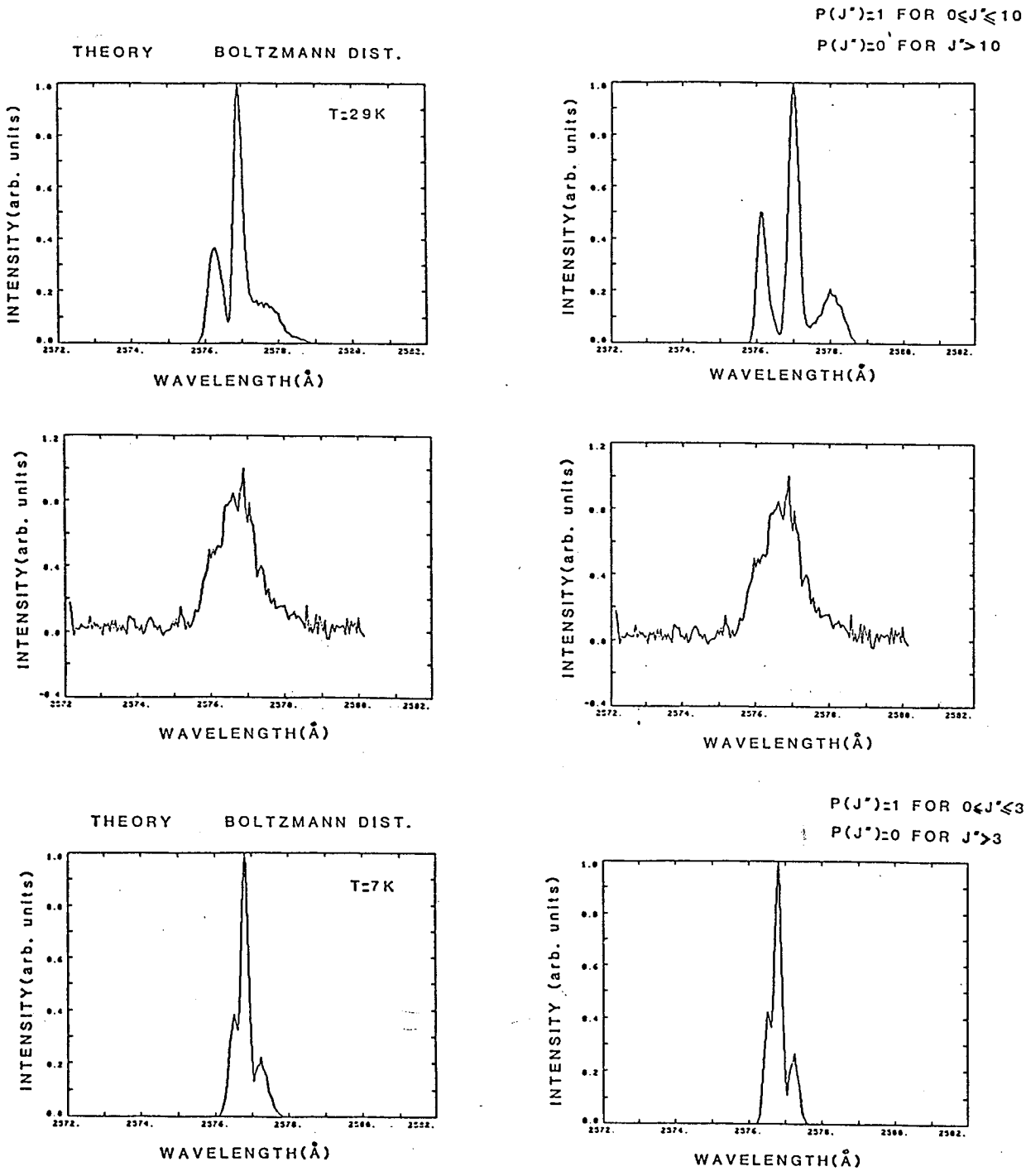

Fig. 3 Two simulated spectrum using a Boltzmann distribution of rotational levels. The Halley spectrum is included for comparison.

Fig. 4 Two simulated spectra using a uniform distribution. The Halley spectrum is included for comparison.

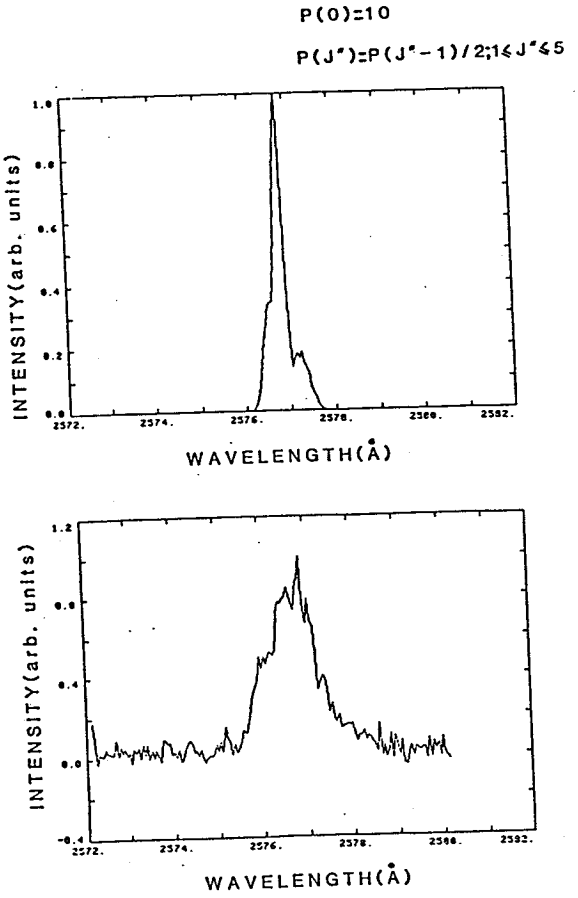

Fig. 5 A simulated spectrum using a linear distribution.

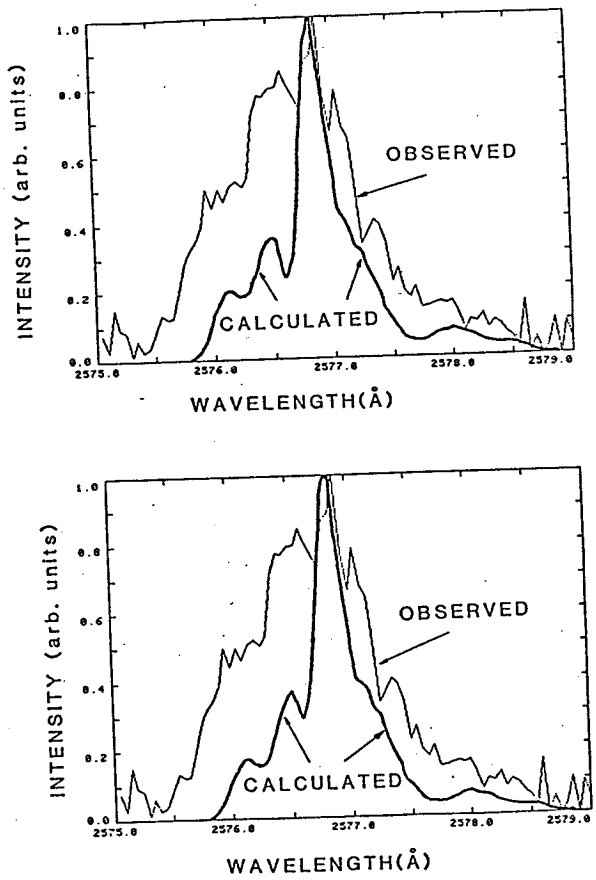

Fig. 6 Simulated Spectra obtained using bimodal distributions. The top figure has relative populations of 10, 10, 10, 10, 5, 0.5, 0.5, 0.5, 0.5, 0.5, 0.2, and 0.2 for the J" = 0, 1, 2, 3, 4, 5, 6, 7, 8, 9, 10 and 11 respectively. The bottom figure has a relative population of 10, 15, 20, 10, 5, 0.5, 0.5, 0.5, 0.5, 0.5, 0.2 and 0.2 respectively.

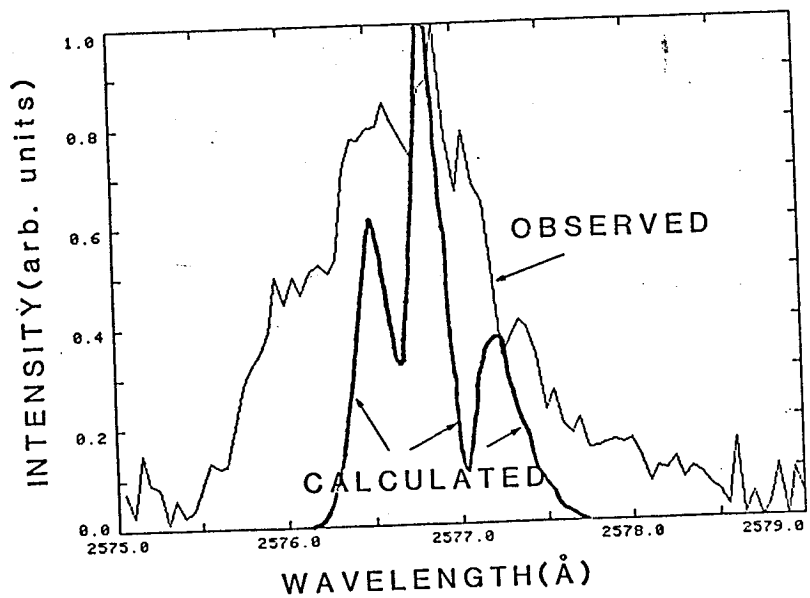

Fig. 7 An inversion using the theory described in the text.

The inversion which was previously described tries to obtain a match by fitting J" rather than the rotational energy. It is now thought that it would be better (to fit the rotational energy) because the simulation procedures suggest that only a few J" levels are involved.

The poor fit with the observations is not the only reason that the present inversion is unsatisfactory. The inversion procedure should yield the average populations, <P(J")>, in several rotational levels as well as the error in those estimates. The average populations <P(0) + P(1)>, <P(2) + P(3)>, and <P(4) + P(5)> were found to be -4.89 ± 1.8, 1.97 ± 0.61, and 0.86 ± 0.2, respectively. Thus, the inversions yield a negative population for the average of the J" = 0 and 1 levels. This is obviously physically unrealistic. The error in the populations are also unacceptably large. These preliminary results suggest, inversion procedure needs to be done as a global fit in energy rather than in J" populations.

The inversion procedure will only give a good fit if a correct functional form is assumed for the distributions. Which is why the simulations are important so that one can obtain a feel for the correct functional form. Once a good functional form is determined, the inversion procedure can be used to yield a quantitative measure of the parameters that give the best fit.

From all of the simulations done thus far, it is clear that the low J" levels are the principal contributors to the observed Halley spectrum. This can be explained by considering the characteristic times for electronic excitation, rotational radiative relaxation, and collisional process. These times are collected in Table 1. The average CS radical will be produced 600 s after the CS_2 radical has been released from the nucleus. It will then take an average of 1400 s before it will be excited by a solar photon. Experimental evidence[5[is available which shows that the CS radicals are born with up to 12 quanta of vibrational energy and 100 quanta of rotational energy. The vibrational energy is unimportant in determining the observed line profiles because excited vibrational levels will radiate in time of the order of milliseconds. A similar argument can be made for the upper rotational levels of CS, which according to the theoretical formula given in Table 1, will have short radiative lifetimes. At 500 km the time between collisions is 14 s, so that all of the CS radicals in rotational levels with J" above 24 will have radiated before the molecule has had a chance to collide. The CS radicals that now all have $J" \leq 24$, will then undergo approximately 200 collisions before it can be electronically excited. This collision rate has been calculated using a spherical model for fluid flow in the coma [11] and a production rate for water in Halley of 5×10^{29} s^{-1}. If collisions have unit efficiency for rotational relaxation, then all of the CS radicals will end up in J" = 0 because 24 levels are excited. It is clear that this is not the case, since the observed spectrum cannot be fitted with such a model. This means that collisions with H_2O do not have a unit efficiency for relaxing the rotationally excited CS radical.

The efficiency for rotationally quenching the CS radical by water will probably depend upon the energy difference between the rotational levels of water accepting the energy and the CS molecules giving up the energy. The greater the energy gap between the H_2O molecules and the CS radical, the lower the probability [12] that the radical can be deexcited by collisions with H_2O. The energy difference for CS radicals in the J" = 24 and J" = 23 levels is 39.4 cm^{-1} which is 3.0 cm^{-1} below the lowest rotational level of water, the 1_{10} level. The probability for deactivation by collision will be higher for this level than for the lower rotational levels. This probability should also decrease exponentially as the energy difference increases.

Collisions could also rotationally excite the CS molecule by T to R transfer. The translational temperature of the gas should be of the order of 200 to 300 K. This corresponds to energies of the order of 147 to 220 cm^{-1} and collisions could then excite the CS radicals to higher rotational energy levels. The efficiency of excitation versus deexcitation by radiative relaxation will depend upon the competition between the two processes.

The above discussion suggests that collisions will not be completely effective in quenching the rotationally excited CS radicals in the first 2500 s before the radical is excited. The spectrum obtained from radicals that have been newly created will be superimposed upon a spectrum of radicals that have undergone multiple excitations in the collisionless regime. This suggests that a bimodal rotational distribution is needed to fit the observed spectrum. One of the main results of our modelling so far has been that there is no one single rotational distribution that will fit the observed spectrum. As Fig. 6 shows, the bimodal rotational distribution gives a better overall fit than a single distribution. It remains to be determined just what kind of bimodal distribution should be used.

The simulations and inversions have all been done with spectral intensities of the central solar region given in Kohl, Parkinson, and Kurucz [13]. These spectra were averaged over 0.005 nm bins. In future work, the averaged solar disk spectrum A'Hearn et al. [14] will be used. It is expected that this will make the rotational profile more sensitive to the radial velocity of the comet but should not produce the broader profiles.

TABLE I

Some Characteristic Times for Elementary Processes involving CS in Comets at 1 AU

Process	Time(s)	Reference
Electronic Excitation	1,400	3
Rotational Radiative Relaxation	$1.9 \times 10^5/(J")^3$	9,10†
for J" = 5	1500	
for J" = 4	2970	
Time between Collisions	$5.7 \times 10^{-15}(r)^2$	11
for r = 500 km	14	
for r = 1900 km	206	
for r = 5000 km	1425	
Photochemical Production	600	4

† The lifetime was calculated using the dipole moment of Reference 9 and the method of Reference 10.

Acknowledgments

William M. Jackson would like to thank Gibor Basir for the ANA program and all of his help in using it. He would also like to thank P. Butterworth for his aid in this project. This work was supported by NASA under grant NAGW-446 and NAGW-903.

References

1. W. M. Jackson, J. Rahe, B. Donn, A. M. Smith, H. U. Keller, P. Benvenutti, A. H. Delsemme, and T. Owen, Astron. Astrophys., 73, L7 (1978).
2. P. D. Feldman, H. A. Weaver, M. C. Festou, M. F. A'Hearn, W. M. Jackson, B. Donn, J. Rahe, A. M. Smith, P. Benvenutti, Nature, 286, 132 (1980).
3. W. M. Jackson, J. B. Halpern, P. D. Feldman, and J. Rahe, Astron. Astrophys., 107, 385 (1982).
4. W. M. Jackson, P. S. Butterworth, and D. Ballard, Ap. J., 304, 515 (1986).
5. V. R. McCrary, R. Lu, D. Zakheim, J. A. Russell, J. B. Halpern, and W. M. Jackson, J. Phys. Chem., 83, 3481 (1985).
6. M. G. Prisant and R. N. Zare, J. Chem. Phys., 83, 5458 (1985).
7. A. Boggess, Nature, 275, 377 (1972).
8. M. G. Prisant and R. D. Levine, unpublished.
9. G. Winnewisser and R. L. Cook, J. Molec. Spect., 28, 266 (1968).

10. W. A. Guillory, **An Introduction to Molecular Structure and Spectroscopy**, Allyn and Bacon, Boston, 33 (1977).

11. W. M. Jackson and B. Donn, **Nature et Origine des Comètes**, Mémoires de La Societe Royale des Science, V Series, Vol XII, 133 (1966).

12. J. T. Yardley, **Introduction to Molecular Energy Transfer**, Academic Press, New York, 108 (1980).

13. J. L. Kohl, W. H. Parkinson, and R. L. Kurucz, **Center and Limb Solar Speetrum in High Spectral Resoluion 225.2 nm to 319.6 nm**, Harvard-Smithsonian Center for Astrophysics, Harvard University Press, Cambridge, Mass. (1978).

14. M. F. A'Hearn, J. T. Ohlmacher, and D. G. Schleicher, **A High Resolution Solar Atlas for Fluorescence Calculations**, University of Maryland Technical Report, Tr Ap83-044, (1983).

#72

IUE observations of Comet Halley: Evolution of the ultraviolet spectrum between September 1985 and July 1986

P. D. Feldman,[1*] M. C. Festou,[2*] M. F. A'Hearn,[3*] C. Arpigny,[4*] P. S. Butterworth[5*] C. B. Cosmovici[6*] A. C. Danks,[7*] R. Gilmozzi,[8*] W. M. Jackson,[9*] L. A. McFadden,[3] P. Patriarchi,[10*] D. G. Schleicher,[11] G. P. Tozzi,[10*] M. K. Wallis,[12*] H. A. Weaver,[13*] T. N. Woods[1]

[1]Johns Hopkins University, Baltimore, Maryland 21218, USA
[2]Observatoire de Besançon, 25000 Besançon, France
[3]University of Maryland, College Park, Maryland 20742, USA
[4]Institut d'Astrophysique de Liège, B-4200 Liège, Belgium
[5]NASA/Goddard Space Flight Center, Greenbelt, Maryland 20771, USA
[6]IFSI-CNR, 00044 Frascati, Italy
[7]Florida International University, Miami, Florida 33199, USA
[8]IUE Tracking Station, ESA/Vilspa, 28080 Madrid, Spain
[9]University of California, Davis, California 95616, USA
[10]Osservatorio Astrofisico di Arcetri, 50125 Firenze, Italy
[11]Lowell Observatory, Flagstaff, Arizona 86001, USA
[12]University College, Cardiff CF1 1XL, UK
[13]Space Telescope Science Institute, Baltimore, Maryland 21218, USA

To be published in *Astronomy and Astrophysics*, Main Journal, Proceedings of the ESLAB symposium *The Exploration of Halley's Comet*, Heidelberg, FRG, 27-31 October 1986.

*Guest Observer with the *International Ultraviolet Explorer* satellite observatory.

8 April 1987

Summary

The ultraviolet spectrum of comet P/Halley (1982 i) was monitored with the *International Ultraviolet Explorer* (*IUE*) satellite observatory between 12 September 1985 and 8 July 1986 ($r < 2.6$ AU pre- and post-perihelion) at regular time intervals except for a two-month period around the time of perihelion. A complete characterization of the UV spectrum of the comet was obtained which allows us to derive coma abundances and to study the light emission mechanisms of the observed species. *IUE* observations at the time of the *Giotto* encounter provide a unique opportunity to compare the *in situ* measurements with remote observations of the principal coma species. The Fine Error Sensor (FES) camera of the *IUE* was used to photometrically investigate the coma brightness variation on time scales of the order of hours. Spectroscopic observations as well as FES measurements show that the activity of the nucleus was highly variable, particularly at the end of December 1985 and during March and April 1986. The production rates of OH, CS and dust are derived for the entire period of the observations. The total water loss rate for this period is estimated to be 3×10^8 metric tons.

Keywords: comet Halley, spectroscopy, ultraviolet

1. Introduction

The *IUE* was used in an extensive joint U.S.-European program to monitor the spectral characteristics and evolution of comet Halley between September 1985 and July 1986, corresponding to heliocentric distance $r < 2.6$ AU both pre- and post-perihelion. Observations, from both Goddard Space Flight Center and Vilspa, were made at regular intervals during this period except between January 1 and March 8, 1986 when the solar elongation angle of the comet was too small. A special observing technique, developed by the GSFC *IUE* staff, made possible the almost daily observations during the week of the *Vega-2* and *Giotto* encounters.

An unexpected benefit of the *IUE* program was the use of the Fine Error Sensor (FES) as a photometric monitor over relatively long time periods of short-term fluctuations in cometary activity. Large amplitude variations in brightness (in the 18 arc-seconds square central region of the coma) were particularly evident the last week of December 1985 and throughout March and April 1986. These variations are attributed to a combination of nucleus rotation and outburst of individual jets or active areas on the surface of the nucleus. Contiguous observing shifts have made it possible to study the behavior of the UV emissions during several periods of outburst activity.

This report presents a summary of the observations made through July 1986 and a preliminary analysis of the long-term evolution of the gaseous coma of P/Halley. The highlights of the observations made during the spacecraft encounters have been presented by Festou *et al.* (1986). In this regard it is worth

noting the excellent agreement obtained between the water production rate based on *IUE* measurements of OH emission and the vectorial model of Festou (1981) and that based on the *in situ* neutral mass spectrometer data from *Giotto* (Krankowsky *et al.*, 1986). The *in situ* measurements also showed the validity of the inverse square distribution and radial outflow velocity (0.9 ± 0.2 km s^{-1}) of the H_2O parent molecules used in the coma models, even though some question remains concerning the value of the photodestruction lifetime of H_2O.

2. Spectroscopy

The first spectrum of comet Halley ever recorded from space, a long wavelength three-hour exposure taken on 12.0 September 1985, is shown in Figure 1. The OH (0,0) band at 3085 Å is readily apparent, indicating a significant H_2O production rate already at 2.59 AU. Typical of the period following perihelion is the exposure from 11 March 1986, shown in Figure 2, which displays all of the known neutral cometary emission features in this spectral range as well as a very strong component of sunlight reflected by particulate grains in the coma. Comparison with the measured solar spectrum (Mount and Rottman, 1981), shown as the dotted curve in Figure 2, indicates that the reflected spectrum is more reddened (7% per 100 Å) than that of more distant, dusty comets observed previously by the *IUE* (Feldman and A'Hearn, 1985). The source of the reddening remains uncertain and is contrary to the behavior expected from the large population of small grains detected by the *in situ* dust experiments. The strong solar component tends to mask the emission from the CO_2^+ doublet near 2890 Å. However, when a properly reddened solar spectrum is subtracted from a spectrum such

as in Figure 2, the resultant CO_2^+ emission suggests an abundance relative to OH comparable to that found in other comets (Festou, Feldman and Weaver, 1982). The absence of detectable CO^+ First Negative band emission near 2200 Å probably results from a combination of lower fluorescence efficiency for these transitions (relative to the blue Comet Tail bands) (Magnani and A'Hearn, 1986) and the poor sensitivity of the LWP camera in this spectral range.

As with the long-wavelength spectra, the short-wavelength spectrum (Figure 3) does not show any previously undetected cometary emission features. In fact, the apparent weakness of O I, C I and S I, relative to those emissions in the spectrum of comet Bradfield (1979 X) (Weaver *et al.*, 1981), may reflect lower fluorescence efficiencies and photodissociation rates due to the lower solar UV fluxes characteristic of solar minimum as compared with 1980 which was the year of solar maximum.

3. Variability

Visible light photometric monitoring of P/Halley was accomplished by using the Fine Error Sensor (FES) camera of the *IUE* (normally used for target acquisition and tracking) as a broad-band (4000 - 6500 Å) photometer. In this mode, the FES samples a region approximately 18 arc-seconds square around the center of brightness of the comet. These observations are made automatically as the *IUE* tracking of the moving comet is verified at intervals of ~30 to 60 minutes. The short-term variability of comet Halley can be seen in Figures 4 and 5 which show the FES data for December 1985 and March-April 1986, respectively. The

FES responds to a mixture of gas and dust emission and a comparison with the ultraviolet spectra (taken at much less frequent intervals) indicates that both the UV continuum and the CS emission follow the changes in cometary activity more rapidly than does the OH emission, which arises from a parent molecule whose lifetime is about 1 day (McFadden *et al.*, 1987). Amongst many apparent transient events seen in Figure 5, a sharp outburst on 18-19 March was found to be correlated with CO_2^+ emission observed by *IUE* 150,000 km tailward from the nucleus during the outburst and with ground-based observations of a large detached CO^+ cloud on 20 March 1986 (Feldman *et al.*, 1986). Otherwise, the variations in Fig. 5 are found to closely follow the 7.4-day period light curve derived from ground-based photometry by Millis and Schleicher (1986). However, it should be noted that *IUE* observations made after April did not show any significant variation in the FES count rate during an 8-hour observing shift.

4. Production Rates

One of the principal goals of the *IUE* Halley program was the determination of the variation of gas production rate with heliocentric distance both before and after perihelion. The derivation of this rate from the observed surface brightness is generally achieved with the use of steady-state, spherically symmetric models. Although the validity of these assumptions is clearly questionable in light of both *in situ* and remote observations of P/Halley, they provide the only means of intercomparing observations made over a large range of heliocentric and geocentric distances. However, as noted above, the preliminary results from the *Giotto* neutral mass spectrometer experiment (Krankowsky *et al.*, 1986) confirmed two of the

basic assumptions of the models, the radial outflow velocity and the inverse square density distribution of the parent molecules. For the present, only the production rates of the parents of OH and CS are considered. For the grains, the production rate can be related to the quantity $Af\rho$, the product of albedo, filling factor and aperture radius (A'Hearn *et al.*, 1984). The vectorial model (Festou, 1981) and OH fluorescence efficiencies of Schleicher (1983) are used to derive Q_{H_2O}, while Q_{CS}, assumed to be equal to the production rate of its short-lived parent, CS_2 (Jackson, Butterworth and Ballard, 1986), is derived from a Haser model and the assumption of a heliocentric velocity independent fluorescence efficiency. For the parent molecules, the outflow velocity was taken to be 1 km s^{-1}, while the photodissociation lifetimes of both H_2O and OH were taken from Festou (1981). The use of a shorter H_2O scale length, as suggested by Krankowsky *et al.* (1986) would yield values of Q about 60% of those shown in Figure 6. In all three cases, the emissions are assumed to be optically thin. While this is not exactly so for the strongest lines of the OH (0,0) band used in the analysis, the effect of resonance re-radiation on the derived production rates is estimated to be negligible.

The results, shown in Figures 6-8, are somewhat surprising. Both the CS and the dust show larger short-term fluctuations with comet variability than does OH, but also exhibit a uniform decrease in production rate to larger heliocentric distance. The H_2O production rate, on the other hand, while increasing dramatically between 2 and 3 AU pre-perihelion, and then more gradually to 1 AU, did not begin to decrease appreciably until the comet was approaching 2 AU post-perihelion. This behavior suggests that in P/Halley the CS and dust production

are not totally controlled by the water vaporization, a conclusion already reached for two other comets previously observed by *IUE*, IRAS-Araki-Alcock (1983 VII) (Feldman, A'Hearn and Millis, 1984) and P/Encke (A'Hearn *et al.*, 1985).

Finally, we note that the water production rates shown in Figure 6 can be integrated over the entire period from September 1985 through the beginning of July 1986 to estimate the total amount of water lost by P/Halley during this apparition. For the period around perihelion when there are no *IUE* observations, a constant value of $Q = 1 \times 10^{30}$ molecules s^{-1} is used. This value is consistent with the H I Lyman-α observations made by the ultraviolet spectrometer on *Pioneer Venus Orbiter* during this period (Stewart, 1987). The total H_2O lost, estimated this way, is 3×10^8 tons.

5. Conclusion

The *IUE* observations of comet Halley provide a unique source of information about the composition, evolution, and short-term behavior of the cometary coma, and establish a context for the inter-comparison of the *in situ* encounter snapshots of Halley and the large body of Earth-based observations of the comet.

Acknowledgments

We thank the *IUE* staffs at Goddard Space Flight Center and Vilspa for their assistance in the operations and acquisition of data. E. Roettger assisted in the data analysis. This work was supported by NASA grants NSG-5393 to the Johns Hopkins University and NAG 5-252 to the University of Maryland.

References

A'Hearn, M. F., Schleicher, D. G., Feldman, P. D., Millis, R. L., Thompson, D. T.: 1984, *Astron. J.*, **89**, 579-591.

A'Hearn, M. F., Birch, P. V., Feldman, P. D., Millis, R. L.: 1985, *Icarus,* **64**, 1-10.

Feldman, P. D., A'Hearn, M. F., Millis, R. L.: 1984, *Astrophys. J.*, **282**, 799-802.

Feldman, P. D., A'Hearn, M. F.: 1985, in *Ices in the Solar System* (ed. J. Klinger *et al.*), Dordrecht, D. Reidel Publ. Co., 453-461.

Feldman, P. D., A'Hearn, M. F., Festou, M. C., McFadden, L. A., Weaver, H. A., Woods, T. N.: 1986, *Nature,* **324**, 433-436.

Festou, M. C.: 1981, *Astron. Astrophys.*, **95**, 69-79.

Festou, M. C., Feldman, P. D., Weaver, H. A.: 1982, *Astrophys. J.*, **256**, 331-338.

Festou, M. C., Feldman, P. D., A'Hearn, M. F., Arpigny, C., Cosmovici, C. B., Danks, A. C., McFadden, L. A., Gilmozzi, R., Patriarchi, P., Tozzi, G. P., Wallis, M. K., Weaver, H. A.: 1986, *Nature,* **321**, 361-363.

Jackson, W. M., Butterworth, P. S., Ballard, D.: 1986, *Astrophys. J.*, **304**, 515-518.

Krankowsky, D., Lämmerzahl, P., Herrwerth, I., Woweries, J., Eberhardt, P., Dolder, U., Herrmann, U., Schulte, W., Berthelier, J. J., Illiano, J. M., Hodges, R. R., Hoffman, J. H.: 1986, *Nature,* **321**, 326-329.

Magnani, L., A'Hearn, M. F.: 1986, *Astrophys. J.*, **302**, 477-487.

McFadden, L. A., A'Hearn, M. F., Feldman, P. D., Roettger, E. E., Edsall, D. M., Weaver, H. A., Butterworth, P. S.: 1987, *Astron. Astrophys.*, submitted.

Millis, R. L., Schleicher, D. G.: 1986, *Nature,* **324**, 646-649.

Mount, G. H., Rottman, G. J.: 1981, *J. Geophys. Res.,* **86**, 9193-9198.

Schleicher, D. G.: 1983, The fluorescence of cometary OH and CN, Ph.D. Dissertation, University of Maryland.

Stewart, A. I. F.: 1987, *Astron. Astrophys.,* submitted.

Weaver, H. A., Feldman, P. D., Festou, M. C., A'Hearn, M. F., Keller, H. U.: 1981, *Icarus,* **47**, 449-463.

FIGURE CAPTIONS

Figure 1. Long-wavelength spectrum of P/Halley (LWP 6720) obtained on 12 September 1985. The exposure time was 180 minutes.

Figure 2. A long wavelength 15 minute exposure of P/Halley (LWP 7773) obtained on 11 March 1986.

Figure 3. Short-wavelength spectrum of P/Halley (SWP 27884) obtained on 9 March 1986. The exposure time was 45 minutes.

Figure 4. FES photometry for December 1985.

Figure 5. FES photometry for March and April 1986. The times of the *Vega-2* and *Giotto* encounters are indicated.

Figure 6. Water production rate for comet Halley as a function of heliocentric distance as derived from *IUE* observations of OH.

Figure 7. Dust production rate variability as a function of heliocentric distance.

Figure 8. Production rate of CS as a function of heliocentric distance.

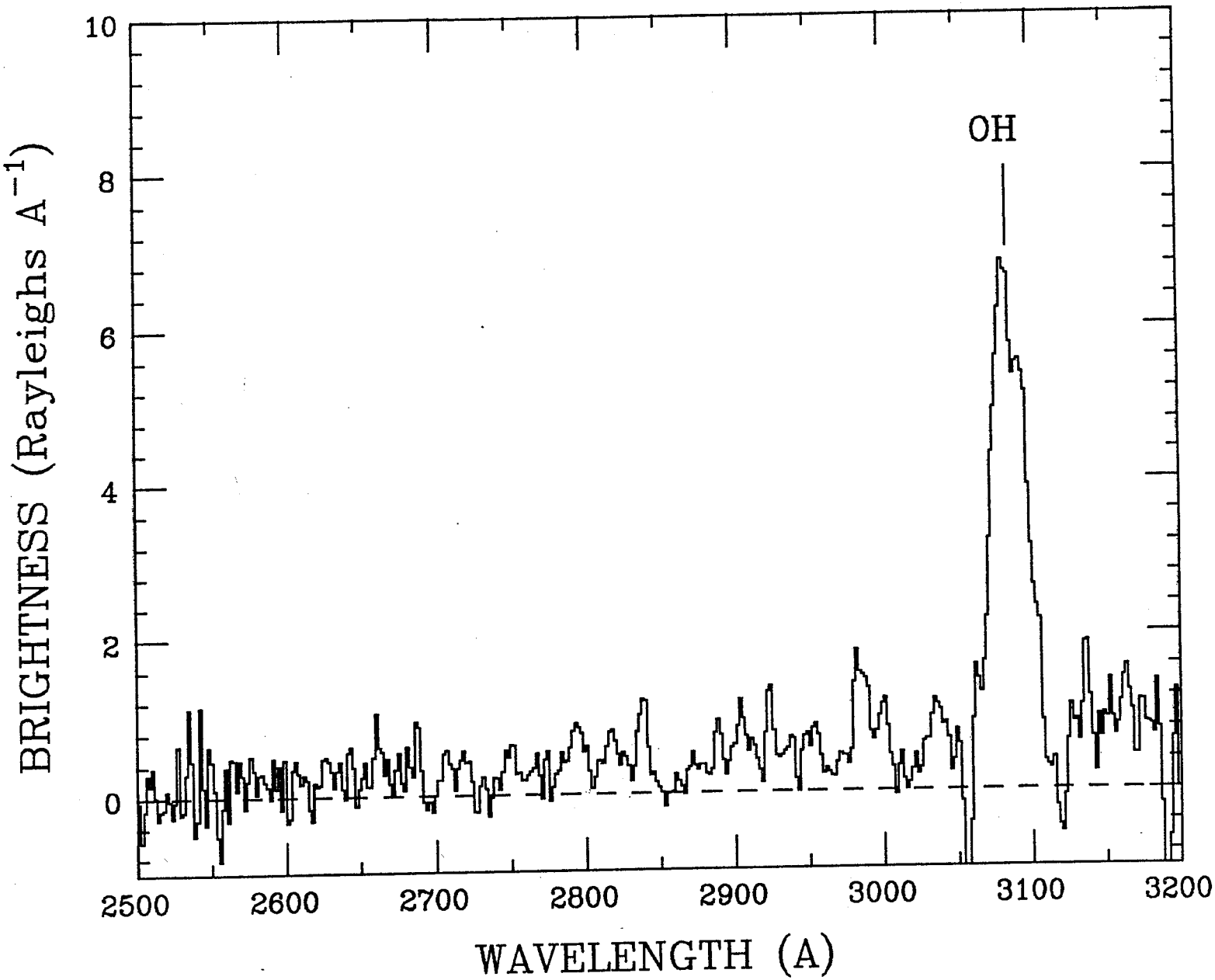
OH
BRIGHTNESS (Rayleighs A^{-1})
WAVELENGTH (A)
10
8
6
4
2
0
2500
2600
2700
2800
2900
3000
3100
3200

Fig. 1

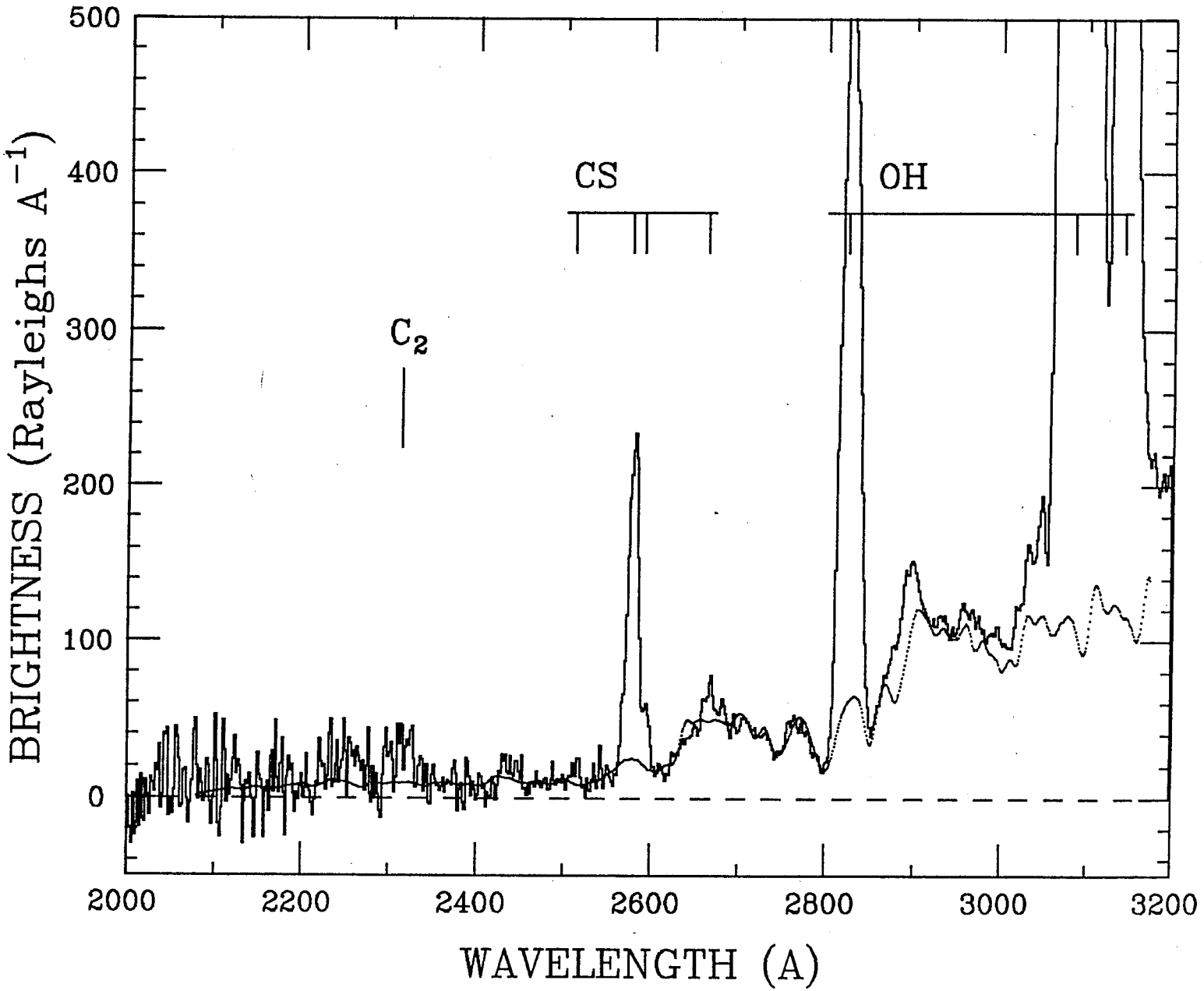
500
400
300
200
100
0
BRIGHTNESS (Rayleighs A^{-1})
CS
OH
C_2
2000
2200
2400
2600
2800
3000
3200
WAVELENGTH (A)

Fig. 2

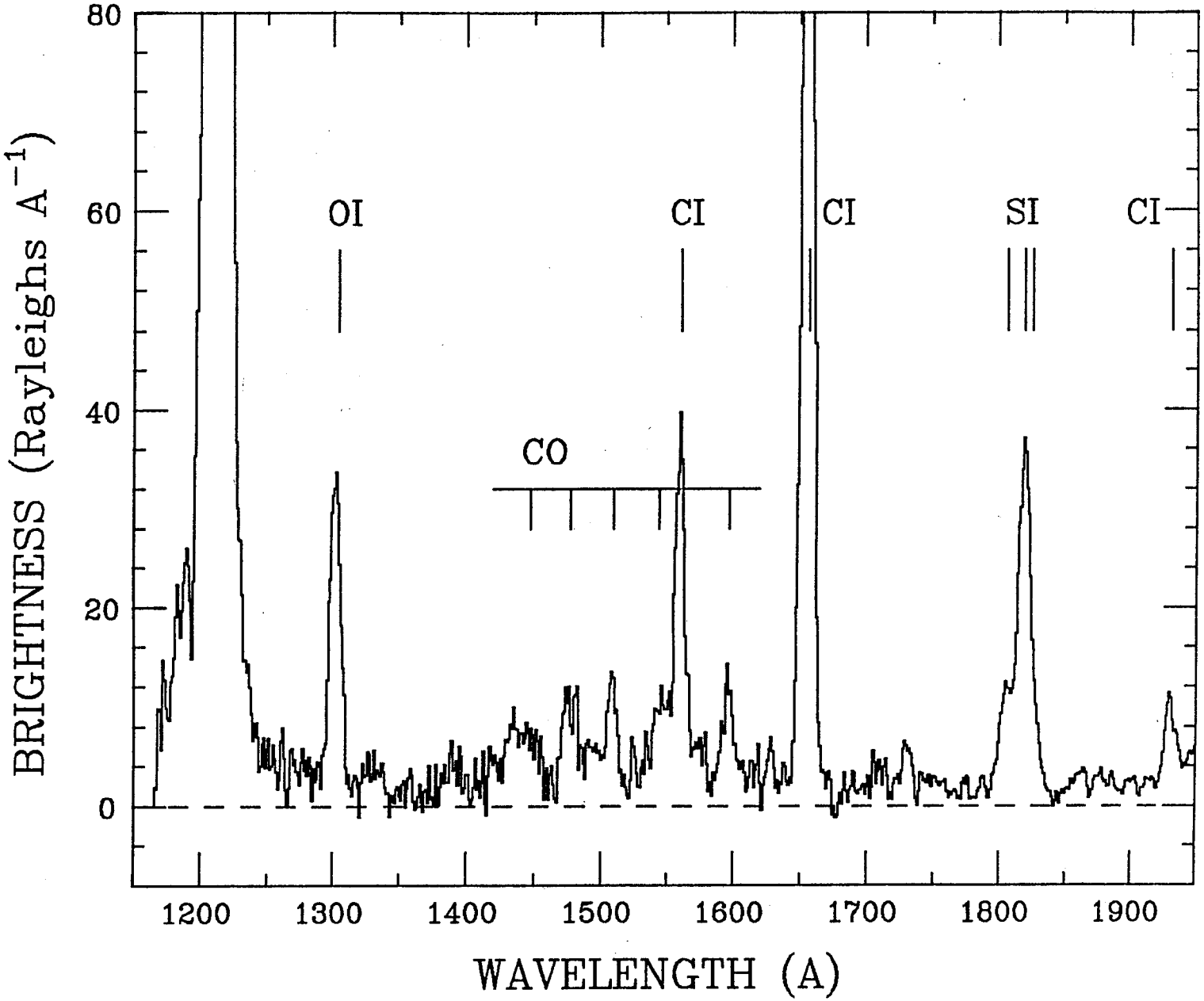
80
60
40
20
0
BRIGHTNESS (Rayleighs A^{-1})
OI
CI
CO
CI
SI
CI
1200
1300
1400
1500
1600
1700
1800
1900
WAVELENGTH (A)

Fig. 3

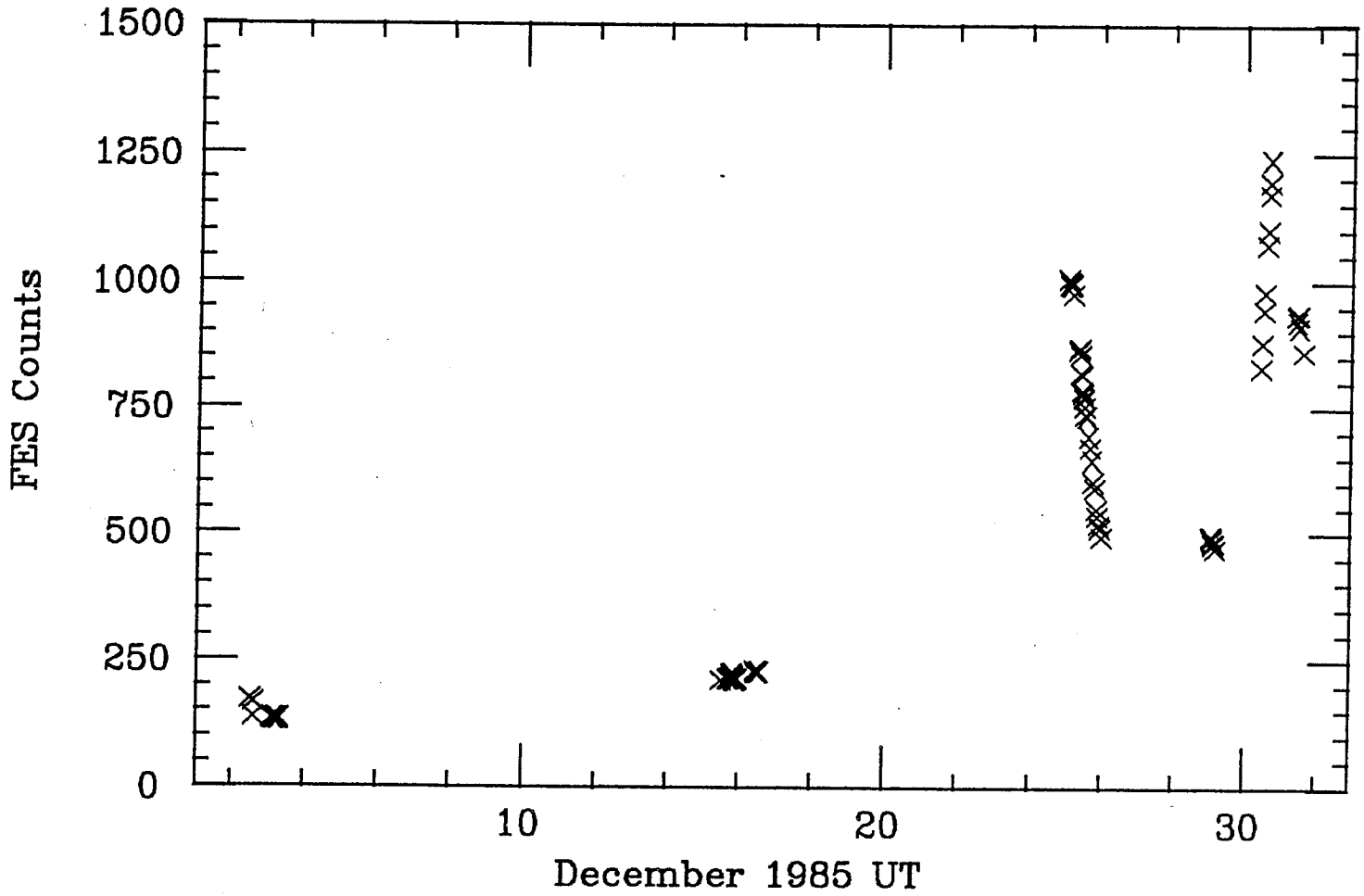
1500
1250
1000
750
500
250
0
FES Counts
10
20
30
December 1985 UT

Fig. 4

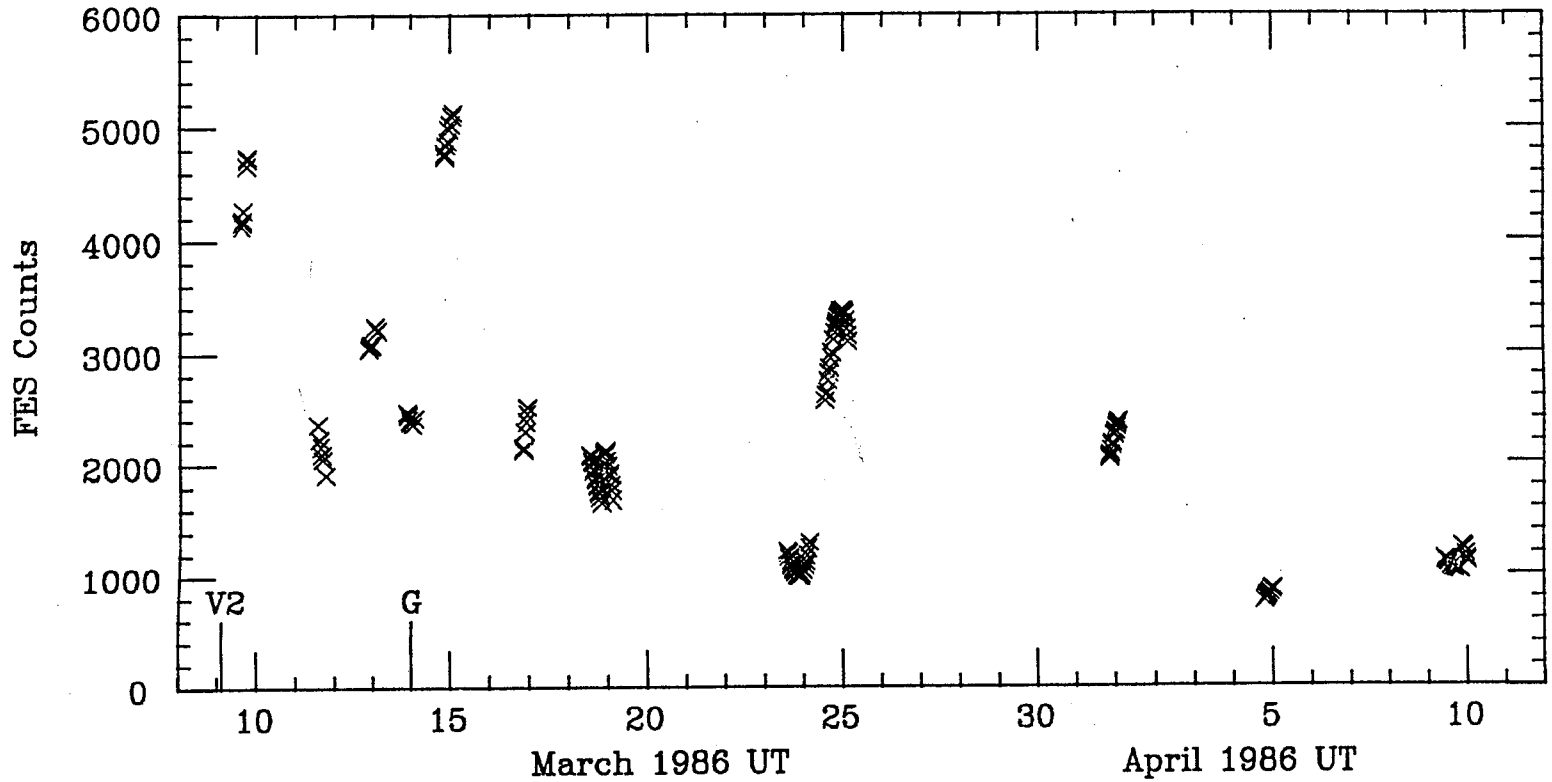
6000
5000
4000
3000
2000
1000
0
FES Counts
V2
G
10
15
20
25
30
5
10
March 1986 UT
April 1986 UT

Fig. 5

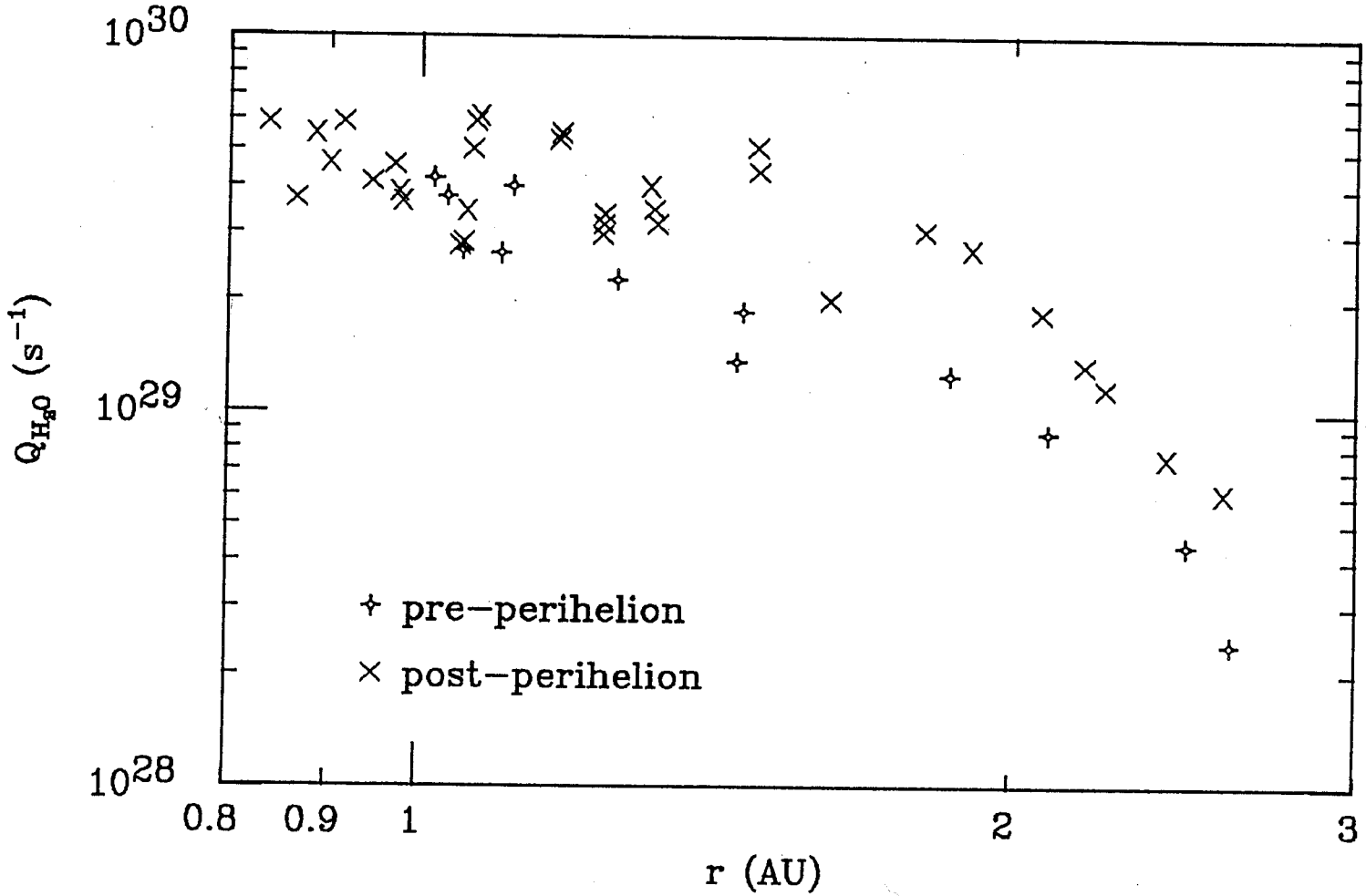
10^{30}
10^{29}
10^{28}
Q_{H_2O} (s^{-1})
pre−perihelion
post−perihelion
0.8
0.9
1
2
3
r (AU)

Fig. 6

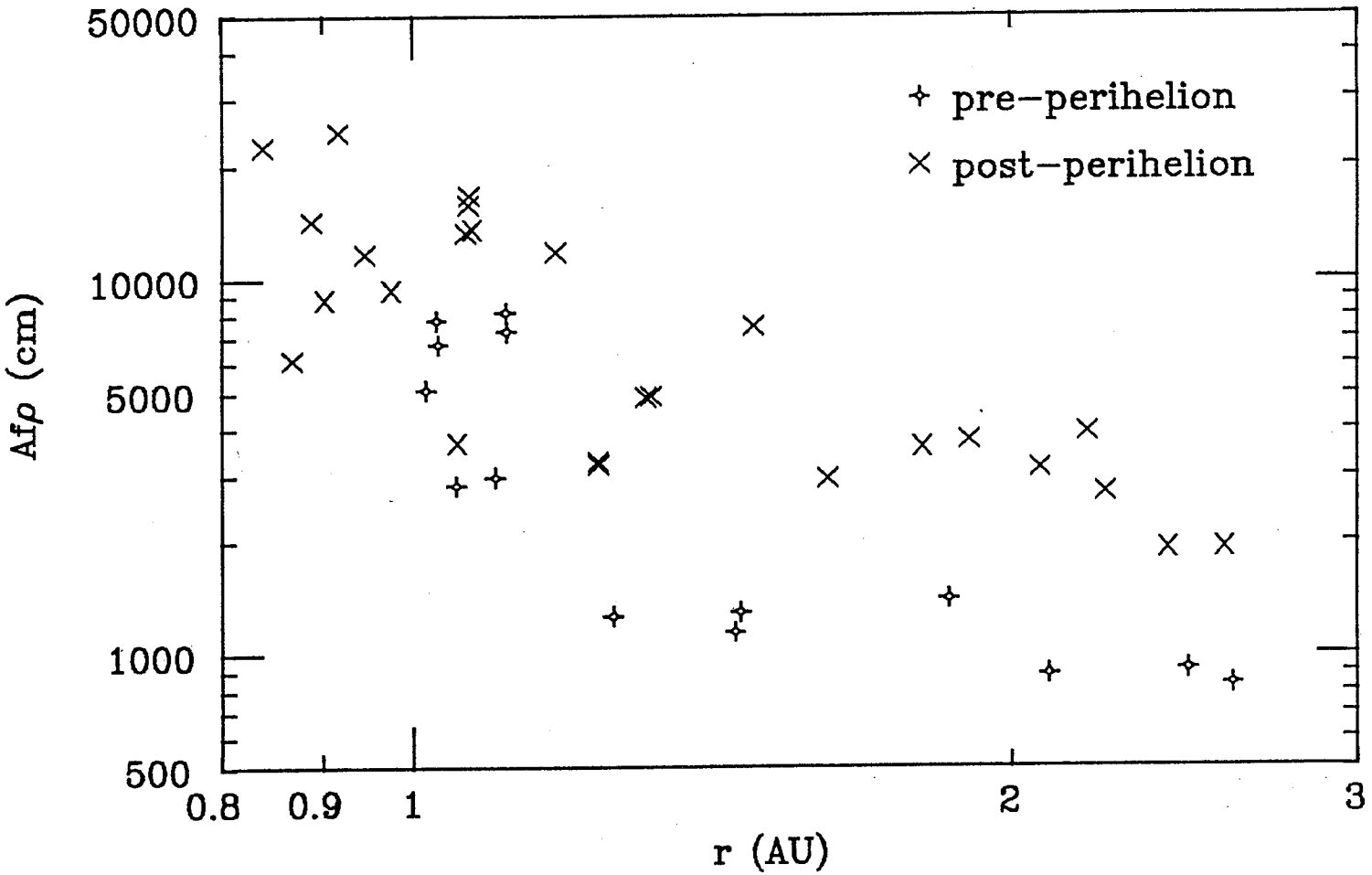
50000
10000
5000
1000
500
Afρ (cm)
0.8
0.9
1
2
3
r (AU)
pre−perihelion
post−perihelion

Fig. 7

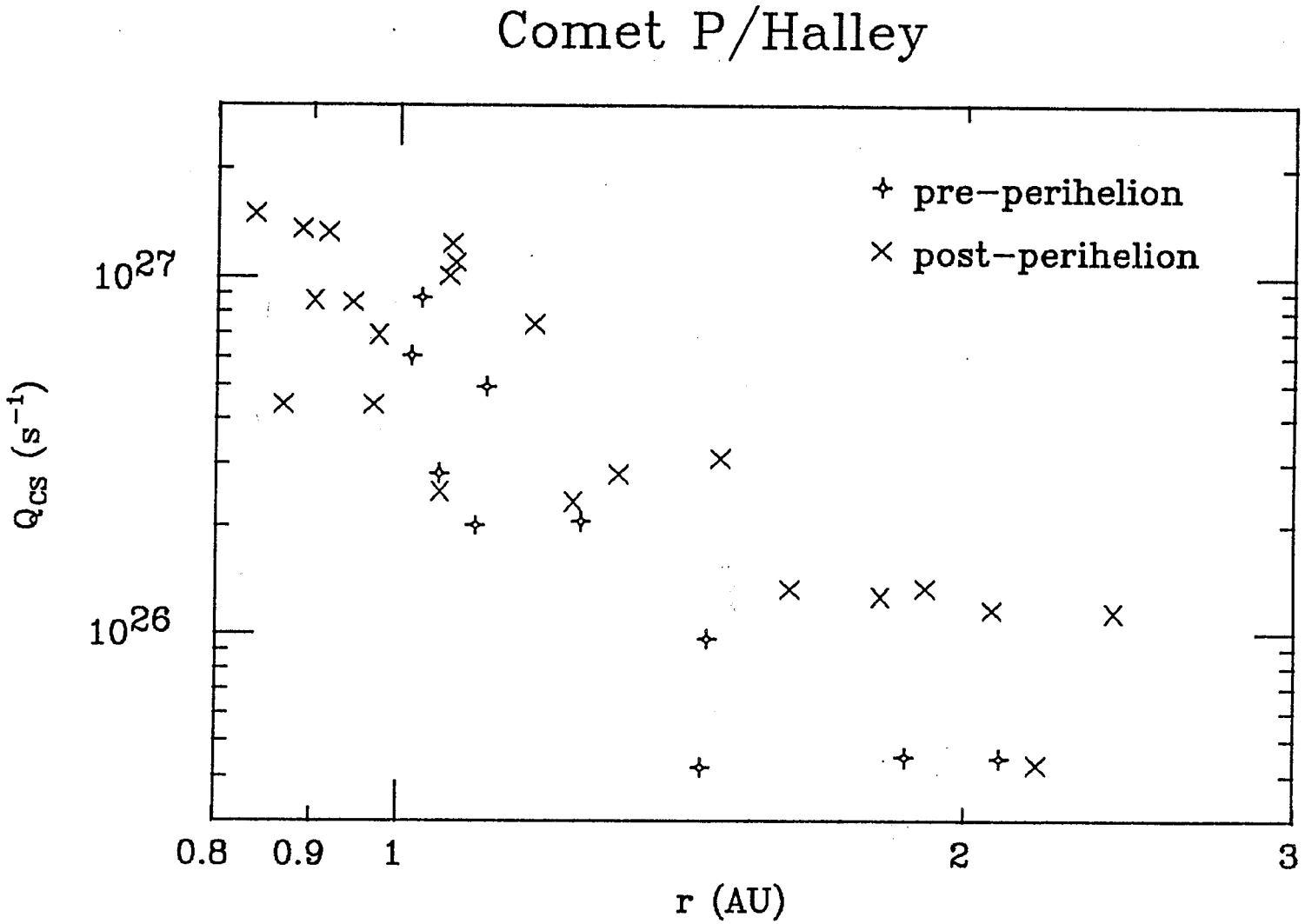
Comet P/Halley
pre-perihelion
post-perihelion
10^{27}
10^{26}
Q_{CS} (s^{-1})
0.8
0.9
1
2
3
r (AU)

Fig. 8

#73

A Comparison of the High Resolution IUE observations of CS emission in Comets Halley and Giacobini-Zinner

William M. Jackson[1*], and M. G. Prisant[2]

[1]Chemistry Department, University of California, Davis, Ca. 95616

[2]Chemistry Department, University of California, Berkeley, Ca. 94720

Abstract

The high resolution spectra of comets Giacobini-Zinner and Halley have been measured in the region of the CS emission. Both spectra have essentially the same shape, but the Halley spectrum has a better signal to noise ratio. Attempts have been made to obtain the rotational distribution of the radical in these comets by using an inversion program and spectral simulation. Both procedures suggest that the rotational distribution is dominated by CS radicals with J" ≤ 5. Despite this it appears that another distribution with higher J"'s is needed to explain the shape of the rotational distribution. Arguments are presented which suggest that this second distribution is due to a balance between collisions and radiation in the inner coma.

Introduction

The CS molecule occupies a unique position in comets. It is the only molecule, which is consistently observed in the spectra of comets that has a short scale length in the coma [1,2,3,4]. Because of this we have speculated that it's spectral signature can be a monitor of the local conditions in this region of the coma. The scale length has been shown to be about 600 km [4] which is still in a region where collisions could affect the rotational populations of the CS radicals. To evaluate this idea a model is needed which would allow one to match the observed high resolution spectra with theoretical profiles. Earlier a very simple model was used that assumed the rotational distribution of the CS radical could be described by a Boltzmann distribution [3]. This amounts to assuming that the CS rotational distribution is a thermometer for the collision region. Subsequently more theoretical analysis and laboratory work [5] has suggested that a more sophisticated model is needed. In particular a model is required that could extract the rotational distribution from the observed spectra, which could then be compared with the expected distributions based upon a molecular model. Recently Prisant and Zare [6] have described an inversion procedure that can be used to obtain the rotational distribution from an observed spectra. In this paper this method will be adapted to analyze high resolution spectra obtained in IUE observations of Comets Giacobini-Zinner during the ICE encounter and Halley's comet on December 25 and 26, 1985. Various simulation procedures have also been used and will be compared with the inversion procedure. The extracted rotational distributions are then discussed in terms of what should be expected from a molecular model.

*Guest observer with the International Ultraviolet Explorer Satellite observatory

Observations

Bogess [7] has previously described the IUE instrumentation and only the observational details and the results will be given in this section. The CS portion of the high resolution spectra which was obtained with the LWP camera during observations of comets Giacobini-Zinner and Halley are shown in Figs. 1 and 2, respectively. The wavelength scale is from the IUE guest observer tape and has not been corrected for the relative motion of the comet and the telescope. A 390 min exposure was used for the Giacobini-Zinner (LWP 6694) spectrum, obtained on 30 August 1985, while a 720 min exposure was used for the Halley spectrum (LWP 7383) observed on the 25 and 26 of December, 1985. The data is presented as is, with no smoothing and the signal to noise ratio is estimated to be 12/1 for Giacobini-Zinner and 33/1 for Halley. The noise was estimated from the negative excursion peaks in the spectra in the region where there should not be any CS rotational lines. The CS spectra was observed in two different orders in both spectra but in this paper only the order that occurs near the center of the camera will be discussed. The IUE instrumental bandwidth is quoted to be 0.2 A for a point source and 0.8 A for an extended source. This is varied in the analysis because the images of these comets completely fill the slit. The true resolution is somewhere between these values.

Theory

The high resolution emission spectrum of both comets obtained from IUE should contain information about the local condition in the inner coma. The production scale lengths of CS had previously been shown to be less than [3,4] 1000 km. Thus this species is formed in the inner coma and may be a probe of this region. The rotational distribution of the CS radical in this region could possibly monitor the local conditions of the inner coma. To determine whether this is the case it is necessary to see if the observed spectra can be fitted with models that require collisions.

There are several approaches that can be taken to match the observed spectra with a model spectra. Earlier work [3] had calculated the high resolution spectra assuming that the rotational distribution could be fitted with a Boltzmann distribution of rotational levels. In the present work that approach will be used as well as the inversion method [6] which has been developed for inverting the distribution from the observed spectra.

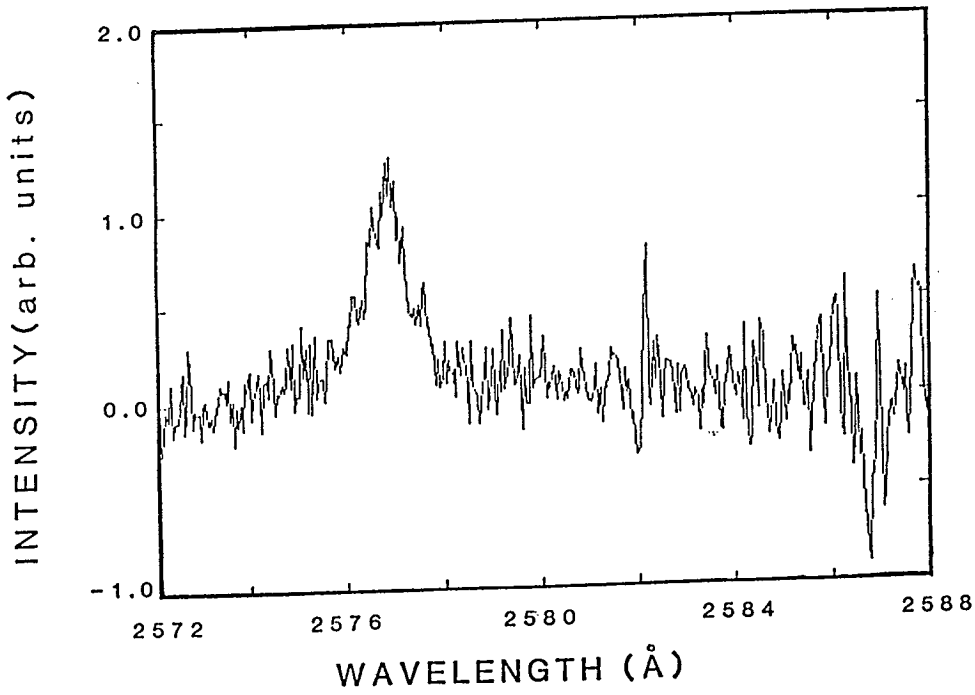

Fig. 1 The CS region of the LWP6694 Giacobini-Zinner spectrum. This is a 390 min exposure and the data is as it is provided to the guest observer on tape. It was extracted from the tape image using ANA software supplied by Gibor Basir.

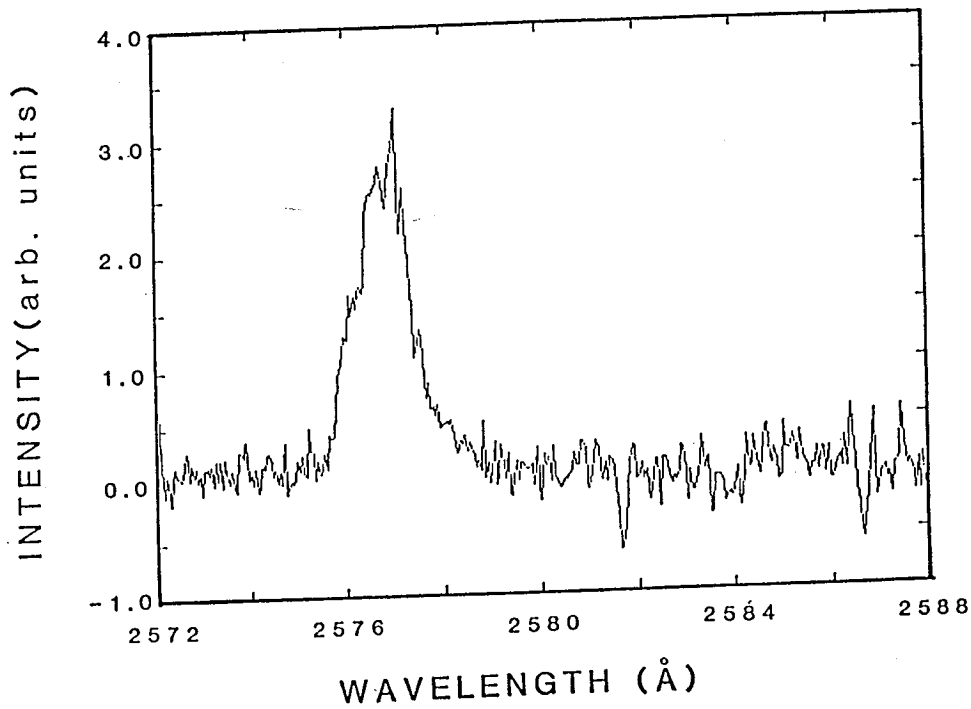

Fig. 2 The same spectral region for comet Halley, but this is a 720 min exposure. The data were taken on 12/25 and 12/26, 1985.

In the analysis it will be assumed that the CS radical is produced by photodissociation of CS_2. Ample evidence has been presented that suggest that this is the most likely source of CS [4]. Photodissociation of CS_2 is known to lead to the production of highly vibrationally and rotationally excited CS radicals [5]. The radicals appear to be formed with internal energy up to the thermodynamic limit, so that at 193 nm they can be formed with up to 12 quanta of vibrational energy and with substantial amounts of rotational energy. Once the radicals are formed in the cometary environment it is unlikely that they will survive in these highly excited vibrational levels. The natural radiative lifetime for a CS radical radiating in the infrared region via the following process,

$$CS(v'') \longrightarrow CS(v''-1) + h\upsilon \qquad (1)$$

is of the order of a few milliseconds. This is much smaller than the solar excitation rate and the collision rate, so that it is unlikely that vibrationally excited radicals will survive long enough to be electronically excited and detected. Similar considerations for the highly excited rotational levels lead to the same conclusion for the upper rotational levels, with large spacings. The exact number of rotational levels that will have to be considered will depend upon radiative relaxation time and the collision time between the CS radical and the gas in the coma.

With the above considerations in mind a model can be developed to try to match the observed high resolution spectra. The overall process can be described by the following series of reactions,

$$CS(X^1\Sigma,v'',J'') + h\upsilon \longrightarrow CS(A^1\Pi,v',J') \qquad (2)$$

$$CS(A^1\Pi,v',J') \longrightarrow CS(X^1\Sigma,v'',J'') + h\upsilon \qquad (3)$$

First, label all of the initial levels of $CS(X^1\Sigma)$ with the index i, the intermediate levels of $CS(A^1\Pi)$ with the index j, and the final levels of $CS(X^1\Sigma)$ with the index k. The levels i are the populated levels in the coma, the levels j are the levels that are optically populated by absorption of solar radiation, and the levels k are the levels that are optically coupled by emission from j. It is this latter emission that is measured by the IUE telescope.

The emission intensity, $I_{jk}(\lambda_l)$, from a given j level to a k level at wavelength λ_l is proportional to,

$$I_{jk}(\lambda_l) = \Sigma_{jk} N_j S_{jk} \upsilon^3_{jk} \phi(\lambda_{jk}-\lambda_l) \qquad (4)$$

where, $\phi(\lambda_{jk}-\lambda_l)$ is the instrument function of the telescope, υ_{jk} is the frequency of the transition between the j and the k levels, S_{jk} is the natural line strength, λ_{jk} is the Doppler shifted transition wavelength, and N_j is the population of the intermediate level j. The natural line strength is given by,

$$S_{jk} = q^2_{v'v''} \mu^2_{jk} S_{jk} \qquad (5)$$

in which $q_{v'v''}$ is the Franck-Condon factor, μ is the transition dipole, and S is the rotational line strength. The sum in the intensity function is over all optically coupled levels in emission and absorption.

The population of the intermediate level j can be determined from the following relationship,

$$N_j = \Sigma_i N_i S_i \upsilon_{ij} O(\upsilon_{ij}) \qquad (6)$$

where, $O(\upsilon_{ij})$ is the intensity of the solar radiation at the Doppler shifted absorption frequency υ_{ij} and all of the other symbols are the same. The equation for the emitted light intensity I_l can now be rewritten as,

$$I_l = \Sigma_i N_i (\Sigma_{jk} S_{ij} \upsilon_{ij} \upsilon^3_{jk} O(\upsilon_{ij}) \phi(\lambda_{jk}-\lambda_l)) \qquad (7)$$

The light intensity at a given line is linearly dependent upon the population of the initial states responsible for that line. If the instrument function is such that all of the lines are resolved then the population of the initial rotational levels are completely defined. In fact since there are three branches, the P,Q, and R branches, we have more equations than unknowns.

The above equation can be written in matrix form as follows,

$$\mathbf{I} = \mathbf{M}\,\mathbf{N} \qquad (8)$$

In this equation the **I** is a L dimensional column vector with L being the number of points measured in the spectrum, and N is an I dimensional column vector with I being the number of ground state rovibrational levels.

The rotational levels can be further parameterized, in terms of J_{max} where J_{max} is defined by $E_{max} = BJ''_{max}\,(J''_{max} + 1)$. Let us define a new variable X, where,

$$X = -1 + (2J/J_{max}) \qquad (9)$$

The population for a given X, P(X), can be expanded in a Legendre Series, so that

$$N(X) = \Sigma_q P_q(X) a_q \qquad (10)$$

where, $a_q = \langle P_q | P \rangle = \int_{-1}^{+1} P_q P d_l X \qquad (11)$

with $\langle P_p | P_q \rangle = \delta_{pq} \qquad (12)$

The a_q are the moments of the distribution.

therefore,

$$I_l = \Sigma_q a_q \Sigma_i P_q(X_i) \Sigma_{jk} S_{ij} S_{jk} \upsilon_{ij} \upsilon^3_{jk} O(\upsilon_{ij}) \phi(\lambda_{jk}-\lambda_l) \qquad (13)$$

since,

$$\mathbf{I_l} = \mathbf{qM} \qquad (14)$$

so,

$$\mathcal{M}_{lq} = \Sigma_{ijk} P_q(X_i) S_{ij} S_{jk} \upsilon_{ij} \upsilon^3_{jk} O(\upsilon_{ij}) \phi(\lambda_{jk}-\lambda_l) \qquad (15)$$

and,

$$\mathbf{q} = \{A_q\} \qquad (16)$$

The a_q are the moments of the distribution and may be independently extracted from the least-square's analysis of the spectrum [8].

Results and Discussion

A careful comparison of Figs. 1 and 2 suggest that the two spectra were identical except for the signal to noise ratio. Because of this, it was decided to only analyze the Halley comet spectra since it has a much better signal to noise ratio.

A synthetic spectra was first derived assuming various Boltzmann temperatures. Some of the results of this simulation procedure are shown in Fig. 3, along with the Halley comet spectra for comparison. The 29 K spectrum has the right width but it has two distinct peaks corresponding to the R branch and the overlapping P and Q branches. The resolution of the IUE instrument is not high enough to resolve these latter two branches. The 7 K spectrum has the right shape, but it is too narrow to match the spectrum that is observed. Increasing the temperature does not improve the match because the two peaks remain and eventually become too wide.

A simulated spectra was them computed using a uniform distribution, such that, $P(J''_i) = P(J''_k)$ for all J''_i and $J''_k < J''_{max}$, and is equal to zero outside of this range. These results are shown in Fig. 4, which show that the shape is better fitted with a distribution that only employs levels with low J. The spectra calculated from distributions with higher J's have too many peaks and eventually become too wide.

Fig. 5 shows, a better shape can be obtained by employing a rotational distribution function that monotonically decreases from J" = 0 to J" = 5, with a slope of one. The width of the simulated spectrum, however, is still too narrow.

Several bimodal distributions have been tried. The best fit that we have been able to obtain thus far with a bimodal distribution is given in Fig. 6. This calculated spectrum is wider than the spectra obtained with a single distribution and has the correct shape. It is still, however, not as wide as the observed spectrum.

Several spectral inversions were attempted using the theory that was described earlier. All of them gave results similar to those shown in Fig. 6, which looks very much like some of the results obtained by direct simulation. In this case it has the undesirable properties that both the width and shape are in poor agreement with the observed spectrum.

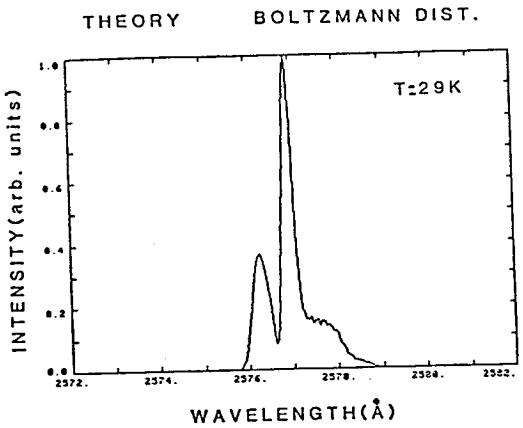

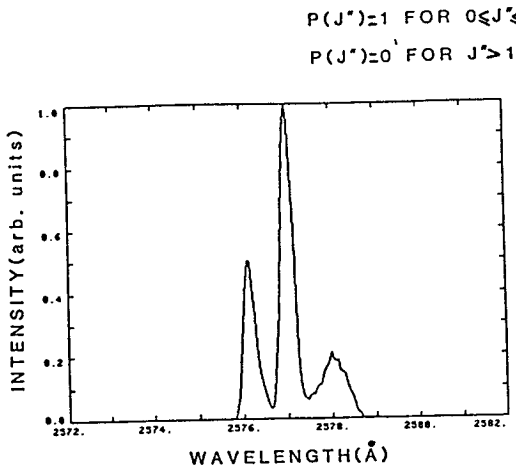

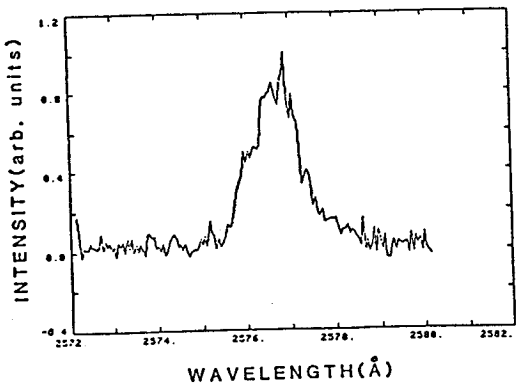

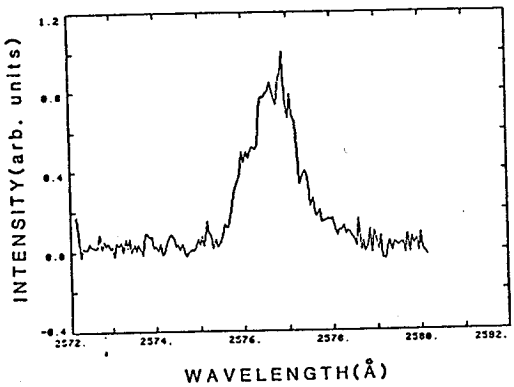

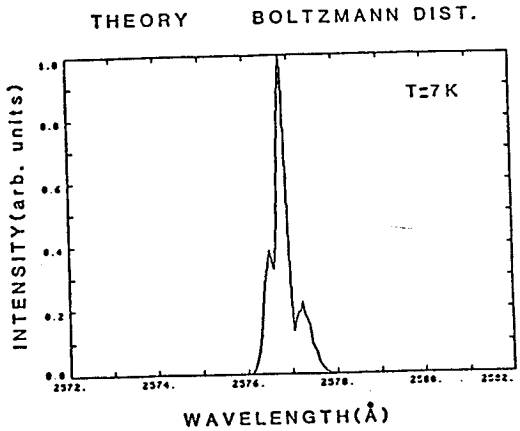

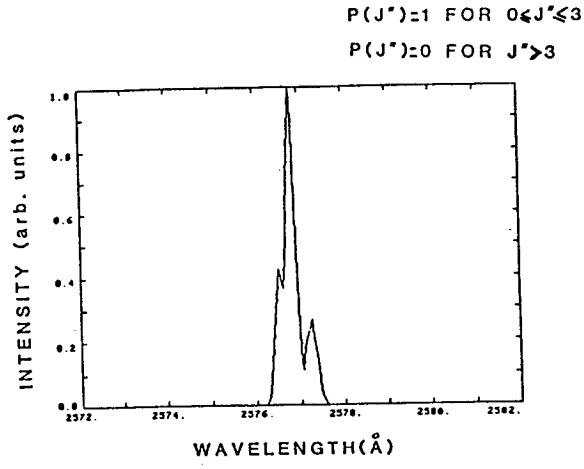

Fig. 3 Two simulated spectrum using a Boltzmann distribution of rotational levels. The Halley spectrum is included for comparison.

Fig. 4 Two simulated spectra using a uniform distribution. The Halley spectrum is included for comparison.

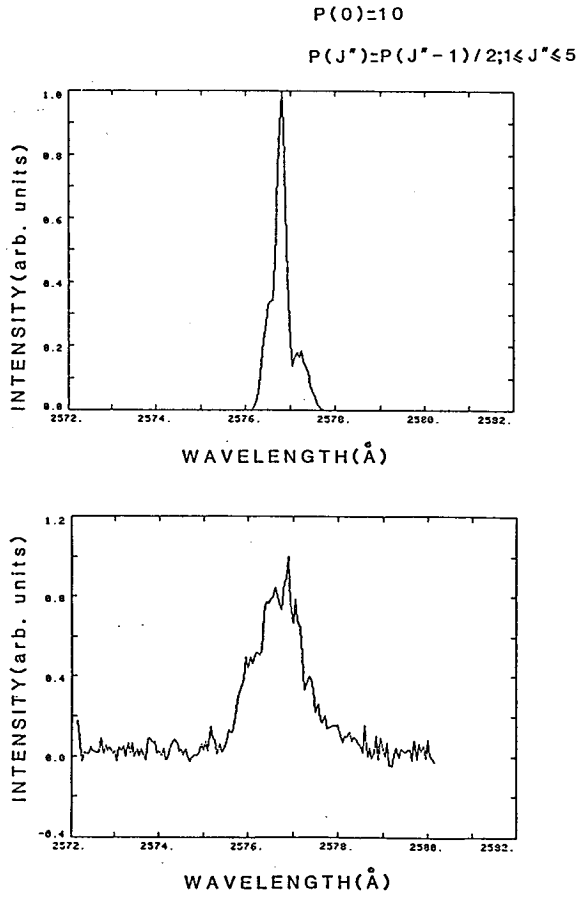

Fig. 5 A simulated spectrum using a linear distribution.

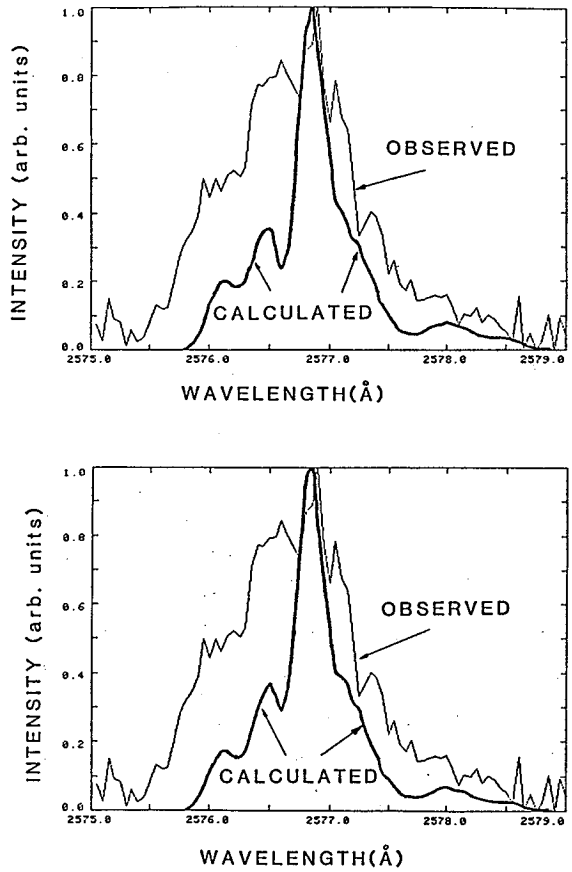

Fig. 6 Simulated Spectra obtained using bimodal distributions. The top figure has relative populations of 10, 10, 10, 10, 5, 0.5, 0.5, 0.5, 0.5, 0.5, 0.2, and 0.2 for the J" = 0, 1, 2, 3, 4, 5, 6, 7, 8, 9, 10 and 11 respectively. The bottom figure has a relative population of 10, 15, 20, 10, 5, 0.5, 0.5, 0.5, 0.5, 0.5, 0.2 and 0.2 respectively.

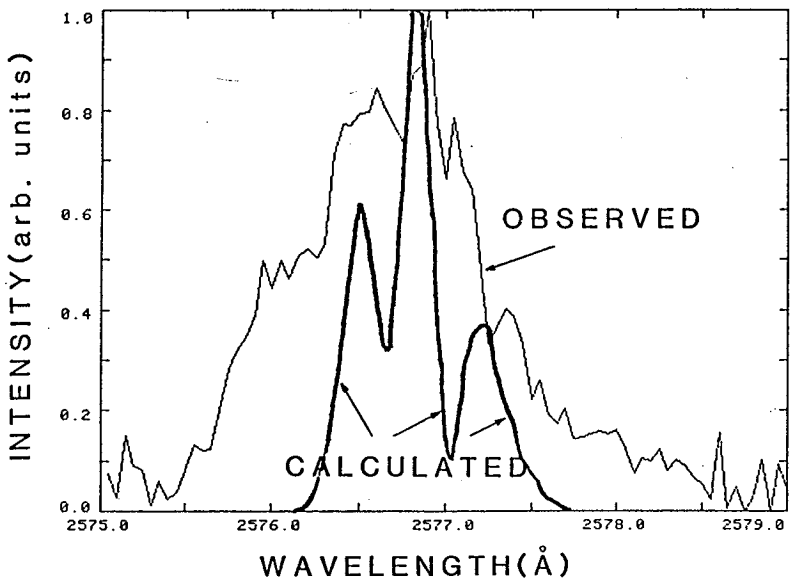

Fig. 7 An inversion using the theory described in the text.

The inversion which was previously described tries to obtain a match by fitting J" rather than the rotational energy. It is now thought that it would be better (to fit the rotational energy) because the simulation procedures suggest that only a few J" levels are involved.

The poor fit with the observations is not the only reason that the present inversion is unsatisfactory. The inversion procedure should yield the average populations, <P(J")>, in several rotational levels as well as the error in those estimates. The average populations <P(0) + P(1)>, <P(2) + P(3)>, and <P(4) + P(5)> were found to be -4.89 ± 1.8, 1.97 ± 0.61, and 0.86 ± 0.2, respectively. Thus, the inversions yield a **negative** population for the average of the J" = 0 and 1 levels. This is obviously physically unrealistic. The error in the populations are also unacceptably large. These preliminary results suggest, inversion procedure needs to be done as a global fit in energy rather than in J" populations.

The inversion procedure will only give a good fit if a correct functional form is assumed for the distributions. Which is why the simulations are important so that one can obtain a feel for the correct functional form. Once a good functional form is determined, the inversion procedure can be used to yield a quantitative measure of the parameters that give the best fit.

From all of the simulations done thus far, it is clear that the low J" levels are the principal contributors to the observed Halley spectrum. This can be explained by considering the characteristic times for electronic excitation, rotational radiative relaxation, and collisional process. These times are collected in Table 1. The average CS radical will be produced 600 s after the CS_2 radical has been released from the nucleus. It will then take an average of 1400 s before it will be excited by a solar photon. Experimental evidence[5[is available which shows that the CS radicals are born with up to 12 quanta of vibrational energy and 100 quanta of rotational energy. The vibrational energy is unimportant in determining the observed line profiles because excited vibrational levels will radiate in time of the order of milliseconds. A similar argument can be made for the upper rotational levels of CS, which according to the theoretical formula given in Table 1, will have short radiative lifetimes. At 500 km the time between collisions is 14 s, so that all of the CS radicals in rotational levels with J" above 24 will have radiated before the molecule has had a chance to collide. The CS radicals that now all have $J" \leq 24$, will then undergo approximately 200 collisions before it can be electronically excited. This collision rate has been calculated using a spherical model for fluid flow in the coma [11] and a production rate for water in Halley of 5×10^{29} s^{-1}. If collisions have unit efficiency for rotational relaxation, then all of the CS radicals will end up in J" = 0 because 24 levels are excited. It is clear that this is not the case, since the observed spectrum cannot be fitted with such a model. This means that collisions with H_2O do not have a unit efficiency for relaxing the rotationally excited CS radical.

The efficiency for rotationally quenching the CS radical by water will probably depend upon the energy difference between the rotational levels of water accepting the energy and the CS molecules giving up the energy. The greater the energy gap between the H_2O molecules and the CS radical, the lower the probability [12] that the radical can be deexcited by collisions with H_2O. The energy difference for CS radicals in the J" = 24 and J" = 23 levels is 39.4 cm^{-1} which is 3.0 cm^{-1} below the lowest rotational level of water, the 1_{10} level. The probability for deactivation by collision will be higher for this level than for the lower rotational levels. This probability should also decrease exponentially as the energy difference increases.

Collisions could also rotationally excite the CS molecule by T to R transfer. The translational temperature of the gas should be of the order of 200 to 300 K. This corresponds to energies of the order of 147 to 220 cm^{-1} and collisions could then excite the CS radicals to higher rotational energy levels. The efficiency of excitation versus deexcitation by radiative relaxation will depend upon the competition between the two processes.

The above discussion suggests that collisions will not be completely effective in quenching the rotationally excited CS radicals in the first 2500 s before the radical is excited. The spectrum obtained from radicals that have been newly created will be superimposed upon a spectrum of radicals that have undergone multiple excitations in the collisionless regime. This suggests that a bimodal rotational distribution is needed to fit the observed spectrum. One of the main results of our modelling so far has been that there is no one single rotational distribution that will fit the observed spectrum. As Fig. 6 shows, the bimodal rotational distribution gives a better overall fit than a single distribution. It remains to be determined just what kind of bimodal distribution should be used.

The simulations and inversions have all been done with spectral intensities of the central solar region given in Kohl, Parkinson, and Kurucz [13]. These spectra were averaged over 0.005 nm bins. In future work, the averaged solar disk spectrum A'Hearn et al. [14] will be used. It is expected that this will make the rotational profile more sensitive to the radial velocity of the comet but should not produce the broader profiles.

TABLE I

Some Characteristic Times for Elementary Processes involving CS in Comets at 1 AU

Process	Time(s)	Reference
Electronic Excitation	1,400	3
Rotational Radiative Relaxation	$1.9 \times 10^5/(J")^3$	9,10[†]
for J" = 5	1500	
for J" = 4	2970	
Time between Collisions	$5.7 \times 10^{-15}(r)^2$	11
for r = 500 km	14	
for r = 1900 km	206	
for r = 5000 km	1425	
Photochemical Production	600	4

[†] The lifetime was calculated using the dipole moment of Reference 9 and the method of Reference 10.

Acknowledgments

William M. Jackson would like to thank Gibor Basir for the ANA program and all of his help in using it. He would also like to thank P. Butterworth for his aid in this project. This work was supported by NASA under grant NAGW-446 and NAGW-903.

References

1. W. M. Jackson, J. Rahe, B. Donn, A. M. Smith, H. U. Keller, P. Benvenutti, A. H. Delsemme, and T. Owen, Astron. Astrophys., **73,** L7 (1978).
2. P. D. Feldman, H. A. Weaver, M. C. Festou, M. F. A'Hearn, W. M. Jackson, B. Donn, J. Rahe, A. M. Smith, P. Benvenutti, Nature, **286,** 132 (1980).
3. W. M. Jackson, J. B. Halpern, P. D. Feldman, and J. Rahe, Astron. Astrophys., **107,** 385 (1982).
4. W. M. Jackson, P. S. Butterworth, and D. Ballard, Ap. J., **304,** 515 (1986).
5. V. R. McCrary, R. Lu, D. Zakheim, J. A. Russell, J. B. Halpern, and W. M. Jackson, J. Phys. Chem., **83,** 3481 (1985).
6. M. G. Prisant and R. N. Zare, J. Chem. Phys., **83,** 5458 (1985).
7. A. Boggess, Nature, **275,** 377 (1972).
8. M. G. Prisant and R. D. Levine, unpublished.
9. G. Winnewisser and R. L. Cook, J. Molec. Spect., **28,** 266 (1968).

10. W. A. Guillory, **An Introduction to Molecular Structure and Spectroscopy**, Allyn and Bacon, Boston, 33 (1977).

11. W. M. Jackson and B. Donn, **Nature et Origine des Comètes**, Mémoires de La Societe Royale des Science, V Series, Vol XII, 133 (1966).

12. J. T. Yardley, **Introduction to Molecular Energy Transfer**, Academic Press, New York, 108 (1980).

13. J. L. Kohl, W. H. Parkinson, and R. L. Kurucz, **Center and Limb Solar Spectrum in High Spectral Resoluion 225.2 nm to 319.6 nm**, Harvard-Smithsonian Center for Astrophysics, Harvard University Press, Cambridge, Mass. (1978).

14. M. F. A'Hearn, J. T. Ohlmacher, and D. G. Schleicher, **A High Resolution Solar Atlas for Fluorescence Calculations**, University of Maryland Technical Report, Tr Ap83-044, (1983).

Astron. Astrophys. 187, 489–496 (1987)

ASTRONOMY
AND
ASTROPHYSICS

A rotational-state population analysis of the high-resolution IUE observation of CS emission in comet P/Halley

M.G. Prisant [1] **and W.M. Jackson** [2,*]

[1] Department of Chemistry, University of California, Berkeley, CA 94720, USA
[2] Department of Chemistry, University of California, Davis, CA 95616, USA

Received February 21, accepted May 13, 1987

Summary. The high resolution spectrum of comet P/Halley has been measured in the region of the CS emission. CS in comet Halley is produced by photodissociation of CS_2 and subsequently re-excited by broad band solar radiation. An inversion procedure is introduced to extract the rotational population distribution from the dispersed fluorescence spectrum. The fluorescence profile from the R branch of the $v' = 0$ to $v'' = 0$ is analyzed using this method. The extracted rotational distribution shows a peak at $J'' = 1$ superimposed on a background extending to $J'' = 29$. The distribution is interpreted by considering radiative and collisional relaxation processes in the comet. Intensity anomalies in the wavelength region corresponding to P and Q branch emission are considered.

Key words: comets – atomic and molecular processes

1. Introduction

The CS molecule holds the potential of playing an important role in our understanding of comet chemistry (Swamy, 1986). The CS radical is produced by photodissociation of CS_2 in the comet. The scale length of the CS daughter has been shown to be greater than 10^5 km: this corresponds to a sufficiently long lifetime for the detection of molecular fluorescence due to subsequent reexcitation by solar radiation (Swamy, 1986; Jackson et al., 1986). The scale length of CS_2 parent, on the other hand, has been shown to be less than 10^3 km (Swamy, 1986): this means that CS radicals are formed in the inner region of the comet coma where collisions could conceivably affect the rotational populations of newly formed product (Swamy, 1986; Jackson, 1986). CS is the only molecule which is consistently observed in the spectra of comets that originates from a parent of such short scale-length. The CS species is thus uniquely positioned to monitor local conditions in the inner region of the comet coma.

The rotational distribution of CS radical reflects conditions in the inner coma. In the case of complete thermalization of CS product, we would expect a rotational distribution well described by a Boltzmann functional form (Jackson et al., 1982); the temperature of this distribution would then be the temperature of the inner coma. In the case of radiative equilibrium (in some sense the opposite extreme) we would anticipate a distribution of a highly non-Boltzmann character in which most molecules were relaxed to very low J levels; a "temperature" determined from such a distribution would bear no relation to the temperature of the inner coma.

The form of the CS rotational distribution as determined from the fluorescence contour thus weights heavily in evaluating the character and content of information which may be learned on the inner coma conditions. Unfortunately the CS spectrum, like many other molecular systems of astrophysical interest, is sufficiently complex and overlapped to prohibit a straightforward determination of individual rotational populations. The procedure generally used – spectral simulation – is not only inappropriate in this situation because it begins by presuming the *form* of the distribution which is of special interest, but also inadequate because it provides no measure of goodness of fit or parameter sensitivity.

The problem of extracting populations from congested spectra has recently been treated by Prisant and Zare (1985) and refined by Prisant and Levine (1986). These authors define a linear transformation connecting spectral intensities and state populations. Definition of this transformation permits direct extraction of population estimates through use of linear regression. In this work, the method of Prisant and Zare will be adapted to analyze high resolution spectra obtained in an IUE observation of comet Halley on 1985 December 25 and 26. As this technique bears on population analysis of astrophysical spectra in a completely general fashion, extensive discussion will be given to the modalities of its application. The results of the analysis are prerequisite to distinguishing between radiative equilibrium and collisional thermalization mechanisms for the production of the CS rotational distribution in Halley's comet.

2. Observation of CS radical in comet fluorescence

CS has been seen in many comets since its first observation in comet West 1976 VI (Prisant and Levine, 1986). Spatial resolution of CS emission in other comet sightings has shown that CS originates not from the comet nucleus but rather from the decay of another molecule at a height of less than 1000 km in the cometary atmosphere. Analysis of emission from comet IRAS-Araki-Alcock 1983d using the model of Haser (Haser, 1957; Festou, 1981) established a scale length of 300 km for the parent of CS (Jackson et al., 1982).

Send offprint requests to: W.M. Jackson

* Guest observer with the International Ultraviolet Explorer Satellite

It has been argued that CS radical is formed in comet atmospheres by the photodissociation of CS_2 (Jackson et al. 1985):

$$CS_2 + h\nu(\text{solar radiation: } 190\,\text{nm} < \lambda < 210\,\text{nm}) \rightarrow CS + S. \quad (1)$$

Identification of CS_2 as the parent species is based on the photochemical unsuitability of other species containing a CS bond found in comet atmospheres as parents of CS and the photochemical suitability of CS_2 as the only simple molecule containing CS with a large absorption coefficient at wavelengths that are reasonably intense in solar radiation (Jackson et al., 1985). We note that CS_2 photodissociates efficiently throughout the 100–210 nm region. Okabe identifies the ground state product as the major channel in the region from 190 to 210 nm and production of $A\,^1\Pi$ as a major primary process in 120 to 140 nm region: the former occurring through predissociation of the $^1B_2$ state and the latter through direct dissociation of Rydberg states. Three lines of reasoning argue for the predissociation mechanism followed by solar excitation as the source of CS emission in the comet. First, the CS parent lifetime deduced from scale length measurements in the comet (500 s) is consistent with the calculated predissociation lifetime from the $^1B_2$ state (590 s) (Jackson et al., 1985). Second, as will be seen, the observed rotational and vibrational distributions in emission are highly relaxed; if CS A state directly produced by photodissociation were a major contributing source of emission intensity, we would expect an emission pattern characteristic of highly excited product. Third, solar intensities are much reduced in 120–140 nm region relative to those in the 190–210 region. In our analysis it will be assumed that the CS observed in cometary fluorescence is produced by photodissociation of CS_2 yielding ground state product and subsequently reexcited by solar radiation.

Photodissociation of CS_2 in laboratory experiments is known to lead to the production of highly vibrationally and rotationally excited CS radicals (McCrary et al., 1985). The radicals appear to be formed with energy up to the thermodynamic limit, so that in excitation at 193 nm vibrational levels up to $v''=12$ and substantial amounts of rotational energy are populated. It is unlikely that CS radicals formed in the cometary environment will survive in the highly excited vibrational levels of the nascent product state distribution. The natural radiative lifetime for the a CS radiacal radiating in the infrared region via:

$$CS(v'') \rightarrow CS(v''-1) + h\nu \quad (2)$$

is on the order of milliseconds. We therefore expect that all radicals formed in vibrationally excited states will cascade down to the ground state on a time scale of 10^{-2} s. This is short compared to the solar excitation rate (on the order of 10^3 s at 1 AU) and the collision rate (on the order of seconds at 300 km from the nucleus). It may therefore be concluded that most of the detected CS radicals are in the $v''=0$ vibrational level.

In contrast to vibration, full radiative relaxation of rotational excitation in the CS radical in the cometary atmosphere is not expected. The B value for the CS radical is $\sim 0.8\,\text{cm}^{-1}$ and approximate spacing between J levels of $2BJ$ suggest that the radiative lifetime of all J'' levels $< J=60$ will be greater than 1 s. This is the largest number of J levels which must be considered in any rotational analysis and defines the dimensionality of the problem.

We now describe the observation of CS in Halley's comet. CS produced in the comet coma is excited by solar radiation; resulting fluorescence is detected by the IUE telescope. The spectrum of the exciting solar radiation is shown in Fig. 1: this data presented by A'Hearn (1983) has been averaged over the solar disk. The solar radiation is unpolarized. Boggess et al. (1978) has previously described the IUE instrumentation: only the observational details and the results will be given in this section. Figure 2 shows the high resolution spectrum obtained with the LWP camera during observation of comet Halley between 257.5 and 257.9 nm. This portion of the spectrum has been assigned to emission from $CS(^1\Pi(v=0) - X^1\Sigma^+(v=0))$. The spectrum was observed using a 720 minute exposure on 1985, 25 and 26 December (LWP 7383). The CS spectrum was observed in two different orders but in this paper we present only the order that occurs near the center of the camera.

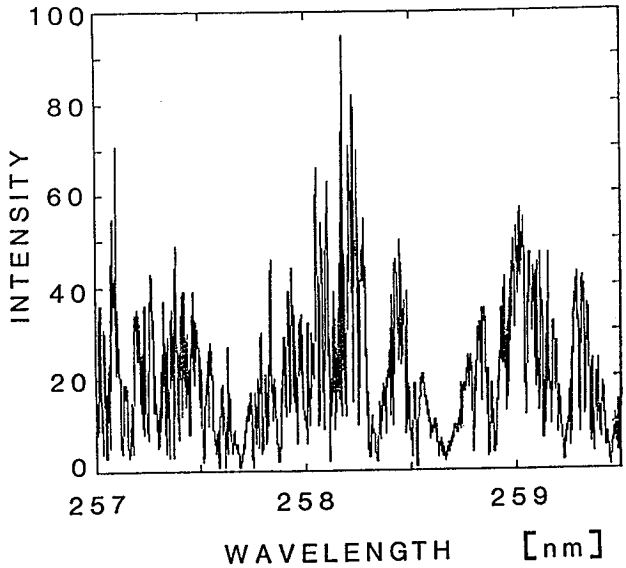

Fig. 1. The solar emission spectrum between 257 and 259 nm. An air wavelength scale is used. The comet sees this spectrum Doppler shifted ~0.02 nm to the blue

3. Theory

3.1. An inversion procedure for extraction of rotational populations from the fluorescence contours of broad-band excitation spectra

The fluorescence contour viewed by the observation telescope is the result of broad band excitation by solar radiation followed by emission. In the discussion which follows we first develop the linear transformation which relates the vector of emission intensities to that of rotational populations. We then go on to develop a parameterization scheme for the rotational populations.

The emission intensity at wavelength λ_l, $I_l(\lambda_l)$ is a linear function of the ground state populations and is given by:

$$I_l(\lambda_l) = K\sum_i \left\{ N_i \left[\sum_{jk} s_{ij} s_{jk} v_{ij} v_{jk}\, {}^3O(v_{ij})\, \phi(\lambda_{jk} - \lambda_l) \right] \right\}, \quad (3)$$

where K is a proportionality constant. The first summation over i is over the populated ground state levels, the second summation over j is over the intermediate levels excited by solar radiation, and the third summation over k is over all ground state levels optically coupled in fluorescence. The terms relevant to the absorption process are: N_i, the population flux of ground state absorbers is in

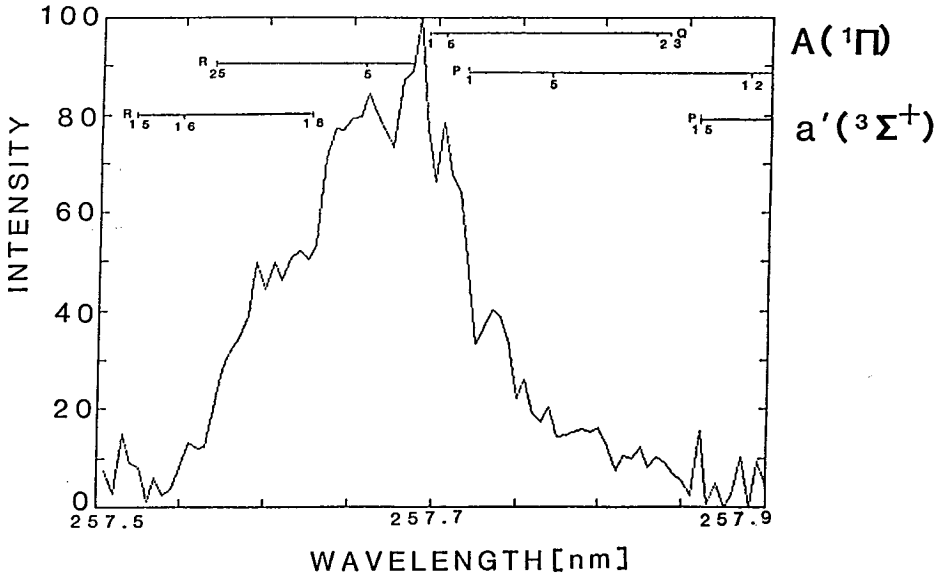

Fig. 2. The portion of the emission spectrum of Halley's comet captured by the IUE satellite assigned to CS emission. An air wavelength scale is used. The motion of the satellite relative to the comet shifts the emission lines ~0.02 nm to the red of their values for a stationary observer. The intensity scale is relative and does not indicate the level of background scattered light not due to CS fluorescence. Positions of the assigned transitions are shown: the R branch line occurs to the blue of 257.68 nm and the P and Q branch lines to the red

state i, v_{ij}, the Doppler shifted absorption frequency, $O(v_{ij})$ the solar radiation flux at v_{ij}, and s_{ij}, the natural line strength of the absorption transition. The terms relevant to the emission process are: $\phi(\lambda_{jk}-\lambda_l)$, the instrument function of the telescope, s_{jk}, the natural line strength of the emission transition, v_{jk}, the Doppler shifted emission frequency, and λ_{jk}, the Doppler shifted emission wavelength. We also make the following notes. Doppler shifts in absorption originate from the motion of the comet from the sun; Doppler shifts in emission originate from the motion of the observer telescope relative to that of the comet. The natural line strength is given by:

$$s_{jk} = q^2(v', v'')\,\mu_e{}^2 S_{jk}/(2J+1), \tag{4}$$

where $q(v'v'')$ is the Franck-Condon factor between levels v' and v'', μ_e is the electronic transition moment, $2J+1$ is the degeneracy of the populated state in emission or absorption with J the total angular momentum quantum number, and S_{jk} is the Hönl-London line strength factor for the transition. Finally the telescope instrument function is taken to be a grating function or triangle with FWHM equal to the instrument resolution.

The original equation for emission intensity may be recast in matrix form such that:

$$\boldsymbol{I} = \mathbf{Q}\boldsymbol{N}, \tag{5}$$

where $\boldsymbol{I}$ is an L-dimensional column vector with L being the number of measured points, $\boldsymbol{N}$ is an I-dimensional vector with I being the number of ground state rovibrational levels, and $\mathbf{Q}$ is an L by I matrix where each element corresponds to the contribution made by a specific ground state level i with unit population to the emission intensity at wavelength l.

If the telescope instrument function is such that all emission lines are resolved then the population of all the initial levels is overdetermined due to the presence of P, Q, and R branches originating from each level. This is generally not the case and we must consider a parameterization of the distribution in order to reduce the number of fitted parameters and define a model matrix which is not rank deficient. Let each population N_i be given by the expansion:

$$N_i(vJ) = \sum_q a_q F_q(N_i)/f_q, \tag{6}$$

where $\{F_q\}$ is a Q-dimensional set of orthogonal basis functions (Prisant and Levine, 1986). The factor f_q is the normalization constant of basis function F_q determined by:

$$f_q = \sum_i F_q(N_i)\,F_q(N_i). \tag{7}$$

The $\{a_q\}$ are the independent moments (Prisant and Levine, 1986) of the population distribution $N(vJ)$ defined by:

$$a_q = \langle N(vJ)|F_q\rangle \tag{8}$$

with

$$\langle F_p|F_q\rangle = f_q\,\delta_{pq} \quad \text{and} \quad \langle N(vJ)|F_q\rangle = \sum_i N_i F_q(N_i). \tag{9}$$

A number of different orthogonal basis sets may be chosen for the parameterization (Prisant and Levine, 1986); in this work we use the spline functions defined by:

$$F_q(N_i) = \begin{cases} 0 & \text{if} \quad i \notin [n(q), n(q+1)) \\ 1 & \text{if} \quad i \in [n(q), n(q+1)), \end{cases} \tag{10}$$

where the $n(q)$ are indices which define the level limits of the spline. The normalization factor is given by:

$$f_q = n(q+1) - n(q). \tag{11}$$

For a spline function basis, the orthogonal moments are proportional to the integrated or average populations over the limits of the spline.

We may now expand the population vector such that $\boldsymbol{N} = \mathbf{F}\boldsymbol{a}$ where $\mathbf{F}$ is a matrix whose elements $F_{iq} = F_q(N_i)$ and $\boldsymbol{a}$ is the vector of moments. Substituting into the matrix equation for the emission intensities we find that:

$$\boldsymbol{I} = \mathbf{M}\boldsymbol{a}, \quad \mathbf{M} = \mathbf{QF}, \tag{12}$$

where $\mathbf{M}$ is the model matrix; each element M_{lq} corresponds to the contribution of basis function q with unit weight to the emission intensity at wavelength l. A set of estimated parameter values $\tilde{\boldsymbol{A}}$ and associated errors which minimize the least squares measure:

$$(\boldsymbol{I}-\boldsymbol{y})^2 = (\boldsymbol{I}-\mathbf{M}\boldsymbol{a})^2 \tag{13}$$

Table 1. Spectroscopic constants of CS electronic states (taken from Bergeman and Cossart, 1981)

State	T_{e0}	ω_e	$\omega_e x_e$	B_e	$\alpha_e [10^{-2}\,\mathrm{cm}^{-1}]$	R_e [Å]
	$[\mathrm{cm}^{-1}]$					
$X^1\Sigma^+$	0.0	1285.154	6.502	0.8200449	0.5921	1.53496
$a^3\Pi$	27030.37	1135.41	7.747	0.78478	0.692	1.5691
$a'^3\Sigma^+$	30695.90	829.24	4.943	0.64727	0.570	1.728
$d^3\Delta$	35041.28	796.17	4.966	0.63685	0.614	1.742
$e^3\Sigma^-$	38040.75	752.93	4.955	0.62251	0.627	1.762
$A^1\Pi$	38255.13	1077.23	10.639	0.78760	0.83	1.566

may be determined using linear regression. Here $\boldsymbol{y}$ is the vector of measured experimental emission intensities corrected for detector response and emission background not due to molecular fluorescence. We remark that the error estimate associated with each parameter a_q determine the variance in the estimated value of the *integrated* populations.

Properly, the inversion procedure determines the best-fit parameters and estimates their associated errors rather than determining the exact form of the distribution itself. The procedure extracts, in the parameterization scheme chosen, the best-fit independent spline moments. Due to the congestion of the spectrum and consequent loss of information, the extracted moments necessarily represent a partial set. The inversion procedure does not distinguish between distributions characterized by this partial set of moments nor does it necessarily determine the best choice of orthogonal basis.

The extracted best-fit moments thus constrain but do not determine the functional form of the actual distribution. The constraints on the form of the reconstructed distribution, $P(vJ)$ are given by:

$$\tilde{a}_q = \langle P(vJ) | F_q \rangle, \tag{14}$$

where the $\tilde{a}_q$ are the fitted values of the moments and

$$P(vJ) > 0 \tag{15}$$

for all vJ contributing to the spectrum.

Any ansatz for reconstruction of the form of the distribution must select one member of the functional family meeting these constraints. This choice is somewhat arbitrary but may be guided by quantitative criterion of the overall variance and qualitative criteria concerning the expected form of the distribution. Acceptable methods for reconstruction of the distribution include generation of all members of the population vector from the partially determined set of moments and truncated fitting basis set or optimization of a second functional form to the values of the determined moments.

3.2. *Spectroscopy of the CS molecule*

Emission detected from comet Halley in the 257–259 nm region corresponds to the $A^1\Pi - X^1\Sigma^+$ electronic band system of CS (Swamy, 1986; Jackson and Prisant, 1986). The lines observed originate from the $v' = 0$ to $v'' = 0$ transition. This band system has been extensively studied and is a model system for the study of spin-orbit perturbations.

Molecular constants and term values for the $X^1\Sigma^+$ have been derived from analysis of microwave and IR spectra (Todd, 1977; Yamada and Hizota, 1979). The Λ doubled energy levels in the $A^1\Pi$ state are perturbed by near-lying levels in the $a^3\Pi$, $a'^3\Sigma^+$, $d^3\Delta$, and $e^3\Sigma^-$ states. A set of deperturbed molecular constants has been derived by Cossart and Bergeman (Bergeman and Cossart, 1981) for this system from the collected emission and absorption data for CS: these are given in Table 1. The deperturbation analysis and term values are fully described in the definitive works of Cossart and Bergeman (Bergeman and Cossart, 1984; Cossart, 1974). It was determined that the most important influence on the $A^1\Pi\,(v=0)$ originates from the $a'^3\Sigma^+\,(v=10)$ level with the $d^3\Delta\,(v=2$ and 4) making more minor contributions (Field and Bergeman, 1971). The rotational "resonance" with the a' state reaches a maximum at $J=16$ ($\approx 10\,\%$ mixing) and thus directly concerns us in this study. The introduction of a' character into the A state has the consequence of altering the energy levels in the A state and diminishing the optical coupling to the X state. Conversely, the introduction of A character into the rotational levels of the a' state means that those levels may be optically coupled to the ground state.

Lefebvre-Brion and Field (1986) point out that the natural line strengths of a perturbed transition depend on "which of the two possible electronic transitions has oscillator strength in the spectral region being monitored; the vibrational and rotational line-strength factors which are applicable for both main and extra lines are those associated with the electronic-vibrational band with nonzero-oscillator strength." Even for levels which emit due to small admixtures of the optically coupled state, the electronic and rovibrational wavefunctions of the non-optically coupled state are completely "irrelevant" to observed linestrengths except insofar as they determine the fractional character of optically coupled state (Lefebvre-Brion and Field, 1986). The CS band system in question is thus to be distinguished from the familiar example of intensity interference seen in NO where the eigenstates are formed from the admixture of two strongly coupled bases, both of which have allowed optical transitions to the ground state.

Accordingly, the form of rotational line strength for the observed CS transitions follows that of a $^1\Pi - {}^1\Sigma^+$ transition. Each J level of the Π state has two lambda doublet components labelled e and f. The inversion parity of the rotational wave functions associated with the e or Π^+ levels is given by $(-1)^J$ and that of those associated with the f or Π^+ levels by $-(-1)^J$. The inversion parity of the rotational wave functions associated with the $^1\Sigma^+$ state is given by $(-1)^J$. The parity selection rule forces all P and R branch transitions to originate from e levels and all Q

branch transitions to originate from f levels of the Π state (Lefebvre-Brior and Field, 1986; Gauyacq et al., 1986). The modified natural line strength for the perturbed CS $^1\Pi - {}^1\Sigma$ transition incorporates Hönl-London factors weighted by the fractional character of optically coupled A state (Lefebvre-Brion and Field, 1986). These may be written:

$$S'_{jk} = p_j S_{jk} \quad \text{with} \quad S_{jk} = \begin{cases} (J''-1)/4 & P(J''=J'-1) \\ (2J''+1)/4 & Q(J''=J') \\ (J''+2)/4 & R(J''=J'+1), \end{cases} \tag{16}$$

where p_j is the fractional A character of the A state rotational level and J'' the quantum number in the X state. We note that the Q branch line strengths are approximately twice of the P and R branches.

4. Analysis and results

We begin by making the following comments on the experimental data presented in Fig. 2. The wavelength scale from the IUE guest observer tape is in air Ångstroms and has not been corrected for the relative motion of the comet and the telescope. The Doppler corrections due to these motions are significant in the analysis of the spectrum. At the time of observation, the comet was moving with a velocity of $\sim -26\,\mathrm{km\,s^{-1}}$ toward the sun and a velocity of $\sim +35\,\mathrm{km\,s^{-1}}$ away from the IUE observer telescope. This corresponds to a blue shift of $3.3\,\mathrm{cm^{-1}}$ or -0.02 nm of solar emission as seen by the comet and a red shift of $-4.5\,\mathrm{cm^{-1}}$ or $+0.02$ nm of comet fluorescence as seen by the telescope camera. Correcting for the Doppler shift in emission, we find that emission to the blue of 257.68 nm originates from R branch transitions and that to the red from P and Q branch transitions. The width of the CS feature suggests rotational states populated up to $J \sim 30$.

The intensity data taken from the IUE tape is reported at 92 irregularly spaced points between 257.5 and 257.9 nm. We have made a projection, using linear interpolation, of this data onto a regular grid of 80 points spaced at 0.005 nm: this projection produces no visible change in the spectrum. The intensity scale in the figure is relative and uncorrected for background light scattering not due to CS fluorescence. The IUE instrumental bandwidth is quoted to be 0.08 nm for an extended source and 0.02 nm for a point source: we find that it is the later which best duplicates the experimental spectrum. The signal to noise ratio may be estimated from the negative excursion peaks in the spectrum – this is found to be ~33/1 in the Halley spectrum. The shape of the intensity profile – peaking near the Doppler shifted band origin – suggests highly rotationally relaxed CS. However, given that the Hönl-London factors for the Q branch are approximately two fold greater than those of the P and R branches and that the P and Q branches overlap, we would expect a spectrum whose intensity fell off more rapidly in the blue with shouldering in the red. The observed spectrum is almost symmetric with slightly more integrated intensity in the wavelength region corresponding to the R branch emission than that in the region corresponding to the Q and P branches.

A computer program has been written which simulates fluorescence spectra excited by broad band solar radiation and extracts estimates of population parameters through direct inversion of experimental intensities. The term values for the $X(v=0)$ state and the term values and fractional A character for the $a'(v=10)$, and $A(v=0)$ states have been tabulated by Cossart and Bergeman (1981). Transition frequencies for the band system are

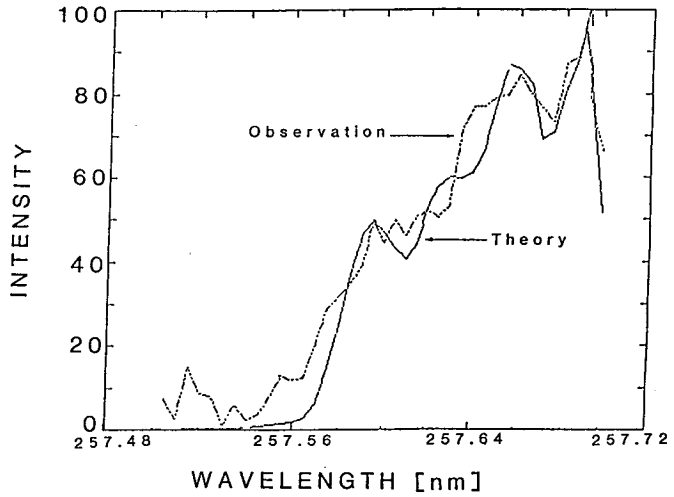

Fig. 3. The fitted R branch of the emission spectrum. The dotted line represents the experimental data; the solid line shows the spectrum simulated according to the parameters of the rotational population distribution extracted in the inversion procedure

calculated through use of these tables. Natural line strengths are calculated through use of Eqs. (4) and (16) subject to the selection rules described in Sect. 3.2. Transitions in absorption are weighted according to the Doppler shifted intensity of solar radiation as given by A'Hearn. For each upper state populated in absorption, all allowed transitions in emission are calculated. For simulation, the Doppler shifted air wavelength is sorted into a histogram bin of regular spaced observation points and weighted by population and a grating instrument function depending on its displacement from the center of the bin. Alternatively a model matrix for inversion may be tabulated by cross-sorting with a parameter index and unit population weighting. Given the tabulated model matrix, a linear regression routine is used to determine the best-fit parameters and associated estimated errors.

Inversion of the R branch portion of the spectrum yields good agreement with reported intensities. Figure 3 compares the spectrum simulated according to extracted population parameters with the experimentally obtained spectrum. Figure 4 shows the population distribution reconstructed from the fitted parameters. The estimated variance for the fitted parameters was sensitive to the choice of orthogonal spline basis set though the overall form of the distribution was not. The $J=1$ and $J=0$ level parameters are the most highly populated; a background extends out to $J \approx 30$ which is at ≈ 0.2 of this maximum level. Attempts to fit the entire spectrum and the P and Q branch portion separately yielded consistently inferior results. If the red portion of the spectrum corresponding to the P and Q branch emission was enhanced by a factor of 2.5 relative to the blue portion corresponding to R branch emission, then a reasonable quality fit was obtained and the population distribution resembles that shown in Fig. 4.

5. Discussion

Initial attempts to model the observed spectrum with a Boltzmann distribution have been described in a previous publication (Jackson and Prisant, 1986); these efforts showed that a Boltzmann distribution cannot account for the observed form of

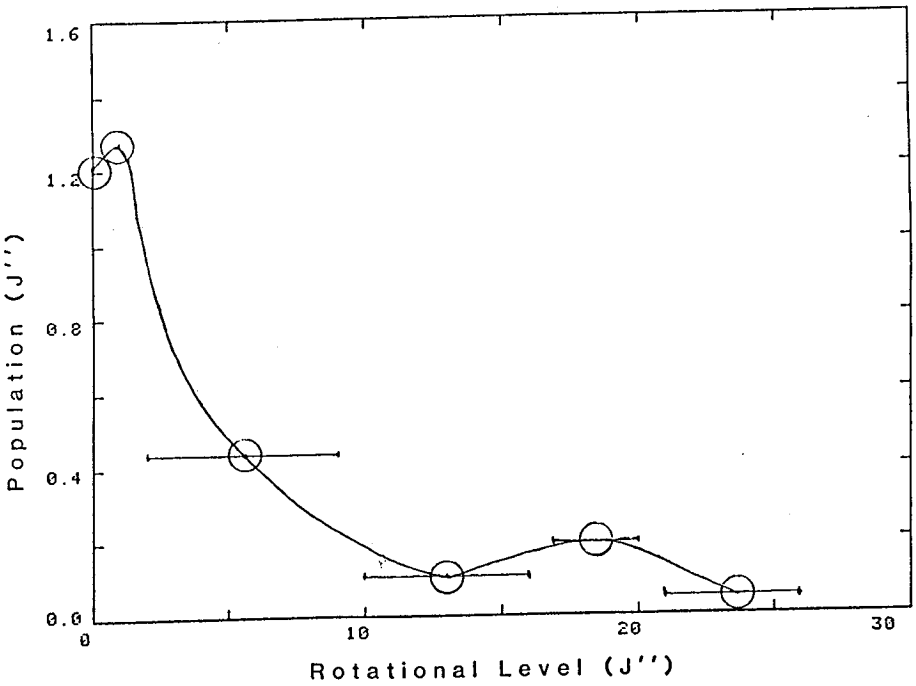

Fig. 4. The rotational population distribution reconstructed from linear regression best fit parameters. The bars represent the bin width and the circles represent the average population per J level over the interval. The nature of the errors are described in the text

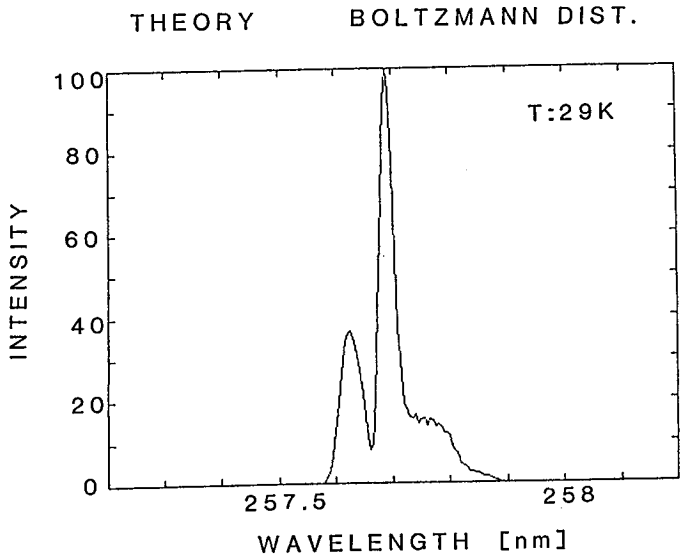

Fig. 5. The $A^1\Pi - X^1\Sigma^+(v=0)(v=0)$ emission simulated for a 29 K Boltzmann distribution of absorbers

the CS fluorescence contour. If a low rotational temperature of the order of 7 K is used, the spectral bandshape is roughly triangular but much narrower than the observed spectrum. Increasing the temperature to broaden the band profile results in the development of a characteristic dip separating the R and P, Q halves of the simulated spectrum. Figure 5 shows a plot of the spectrum resulting from simulation of a 29 K or best-fit Boltzmann rotational distribution. While accounting for the breadth of the fluorescence contour, the overall shape of the spectrum and that of constituent branches are clearly incorrect. No reasonable adjustment of the IUE instrument bandwidth was able to eliminate this disagreement. In earlier work on CS in comet Bradfield (Jackson et al., 1982), a Boltzmann distribution appeared to give a reasonable fit to the observed data. Subsequent consideration suggests that this earlier agreement was fortuitous and due to the lower signal to noise ratio in the Bradfield spectrum and that required excessive smoothing of the original data. Since a Boltzmann distribution does not fit the observed spectra it is unlikely that collisions are responsible for *most* of the CS rotational distribution.

Also examined in a previous publication (Jackson and Prisant, 1986) were simulations resulting from several different functional forms of the rotational distribution. These included a linear distribution peaking at $J''=0$ and monotonically decreasing to $J''=10$, a bimodal distribution peaking at $J''=0$ and at $J''=20$, and uniform distributions that cut off at some upper J'' level. Though none of these distributions provided a satisfactory fit to the overall observed spectrum, the bimodal distributions were superior and provided a better accounting of the general shape of the R branch half of the spectrum.

Use of the inversion procedure showed that the fit variance could be dramatically improved by artificially suppressing the P and Q branches of the spectrum relative to the R branch. In other words, the general form of the spectrum is incompatible with the known rotational line strengths of CS. Because of this incompatibility we have chosen to use the inversion program to only fit the R-branch and derive populations from this branch.

The spectrum simulated with the population distribution reconstructed according to the fitted parameters and the reconstructed distribution itself are shown in Figs. 3 and 4 respectively. The results show reasonable agreement with the experimental observations. To reduce the overall error and improve the fit it is necessary to limit the number of parameters that are determined in the least squares fitting procedure. We have chosen to to this integrating the population in four bins for $J''=2$ through 27. The bin sizes indicated in the figure by the horizontal lines the error on the integrated populations is very low, with a two

Table 2. Some characteristic times for elementary processes involving CS in comets at 1 AU

Process	Time	Ref.
1. Electronic excitation	1400	Jackson (1982)
2. Rotational radiative relaxation	$1.9\ 10^5/(J'')^3$	Winnewisser and
for $J''=5$	1500	Cook (1968)
for $J''=4$	2970	Guillory (1977)
3. Time between collisions	$5.7\ 10^{-15}(r)^2$	Jackson and
for $r=$ 500 km	14	Donn (1966)
for $r=1900$ km	206	
for $r=5000$ km	1425	
4. Photochemical production	500	Jackson (1986)

sigma value indicated by the size of the circles. As would be expected, the estimated errors on the individually fitted populations of the $J''=0$ and 1 levels are much larger, with one sigma values of 0.1 and 0.6, respectively. The errors on the $J''=0$ and 1 populations can be improved with a different choice of basis; the overall form of the reconstructed distribution is not, however, terribly sensitive to this choice. After experimentation with a number of different bases, we found that the distribution reconstructed with the basis shown produced the optimal variance and yielded positive values for all populations even in the high J domain.

The populations derived from fitting the R branch are generally satisfactory if we can find a reasonable explanation for the inability of the inversion procedure to fit the Q and P branches. Several explanations come to mind but as further discussion will indicate most are unlikely. We first consider an optical depth effect. To be suitable, the absorber must have an optical thickness 0.4 units greater in the P and Q branch region of the spectrum than that in the R branch region. Calculations using the oscillator strength and measured production rates to compute column density for CS indicate that its optical thickness is only 0.02; this rules out any explanation invoking self-absorption. The presence of a strong absorber other than CS itself that overlaps just the P and Q branches may be ruled out because 1) there is no indication in the spectrum for such a species and 2) given the large oscillator strength of CS and its production close to the nucleus, it is improbable that another unknown absorber could exist whose optical thickness would exceed that of CS by an order of magnitude. A second possibility is that a polarization effect is being observed in the emission spectrum. This seems unlikely since 1) the exciting radiation is unpolarized and 2) for a given anisotropic ensemble of emitters, the Q branch would be expected to polarized opposite to the P and R branches whereas the observed anomalous relative intensities are for P and Q with respect to R.

A plausible explanation for the observed discrepancy is the contamination of the R branch measured intensity by a higher contribution of scattered sunlight than the P and Q branches. This explanation is suggested by examination of the photowrite images in the region of OH spectrum where there is clear indication that a continuum is present and contributes to the measured emission intensity. Consistent with this hypothesis, the spectral distribution of scattered sunlight overlapping the CS band system (shown in Fig. 1) exhibits a dip in the P and Q branch region.

Halley was 1.08 AU from from the earth at the time of the present measurements. The observed column of emitting gas had a length of 10^5 km and a radius of 4000 km with the telescope observation axis lying along the column axis. Prerequisite to understanding the bimodal rotational distribution are the characteristic times for the various processes involving CS in comets presented in Table 2. The 500 s reciprocal rate of CS photochemical production and the observed 300 km locus of CS production above the comet nucleus are consistent with an outward gas flow velocity of 0.6 km s^{-1}. The reciprocal rate or characteristic time for CS electronic excitation is 1400 s; this means that multiple excitation of individual molecules will contribute to a spreading of the distribution. As the carrier gas expands outward from the comet nucleus diminishing in density, the time between collisions varies from 5 s at 300 km to 74 s at 1140 km. At 300 km, the characteristic collision time is greater than the characteristic radiative relaxation time for all levels above $J''=34$ while at 1140 km, the comparable value is $J''=14$. The rotational population distribution at a given altitude will reflect competition between collisional thermalization and radiative relaxation with radiative relaxation increasing and collisional thermalisation decreasing in importance with increasing distance from the nucleus. The extracted distribution averages over the entire observation volume.

The results reported in the figure are clearly not at odds with the qualitative ideas presented above. The fitted populations are dominated by a low J component that probably originates from those radicals that have radiatively relaxed to the lowest J'' levels. This larger component is superimposed on a weaker component which represents those radicals that sample the inner collisional region. To obtain more quantitative information from the observed distribution a detailed quantitative model is needed which incorporates the qualitative ideas given above.

Acknowledgements. WMJ wishes to thank G. Basir for the ANA program and his help in its use and P. Butterworth for his aid in this project. MGP wishes to acknowledge fertile conversations with J. Rostas, D. Cossart, R.W. Field, and T. Bergeman on the spectroscopy of CS. He also wishes to thank S. Fredin for pointing out the possibility of parity selectivity in consecutive absorption and emission processes. This work was supported by NASA under grants NAGW-446 and NAGW-903.

References

A'Hearn, M.F., Ohlmacher, J.T., Schleicher, D.G.: 1983, *A High Resolution Solar Atlas for Fluorescence Calculations*, University of Maryland Technical Report, TR Ap 83-044

Barrow, R.F., Dixon, R.N., Lagerqvist, A., Wright, C.V.: 1960, *Ark. Fys.* **18**, 543

Bergeman, T., Cossart, D.: 1981, *J. Mol. Spec.* **87**, 119

Boggess, A. et al.: 1978, *Nature* **275**, 377

Cossart, D.: 1974, *Etude a Haute Resolution des Spectres et des Perturbations Electroniques du Radical CS*, These d'Etat, Universite de Paris XI

Cossart, D., Horani, M., Rostas, J.: 1977, *J. Mol. Spec.* **67**, 283

Cossart, D.: 1980, *J. Phys.* **41**, 489

Crawford, F.H., Shurcliff, W.A.: 1934, *Phys. Rev.* **45**, 860

Feldman, P.D., Weaver, H.A., Festou, M.C., A'Hearn, M.F., Jackson, W.M., Donn, B., Rahe, J., Smith, A.M., Benvenutti, P.: 1980, *Nature* **286**, 132

Festou, M.: 1981, *Astron. Astrophys.* **95**, 69

Field, R.W., Bergeman, T.: 1971, *J. Chem. Phys.* **54**, 2936

Gauyacq, D., Fredin, S., Jungen, Ch.: 1986, *Molecular Physics* (submitted)

Guillory, W.A.: 1977, *An Introduction to Molecular Structure and Spectroscopy*, Allyn and Bacon, Boston, p. 33

Haser, L.: 1957, *Bull. Acad. Roy. Belgique, Classe des Sciences* **43**, 740

Haser, L.: 1966, *Mém. Soc. Roy. Sci. Liège. 5e Ser.* **12**, 233

Jackson, W.M., Donn, B.: 1966, *Mém. Soc. Roy. Sci. Liège. 5e Ser.* **12**, 133

Jackson, W.M., Rahe, J., Donn, B., Smith, A.M., Keller, H.U., Benvenutti, P., Delsemme, A.H., Owen, T.: 1978, *Astron. Astrophys.* **73**, L7

Jackson, W.M., Halpern, J.B., Feldman, P.D., Rahe, J.: 1982, *Astron. Astrophys.* **107**, 385

Jackson, W.M., Butterworth, P.S., Ballard, D.: 1986, *Astrophys. J.* **304**, 515

Jackson, W.M., Prisant, M.G.: 1986, *20th ESLAB Symp.* ESA SP-250, 545

Lagerqvist, A., Westerlund, H., Wright, C.V., Barrow, R.F.: 1958, *Ark. Fys.* **14**, 387

Lefebvre-Brion, H., Field, R.W.: 1986, *Perturbations in the Spectra of Diatomic Molecules*, Academic Press, New York, Chap. 5

McCrary, V.R., Lu, R., Zakheim, D., Russel, J.A., Halpern, J.B., Jackson, W.M.: 1985, *J. Phys. Chem.* **83**, 3481

Prisant, M.G., Zare, R.N.: 1985, in *Gas Phase Chemiluminescence and Chemi-Ionization*, ed. Fontijn, A., North-Holland, Amsterdam, p. 189

Prisant, M.G., Zare, R.N.: 1985, *J. Chem. Phys.* **83**, 5458

Prisant, M.G., Levine, R.D.: 1986 (unpublished)

Robbe, J.-M., Schamps, J.: 1972, *Chem. Phys. Lett.* **15**, 596

Smith, A.M., Stecher, T.P., Caswell, L.: 1980, *Astrophys. J.* **242**, 402

Swamy, K.S.K.: 1986, *The Physics of Comets*, World Scientific, Philadelphia

Todd, T.R.: 1977, *J. Mol. Spec.* **66**, 162

Todd, T.R., Olson, W.B.: 1979, *J. Mol. Spec.* **74**, 190

Winnewisser, G., Cook, R.L.: 1968, *J. Mol. Spec.* **28**, 266

Yamada, C., Hirota, E.: 1979, *J. Mol. Spec.* **74**, 203

#69

LABORATORY STUDIES OF PHOTODISSOCIATION PROCESSES RELEVANT TO THE FORMATION OF COMETARY RADICALS

R.S. URDAHL, Y. BAO, AND W.M. JACKSON
Department of Chemistry, University of California, Davis, CA 95616

The strength of the $C_2(d^3\Pi_g \rightarrow a^3\Pi_u)$ Swan band emission in the spectra of cometary comae identifies this species as a prominent constituent of the coma gas, although its photochemical origin remains yet uncertain. It was previously suggested[1] that the formation of cometary C_2 proceeds via the secondary photolysis of the C_2H radical, which is itself generated by dissociation of the stable acetylene molecule. The detection of C_2H in the interstellar medium[2] and the recent analysis of the radial variation in $C_2(\Delta V=0)$ surface brightness of Comet Halley[3] support the postulate that C_2 is a third-generation molecule. Although these astrophysical observations provide evidence for the proposed two-step dissociation process, laboratory verification of the mechanism is currently incomplete.

Measurement of the C_2 and C_2H translational energy distributions produced from the multiphoton dissociation (MPD) of acetylene at 193nm[4] identifies the primary processes to be:

$$C_2H_2(X^1\Sigma_g^+) + h\nu_{193nm} \text{ ----> } C_2H(X^2\Sigma^+, A^2\Pi) + H(^2S) \quad (1)$$

$$C_2H(X^2\Sigma^+, A^2\Pi) + h\nu_{193nm} \text{ ----> } C_2(X^1\Sigma_g^+, a^3\Pi_u, A^1\Pi_u) + H(^2S) \quad (2)$$

Time-resolved FTIR emission studies of the nascent C_2H radical formed in reaction (1)[5] verify that this species is produced both vibrationally and electronically excited. A survey of the internal energy distributions of the C_2 fragments produced from the MPD of acetylene using a high intensity ArF laser is currently in progress in this laboratory. Previous results using the techniques of laser-induced fluorescence (LIF) and time-resolved emission[6] allowed estimation of nascent radical concentrations, with $[C_2(A^1\Pi_u)] >> [C_2(C^1\Pi_g)]$, $[C_2(a^3\Pi_u)] > [C_2(d^3\Pi_g)]$, and $[C_2(a^3\Pi_u)] \simeq [C_2(A^1\Pi_u)]$.

Recent experiments have focused on the measurement of rotational energy distributions for the $C_2(A^1\Pi_u, a^3\Pi_u)$ fragments. Figure 1 illustrates the distribution of rotational energies for the nascent $C_2(A^1\Pi_u)$ fragment produced during the MPD of various C_2H precursors. The distributions can each be fit using low and high temperature components, which implies the dissociation of C_2H occurs through a statistical process such as predissociation or internal conversion to the ground state continuum. The rotational energy distribution of nascent $C_2(a^3\Pi_u)$ from the MPD of acetylene is shown in Figure 2. Although the fit to a single temperature is fair, there is some indication of a low temperature component in the region of low rotational energies. Since the measurement of this distribution requires the use of low gas

pressures and short pump/probe delay times, interference from $C_2(d^3\Pi_g \rightarrow a^3\Pi_u)$ emission limits the achievable signal to noise ratio. We are currently trying to improve our $C_2(a^3\Pi_u)$ detection capability by performing this experiment in a molecular beam, thus allowing for discrimination between initial emission and LIF.

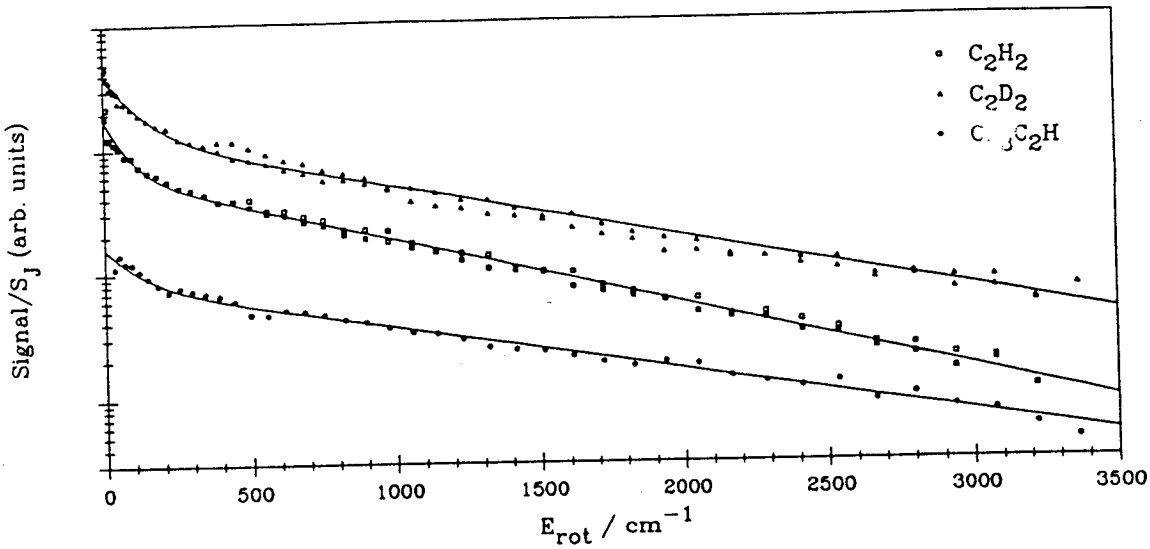

Figure 1. Rotational energy distributions for nascent $C_2(A^1\Pi_u, v''=0)$ formed in the photolysis of various C_2H precursors. The solid curves are fit to the temperature pairs of 100K+1200K, 150K+1500K, and 150K+1800K for C_2H_2, C_2D_2, and CF_3C_2H, respectively.

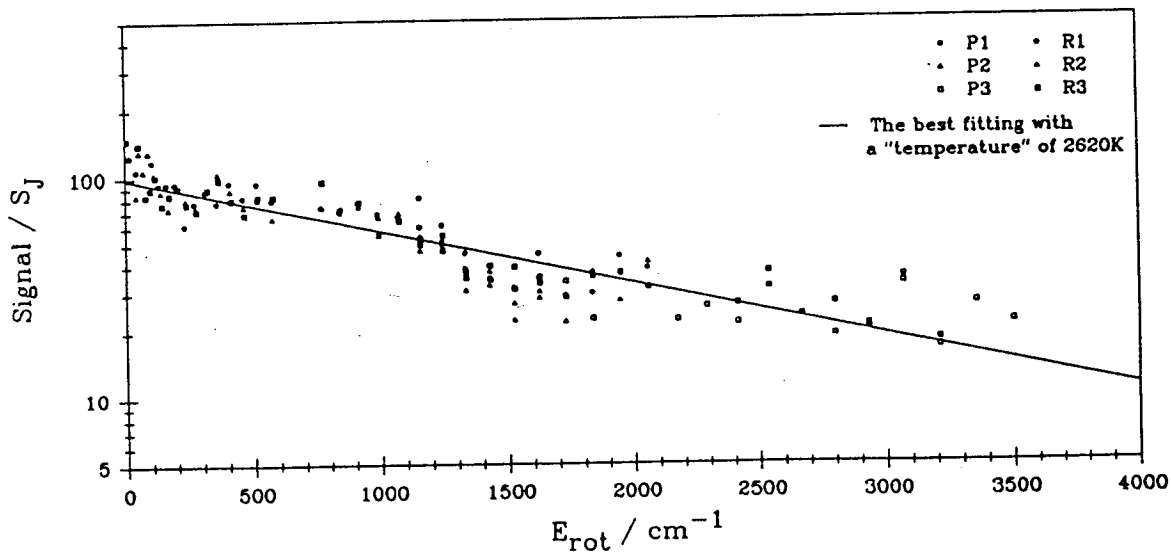

Figure 2. Rotational energy distribution for nascent $C_2(a^3\Pi_u, v''=0)$ formed in the photolysis of C_2H_2.

A portion of the two-photon laser excitation spectrum of $C_2(X^1\Sigma_g^+)$ is shown in Figure 3. Since the signal was only observable after the inclusion of a buffer gas, it appears that $C_2(X^1\Sigma_g^+)$ is not formed appreciably during the initial dissociation process but rather as a result of radiative and collisional quenching of the $A^1\Pi_u$ and $a^3\Pi_u$ primary fragments.

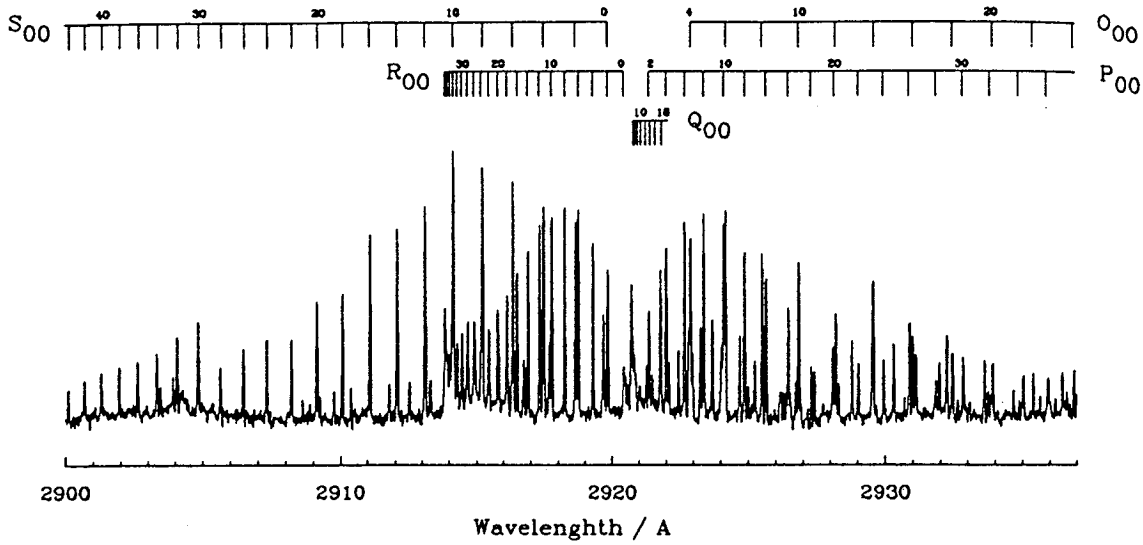

Figure 3. Two-photon laser excitation spectrum of $C_2(X^1\Sigma_g^+)$ produced in the MPD of C_2H_2 at 193nm, observed at a delay of 2μs (100mtorr C_2H_2, 10torr Ar).

Another class of experiments being performed considers the mechanism and dynamics of CH and C_3 formation during the photodissociation of allene with a focused ArF laser. The laser excitation spectra of $CH(X^2\Pi)$ and $C_3(X^1\Sigma_g^+)$ given in Figures 4 and 5 verify the production of these cometary radicals, but give little insight into whether they are formed by primary or secondary dissociation processes. Again, the extraction of this information may be possible through the use of a molecular beam, since the possibility of forming a product by collisional processes is minimized.

Although the experiments performed to date provide considerable evidence in support of reaction (2), there is an important distinction to be made when comparing the laboratory conditions to those typically found in comets. Since the C_2H radicals generated in the laboratory experiments are formed vibrationally and/or electronically excited, the theoretical calculations of Shih et al.[7] predict 193nm vertical excitation of the bent(115°) $C_2H(1^2A' \rightarrow 2^2A'')$ transition. Alternatively, any rotationally/vibrationally excited C_2H present in cometary comae will quickly undergo radiative relaxation in the infrared to their lowest rotational and vibrational state. The vertical excitation energy for the linear(180°) $C_2H(X^2\Sigma^+ \rightarrow {}^2\Pi)$ transition then increases to $\simeq$8.1eV[7], well into the vacuum UV region. Experiments are currently under

way in our laboratory to confirm the cometary formation of C_2 via the VUV dissociation of cold C_2H.

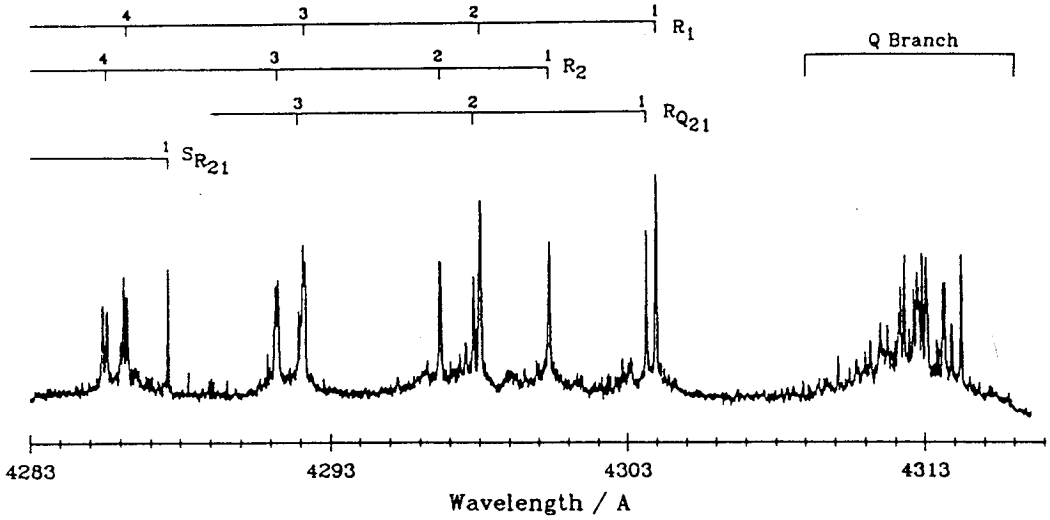

Figure 4. Laser excitation spectrum of CH($X^2\Pi$, v''=0) formed in the photolysis of allene, observed at a delay of 5μs (50mtorr C_3H_4, 10torr Ar).

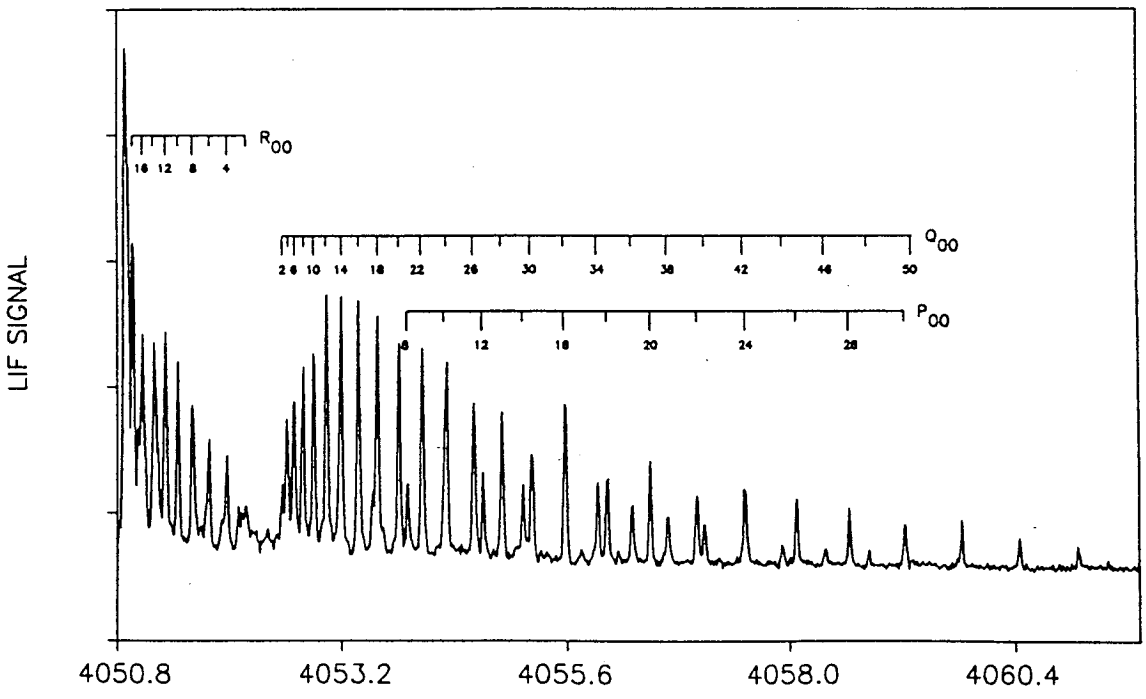

Figure 5. Laser excitation spectrum of $C_3(X^1\Sigma_g^+, 000)$ formed in the photolysis of allene, observed at a delay of 5μs (100mtorr C_3H_4, 10torr Ar).

ACKNOWLEDGEMENTS

The allene dissociation experiments were performed in cooperation with Dr. D. Winkoun. The authors gratefully acknowledge support by the Planetary Atmospheres Program of NASA under grant NAGW-903.

REFERENCES

1. W.M. Jackson, J. Photochem. 5, 107 (1976).
2. K.D. Tucker, M.L. Kutner, and P. Thaddeus, Astrophys. J. 193, L115 (1974).
3. C.R. O'Dell, R.R. Robinson, K.S.K. Swamy, P.J. McCarthy, and H. Spinrad, Astrophys. J. 334, 476 (1988).
4. A.M. Wodtke and Y.T. Lee, J. Phys. Chem. 89, 4744 (1985).
5. T.R. Fletcher and S.R. Leone, J. Chem. Phys. 90, 871 (1989).
6. R.S. Urdahl, Y. Bao, and W.M. Jackson, Chem. Phys. Lett. 152, 485 (1988).
7. S. Shih, S.D. Peyerimhoff, and R.J. Buenker, J. Mol. Spectrosc. 64, 167 (1977); 74, 124 (1979).

J. Phys. Chem. **1990**, *94*, 1869–1873

Photochemistry of Cyano- and Dicyanoacetylene at 193 nm

J. B. Halpern,* L. Petway,† R. Lu,‡ W. M. Jackson,§ V. R. McCrary,⊥

Department of Chemistry, Howard University, Washington, D.C. 20059

and W. Nottingham

Department of Chemistry, The University of the District of Columbia, Washington, D.C. 20008

(Received: March 30, 1989; In Final Form: August 10, 1989)

The far-UV photochemistry of cyano- and dicyanoacetylene has been studied. In particular, those photolysis channels have been characterized that lead to the production of excited-state fragments and CN in the ground electronic state. Following photolysis of HC_3N, in addition to direct production of CN and C_2H, there is a second dissociation channel leading to C_3N and H atoms. The results also show that at high laser intensity the HC_3N dissociates by two-photon photolysis and that the C_3N undergoes secondary photolysis. Photolysis of C_4N_2 produces CN and C_3N radicals.

Introduction

In 1920, Moreau and Bongrand synthesized the first members of the cyanoacetylene family, cyano-[1] and dicyanoacetylene.[2] Since that time, several additional cyano polyenes of the series $H(C{\equiv}C)_nCN$ and $NC(C{\equiv}C)_nCN$ have been synthesized. Chemists, and particularly spectroscopists, have studied the cyanoacetylenes because of their linear structure. Interest in these molecules increased in 1971, when Turner observed the rotational spectrum of HC_2CN in the interstellar medium.[3] This spectrum had first been measured in the laboratory by Westenberg and Wilson.[4] HC_2CN has also been observed in Titan's atmosphere by the Voyager missions to Saturn[5] and has been shown to play an important role in the odd nitrogen chemistry of that enormous moon.[6]

Our laboratory has been studying the photochemistry of XCN species and C_2N_2 for some time.[7] This study was started because of the astrochemical relevance of cyanoacetylene photochemistry and also to see if there were any dynamic effects in photolysis that could be related to the increase in molecular size as compared to C_2N_2.

This article reports on the photolysis of cyano- and dicyanoacetylene at 193 nm. Measurements have been made of emission spectra from excited fragments and laser-induced fluorescence (LIF) spectra of ground-state CN fragments. The photolysis was accomplished by an unfocused ArF laser whose intensity was varied over more than 2 orders of magnitude.

Previous work on cyanoacetylene photochemistry has used vacuum-UV light. Okabe and Diebler have studied the photodissociative excitation and photoionization of HC_2CN below 150 nm.[8] Sabety-Dzvonik et al. characterized the quantum-state distribution of CN produced in the 160-nm photolysis of HC_2CN[9] and C_4N_2.[10]

The UV spectrum of HC_2CN from 290 to 200 nm has been measured and assigned by Job and King.[11,12] Conners et al. have measured the vacuum-UV spectrum below 170 nm but have not assigned it.[13] Miller and Hannon have measured the UV spectrum of C_4N_2 between 290 and 220 nm and partially assigned the vibrational structure.[14] Conners et al. also measured the vacuum-UV spectrum of C_4N_2 below 200 nm.[13] Halpern, Miller, and Okabe have measured the absorption cross sections of HC_2CN in the UV and the heat of formation of C_3N.[15] Bruston et al.[16] measured the UV absorption cross sections of cyanoacetylene at approximately the same resolution as Job and King[12] and much higher resolution than Halpern et al.[15] used. They point out that the presence in the spectrum of $\Delta v_\pi = \pm 2, \pm 4$ and $v_p' = 1 - v_\pi''$ = 1 transitions establishes the 230-nm system as $X^1\Sigma^+ \rightarrow A^1\Delta$. Above 195 nm, their absorption coefficients agree with those of ref 15 but are lower at shorter wavelengths, probably because of oxygen molecule interferences in the latter paper.

Seki studied emission from cyanoacetylene.[17] He varied the excitation frequency from 265 to 215 nm and recorded the dispersed emission. In the region from 265 to 250 nm, relatively strong direct fluorescence was seen centered at the irradiation wavelength. Following excitation below 230 nm, there was a broad emission between 300 and 400 nm. In addition, there was a sharp peak at the excitation wavelength that was attributed to scattered light; however, no such scattering was seen at 240 nm where the absorption cross section is zero. The total emission following excitation below 240 nm was much lower than that above 250 nm, even though the peak absorptions are much larger at the lower wavelengths. This is understandable because the dissociation limit of HC_3N to H + C_3N is 244 nm.[15]

Experimental Section

The experimental apparatus has been described in detail elsewhere.[18] An ArF excimer laser (Lambda Physik EMG101) was used to photolyze gas samples in a static reaction cell and in an effusive molecular beam. The CN ($X^2\Sigma^+$) fragments formed in the photolysis were detected by LIF of the CN ($B^2\Sigma^+ \rightarrow X^2\Sigma^+$)

† Present address: Lawrence Livermore National Laboratories, Livermore, CA.

‡ Present address: Dalian Institute of Chemical Physics, Dalian, People's Republic of China.

§ Present address: Department of Chemistry, University of California, Davis, CA.

(1) Moreau, C.; Bongrand, J. C. *Ann. Chim. (Paris)* **1920**, *14*, 47.
(2) Moreau, C.; Bongrand, J. C. *Ann. Chim. (Paris)* **1920**, *14*, 5.
(3) Turner, B. *Astrophys. J. Lett.* **1971**, *L35*, 163.
(4) Westenberg, A.; Wilson, E. B., Jr. *J. Am. Chem. Soc.* **1950**, *72*, 199.
(5) See: *Science* **1981**, *212*. *Nature* **1981**, *292*. *J. Geophys. Res.* **1982**, *87*.
(6) Yung, Y. L.; Allen, M.; Pinto, J. *Astrophys. J. Suppl.* **1984**, *55*, 465.
(7) (a) Miller, G. E.; Halpern, J. B.; Jackson, W. M. *J. Chem. Phys.* **1979**, *70*, 2373. (b) Halpern, J. B.; Jackson, W. M. *J. Phys. Chem.* **1982**, *86*, 973. (c) Halpern, J. B.; Jackson, W. M. *J. Phys. Chem.* **1982**, *86*, 3528.
(8) Okabe, H.; Diebler, V. H. *J. Chem. Phys.* **1973**, *59*, 2430.
(9) Sabety-Dzvonik, M. J.; Cody, R. J.; Glicker, S. *J. Chem. Phys.* **1986**, *82*, 3100.
(10) Sabety-Dzvonik, M. J.; Cody, R. J.; Jackson, W. M. *Chem. Phys. Lett.* **1976**, *44*, 131.
(11) Job, V. A.; King, G. W. *J. Mol. Spectrosc.* **1966**, *19*, 155.
(12) Job, V. A.; King, G. W. *J. Mol. Spectrosc.* **1966**, *19*, 178.
(13) Conners, R. E.; Roebber, J. L.; Weiss, K. *J. Chem. Phys.* **1974**, *60*, 5011.
(14) Miller, F. A.; Hannon, R. B., Jr. *Spectrochim. Acta* **1958**, *12*, 321.
(15) Halpern, J. B.; Miller, G. E.; Okabe, H. *J. Photochem. Photobiol.* **1988**, *A42*, 63.
(16) Bruston, P.; Poncet, H.; Raulin, F.; Cossart-Magos, C.; Courtin, R. *Icarus* **1989**, *78*, 38.
(17) Seki, K. Ph.D. Thesis, Tokyo, 1985.
(18) Russell, J. R.; McLaren, I. A.; Jackson, W. M.; Halpern, J. B. *J.*

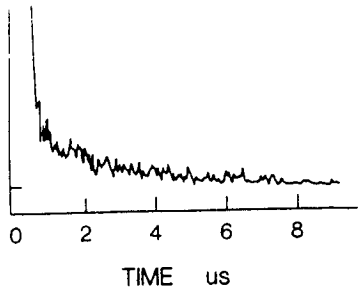

Figure 1. Temporal profile of the total emission signal following the photolysis of HC_2CN by an unfocused ArF laser of 50 mJ/cm² fluence.

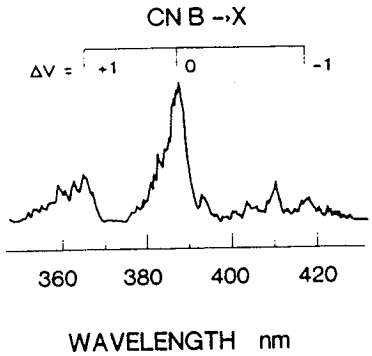

Figure 2. Dispersed fluorescence from the high-intensity photolysis of HC_2CN in the initial part of the temporal profile shown in Figure 1.

violet system. The LIF was excited by a nitrogen-laser-pumped dye laser. The nitrogen laser could be pulsed at an arbitrary and adjustable delay after the excimer laser.

The fluorescence excited in the interaction region was detected by a photomultiplier tube (EMI 9789QB) placed at right angles to both the molecular beam and the lasers. The fluorescence was averaged by a boxcar analyzer (PAR 160). In early experiments, the signal was displayed on a strip-chart recorder. Later experiments recorded the signal in a IBM PC/XT-based data acquisition system designed in our laboratory. Direct fluorescence from multiphoton excited fragments was measured through a 0.25-m monochromator (Jobin-Yvon H20-UV) with a slit width of 1 mm and a dispersion of 4 nm/mm. The LIF signal was measured with an appropriate band-pass filter between the photomultiplier and the cell.

The excimer laser power was monitored by a Scientech power meter. Corrections were made for variation in the dye and excimer laser intensities.

The HC_2CN sample, synthesized by the method of Moreau and Bongrand[1] as modified by Miller and Lemmon,[19] was furnished by Dr. Hideo Okabe. C_4N_2 was synthesized by the method of Moreau and Bongrand.[2] GC/MS analysis of both samples showed no impurities.

Results

A. Photolysis of Cyanoacetylene. Photodissociation of HC_2CN in a static gas cell at a pressure of 20 mTorr with 50 mJ/cm² of ArF laser light produced a fairly strong fluorescence. Figure 1 shows the temporal profile of the total fluorescence with a resolution of 30 ns. The vertical scale has been expanded to emphasize the weak emission. There is a strong fluorescence with a lifetime of about 250 ns followed by a weak emission with a 3-μs lifetime. The actual decay of the sharp peak may be faster but is broadened by a jitter of about 50 ns in the firing of the excimer laser due to an old thyratron. In any case, the bimodal characteristic of the fluorescence decay is evident.

Figure 2 shows the dispersed fluorescence about 100 ns after the excimer laser fired. This spectrum is dominated by the CN ($B^2\Sigma^+ \rightarrow X^2\Sigma^+$) violet bands. Their intensity varies as the second power of the laser flux. There is also some emission from the C_2 ($c^3\pi_u \rightarrow a^3\pi_g$) Swan bands. The fluorescence at times greater than 1 μs after the photolysis was much weaker. Most of this slower decaying emission appears in the CN violet system.

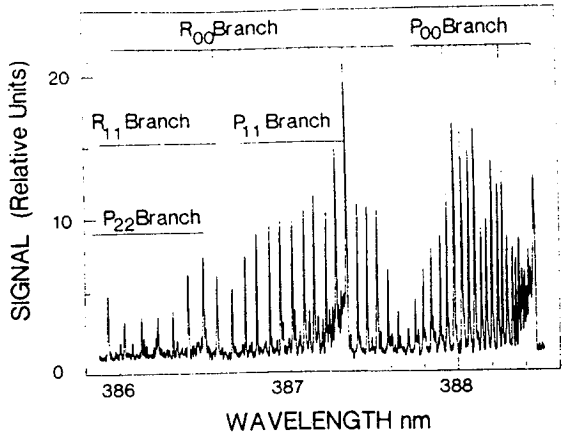

Figure 3. LIF spectra of ground-state CN fragments produced in the photolysis of HC_2CN at 193 nm. The laser fluence was 50 mJ/cm².

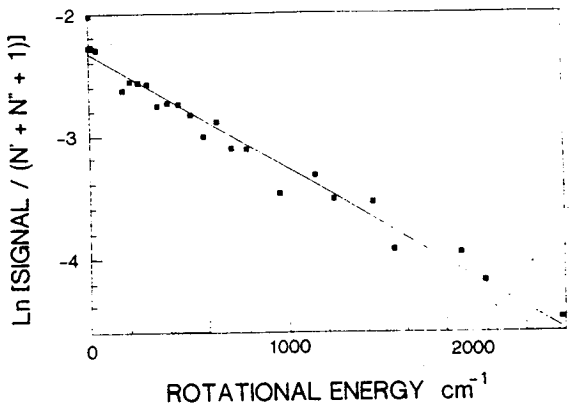

Figure 4. Quantum-state distribution of CN $v'' = 0$ from the photolysis of HC_2CN at high laser energy.

The strong peak between 380 and 390 nm comes from the $\Delta v = 0$ progression of the CN violet system. Weaker, associated $\Delta v = +1$ and -1 progressions of this system can be seen at 360 and 415 nm. The peaks between 390 and 410 nm are from excited C_2. Some other bands from C_2 would be hidden below the CN violet bands, and we saw emission between 460 and 480 nm.

The lifetime of the C_2 Swan transitions is 170 ns,[20] which would fall into the region of the fast emission in Figure 1. Black carbon deposits on the window are also consistent with C_2 production. We have not used LIF to look for ground-state C_2 or C_2 in the $a^3\pi$ state.

LIF measurements of the rotational and vibrational distribution of the CN ($X^2\Sigma^+$) fragments have been performed at a variety of dissociating laser intensities. The delay time between the excimer and the dye laser was fixed at 500 ns, which maintained a collision-free condition while eliminating interference from the immediate fluorescence. As seen in Figure 3, vibrationally and rotationally hot excitation spectra were observed after photolysis at the highest laser intensity (50 mJ/cm²). The nascent quantum-state distributions are shown in Figure 4. The LIF signal of CN in the $v'' = 1$ level varies as the second power of the excimer laser intensity. Figure 5 shows that the population of levels other than $v'' = 0$ disappeared when the excimer laser intensity was decreased to 1 mJ/cm². Dramatic changes were seen in the rotational envelope of the excitation spectrum. Under these conditions, both vibrational and rotational distributions were cold. Bandheads and lines in the 1–1 and 2–2 bands disappeared into the noise. The intensity of this LIF spectrum increased linearly

(19) Miller, F. A.; Lemmon, D. H. *Spectrochim. Acta, Part A* **1967**, *23*,

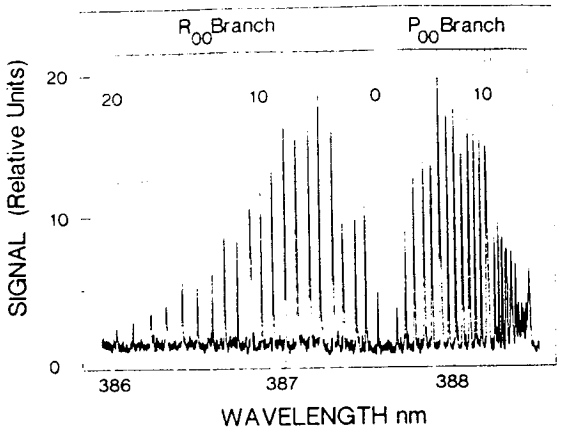

Figure 5. LIF spectrum of ground-state CN $v'' = 0$ fragments following low-intensity photolysis (1 mJ/cm^2).

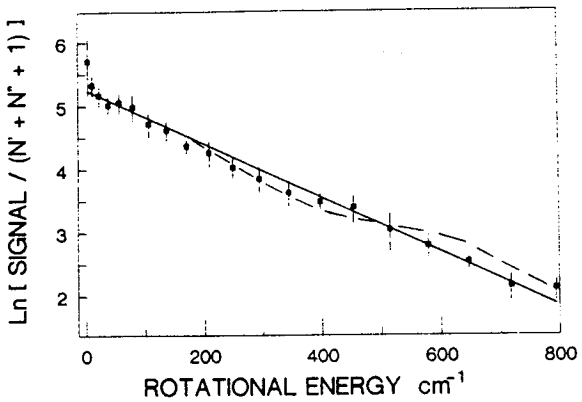

Figure 6. Quantum-state distribution of CN $v'' = 0$ as measured from the spectrum shown in Figure 5. There was no population of the $v'' = 1$ levels at this photolysis intensity.

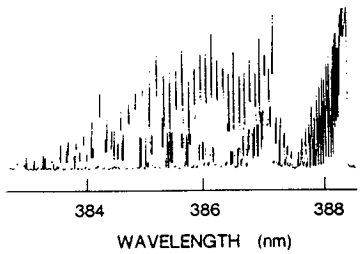

Figure 7. LIF spectra of CN fragments from the photolysis of C_4N_2 at 193 nm under conditions of low laser intensity.

with the laser flux. The spectrum of Figure 5 can be converted into the quantum-state distribution shown in Figure 6.

B. Photolysis of Dicyanoacetylene. The direct fluorescence from the photolysis of C_4N_2 at 193 nm was much weaker than that observed from HC_2CN photolysis under similar conditions. On the other hand, the LIF signals from CN ($X^2\Sigma^+$) were much stronger than those seen following HC_2CN photolysis. As a result of this, the fluorescence could be ignored when the ArF laser power was kept below a 20 mJ/cm^2 pulse. The LIF spectrum of the CN product is shown in Figure 7, and the Boltzmann-like fits to the observed quantum-state distributions are shown in Figure 8. The latter are single-exponential functions described by thermodynamic temperatures of 1400 and 1220 ± 60 K for CN fragments in the $v'' = 0$ and 1 levels, respectively.

Discussion

A. Cyanoacetylene. The absorption spectrum of cyanoacetylene between 260 and 200 nm has been studied by Job and King,[12,13] and the vacuum-UV absorption between 165 and 105 nm has been examined by Conners et al.[14] Job and King found a structured, but very weak, absorption system at 260 nm and a stronger system, described as a structured continuum, starting at 230 nm and

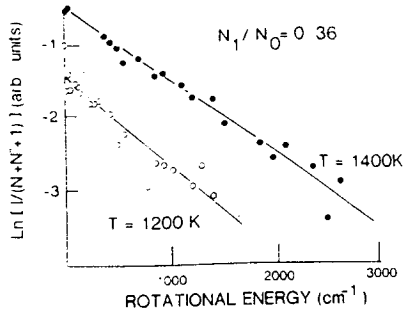

Figure 8. Quantum-state distribution of CN as measured from the spectrum shown in Figure 7. Filled symbols refer to the population in the $v'' = 0$ level, and open symbols refer to the population in the $v'' = 1$ level.

TABLE I: Heats of Formation and Heats of Reaction for Ground-State Molecules and Radicals

species formed	ΔH_f,[a] kJ/mol	species formed	ΔH_f,[a] kJ/mol
HC_2CN	356 ± 4	C_2	829.3 ± 3
C_4N_2	533 ± 4[23]	C_3	833 ± 1.5
H	216.03 ± 0.004	C_3N	629 ± 17[15]
CN	422 ± 4	N	471 ± 4
C_2H	531 ± 1		

reaction	ΔH_R, kJ/mol	threshold, nm
$HC_2CH\ h\nu \rightarrow H + C_3N$	490	244
$\rightarrow CN(X) + C_2H$	599	200
$C_4N_2 + h\nu \rightarrow CN(X) + C_3N$	515	232
$C_3N + h\nu \rightarrow C_2 + CN(X)$	621	193
$\rightarrow C_3 + N$	656	182

[a] All heats of formation are from ref 24 unless otherwise noted.

extending to lower wavelengths. It was noted that the 260-nm bands became diffuse below 240 nm. The 230-nm system of cyanoacetylene consists of a number of diffuse sets of bands with a spacing of 2100 cm^{-1} between the sets. The 2100-cm^{-1} interval corresponds to the excited-state stretching frequency ν_2. The bands have a half-width of 5 cm^{-1} at 230 nm, which increases to 25 cm^{-1} at 200 nm.

Job and King's assignments can be extended to show that the state excited by the 1-nm-bandwidth ArF laser at 193 nm is the $2_0^3 4_0^1 5_0^1$ level at 51 821 cm^{-1}. This lies 2120 cm^{-1} above the assigned $2_0^2 4_0^1 5_0^1$ level at 49 701 cm^{-1}. The forbidden $^1\Sigma^+ \rightarrow {}^1\Delta$ transition is made allowed by excitation of υ_π modes.

Because of the similarity of the low-frequency bending modes in the ground and excited state, the ArF laser also excites some hot bands in the room-temperature gas. The absorption at the ArF frequency has been measured by us, using a 0.1-nm resolution spectrophotometer[15] and by Bruston et al.[16] using a purged monochromator at 0.02-nm resolution. In addition to the vibronic structure, there is a relatively strong continuum, rising smoothly from 230 nm. At 193 nm, the absorption of cyanoacetylene is 2.4×10^{-19} cm^2.[16] Most of this is a continuum contribution.

The thermochemistry of cyano- and dicyanoacetylene is summarized in Table I. Energetically allowed single-photon photolysis processes for cyanoacetylene photolysis at 193 nm are as follows:

$$HC_2CN + h\nu \rightarrow C_2H + CN \qquad \Delta H = 599 \pm 4 \text{ kJ/mol} \quad (1)$$

$$HC_2CN + h\nu \rightarrow H + C_2CN \qquad \Delta H = 490 \pm 21 \text{ kJ/mol} \quad (2)$$

$$HC_2CN + h\nu \rightarrow HCN + C_2 \qquad \Delta H = 609 \pm 17 \text{ kJ/mol} \quad (3)$$

The heat of reaction 2 is based on our measurement of the heat of formation of C_3N from the photodissociative excitation of C_4N_2.[15] The thresholds for processes 1–3 are 200, 244, and 196 nm, respectively.

Reaction 3, in addition to being the most endothermic, requires a rearrangement of the molecular structure. Because the excited

state is linear, there should be a substantial barrier in this channel. Thus, we consider it justified to neglect reaction 3.

The width of the vibrational bands increases smoothly from 230 nm down without sudden large increases at the thresholds of processes 1 and 3. Although the absorption of HC_2CN at 193 nm is four times stronger than that of C_4N_2, the CN LIF signal following HC_2CN photolysis is much weaker. Therefore, it is clear that process 2 is the main contributor to dissociation at 193 nm and at all wavelengths above 190 nm as was suggested in ref 15. The branching ratio between channels 1 and 2 was found to be 1:20 at 193 nm.[15]

Absorption of a second photon by C_3N would lead to

$$C_2CN + h\nu \rightarrow C_2 + CN \qquad \Delta H = 621 \pm 25 \text{ kJ/mol} \qquad (4)$$

with a threshold of 193 nm for ground-state C_2CN.

CN can only be produced in the lowest vibrational level following 193-nm photolysis via reactions 1 and 4. With respect to 193-nm photolysis, process 1 is 21 kJ/mol exothermic and process 4 is roughly thermoneutral, but with a large uncertainty. Thus, no vibrational excitation of the CN stretch can be produced directly from reactions 1 and 4.

Channel 2 is about 130 kJ/mol exothermic with respect to 193-nm photolysis, but again, there is a large associated uncertainty. Some of this energy can remain in the CN fragment following photolysis of C_3N. The maximum energy available to the CN fragment in the two-step sequential process 2 followed by 4, would be 127 ± 4 kJ/mol. It is barely energetically possible that some of the CN could be produced in the excited ($A^2\pi_i$) state.

No vibrationally excited CN fragments are produced in the low-intensity photolysis. The intensity of the R_{00} (4) line varies linearly with the photolysis laser intensity, indicative of a single-photon process. Thus, process 1 appears to be the only source of CN radicals at low photolysis energies. As shown in Figure 6, the quantum-state distribution of $CN(X^2\Sigma^+, v'' = 0)$ fragments can be fit by a Boltzman distribution with a temperature parameter of 240 cm^{-1} or 360 K (solid line), which is very close to the 300 K rotational temperature of the parent molecule.

We have attempted to reproduce the nascent CN radical rotational-state distribution with a phase-space model similar to the one developed by Eres and McDonald[21] to model photolysis of C_2N_2 at 193 nm. They obtained an excellent fit to the experimental results, using an adjustable impact parameter of 0.25 nm. We have reproduced their results for C_2N_2 photolysis but found that the best fit impact parameter is about 0.09 nm, close to the equilibrium bond length. This difference is probably due to a choice of reduced mass. We used the reduced mass for two CN radicals, 13 amu, while Eres and McDonald appear to have used the mass of a single CN radical. This model then becomes parameterless. In any case, the dissociation of C_2N_2 produces CN radicals with an almost statistical distribution of energy between rotation and translation.

Little or no excess energy ends up in the rotation of the fragments following the photolysis of HC_3N. Intuitively, this shows that the dissociation is linear and that there is no excitation of bending modes in the transition. The best match to the phase-space calculation is obtained when the impact parameter is 0.0075 nm (shown as the dashed line in Figure 6). The precision of the fit is perhaps fortuitous, but the small size of the impact parameter agrees with the above argument. Thus, along pathways leading to $CN + C_2H$ in the region available to Franck–Condon excitation, curvature in the bending coordinate of the potential energy surface (PES) must be positive.

Figure 3 shows the vibrationally excited LIF spectrum obtained following photolysis at high laser intensity. The rotational distributions are hot as can be seen from the absence of a clear band gap between the P_{00} and R_{00} bands. As can be seen in Figure 4, the distribution can be fit by a Boltzmann distribution with a temperature of 1000 cm^{-1} or 1400 K. There is population in rotational states at least as high as $N = 60$.

The process leading to the observed $CN(X^2\Sigma^+)$ distribution at high laser intensities is most likely reaction 2 followed by 4. The total excess energy available to the $CN(X^2\Sigma^+)$ after these two steps is about 10656 ± 1050 cm^{-1}. Some of the excited radicals have more than 7300 cm^{-1} of rotational energy, which would be a remnant of internal energy left in the C_3N fragment after reaction 2. The second-order dependence of the LIF signal for higher vibrational and rotational levels is consistent with the proposed sequential two-step mechanism.

Another energetically allowed channel that could lead to such vibrationally and rotationally excited CN radicals would be simultaneous absorption of two photons in the cyanoacetylene. Concerted dissociation to $H + C_2 + CN$ is most unlikely. Such a doubly excited state should first decompose to $CN + C_2H$ or $H + C_3N$. Enough energy could be left in the C_2H or C_3N fragments to allow unimolecular dissociation of these fragments. Still, at least some of the doubly excited HC_3N should form CN with much more vibrational and rotational excitation than was observed.

At low intensities, channel 2 dominates over the process, leading to vibrationally and rotationally excited CN by a factor of about 20.[15] Channel 1 produces CN following absorption of a single photon at all intensities. For reasons that have been dealt with in detail in Xie et al.,[22] ground-state CN radicals cannot absorb a second photon at 193 nm. Only a few levels of the $CN(A^2\pi_i)$ state can do so, and the resulting fluorescence is well characterized, leading to emission from the F and E states of CN. Even at the highest intensities, no such direct emissions were seen after the photolysis of either HC_2CN or C_4N_2. The 193-nm HC_2CN absorption cross section is 2.4×10^{-19} cm^2,[16] so even at the highest laser intensities, less than 1% of the HC_2CN molecules will be photolyzed via reactions 1 and 2.

If the mechanism producing the hot CN radicals is sequential absorption of two photons by cyanoacetylene, then the effective cross section for absorption of a second photon includes a factor that is the ratio between the laser pulse length and the lifetime of the excited state reached by absorption of the first photon. The bandwidth of lines at 193 nm corresponds to a lifetime of less than 1 ps. However, most of the absorption is from an underlying continuum (i.e., from shorter lived states).

Simple kinetics shows that the ratio of CN produced by the one-photon process to that produced by either the sequential two-step process of reaction 1 followed by reaction 4 or the sequential absorption of two photons by the cyanoacetylene will be

$$R = (q_1/q_2)(\sigma_i E_{\text{laser}})^{-1} \qquad (5)$$

where q_i is the relative quantum yield of reaction i and σ_i the cross section for absorption of the second photon. q_1/q_2 is about 0.05 at 193 nm.

At a laser flux of 5×10^{15} photons/(cm^2-pulse), channel 1 dominates and R is at least 10. This has been estimated by comparing the amounts of vibrationally excited CN in Figure 3 (high-intensity photolysis) and Figure 5 (low-intensity photolysis). Increasing the flux by 1 order of magnitude increased the relative yield of radicals from the two-photon mechanism above that from channel 1. If the high-intensity channel were sequential absorption of two photons by HC_3N, the absorption cross section would be greater than 10^{-14} cm^2, which is unrealistically large.

On the other hand, the sequential processes of reaction 2 followed by reaction 4 yields crude limits for the 193-nm absorption of C_2CN of between 1×10^{-18} and 5×10^{-17} cm^2. The branching between reactions 1 and 2 accounts for the much smaller LIF signal when HC_2CN is photolyzed as against when C_4N_2 is irradiated.

Excited fragments are also created in the photolysis. Thermochemically, absorption of at least two photons is needed to form

(21) Xie, X.; McCrary, V. R.; Halpern, J. B.; Pugh, E.; Jackson, W. M. J. Phys. Chem. 1986, 90, 2670.

(22) Eres, D.; Gurnick, M.; McDonald, J. D. J. Chem. Phys. 1984, 81, 5552.

(23) Armstrong, G. T.; Marantz, S. J. Phys. Chem. 1960, 64, 1776.

(24) Okabe, H. Photochemistry of Small Molecules; Wiley: New York,

excited radicals. Production of $CN(B^2\Sigma^+)$ can only proceed via the two-photon process

$$HC_2CN + 2h\nu \rightarrow C_2H + CN(B^2\Sigma^+) \qquad \Delta H = -332 \text{ kJ/mol} \tag{6}$$

or the overall three-photon process of reaction 2 followed by

$$C_2CN + 2h\nu \rightarrow C_2 + CN(B^2\Sigma^+) \qquad \Delta H = -322 \text{ kJ/mol} \tag{7}$$

or the three-photon process

$$HC_2CN + 3h\nu \rightarrow H + C_2 + CN(B^2\Sigma^+) \qquad \Delta H = -442 \text{ kJ/mol} \tag{8}$$

where we have included the energy of the necessary 193-nm photons in the heats of reaction.

Figures 1 and 2 show that the emission is dominated by the CN violet system. There is also some emission observed at positions corresponding to lines in the Swan bands of C_2. The intensity of the CN ($B^2\Sigma^+ \rightarrow X^2\Sigma^+$) fluorescence varies as the second power of the laser intensity. This favors the direct two-photon absorption mechanism as the source of excited CN. Dissociation of C_3N to excited CN would require three photons overall. Moreover, if this were the mechanism, the same pattern and strength of emission should be seen following the photolysis of C_4N_2. The direct emission following the high-energy photolysis of C_4N_2 is much lower than that seen after the photolysis of HC_3N.

B. Dicyanoacetylene. The UV absorption spectrum of C_4N_2 has been studied by Miller and Hannon,[15] and the vacuum-UV spectrum has been studied by Conners, Roebber, and Weiss.[14] As for HC_2CN, Miller and Hannon found that there are two UV absorption systems in C_4N_2, a weak, red degraded system starting at 280 nm and a stronger system starting at 264 nm. They list four bands of this system centered at 264, 250, 237, and 226 nm. No other bands are listed, but there is a notation that the spectrophotometer that was used could not maintain its narrowest resolution (0.1 nm) for the last band. There is some possibility that the lamp was running out of intensity below 225 nm, and there may be one or more bands further to the blue. The band at 250 nm is by far the strongest.

Miller and Hannon were able to resolve sharp vibrational structures in the 280-nm system using a 2-m spectrograph with a 0.52 nm/mm dispersion, but in no case did they have enough resolution to measure rotational structure. Judging from the low-resolution spectrum and assignments, the bands at 264 and 250 nm are equally sharp, while the 237-nm band is only a bit more diffuse and the 226-nm band is obviously broadened. None of this is conclusive as to the dissociation limit, but it is consistent with the thermochemical limit measured in ref 15.

Conners et al. see an irregular absorption growing from 50 100 to 55 000 cm^{-1} (198 to 180 nm) where a far stronger system begins. They offer no assignment, but using a CNDO/2 method SCF-MO calculation, they find that there are five possible states in the region that may be responsible for this absorption. Briefly, they are $^1\Sigma^-_g$, $^1\Delta_g$, $^1\Sigma^-_u$, $^1\Delta_u$ (different from the pair of the same symmetries responsible for the 264 absorption), and $^1\Sigma_g$. The 198-nm absorption is not broadened by many atmospheres of helium so it is a valence transition. The absorption cross section at 193 nm is about 1×10^{-19} cm^2. From the shape of the spectrum, this absorption is not a continuation of the 264-nm system, and indeed the peaks do not fall where one would expect the ν_1 progression of the 264 system. The electronic origin of this third electronic state must be near 198 nm. Absorption at 193 nm (51 813 cm^{-1}) would not excite any high-frequency stretching modes (ν_1–ν_5) of the C_4N_2 but might involve excitation of a few low-frequency stretches and, of course, thermally excited hot bands of such modes. For most of the possible electronic species, at least 1 quanta of the π_g ν_6 or ν_7 modes would have to be excited to make the transition vibrationally allowed.

In the photolysis of C_4N_2, the first step will be

$$C_4N_2 + h\nu \rightarrow CN + C_3N \qquad \Delta H = 515 \pm 6 \text{ kJ/mol} \tag{9}$$

followed, possibly, by reaction 4. At 193 nm, process 9 would leave 8723 cm^{-1} of excess energy in the modes of motion of the fragments. The thermochemical threshold is 232 ± 1 nm.[15] Excited CN could be formed by the two-photon excitation of C_4N_2 or reaction 7.

The photolysis of thermal C_4N_2 at 193 nm produced a fairly strong $CN(X^2\Sigma^+)$ LIF signal. The signal intensity in the bandhead region was measured as a function of laser intensity and found to be linear. This confirms the photolytic reaction 9 as the primary process. Thermochemically, the CN fragment can have up to 8700 cm^{-1} of excess energy. The LIF spectrum shows that CN ($X^2\Sigma^+$) is formed in $v'' = 0$ and 1 levels. Little or no population is seen in higher vibrational levels. Vibrational population distributions are probably controlled by Franck–Condon factors in the parent molecule. The populated state with the highest internal energy has between 3000 and 3500 cm^{-1}. About 36% of the CN is created in the $v'' = 1$ level. We have attempted to match the measured distributions with a phase-space calculation. The best matches are found with an impact parameter of 0.03 nm, assuming no vibrational excitation of the C_3N fragment. Higher values of the impact parameter partition too much energy to rotation. This indicates that either the dissociation is linear, or that about half of the energy is partitioned to vibrational excitation of the C_3N fragment.

Conclusions

The single-photon photolysis mechanism of cyano- and dicyanoacetylene has been studied. Quantum-state distributions of CN fragments have been measured. Multiphoton photolysis schemes of these two molecules have also been determined and some characteristics of the fragments measured.

It has been shown that secondary photolysis of the C_3N radical leads to the formation of CN radicals, from which we infer that the photolysis is also a source of C_2 radicals. Some excited C_2 has been seen as a product of simultaneous absorption of two photons by the HC_3N. An estimate of the cross section of the C_3N radical at 193 nm has been made.

Cyanoacetylene is commonly found in the interstellar medium, nitrogen–methane atmospheres, and probably in comets. On a simple calculation, it should be the second most common odd nitrogen species in these environments. A simple, two-step photodissociation of cyanoacetylene has been shown to lead to formation of both C_2 and CN radicals.

Acknowledgment. We acknowledge the support of the Office of Naval Research and the National Aeronautics and Space Administration. J.B.H. was also supported by the National Science Foundation. W.M.J. acknowledges the support of NASA under Grant NASA-903. We thank Hideo Okabe and M. Drewniak-Deyrup for many helpful discussions and the gift of the cyanoacetylene sample. We also thank George E. Miller for his comments on this work.

Registry No. HC_2CN, 1070-71-9; C_4N_2, 1071-98-3; CN, 2074-87-5; C_2H, 2122-48-7; C_3N, 62435-43-2; H, 12385-13-6; C_2, 108481-51-2.

Detection of $C_2(B'\,^1\Sigma_g^+)$ in the multiphoton dissociation of acetylene at 193 nm

Yihan Bao, R. S. Urdahl, and William M. Jackson
Department of Chemistry, University of California, Davis, California 95616

(Received 1 October 1990; accepted 23 October 1990)

Various electronic states of C_2 have previously been identified in the following two-photon sequential photochemical process[1]

$$C_2H_2 + h\nu_{193\ nm} \rightarrow C_2H + H,$$
$$C_2H + h\nu_{193\ nm} \rightarrow C_2 + H.$$

The existence of $C_2(A\,^1\Pi_u)$ as a primary photofragment was established early on by the observation of the Phillips band ($A\,^1\Pi_u$–$X\,^1\Sigma_g^+$) emission upon photolysis.[2] Subsequent experiments using laser-induced fluorescence (LIF)[3] showed the presence of nascent $C_2(a\,^3\Pi_u)$, whereas REMPI detection schemes have verified the formation of both $C_2(B\,^1\Delta_g)$ and $C_2(b\,^3\Sigma_g^-)$.[4] The existence of $C_2(B'\,^1\Sigma_g^+)$ has been predicted theoretically for a number of years,[5–7] but has only recently been observed experimentally.[8] Using a high-resolution FTIR spectrometer, Douay *et al.* recorded the $C_2(B'\,^1\Sigma_g^+$–$A\,^1\Pi_u)$ emission spectra excited during a microwave discharge in various hydrocarbon mixtures. Subsequent line position analysis allowed the first derivation of precise molecular constants for the $B'\,^1\Sigma_g^+$ state. We report here the first observation of $C_2(B'\,^1\Sigma_g^+)$ in the two-step 193 nm photolysis of C_2H_2, which is the highest lying electronic state of C_2 detected to date in this process.

The nascent $C_2(B'\,^1\Sigma_g^+, v'' = 0,1,2)$ radicals were produced by the two-photon sequential dissociation of acetylene in a supersonic jet. The molecular beam was formed by expanding acetylene (Matheson, 99.6%, purified using a dry ice/acetone slush trap) through the 0.5 mm orifice of a Newport BV-100 pulsed valve, operated at a source pressure of 200 Torr. Approximately 5 mJ of light from a 193 nm excimer laser (Lambda Physik EMG101MSC) was focused using a 38-cm focal length UV fused silica lens prior to intersecting the jet expansion at 90°, ~10 nozzle diameters downstream from the exit plane of the nozzle. The C_2 fragments are detected by laser-induced fluorescence, using a XeCl excimer pumped tunable dye laser (Lambda Physik EMG101MSC/FL2002) operated with DMQ in dioxane to excite the $D\,^1\Sigma_u^+$–$B'\,^1\Sigma_g^+$ transition at ~356 nm. The dye laser also intersects the molecular beam at 90°, and spatially overlaps the focal point of the photolysis laser. Fluorescence from the Mulliken system ($D\,^1\Sigma_u^+$–$X\,^1\Sigma_g^+$) was collected normal to the plane formed by the axes of the dye laser and molecular beam, isolated with a 25 nm FWHM interference filter centered at 239 nm (Corion), and imaged onto the cathode of a Thorn-EMI 9789QB photomultiplier tube. The PMT signal was processed by an Evans 4130A gated integrator, whose output was digitized, averaged, and stored using a Laser Interfaces LI1000 series data acquisition system. The PC-XT based LI1000 also served as the experimental time base, providing programmable timers necessary to trigger the various instruments.

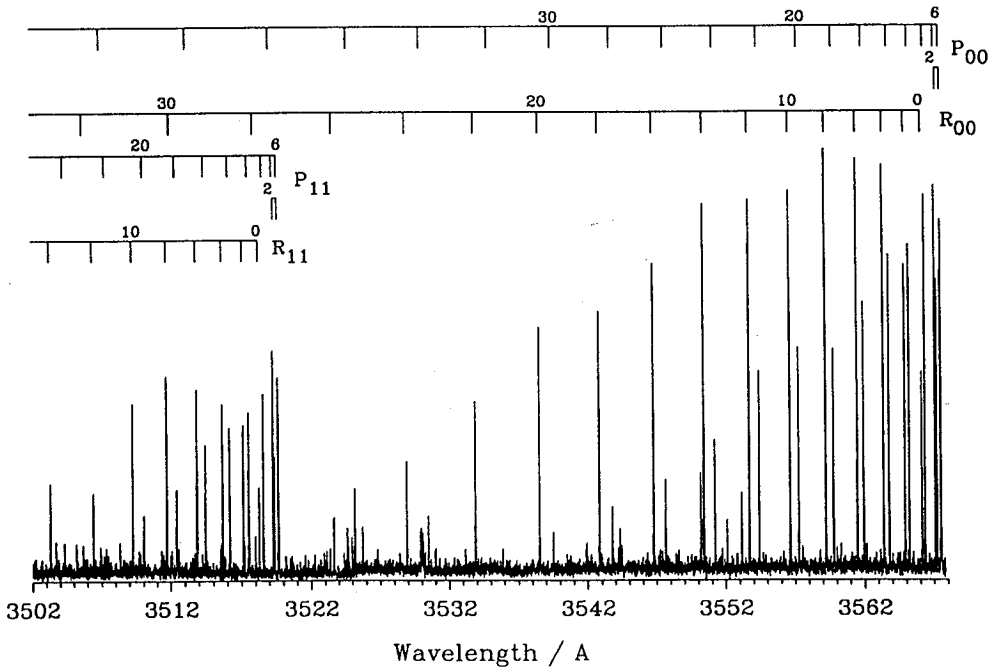

FIG. 1. LIF spectrum of $C_2(B'\,^1\Sigma_g^+)$ produced during the photodissociation of jet-cooled C_2H_2.

 0021-9606/91/010808-02$03.00

The partial $C_2(B'\,^1\Sigma_g^+)$ LIF spectrum is shown in Fig. 1. Assignment of the spectral lines was made using the molecular constants of Douay *et al.* $(B'\,^1\Sigma_g^+)$[8] and Herzberg $(D\,^1\Sigma_u^+)$.[9] Clearly evident in the spectrum are the lack of a Q branch and the absence of odd-numbered rotational lines. These are the expected spectral features of a $^1\Sigma$–$^1\Sigma$ transition in a homonuclear diatomic molecule with zero nuclear spin. It should also be noted that the spectrum was taken by saturating the $D\,^1\Sigma_u^+$–$B'\,^1\Sigma_g^+$ transition in order to maximize the observed LIF signal.

Detailed measurement of the $C_2(B'\,^1\Sigma_g^+)$ rotational and vibrational populations is currently in progress. A discussion of their implications to the dynamics of acetylene dissociation is forthcoming.

This work was supported by the Planetary Atmospheres Program of NASA under Grant No. NAGW-903.

[1] A. M. Wodtke and Y. T. Lee, J. Phys. Chem. **89**, 4744 (1985).
[2] J. R. McDonald, A. P. Baronavski, and V. M. Donnelly, Chem. Phys. **33**, 161 (1978).
[3] R. S. Urdahl, Y. Bao, and W. M. Jackson, Chem. Phys. Lett. **152**, 485 (1988).
[4] P. M. Goodwin and T. A. Cool, J. Mol. Spectrosc. **133**, 230 (1989).
[5] P. F. Fougere and R. K. Nesbet, J. Chem. Phys. **44**, 285 (1966).
[6] J. Barsuhn, Z. Naturforsch. Teil A **27**, 1031 (1972).
[7] K. Kirby and B. Liu, J. Chem. Phys. **70**, 893 (1979).
[8] M. Douay, R. Nietmann, and P. F. Bernath, J. Mol. Spectrosc. **131**, 261 (1988).
[9] K. P. Huber and G. Herzberg, *Molecular Spectra and Molecular Structure* (Van Nostrand Reinhold, New York, 1979), Vol. IV.

#96

An experimental determination of the heat of formation of C_2 and the C–H bond dissociation energy in C_2H

Randall S. Urdahl, Yihan Bao and William M. Jackson
Department of Chemistry, University of California, Davis, CA 95616, USA

Received 5 November 1990; in final form 4 January 1991

The rotational cutoff levels of $C_2(B'\,^1\Sigma_g^+, v''=1, 2)$, produced in the multiphoton dissociation of jet-cooled acetylene at 193 nm, have been measured using laser-induced fluorescence. This data is used to calculate the values $\Delta H_{f,0}(C_2) = 194.8 \pm 0.5$ kcal/mol and $D_0(CC\text{–}H) = 112.0 \pm 0.8$ kcal/mol, in excellent agreement with the latest theoretical calculations.

1. Introduction

Recently Ervin et al. [1] reported on the C–H bond dissociation energies of acetylene, ethylene, and the vinyl radical, which were derived from their studies of negative ion photoelectron spectroscopy and gas phase proton transfer kinetics. The recommended values for $\Delta H_{f,0}(C_2)$ and $D_0(CC\text{–}H)$ are given to be 199.0 ± 2.5 and 116.3 ± 2.6 kcal/mol, respectively, with $D_0(CC\text{–}H)$ being critically dependent upon the value of $\Delta H_{f,0}(C_2)$. Newly published theoretical calculations by Bauschlicher and Langhoff predict $D_0(CC\text{–}H)$ at 112.4 ± 2.0 kcal/mol [2], just within the error bars of the experimental value. Due to the importance of thermodynamic data for these simple radicals in combustion and astrophysics, accurate experimental values for these quantities are needed. Not only will more accurate experimental data help in the modeling of combustion and astrophysical systems, but it will also allow the theorist to better calibrate the computational methods used to calculate such quantities.

In a previous communication [3], we reported the first observation of $C_2(B'\,^1\Sigma_g^+)$ in the photolysis of acetylene. Since the $B'\,^1\Sigma_g^+$ is the highest lying electronic state of C_2 yet detected in the two-photon dissociation of jet-cooled acetylene at 193 nm, locating the high-J cutoffs enables the accurate measurements of C_2 fragments with maximum internal energy. In this Letter, we report our measurement of the $C_2(B'\,^1\Sigma_g^+)$ ro-vibrational cutoff levels, from which we were able to derive firm upper limits for $\Delta H_{f,0}(C_2)$ and $D_0(CC\text{–}H)$ with uncertainties that are far below those previously reported.

2. Experimental

The experimental conditions used were similar to those described earlier [3] with only a few minor changes, and are briefly summarized here. The pulsed supersonic jet was formed by expanding 200 Torr of neat acetylene (purified using a dry ice/acetone slush trap) through the 0.5 mm orifice of a Newport BV-100 pulsed valve. Light from both an ArF excimer and a tunable dye laser spatially overlap while crossing the expansion at 90°, ≈20 nozzle diameters downstream from the valve orifice. The ≈5 mJ photolysis laser beam (Lambda Physik EMG101MSC) was focused using a 38 cm focal length UV fused silica lens. The XeCl-pumped tunable dye laser (Lambda Physik EMG101MSC/FL2002) operated with a dye mixture of PTP and DMQ in dioxane, and was used to excite the $C_2(D\,^1\Sigma_u^+ - B'\,^1\Sigma_g^+)$ transition. Subsequent Mulliken band emission $(D\,^1\Sigma_u^+ - X\,^1\Sigma_g^+)$ was collected by a lens set normal to the plane formed by the intersection of the dye laser and molecular beam axes. This fluorescence was isolated from other scattered light by a 25 nm fwhm

interference filter centered at 239 nm (Corion), and detected with a photomultiplier tube (Thorn-EMI 9789QB). The signal from the PMT was processed by a gated integrator (Evans 4130A), digitized, averaged, and stored in a PC-XT computer.

3. Results and discussion

A portion of the LIF spectrum obtained in the manner described above is given in fig. 1. This figure shows the high rotational level cutoffs in both the $v''=1$ and 2 vibrational levels. The J_{max} positions were determined after assigning the spectrum using the constants for the $B'\,^1\Sigma_g^+$ state obtained by Douay et al. [4] and those for the $D\,^1\Sigma_u^+$ state of Huber and Herzberg [5]. For the $v''=1$ and 2 vibrational levels, J_{max} was found to be 34 and 14, respectively.

By considering the following reaction scheme:

$$C_2H_2 + h\nu_{193\,nm} \rightarrow H + C_2H\,,$$

$$C_2H + h\nu_{193\,nm} \rightarrow H + C_2(B'\,^1\Sigma_g^+, v, J)\,,$$

the upper limits for $\Delta H_{f,0}(C_2)$ and D_0(CC–H) can be determined from the following equations:

$$\Delta H_{f,0}(C_2) \leqslant 2h\nu_{193\,nm} + \Delta H_{f,0}(C_2H_2) - 2\Delta H_{f,0}(H) - T_v[C_2(B'\,^1\Sigma_g^+)] - B_v[C_2(B'\,^1\Sigma_g^+)]J_{max}(J_{max}+1)\,,$$

$$D_0(CC\text{–}H) \leqslant 2h\nu_{193\,nm} - D_0(HCC\text{–}H) - T_v[C_2(B'\,^1\Sigma_g)] - B_v[C_2(B'\,^1\Sigma_g^+)]J_{max}(J_{max}+1)\,.$$

Using the $C_2(B'\,^1\Sigma_g^+)$ molecular constants derived by Douay et al. [4] and the values $\Delta H_{f,0}(C_2H_2) = 54.68 \pm 0.17$ kcal/mol, $\Delta H_{f,0}(H) = 51.6336 \pm 0.0014$ kcal/mol, and $D_0(HCC\text{–}H) = 131.3 \pm 0.7$ kcal/mol [1], one can calculate $\Delta H_{f,0}(C_2) = 194.8 \pm 0.5$ kcal/mol and $D_0(CC\text{–}H) = 112 \pm 0.8$ kcal/mol. The quoted errors in both these values reflect the 0.8 nm bandwidth of the ArF laser, as well as the additional 0.17 kcal/mol uncertainty in $\Delta H_{f,0}(C_2H_2)$ for $\Delta H_{f,0}(C_2)$, and the 0.7 kcal/mol uncertainty in $D_0(HCC\text{–}H)$ for $D_0(CC\text{–}H)$.

Table 1 summarizes our measured values for $\Delta H_{f,0}(C_2)$ and $D_0(CC\text{–}H)$ along with some previous

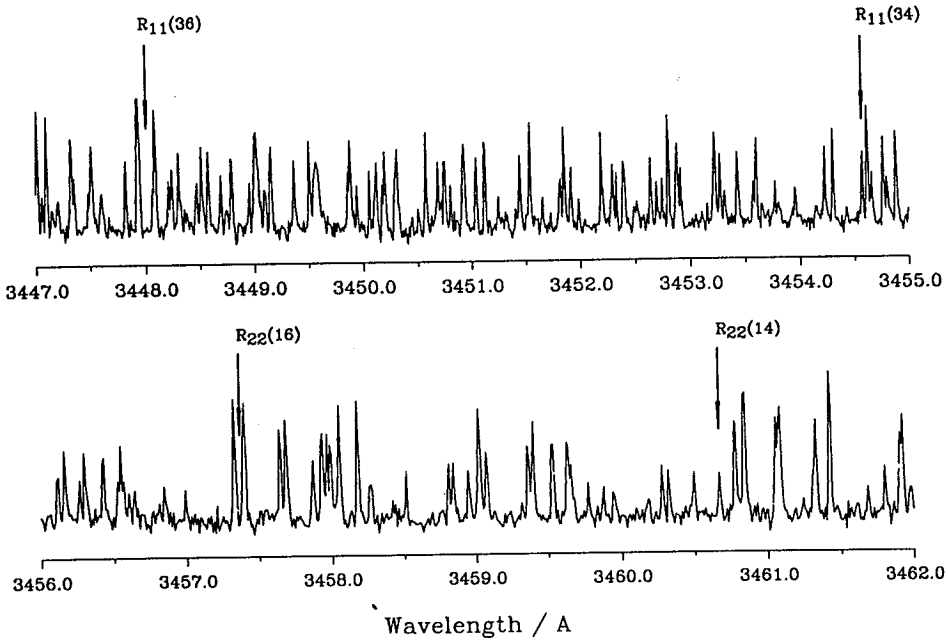

Fig. 1. Region of the $C_2(B'\,^1\Sigma_g^+)$ LIF spectrum highlighting the high-J cutoffs in the (1, 1) and (2, 2) vibrational bands. Most of the numerous unmarked lines appear due to an unidentified transition, and are currently under investigation.

Table 1
Bond dissociation energies and heats of formation

Species	$\Delta H_{f,0}$ (kcal/mol)	D_0 (kcal/mol)	Ref.
C_2	194.8±0.5	145.2±0.5	this work (exp.)
	199.0±2.5	141.0±2.5	[1]
		142.2±2.5	[6] (exp.)
		143.2±2.3	[7] (theor.)
C_2H		112.0±0.8	this work (exp.)
	134.3±0.7	116.3±2.6	[1] (exp.)
		(112.1±0.9)	[1] [a]
	134.0±4.7	112.4±2.0	[2] (theor.)

[a] Value if $\Delta H_{f,0}(C_2)$ measured in this work is used.

experimental data determined by others and the latest theoretical values for these constants. Our value for $\Delta H_{f,0}(C_2)$ is markedly lower than that adopted by Ervin et al. [1], which in turn leads to a significantly higher value for $D_0(C_2)$. Bauschlicher and Langhoff [2] have already pointed out that $\Delta H_{f,0}(C_2) = 199.0 \pm 2.5$ kcal/mol was probably too high, and the present experiments confirm this. We note that both the earlier experimental [6] and latest theoretical [7] values for $D_0(C_2)$ are in better agreement with our result than they are with the value adopted by Ervin et al.

The agreement between our value for D_0(CC–H) and the theoretical value is excellent. There is clearly less of a consensus between our value for D_0(CC–H) and that of Ervin et al., but these results can also be reconciled if the $\Delta H_{f,0}(C_2)$ determined in this work is used to recalculate D_0(CC–H) from their experimental results.

In order to clarify the accuracy of the current measurements, one must consider the effects of the various possible sources of error. These include the existence of rotational levels higher than the observed cutoffs, the energy contained in H atom translational motion, the excitation of hot bands in C_2H_2, and the production of C_2 via a three-photon process.

Due to the zero nuclear spin of ^{12}C, the next highest rotational level past the observed $R_{22}(14)$ cutoff would be the $R_{22}(16)$ line. If we assume that $C_2(B'\,^1\Sigma_g^+, v''=2, J''=16)$ is produced at a concentration below the sensitivity of LIF detection, then the upper limit measured for $\Delta H_{f,0}(C_2)$ would drop by ≈0.3 kcal/mol. However, the $R_{22}(16)$ line is clearly not visible in the spectrum shown in fig. 1, which was taken under saturation conditions of the $C_2(D\,^1\Sigma_u^+ - B'\,^1\Sigma_g^+)$ transition. Since the S/N ratio of the spectrum should allow easy identification of any line with an intensity of less than even half the $R_{22}(14)$ and $R_{11}(34)$, we conclude that the $R_{22}(14)$ and $R_{11}(34)$ lines represent a cutoff in available energy rather than just the detection limit of the experiment.

Another important consideration in the error analysis is the magnitude of the correction necessary to account for the translational energy carried by the H atoms. Implicit in the calculation of $\Delta H_{f,0}(C_2)$ and D_0(CC–H) is the assumption that the corresponding H atoms are produced with either little or no translational energy. However, strictly speaking, conservation of angular momentum applied to the half-collision event will impose a non-zero lower limit on the H atom recoil velocity. The most stringent case we must consider is the formation of $C_2(B'\,^1\Sigma_g^+, v''=1, J''=34)$, in which an impact parameter of 7.5 Å is required for both dissociations, each producing an H atom with ≈0.5 kcal/mol translational recoil energy. Impact parameters of this magnitude or even larger are reasonable if we allow the dissociations to occur with a distribution of impact parameters, thus producing a corresponding distribution of H atom translational energies. The dissociation forming $C_2(B'\,^1\Sigma_g^+, v''=1, J''=34)$ would then necessarily proceed via impact parameters and H atom energies found at the upper and lower limits of their respective distributions. Although we cannot determine the exact H atom recoil velocity coincident with the production of a given ro-vibronic state of C_2, any amount of energy partitioned into this degree of freedom will clearly lower the value calculated for $\Delta H_{f,0}(C_2)$.

The existence of another systematic error in the present values is possible, if in the photolysis process we are exciting hot bands in C_2H_2. We think that this scenario is unlikely, since Wodtke and Lee [8] have shown that the hot band signal leads to fast fragments which would necessarily have very little internal energy. It would be rather perverse if the hot bands made a substantial contribution to the production of C_2H fragments with a significant amount of internal energy and very little recoil translational energy.

Finally, the presence of the observed cutoff levels due to a three-photon absorption process is dis-

counted on the basis that the resulting value of $\Delta H_{f,0}(C_2)$ would be unreasonably high by ≈ 148 kcal/mol.

4. Conclusions

We have derived new values for $\Delta H_{f,0}(C_2)$ and $D_0(CC\text{–}H)$ from experimental measurements of the ro-vibrational cutoffs in the LIF spectrum of $C_2(B'\,^1\Sigma_g^+)$, allowing the determination of $D_0(C_2)$. The uncertainty in our measurements is less than those in previously reported values since they are based on a spectroscopic method. These newly determined thermodynamic quantities now resolve any conflict between previous theoretical and experimental values, and confirm that current theoretical techniques can provide accurate energies for these small free radicals. They also provide additional experimental evidence for the use of $D_0(HCC\text{–}H) = 131.3$ kcal/mol, because one could not obtain such agreement between these various quantities if the smaller value of $D_0(HCC\text{–}H) = 127$ kcal/mol [9,10] is used.

It should be noted that after the initial writing of this paper, two new measurements [11,12] of $D_0(HCC\text{–}H)$ have appeared which lend further support to the ≈ 131 kcal/mol C–H bond dissociation energy of acetylene.

Acknowledgement

The authors would like to thank Professor Y.T. Lee for his critical reading of the manuscript, and Professor D.M. Volman and Professor K.M. Ervin for their useful comments. This work was supported by the National Science Foundation under grant CHE-9008095 and the Planetary Atmospheres Program of NASA under grant NAGW-903.

References

[1] K.M. Ervin, S. Gronert, S.E. Barlow, M.K. Gilles, A.G. Harrison, V.M. Bierbaum, C.H. DePuy, W.C. Lineberger and G.B. Ellison, J. Am. Chem. Soc. 112 (1990) 5750.
[2] C.W. Bauschlicher Jr. and S.R. Langhoff, Chem. Phys. Letters 173 (1990) 367.
[3] Y. Bao, R.S. Urdahl and W.M. Jackson, J. Chem. Phys., to be published.
[4] M. Douay, R. Nietmann and P.F. Bernath, J. Mol. Spectry. 131 (1988) 261.
[5] K.P. Huber and G. Herzberg, Molecular spectra and molecular structure, Vol. 6 (Van Nostrand Reinhold, New York, 1979).
[6] J. Kordis and K.A. Gingerich, J. Chem. Phys. 58 (1973) 5058.
[7] C.W. Bauschlicher Jr., S.R. Langhoff and P.R. Taylor, Astrophys. J. 332 (1988) 531.
[8] A.M. Wodtke and Y.T. Lee, J. Phys. Chem. 89 (1985) 4744.
[9] P.G. Green, J.L. Kinsey and R.W. Field, J. Chem. Phys. 91 (1989) 5160.
[10] J. Segall, R. Lavi, Y. Wen and C. Wittig, J. Phys. Chem. 93 (1989) 7287.
[11] B. Ruscic and J. Berkowitz, J. Chem. Phys. 93 (1990) 5586.
[12] D.P. Baldwin, M.A. Buntine and D.W. Chandler, J. Chem. Phys. 93 (1990) 6578.

#98

RECENT LABORATORY PHOTOCHEMICAL STUDIES AND THEIR RELATIONSHIP TO THE PHOTOCHEMICAL FORMATION OF COMETARY RADICALS

WILLIAM M. JACKSON
Department of Chemistry
University of California
Davis, California 95616
United States of America

ABSTRACT. Experimental laboratory techniques used in studying the photochemistry of stable and unstable molecules are discussed. The laboratory evidence for the photochemical formation of C_2 from C_2H, C_3 from C_3H_2, and NH from NH_2 is presented. Other recent results obtained in laboratory studies of H_2O, H_2S, NH_3, and HCN are reported.

1. Introduction

The chemistry of comets is dominated by photochemistry (Wurm 1943, Mendis and Houpis 1982), so it is natural that a review of laboratory studies as they relate to comets should also be dominated by photochemistry. Most of the cometary photochemistry occurs under conditions that are very different from the typical conditions used for laboratory photochemical studies. In comets, the photochemical light source is the Sun, with a broad spectral distribution that extends from 300 nm to 140 nm, with a secondary peak at 121.6 nm (Huebner and Carpenter 1979). The density of the gas is low enough that there is a long time between collisions even in the collision regime of the coma, and a large portion of the photochemistry occurs in the collisionless region of the coma. Secondary photolysis of primary products can and often does occur in comets (Cochran 1985, O'Dell et al. 1988), while in the laboratory, attempts are generally made to minimize this. A comet's conditions, of course, cannot really be duplicated in the laboratory, so it is important that systematic laboratory studies of the important molecules are done so the results can be intelligently applied to comets. This is a formidable task because of the wide spectral range that must be covered, the transitory existence of some of the molecules, e.g., free radicals, that must be studied, and the unique internal energies of these molecules. Every modern tool of the photochemist, including lasers and molecular beams, is required to address this problem. Fortunately, there has been a tremendous increase in the

R. L. Newburn, Jr. et al. (eds.), Comets in the Post-Halley Era, Vol. 1, 313–332.

experimental arsenal of the photochemist in recent years, and some of the important questions can now be answered. In this short review, not all of the detailed knowledge about photochemistry that has been recently obtained can be covered, but many good reviews are available (Ashfold and Baggott 1987, Ashfold et al. 1979, Jackson and Okabe 1986, Leone 1982, Okabe 1978, Royal Society of Chemistry 1986, Sato 1986). Instead, the key areas that apply to comets will be identified and discussed with a special emphasis on how the experiments and their theoretical interpretations can be used to enhance our understanding of the chemistry of comets.

Despite the fact there is general agreement that photochemistry is the most important source of radicals in comets, there have been other models that include ion-molecule reactions (Mendis and Houpis 1982). These models explain some of the ions, but are unlikely to explain most of the neutrals (Mendis and Houpis 1982). One problem all of these models have is accounting for the low-density fluid flow of the gas. Supersonic expansion of the gas develops within a few hundred kilometers of the nucleus. Once this happens, unless outside forces intervene, the molecules will not have a component of velocity perpendicular to the flow that is large enough to maintain collisions. It is analogous to two boats moving in a fast flowing river—they will never collide unless there is some turbulence, a rock, etc. The outside forces acting on the molecules flowing in comets are solar photolysis and the solar wind, both of which take time to affect the gas. When these outside forces finally couple to the gas, the density should be low enough that most molecules will undergo only a few collisions.

In the balance of this review, the new experimental techniques of photochemistry will be summarized briefly. This summary will be followed by a discussion of the use of these techniques to study the fundamental photochemical processes that can lead to the formation of cometary radicals such as C_2, C_3, NH, CN, and SH.

2. New Experimental Techniques

2.1. Time-of-Flight (TOF) Photofragment Spectroscopy

The most universal technique for the study of photochemistry is the TOF photofragment spectroscopic technique. This technique combines the wavelength specificity of lasers with molecular beams and the universal detection technique of mass spectrometry. In its most elegant form, the TOF analysis is done as a function of angle so that a momentum balance may be obtained for the two fragments (Wodtke and Lee 1987). From this information, the center-of-mass recoil velocity vectors can be obtained, which then define the amount of internal energy remaining in the fragments. The method requires a fairly intense laser light and a mass spectrometer with a very low background pressure. With this method, however, certain generalizations are possible about the photodissociation process. Molecules that undergo statistical types of dissociation such as predissociation and internal conversion generally release very little of the available energy to the translational degrees of freedom. Molecules that undergo direct dissociation or predissociation into molecular fragments release a great deal of the available energy into the translational recoil motion. The first generalization can be understood in terms of unimolecular reaction theory. Molecules that undergo indirect dissociation and internal conversion will tend to randomize the excitation energy into the internal degrees of

freedom, resulting in the highest probability for dissociation to occur near the energy threshold for the process. As a result, most of the fragments will have very little translational energy and more internal energy.

In direct dissociation, the excited molecule is produced on the repulsive part of an excited potential energy surface, which is significantly above the dissociation limit. Hence, the fragments are produced with large amounts of translational energy. Predissociation into molecular fragments generally requires the excited molecule to overcome an energy barrier in the potential energy surface before it can rearrange itself into stable molecular fragments. The barrier is generally higher than the threshold energy for dissociation, which results in large amounts of translational recoil energy.

The basic disadvantage of this method is its requirement for an intense laser light source. This means that it is difficult to study the effects of energy on the dissociation process, which is particularly important for comets. The situation is further complicated by the fact that the most important wavelength region for comets is below 200 nm where there are few strong laser sources. As more intense vacuum ultraviolet (VUV) laser sources or new sources such as the Advanced Synchrotron Light Source become available, this technique will be increasingly important for cometary studies. Already, as the discussion on the formation of C_2 and C_3 will show, some of the results that have been obtained with this technique can be used to provide key information about some important cometary molecules.

2.2. LASER-INDUCED FLUORESCENCE (LIF) STUDIES

The detection of photochemical fragments using the LIF method has been one of the most successful experimental techniques used in photochemistry (Jackson 1973, Jackson and Cody 1974). This technique has great sensitivity and can be used to detect and identify very low concentrations of fragments formed during photodissociation. The internal energy of the fragments can be characterized, and in favorable cases, the recoil velocity can be measured by determining the Doppler profile of the line. Polarized lasers can be employed to investigate the alignment of fragments during photodissociation, which in turn provides information about the symmetry of the excited states of the parent molecules used to produce the fragments. The use of polarized lasers for both dissociation and characterization can also provide information about the correlation between the recoil velocity vector, $\mathbf{v}$, the electronic transition dipole vector, μ, and the angular momentum vector, $\mathbf{J}$.

The LIF method does have its limitations, despite the wonderful information that can be obtained when it is used. It can only be used for fragments that emit light after being excited to the excited state by the laser. This is less of a problem for cometary science than it is for chemistry in general, because some of the most important cometary fragments—e.g., CH, C_2, OH, H, C, O, C_3, NH_2, CO^+, N_2^+, S_2, and CS—meet this criteria. It is often difficult to analyze a nascent radical spectrum, i.e., one obtained before collisions, because of the complexity of the spectrum when the molecules are rotationally and vibrationally excited. A spectrum can also be complex because of perturbations from other excited states, while another may be complex because the internuclear axis changes between the ground and excited state, resulting in its being spread over thousands of angstroms. The CS molecule is an example of the former case, while the NH_2 radical is an example of the latter case. Finally, to obtain all of the information needed for comets, it is

still important to determine the photochemistry at a variety of wavelengths, because the whole character of the photodissociation process may change within a few hundred angstroms.

2.3. LASER IONIZATION TECHNIQUES

There are several classes of ionization techniques that can be used to study the chemistry occurring during photodissociation. One of these is to use the multi-photon ionization technique to characterize those fragments that do not emit light. In this method, a visible laser is tuned to a wavelength that coincides with a single- or multi-photon resonance in the fragment. After exciting the fragment to the excited state, another photon is used to ionize the fragment. These ions may then be detected and characterized using some type of mass analysis such as a quadrupole or a time-of-flight mass spectrometer.

Another type of ionization technique that can be employed in photochemical studies is the single-photon ionization technique. This generally requires a laser in the VUV region of the spectrum that has enough energy to ionize the fragments. After ionization, the fragments may also be mass-analyzed so that they can be identified. If the laser is tunable, it is often possible to obtain information about the internal energy distribution of the fragments, if the rotational and vibrational states can be resolved.

Other variations on the ionization technique include photoelectron spectroscopy on the recoiling photoelectron. This can often be used to identify the intermediate fragments, as well as obtain information about their internal state.

Some of the same information that is obtained with the LIF method can be obtained with the ionization methods. Time-of-flight analysis can be used to determine the velocity distributions if complicating effects such as stray electric and magnetic fields and space charges can be accounted for or minimized.

Relative population measurements are often difficult to obtain using multi-photon ionization techniques, because of fluctuations in laser power and unknown multi-photon cross-sections. Similar problems can occur with the single photoionization techniques, because laser VUV light is generally obtained by a nonlinear process that reflects itself in large variations of laser intensity. Despite these difficulties, much important and useful information about photochemistry has been obtained using these methods.

3. Recent Photochemical Results

3.1. C_2 FORMATION

Some time ago (Yamamoto 1981), it was suggested that the C_2 radical was formed in comets by the following mechanism:

$$C_2H_2 + h\nu \rightarrow C_2H + H$$
$$C_2H + h\nu \rightarrow C_2 + H$$

Analysis of the radial profiles from the C_2 emission in comets (Cochran 1985, Jackson 1976, Yamamoto 1981) also suggests that a two-step photochemical mechanism is required. Very recent data of O'Dell et al. (1988) suggest that the C_2 emission can be

caused by a three-step dissociation. If this is the case, it is not in accord with the present proposal. It will require a second intermediate radical other than C_2H, which in turn will mean that further laboratory work will be required.

Emissions from the radicals $C_2(C^1\Pi_g)$ (McDonald et al. 1978), $C_2(d^3\Pi_g)$ (Craig et al. 1982, Jackson et al. 1978, Okabe 1975, Okabe et al. 1985), and $CH(A^2\Delta)$ (Craig et al. 1982, Jackson et al. 1978) have been observed during laboratory experiments of the 193-nm laser photolysis of acetylene. There is not enough energy in a single laser photon to produce these excited species, so they must have been produced by a multi-photon process. Both infrared (Fletcher and Leone 1989, Shokoohi et al. 1986) and broadband visible emissions (Ashfold et al. 1979, Becker et al. 1971, Saito et al. 1984, Stief et al. 1965, Urdahl et al. 1988) from the vibrationally and electronically excited C_2H radical have also been observed. Time-of-flight studies of the C_2 and C_2H fragments that are produced during the 193-nm photolysis of C_2H_2 have been performed (Wodtke and Lee 1983). These studies show the primary photochemical process to be the production of the C_2H radical via the first reaction above. No evidence was found for the single-photon production of H_2 and C_2. Recently (Urdahl et al. 1988), LIF and time-resolved emission studies have shown that the yields of $C_2(A^1\Sigma_u)$ and $C_2(a^3\Sigma_u)$ are much greater than the yields of $C_2(C^1\Pi_g)$ and $C_2(d^3\Pi_g)$ radicals. An example of the nascent LIF spectra obtained in these studies is shown in Figure 1. From the time-resolved emission, it was suggested that the $C_2(A^1\Sigma_u)$ and $C_2(a^3\Sigma_u)$ radicals are formed from the same electronic state of C_2H. The $C_2(X^1\Sigma_g^+)$ ground state has been probed by two-photon excitation to the $C_2(C^1\Pi_g)$ state. The two-photon spectrum observed for $C_2(X^1\Sigma_g^+)$ from this process is shown in Figure 2. This spectrum was only observed when the probe laser was delayed 10 microseconds after the photolysis laser, which indicates that the ground state of C_2 is probably being formed as a result of fluorescence from an excited state of the C_2 radical. We have recently used transient infrared spectroscopy to show that $C_2(b^3\Sigma^-_g \rightarrow a^3\Pi_u)$ is also observed when C_2H is photolyzed.

The postulate that C_2 is formed from the photolysis of C_2H was further checked by photolyzing C_2D_2 and CF_3C_2H. As Figure 3 shows, in both cases, the Deslandres-d'Azambuja could be excited using the LIF technique, indicating that the C_2 molecule is being produced. The only common fragment in all three molecules is the C_2H radical, which suggests that it is the source of the observed C_2.

The nascent distributions obtained from the LIF measurements of the C_2 fragments in the photodissociation of the above acetylene derivatives are illustrated in Figure 4. The results indicate that there is very little difference between the observed distributions for the various molecules. All of them are Boltzmann-like in character, indicating that dissociation occurs via a statistical process. This in turn means that dissociation probably occurs via predissociation or internal conversion to the ground state continuum. In such a process, the nascent product state distributions may be calculated using a statistical theory such as phase space theory or the modified phase space theory of Wittig (Buelow et al. 1986). This is an extremely important result for cometary science because it means the dissociation of this free radical in this particular electronic state can be described using these theories as compared to more complex theories (Kresin and Lester 1986; Schinke 1988, 1989a, 1989b). As a result, if the spectroscopy and the electronic state of this radical are known, the photochemistry in this particular band could, in principle, be theoretically calculated.

The distributions in Figure 4 can be decomposed into two statistical distributions. One of these distributions can be characterized by a temperature below room temperature,

(a)

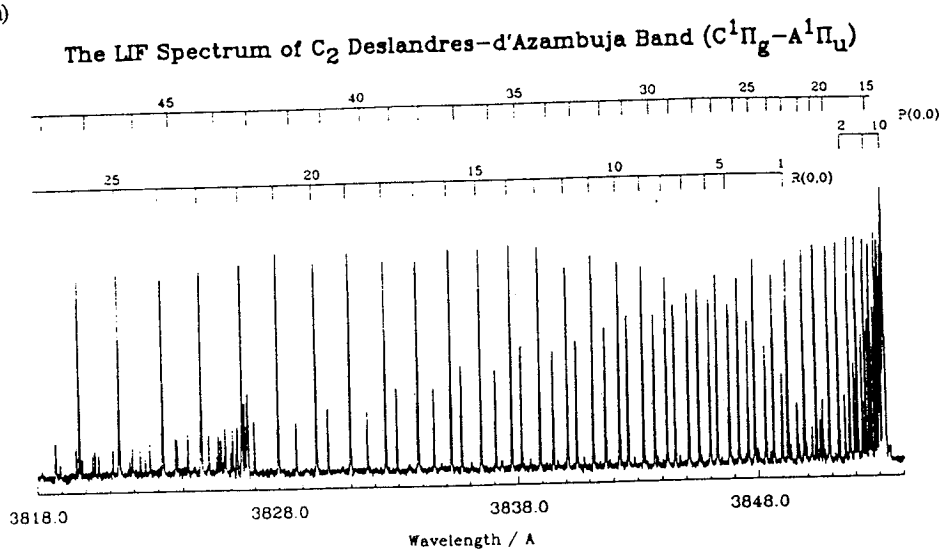

(b)

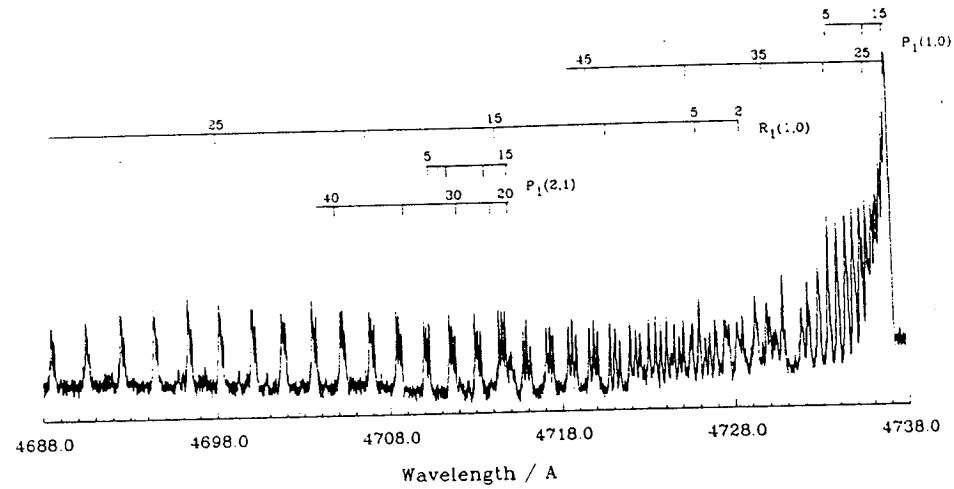

Figure 1. (a) The nascent LIF C_2 spectrum from the 193.3-nm photolysis of C_2H produced in the 193.3-nm photolysis of C_2H_2. (b) The nascent LIF spectrum of the Swan system obtained from the photolysis of C_2H formed in the 193-nm photolysis of C_2H_2.

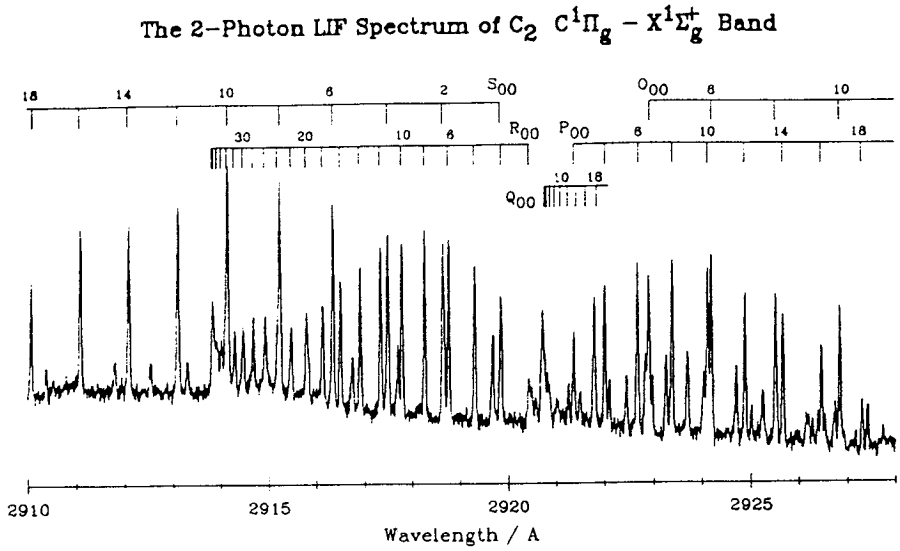

Figure 2. The two-photon spectrum of ground state C_2 is observed only after a 10-microsecond delay, so it is not a nascent product.

and the other by a distribution above room temperature. There is very little change in either of these distributions when the source of the C_2H radical is changed. In the case of the CF_3 radical, the C-C bond dissociation energy is smaller that it is in C_2H_2 or C_2D_2, yet the distributions are very similar. Such a result is understandable on the basis of a statistical theory, because most of the available energy comes when the second 193-nm photon is absorbed. A dynamical explanation of the results should exhibit a more drastic change as the masses change. If a CF_3 radical recoils via a repulsive interaction from an excited CF_3C_2H molecule, the C_2H radical could exhibit a lot of rotational excitation, which in turn should be reflected in the rotational excitation of the C_2 radical. This is evidently not the case in either this molecule or in the C_2D_2 molecule, in agreement with the notion of a statistical dissociation in this absorption band.

The results described above depend upon the C_2H radical being formed vibrationally excited, because the theoretical calculations of Shiu et al. (1979) indicate that a second photon does not have enough energy to excite a linear C_2H fragment to an allowed excited state. However, in the bent configuration, the energy of the excited state that correlates to a C_2 radical in the $A^2\Sigma$ is decreased, so that it could be accessed by a second 193-nm photon. Further experiments are required using vibrationally cold C_2H radicals to determine the wavelengths that can be used for dissociation. Vibrationally cold C_2H radicals are the type of radicals that should be present in comets.

This example illustrates the synergistic relationship between theory, and TOF and LIF observations. It also illustrates how a systematic study using several molecules can help us understand the photochemistry of free radicals.

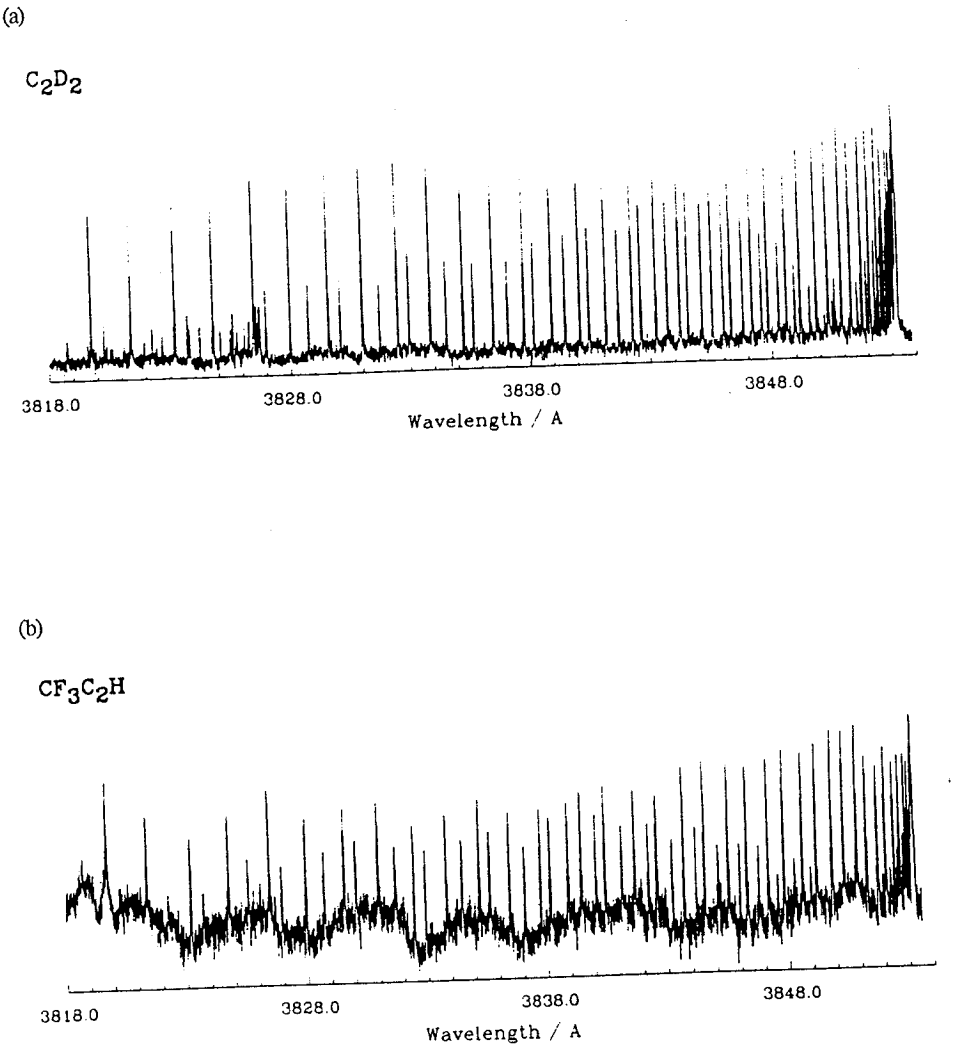

Figure 3. (a) The nascent LIF spectrum of C_2 of the $A^1\Sigma_u$ state formed in the 193.3-nm photolysis of C_2D formed in the 193.3-nm photolysis of C_2D_2. (b) The nascent LIF spectrum of C_2 of the $A^1\Sigma_u$ state formed in the 193.3-nm photolysis of C_2H formed in the 193.3-nm photolysis of CF_3C_2H.

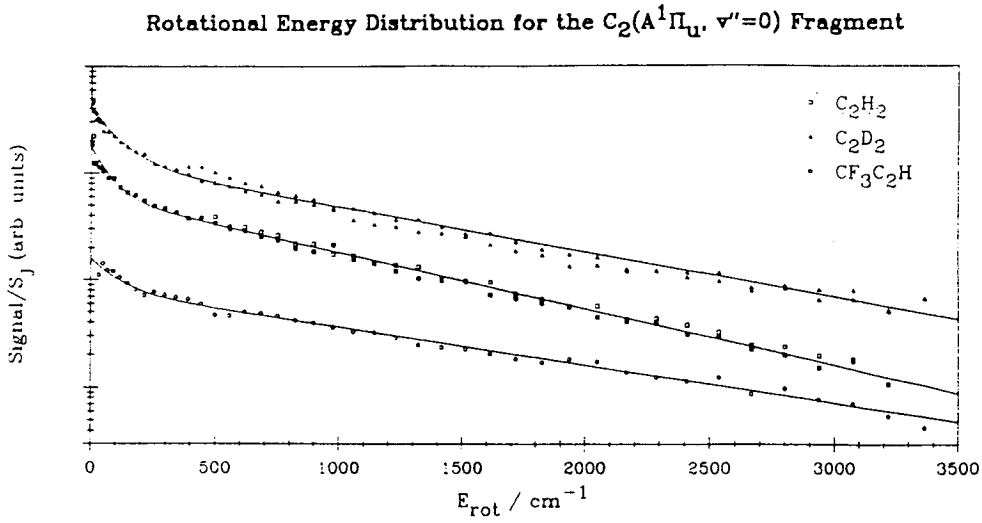

Figure 4. Rotational distributions obtained from the LIF spectrum shown in Figures 1(a) and 3.

It is interesting to compare the laboratory distribution with the rotationally resolved C_2 distribution in the Swan bands obtained from comet Halley (Gredel et al. 1989). It is well-known that the observed rotational distribution of C_2 in comets should be due to resonance fluorescence excitation from solar radiation. The observations suggest that the rotational temperature is lower on the nucleus that it is off the nucleus. It has been suggested that this may be due to shielding of the solar radiation in the inner portion of the coma of the comet by dust. O'Dell et al. (1988) have argued that this is not the case. An alternate explanation is that the nucleus observations have a higher fraction of C_2 radicals that have not undergone many fluorescent cycles and thus are reflective of the rotational distributions originally produced as a result of the photodissociation process that produces the C_2 radical. The C_2 radical should be particularly sensitive to this, since it is a homonuclear molecule and it will not undergo pure rotational and vibrational transitions in the infrared region. Thus, it will lose its original rotational distribution only by many successive electronic transitions. Clearly, the nucleus spectra will have the highest number of radicals that have undergone the least number of electronic transitions.

3.2. C_3 FORMATION

The problem of C_3 formation in comets has also attracted the attention of cometary scientists for years (Marsden 1974). In comets, emission from the C_3 radical is observed before emission from the C_2 radicals as the comet approaches the Sun (Delsemme 1975, Marsden 1974). This radical is probably formed as a result of secondary photolysis of a primary photolytic product, because laboratory investigations indicate that there are no

likely parent molecules that could produce these radicals in a single photochemical step (Jackson 1976, 1982; Payne and Stief 1972). The experiments described above provided firm evidence for the production of C_2 radicals from the photolysis of C_2H during the high-intensity photolysis of C_2H_2. Yet there have been no reports of similar evidence for the C_3 radical. In this section, the results of new experiments will be presented that provide direct confirmation for the production of C_3 via the secondary photolysis of the C_3H_2 radical. The results of these experiments, along with the results of previous experiments, will be discussed in terms of their cometary implications.

The allene molecule, C_3H_4, was chosen as a likely candidate for a parent molecule that may photodecompose to a C_3H_x intermediate, which in turn could absorb a photon to produce the C_3 radical. Earlier infrared (IR) diode laser absorption studies had indicated that this radical is present in a system in which allene is photolyzed with an ArF laser at 193 nm (Matsumura et al. 1988). The conditions under which these experiments were performed did not permit the determination of the photochemistry occurring in the system.

The absorption spectrum of allene (Rabalais et al. 1971) extends up to 260 nm, which means that it overlaps the strong ultraviolet (UV) solar spectrum and suggests this molecule may have a short photochemical lifetime. This is certainly desirable if the C_3 radical is to be produced in comets by the photolysis of a radical produced in the initial photolysis of C_2H_4.

Time-of-flight experiments were performed using two different molecular beam machines. One of these machines is a rotating source machine (RSM), which was specifically designed for photochemical studies (Wodtke and Lee 1987), and was used to detect fragments with masses from m/e = 12 to 39. In the RSM, the allene is seeded in a He carrier gas, and it has a beam velocity of 2×10^5 cm/s. The other beam machine that was used was optimized for the detection of H and H_2 (Continetti 1989), and it employs an unseeded pulsed molecular beam of pure allene. The speed of this beam is about 8×10^4 cm/s, and this machine is designated as the hydrogen beam machine (HBM).

In the RSM, fragment ions with m/e's = 39, 38, 37, 36, and 26 are observed at scattering angles from 7° to 30°. No mass 40 is observed at these angles, proving that the radicals that are observed are not the result of photofragmentation of dimers. A typical set of TOF spectra for masses 39, 38, 37, 36, and 26 that were obtained in these experiments is shown in Figures 5, 6, 7, 8, and 9.

The observation of mass 39 unequivocally shows that the C_3H_3 radical is formed as a primary reaction product in the photolysis of allene. Masses 38, 37, 36, and 26 could have all been due to dissociative ionization of this C_3H_3 fragment in the mass spectrometer ionizer, but the angular distributions of the TOF spectra showed that each of these masses had an additional component due to a new neutral fragment. The identity of these neutral fragments was determined by fitting the TOF measurements at the various angles. These fits were accomplished by using the forward convolution technique that has been described previously (Zhao 1988). The solid curve is the result of the fits with this forward convolution technique. It is made up of time-of-flight curves of the fragments from the following primary and secondary photochemical reactions:

$$C_3H_4 + h\nu \rightarrow C_3H_2 + H_2 \quad (1)$$

$$\rightarrow C_3H_3 + H \quad (2)$$

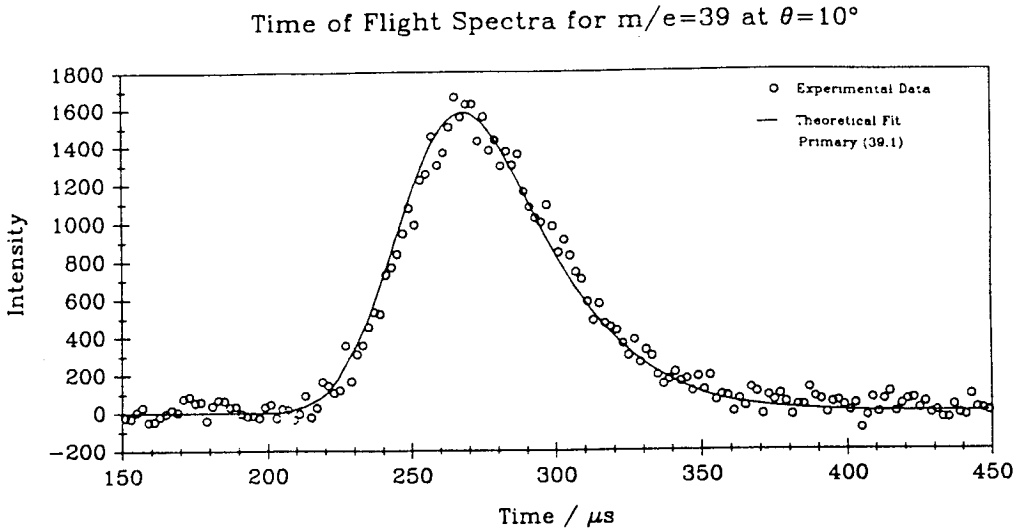

Figure 5. TOF spectrum from the 193.3-nm photolysis of C_3H_4. The theoretical fit is obtained using only one primary channel that produces C_3H_3 and H.

C_3H_3	+	hν	→	C_2H_2	+	CH	(3)
			→	C_3H_2	+	H	(4)
			→	C_3H	+	H_2	(5)
C_3H_2	+	hν	→	C_3H	+	H	(6)
			→	C_3	+	H_2	(7)

A fit was considered successful only if the derived translational energy distribution would fit both fragments at all of the observed laboratory angles. This means, e.g., the same translational energy distribution must be able to fit the data for mass 26 and mass 13 in reaction 3. The translational energy distributions for reactions 1, 2, 4, 5, 6, and 7 also fit the mass 1 and 2 time-of-flight spectra.

The translational energy distributions derived from these fits are given in Figure 10. Reaction 2 leads to the formation of a H atom and C_3H_3, and the translational energy distribution is peaked at low translational energies with a long exponential tail. The shape of the translational energy curve for the H atom in Reaction 4 is the same, but it has been shifted out to larger energies. A H atom is also produced in Reaction 6, and it has a $P(E_T)$ that is very similar to the translational energy curve for Reaction 4. This systematic shifting of the $P(E_T)$ to higher energies, when the fragment absorbs a second photon, is also apparent in the H_2 channels, as a comparison of the $P(E_T)$ for Reactions 1, 5, and 7 shows. In this case, however, the initial $P(E_T)$ for the first fragment via Reaction 1 starts out at higher energies. The reaction that produces the CH radical and the C_2H_2 molecule is also peaked at low energies, which is consistent with its being a free-radical elimination

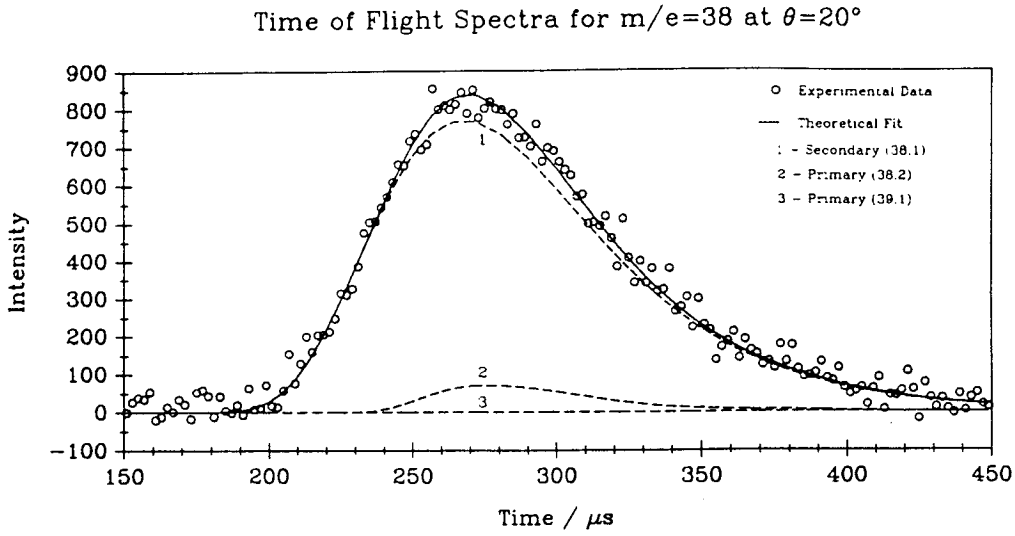

Figure 6. TOF spectrum from the 193-nm photolysis of C_3H_4. Three channels are needed for the theoretical fit: two primary channels and one secondary channel.

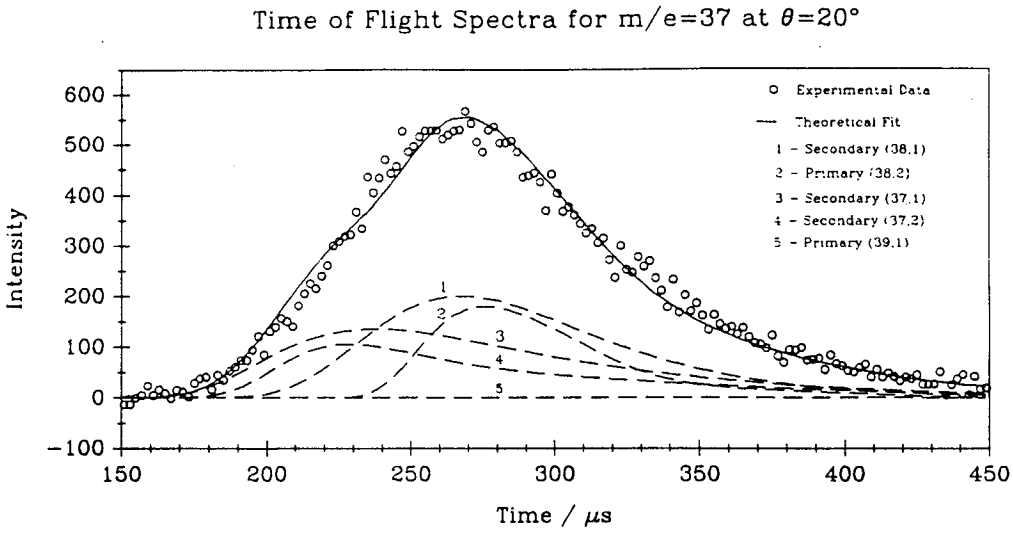

Figure 7. TOF spectrum from the 193.3-nm C_3H_4 photolysis. Five channels are needed for the fit: two primary and three secondary channels.

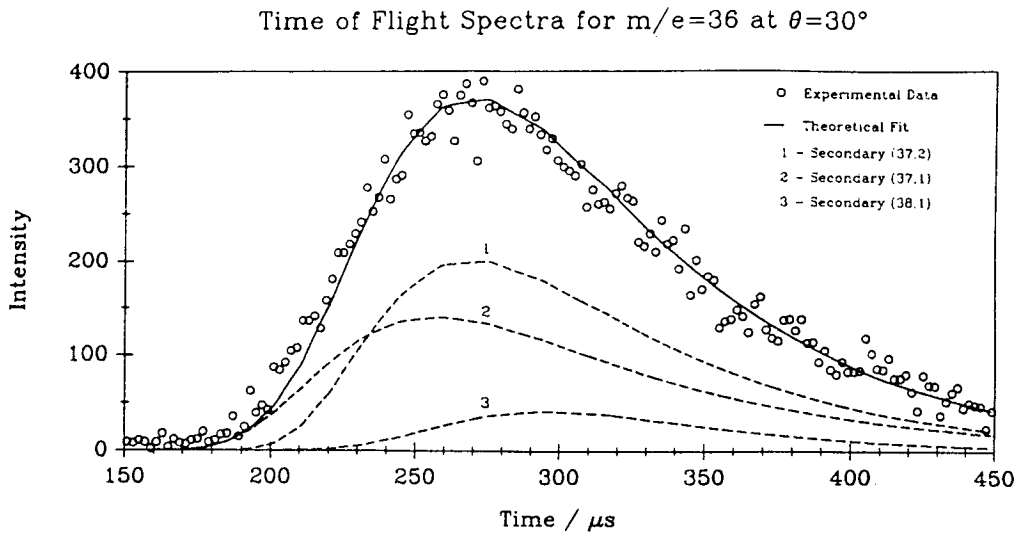

Figure 8. TOF spectrum from the 193.3-nm photolysis of allene. Four secondary channels are required to fit the data.

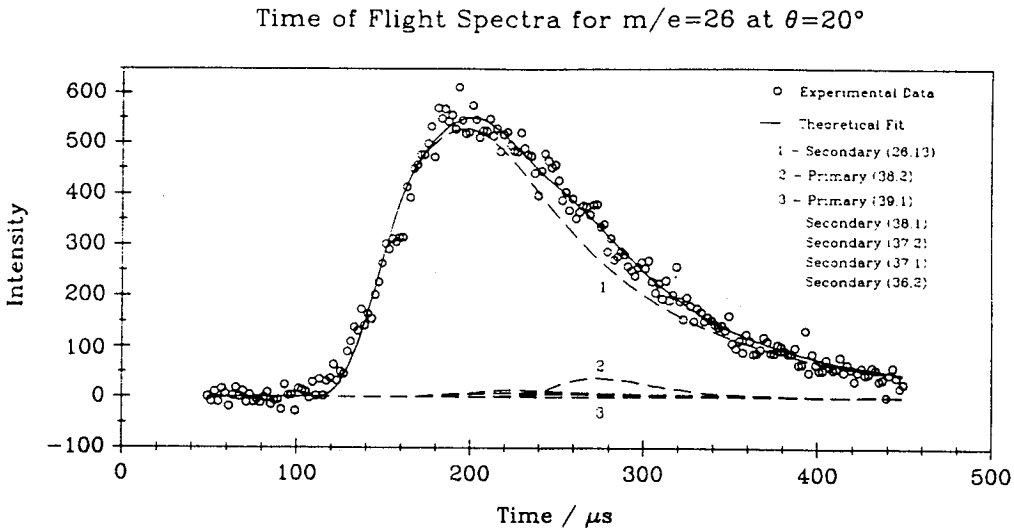

Figure 9. TOF spectrum from the photolysis of C_3H_4 at 193.3-nm. The principal channel that fits this data produces CH and C_2H_2 from C_3H_3.

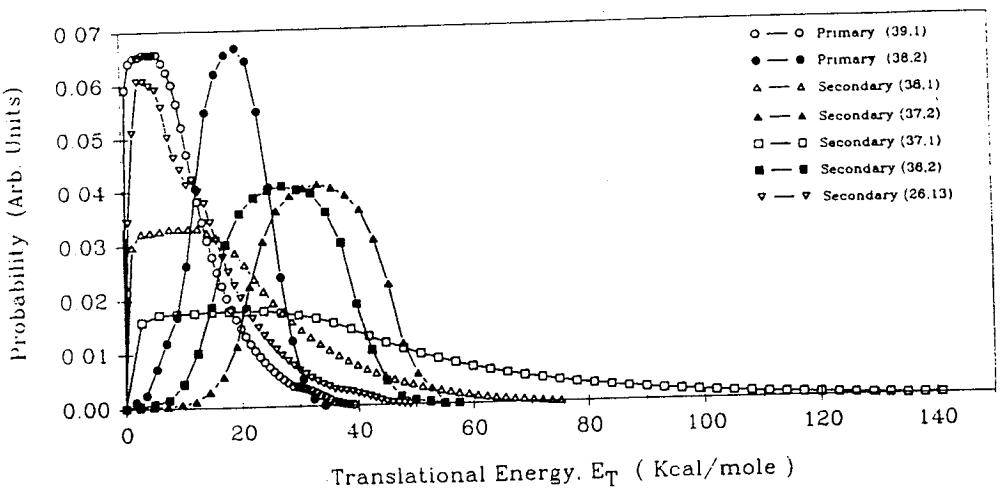

Figure 10. Translational energy distributions derived from fitting all of the data at all masses and angles.

reaction. These observations are all compatible with the earlier generalizations about energy distributions in photochemical reactions.

Reaction 3 is of particular interest to cometary science, since it suggests an alternate means of producing a CH radical in comets. Recent radio observations of the interstellar medium suggest that cyclopropenylidene (C_3H_2) is widespread throughout the galaxy (Madden et al. 1989). Thus, it is not unreasonable to suppose that the cyclic C_3H_3 is also widely dispersed. It is thought that it is this cyclic version of the C_3H_3 radical that is being photolyzed in Reaction 3.

3.3. PHOTOCHEMISTRY OF WATER

The photochemistry of water has recently been reviewed by Crovisier (1989), and he has covered most of the published results. The detailed dynamics for the photodissociation in the first absorption continuum have been studied at 157 nm in great detail by Andresen and his colleagues (Andresen and Schinke 1987). From the structure in the absorption band and the theoretical potential energy curve, it is doubtful whether there will be surprises in the photochemistry in this region. One should be able to get a good idea about the energy partitioning in the fragments by using the theoretical curve and current theories for photodissociation. However, since even at this level, approximations have to be made in the theory, it is probably a good idea if the theoretical predictions are checked at another wavelength. This, of course, will require a laser at a wavelength between 180 nm and 140 nm.

While the water photochemistry and the energy partitioning among the fragments are known in the first continuum, they have not been completely described at 121.6 nm, which is the second most important photochemical region for H_2O (Krautwald et al. 1986).

It is known that the reaction channel leading to OH in the $A^2\Sigma^+$ state represents only about 10% of the total quantum yield. Recent measurements of the recoil velocity by determining the Doppler width of the laser-induced fluorescence of the recoiling H atom suggest the average kinetic energy in the H atom is 1.29 ± 0.3 eV (Krautwald 1986). This is the velocity of the H atom coming from the channel that produces $OH(X^2\Pi)$ state. The H atom associated with the $OH(A^2\Sigma^+)$ has a much lower recoil velocity of 0.26 eV, which was not detected. Nevertheless, this gives us the information to analyze the hydrogen coma in comets. These results indicate that $OH(X^2\Pi)$ radical is produced highly rotationally excited and explains why it cannot be detected using LIF, since the higher rotational levels of the $A^2\Sigma^+$ are strongly predissociated and do not emit.

3.4. PHOTOCHEMISTRY OF AMMONIA

The photoionization TOF flight method for determining the energy partitioning has also been used by two groups to determine the energy partitioning in the photodissociation of NH_3. These studies have been carried out by Wittig and his colleagues at 193 nm (Xu et al. 1989) and Welge and his colleagues (Biesner et al. 1988, 1989) at a variety of different wavelengths. Energy partitioning between the H atom and the NH_2 radical is not simply described. Near-threshold tunneling occurs, and the internal energy distribution of the NH_2 fragment reflects this. Changes occur when the NH_3 molecule is excited to different vibrational and rotational levels of the excited state. However, as the photolysis energy increases, tunneling becomes less important, and the internal energy distribution is peaked at higher vibrational levels, in accord with our previous expectations for simple bond rupture.

Even though the NH_2 radical absorbs and emits light in the visible region of the spectrum, LIF studies have not been very successful in determining the nascent internal energy after photolysis. The reason for this difficulty is that NH_2 is produced with a large amount of internal energy as a result of the photodissociation process. Because of this, many different vibrational bands have to be measured over hundreds of angstroms, which requires many different dyes and very long scans. Quantitative results also require calibration of the detection system over this large wavelength range. Analysis is hence more complicated, so the TOF methods have a unique advantage for this particular molecule. This case illustrates in particular how many different techniques are necessary to completely unravel the photochemistry.

3.5. NH_2 PHOTOLYSIS AND THE FORMATION OF NH IN COMETS

Many years ago, it was suggested that NH was formed in comets by the sequential photolysis of NH_3 via the following type of mechanism (Jackson 1976):

$$NH_3 + h\nu \rightarrow NH_2 + H$$
$$NH_2 + h\nu \rightarrow NH + H$$

Recently, wavelength-resolved fluorescence studies using two ArF lasers at 193 nm have shown that this mechanism is correct at least for $NH(A^3\Pi)$ state radicals (Kenner et al. 1988). The researchers found that the lambda doublet population is preferentially populated in the antisymmetric lambda doublet. As discussed above, it is known that the

NH_2 radical is produced with considerable internal energy. The researchers point out that cold $NH_2(X^2B_1)$ should show different photodissociation dynamics. In this case, the alignment will be higher, the symmetric lambda doublet should be preferentially populated, and the rotational excitation will decrease as more energy appears in the translational degrees of freedom. These studies with cold NH_2 have not been done, and it will be interesting to see if these predictions are correct when the studies are performed. The predictions do point out, however, the importance of carrying out photodissociation dynamics studies with cold free radicals, since these are the radicals that are expected to be present in the coma of comets and the dynamics can be dependent upon the internal energy of the radical.

The work on NH_2 that has been reported thus far is for electronically excited NH. It is important to determine if dissociation of this radical leads to ground-state NH, and if it does, what the dynamics will be. Other questions will arise if ground-state NH is produced, such as "what is the branching ratio between the two channels as a function of wavelength?" and "if the dynamics are different between these two channels, do the dynamics change as the wavelengths change?" These are important questions that will have to be answered successfully to model the NH emission in comets.

3.6. SH Formation and Destruction

There have been four recent results on the photochemistry of H_2S, which is thought to be the parent of SH in comets (Continetti 1989, Weiner et al. 1989, Xie et al. 1989, Xu et al. 1989). Three of these studies used some type of time-of-flight technique, while the other used laser-induced fluorescence to measure the rotational population of the SH radical in the v" = 0 level. The TOF studies resolved the vibrational distribution of the SH and the spin orbit population of the SH radical. One of these TOF studies showed that the peak of the translational energy distribution decreases with decreasing amounts of available energy, but in all cases it is peaked away from zero (Kenner et al. 1988). This is unlike most radical elimination processes. The LIF study determined the rotational distribution at several different wavelengths, and the researchers found the average rotational energy decreases with decreasing energy (Xu et al. 1989). In both of these studies, a detailed model is presented to interpret the results. In one of the TOF studies, the laser fluence was high enough so that secondary photolysis of the SH radical was observed, but the data have yet to be analyzed.

3.7. Photochemistry of HCN

Radio observations of comets prove that HCN is present in comets (Huebner et al. 1974). In the solar radiation field, most of this HCN will be dissociated at Lyman alpha (121.6 nm) (Bockelee-Morvan and Crovisier 1985, Jackson 1973). The branching ratios for the three reactions that produce CN in the $X^2\Sigma$, $A^2\Pi$, and $B^2\Sigma$ states have been determined from the TOF spectra of the H atom to be 0.43, 0.45, and 0.12, respectively. The same spectra were used to determine the vibrational and rotational populations for the channel that produces CN in the $X^2\Sigma$ state. The relative populations of the v" = 0, 1, 2, and 3 levels were found to be 1.0, 0.6, 0.3, and 0.1, respectively. The rotational population of the v" = 0 level peaks at N" = 40 and decreases sharply on both sides of

this peak. The vibrational and rotational distributions of the $A^2\Pi$ could not be unambiguously determined from the data.

4. Conclusions

Great progress has been made in understanding the photochemistry of some of the key stable molecules that are responsible for the radicals that are observed in comets. A variety of techniques have been used to determine the primary reaction products and the partitioning of energy among the fragments. In some cases, these studies need to be extended to molecules with the vibrational and rotational energy appropriate to comets, and in other cases, the effects of photolysis wavelength need to be carefully determined. No experimental technique appears to be completely satisfactory for obtaining all of the required data, but the H-atom photoionization TOF method of K. Welge (Krautwald 1986, Krautwald et al. 1986) and the angular TOF method of Y.T. Lee (Wodtke and Lee 1987) both appear to be extremely powerful tools for cometary photochemistry.

The situation is less satisfactory for those radicals that are granddaughter species, which means they are formed by photodissociation of unstable free radicals. Even so, progress has been made in this sphere, with laboratory evidence for the formation of C_2, C_3, and NH from the secondary photolysis of C_2H, C_3H_2, and NH_2. More work needs to be done with the photolysis of the cold precursor radicals at a variety of different wavelengths. Absorption spectra of the intermediate radicals at wavelengths where they dissociate are desperately needed to be able to evaluate the profiles of the granddaughter radicals.

Theoretical advances in photochemistry have also been made, and as these are put on firmer footing by comparisons with a body of experimental data, they will be more useful for cometary sciences. Already, the experimental and theoretical advances can probably adequately describe for comets the photochemistry of H_2O. Newer experimental techniques such as the Advanced Synchrotron light source, stronger VUV lasers based upon resonance sum frequency generation, and pulsed rare-gas dimer lasers will probably accelerate our knowledge of photochemistry and hence the chemistry of comets.

5. Acknowledgments

The author gratefully acknowledges the Guggenheim Foundation, the Miller Foundation, and the Planetary Atmospheres program of NASA under grant number NSG-903 for their support when this review was written. He also acknowledges Deon Anex, Barbara Balko, and Robert Continetti for their assistance in taking and analyzing the allene data and Y.T. Lee for his hospitality, encouragement, and advice during this time. The experimental LIF work on C_2 was obtained by the author's graduate students Randy Urdahl and Yihan Bao. Last but not least, the author would like thank K. Welge and F. Sthul for their helpful discussions and the sharing of data about their experiments.

References

Andresen, P., and Schinke, R. (1987). 'Dissociation of Water in the First Absorption Band: A Model System for Direct Photodissociation,' in Molecular Photodissociation Dynamics: Advances in Gas-Phase Photochemistry and Kinetics, M.N.R. Ashfold and J.E. Baggott (eds.), Royal Society of Chemistry, London, pp. 61–113.

Ashfold, M.N.R., and J.E. Baggott, eds. (1987). Molecular Photodissociation Dynamics: Advances in Gas-Phase Photochemistry and Kinetics, Royal Society of Chemistry, London.

Ashfold, M.N.R., M.T. Macpherson, and J.P. Simons (1979). 'Photochemistry and Spectroscopy of Simple Polyatomic-Molecules in the Vacuum Ultraviolet,' Topics in Current Chemistry, 86, 1–90.

Becker, K.H., D. Haaks, and M. Schurgers (1971). 'Fluorescence by the Vacuum-UV Photolysis of Acetylene,' Z. Naturforsch., A 26, 1770.

Biesner, J., L. Schnieder, J. Schmeer, G. Ahlers, X. Xie, K.H. Welge, M.N.R. Ashfold, and R.N. Dixon (1988). 'State Selective Photodissociation Dynamics of A State Ammonia. I,' J. Chem. Phys., 88, 3607–3616.

Biesner, J., L. Schnieder, G. Ahlers, X. Xie, K.H. Welge, M.N.R. Ashfold, and R.N. Dixon (1989). 'State Selective Photodissociation Dynamics of A State Ammonia. II,' to be submitted to J. Chem. Phys.

Bockelee-Morvan, D., and J. Crovisier (1985). 'Possible Parents for the Cometary CN Radical: Photochemistry and Excitation Conditions,' Astron. Astrophys., 151, 90–100.

Buelow, S., M. Noble, G. Radhakrishnan, H. Reisler, C. Wittiz, and G. Hancock (1986). 'The Role of Initial Conditions in Elementary Gas-Phase Processes Involving Intermediate "Complexes",' J. Phys.Chem., 90, 1015–1027.

Cochran, A.L. (1985). 'C_2 Photolytic Processes in Cometary Comae,' Astrophys. J., 289, 388–391.

Continetti, R.E. (1989). Ph.D. Thesis, University of California.

Craig, B.B., W.L. Faust, and L.S. Goldberg (1982). 'UV Short Pulse Fragmentation of Isotopically Labeled Acetylene: Studies of Emission With Subnanosecond Resolutions,' J. Chem. Phys., 76, 5014–5021.

Crovisier, J. (1989). 'The Photodissociation of Water in Cometary Atmospheres,' Astron. Astrophys., 213, 459–464.

Delsemme, A.H. (1975). 'The Volatile Fraction of the Cometary Nucleus,' Icarus, 24, 95.

Fletcher, T.R., and S.R. Leone (1989). 'Photodissociation of C_2H_2 at 193 nm: Vibrational Distributions of the CCH Radical and the Rotational State Distribution of the A(101) State by Time-Resolved Fourier Transform Emission,' J. Chem. Phys., 90, 871–879.

Gredel, R., E.F. van Dishoeck, and J.H. Black (1989). 'Fluorescent Vibration-Rotation Excitation of Cometary C_2,' Astrophys. J., 338, 1047–1070.

Huebner, W.F., and C.W. Carpenter (1979). 'Solar Photo Rate Coefficients,' Rep. LA-8085-MS, Los Alamos Sci. Lab., Los Alamos, New Mexico.

Huebner, W.H., L.E. Snyder, and D. Buhl (1974). 'HCN Radio Emission From Comet Kohoutek (19737),' Icarus, 23, 580–584.

Jackson, W.M. (1973). 'Laser Induced Fluorescence of CN Radicals,' J. Chem. Phys., 59, 960–961.

Jackson, W.M. (1976). 'The Photochemical Formation of Cometary Radicals,' J. Photochem., 5, 107–118.
Jackson, W.M. (1982). 'Laboratory Studies of Photochemistry,' in Comets, L.L. Wilkening (ed.), University of Arizona Press, Tucson, pp. 480–495.
Jackson, W.M., and R.J. Cody (1974). 'Laser Photoluminescence Spectroscopy of Photodissociation Fragments,' J. Chem. Phys., 61, 4183–4185.
Jackson, W.M., and H. Okabe (1986). 'Photodissociation Dynamics of Small Molecules,' in Advances in Photochemistry, D.H. Volman, G.S. Hammond, and K. Gollnick (eds.), John Wiley and Sons, New York, 13, pp. 1–94.
Jackson, W.M., J.B. Halpern, and C.S. Lin (1978). 'Multiphoton UV Photochemistry,' Chem. Phys. Lett., 55, 254.
Kenner, R.D., R.K. Browarzik and F. Sthul (1988). 'Two Photon Formation of NH/ND($A^3\pi$) in the 193 nm Photolysis of Ammonia II. Photolysis of NH_2,' J. Chem. Phys., 121, 457–471.
Krautwald, H.-J. (1986). 'Photodissoziationasdynamik einfacher Hydrid-Molekule im Vakuumultravioletten Spektralbereich,' Fakultat fur Physik Universitat Bielefeld.
Krautwald, H.-J., L. Schnieder, K. Welge, and M.N.R. Ashfold (1986). 'Hydrogen-Atom Photofragment Spectroscopy,' Faraday Discus. Chem. Soc., 82, 99–110.
Kresin, V.Z., and W.A. Lester, Jr. (1986). 'Quantum Theory of Polyatomic Photodissociation,' in Advances in Photochemistry, D.H. Volman, G.S. Hammond, and K. Gollnick (eds.), John Wiley and Sons, New York, 13, pp. 95–163.
Leone, S.R. (1982). 'Photofragment Dynamics,' in Advances in Chemical Physics, K.P. Lawley (ed.), John Wiley and Sons, Chichester, 50, p. 255.
Madden, S.C., W.M. Irvine, H.E. Matthews, P. Friberg, and D.A. Swade (1989). 'A Survey of Cyclopropenylidene (C_3H_2) in Galactic Sources,' Astron. J., 97, 1403–1422.
Marsden, B.G. (1974). 'Comets,' Ann. Rev. of Astron. and Astrophys., 12, 1–21.
Matsumura, K., H. Kanamori, K. Kawaguchi, and E. Hirota (1988). 'Infrared Diode Laser Kinetic Spectroscopy of the ν_3 Band of C_3,' J. Chem. Phys. 89, 3491–3494.
McDonald, J.R., A.P. Baronavski, and V.M. Donnelly (1978). 'Multiphoton VUV Laser Photodissociation of C_2H_2: Emission From Electronically Excited Fragments,' Chem. Phys., 33, 161.
Mendis, D.A., and H.L.F. Houpis (1982). 'The Cometary Atmosphere and its Interaction With the Solar Wind,' Rev. of Geophys. and Space Phys., 20, 885–928.
O'Dell, C.R., R.R. Robinson, K.S.K. Swamy, P.J. McCarthy, and H. Spinard (1988). 'C_2 in Comet Halley: Evidence for its Being Third Generation and Resolution of the Vibrational Population Discrepancy,' Astrophys. J., 334, 476–488.
Okabe, H. (1975). 'Photodissociation of C_2H_2 and C_2H Br in the VUV. Production of Electronic Excitation of C_2H and $C_2{}^1$,' J. Chem. Phys., 62, 2782.
Okabe, H. (1978). Photochemistry of Small Molecules, John Wiley and Sons, New York.
Okabe, H., R.J. Cody, and J.E. Allen (1985). 'Laser Photolysis of C_2H_2 and CF_3C_2H at 193 nm: Production of $C_2(d^3\Pi_g)$ and $CH(A^2\Delta)$ and Their Quenching by Xe,' Chem. Phys., 92, 67.
Payne, W.A., and L.J. Stief (1972). 'Hydrogen Formation in the Photolysis of Propyne at 1236 A,' J. Chem. Phys., 56, 3333–3336.

Rabalais, J.W., J.M. McDonald, V. Scheer, and S.P. McGlynn (1971). 'Electronic Spectroscopy of Isoelectronic Molecules. II. Linear Triatomic Groups Containing Sixteen Valence Electrons,' Chem. Rev., 71, 73–108.

Royal Society of Chemistry (1986). Dynamics of Molecular Photofragmentation, Faraday Discussions of the Chemical Society, The Royal Society of Chemistry, London, Number 82.

Saito, Y., T. Hikida, T. Ichimura, and Y. Mori (1984). 'Fluorescence of Excited Ethynyl Radicals Produced by the Pulsed VUV Photolysis of C_2H_2, C_2D_2, and C_2HBr,' J. Chem. Phys., 80, 31.

Sato, H. (1986). 'Photodissociation of Simple Molecules in the Gas Phase,' Research Reports of the Faculty of Engineering, Mie Univ., 11, 123–173.

Schinke, R. (1988). 'Rotational Distributions in Direct Molecular Photodissociation,' Ann. Rev. Phys. Chem., 39, 39–68.

Schinke, R. (1989a). 'Dynamics of Molecular Photodissociation,' in Collision Theory for Atoms and Molecules, F.A. Gianturco (ed.), Plenum, New York, pp. 229–285.

Schinke, R. (1989b). 'Rotational Excitation in Direct Photodissociation and its Relation to the Anisotropy of the Excited State Potential Energy Surface. How Realistic Is the Impulsive Model?', Comments, At. Mol. Phys., 23, 15–44.

Shiu, S., S.D. Peyerimhoff, and R.J. Bunker (1979). 'Calculated Potential Surfaces for the Description of the Emission Spectrum of the C_2H Radical,' J. Molec. Spectr., 74, 124–135.

Shokoohi, F., T.A. Watson, H. Reisler, F. Kong, A.M. Renlund, and C. Wittig (1986). 'Photolytic Production of C_2H: Collisional Quenching of $A^2\Pi \rightarrow x^2\Sigma^+$ Infrared Emission and the Removal of Excited C_2H,' J. Phys. Chem., 90, 5695.

Stief, L.J., V.J. DeCarlo, and R.J. Mataloni (1965). 'Vacuum-Ultraviolet Photolysis of Acetylene,' J. Chem. Phys., 42, 3113–3121.

Urdahl, R.S., Yihan Bao, and W.M. Jackson (1988). 'Observation of the LIF Spectra of $C_2(a^3\Pi_u)$ and $C_2(a^1\Pi_u)$ From the Photolysis of C_2H_2 at 193 nm,' Chem. Phys. Lett., 152, 485–490.

Weiner, B.R., H.B. Levine, J.J. Valentini and A.B. Baronavski (1989). 'Ultraviolet Photodissociation Dynamics of H_2S and D_2S,' J. Chem. Phys., 90, 1403–1414.

Wodtke, A.M., and Y.T. Lee (1983). 'Photodissociation of Acetylene at 193.3-nm,' J. Phys. Chem., 85, 4744–4751.

Wodtke, A.M., and Y.T. Lee (1987). 'High Resolution Photofragmentation Translational Spectroscopy,' in Advances in Gas-Phase Photochemistry and Kinetics, Molecular Photodissociation Dynamics, M.N.R. Ashfold and J.E. Baggott (eds.), Royal Society of Chemistry, London, pp. 31–59.

Wurm, K. (1943). 'Die Natur der Kometen,' Mitt. Hamb. Sternwartz, 8, Nr, 51.

Xie, X., L. Schnieder, H. Wallmeir, U. Bottner, K.H. Welge, and M.N.R. Ashfold (1989). Photodissociation Dynamics of $H_2S(D_2S)$ Following Excitation Within its First Continuum,' submitted to J. Chem. Phys.

Xu, Z., B. Koplitz and C. Wittig (1989). 'Velocity-Aligned Doppler Spectroscopy,' J. Chem. Phys., 90, 2692–2702.

Yamamoto, T. (1981). 'On the Photochemical Formation of CN, C_2, and C_3 Radicals in Cometary Comae,' The Moon and the Planets, 24, 453–463.

Zhao, X. (1988). 'Photodissociation of Cyclic Compounds in a Molecular Beam,' Lawrence Berkeley Laboratory Report, LBL-26332, Berkeley, California.

JOURNAL OF GEOPHYSICAL RESEARCH, VOL. 96, NO. E2, PAGES 17,569–17,572, SEPTEMBER 25, 1991

Implications of C_2H Photochemistry on the Modeling of C_2 Distributions in Comets

WILLIAM M. JACKSON, YIHAN BAO, AND RANDALL S. URDAHL

Department of Chemistry, University of California at Davis

Laboratory studies of the secondary photolysis of the C_2H radical are summarized and used to explain some discrepancies between models of C_2 emission in comets. These studies show that several states of the C_2 radicals produced in the photolysis of C_2H_2 at 193 nm have bimodal rotational distributions when plotted as a Boltzmann diagram. They also establish that the C_2 radicals are formed with varying degrees of vibrational excitation, so that if they are formed in a similar manner in comets, the C_2 radicals must start out with this initial vibrational excitation.

INTRODUCTION

The C_2 radical has been observed in comets for many years, but its origin and the detailed modeling of the spatial distribution of its emission are continuing problems. Earlier, *Jackson* [1976] suggested that this radical was formed by a two-step photodissociation involving C_2H_2 and C_2H via the following general mechanism:

$$C_2H_2 + h\nu \text{ ---> } C_2H + H \quad (1)$$

$$C_2H + h\nu \text{ ---> } C_2 + H \quad (2)$$

Subsequent to this postulate, both laboratory experiments and observational studies have confirmed that this is a viable mechanism for the formation of C_2 radicals in comets [*Jackson et al.*, 1978; *Wodtke and Lee*, 1985; *McDonald et al.*, 1978; *Cochran*, 1985]. Recently, high-quality studies of both the rotational and spatial distributions of this radical have been obtained [*Lambert et al.*, 1990; *O'Dell et al.*, 1988]. These studies have resulted in attempts to match the observed rotational and vibrational distributions with models of the radiative processes that excite the C_2 radicals in comets. All of these models have assumed that the radicals start in the lowest vibrational and rotational state before radiation pumping by the Sun begins. In this paper, laboratory evidence is presented which suggests that this is probably not the case and as a result these models need to be revised.

EXPERIMENTAL RESULTS

The first laboratory demonstration of the two-step mechanism for the formation of the C_2 radical was the observation of the Phillips and Swan bands in the two-photon dissociation of C_2H_2 at 193 nm [*Jackson et al.*, 1978; *McDonald et al.*, 1978], although it could not be decided between a sequential or simultaneous two-photon process. Later, using the photofragment time-of-flight method, *Wodtke and Lee* [1985] showed that the dominant one-photon process was the production of the C_2H radical via reaction (1) and at high fluxes the C_2 radical via reaction (2). *Balko et al.* [1991] have recently confirmed this result using the same method but detecting the H atom instead of the C_2H and C_2 radicals. Previous work in our laboratory shows that in addition to the $A^1\Pi_u$ state, other electronic states are formed such as the $a^3\Pi_u$, $b^3\Sigma_g^-$, and $B'^1\Sigma_g^+$ [*Urdahl et al.*, 1988; *Bao et al.*, 1991; M. Zahedi et al., unpublished data, 1990]. Most recently, we observed the vibrationally excited $C_2(a^3\Pi_u)$ state up to $v = 8$ in the photodissociation of C_2H_2 at 193 nm. *Goodwin and Cool* [1989] have shown by the resonance-enhanced multiphoton ionization (REMPI) technique that the $B^1\Delta_g$ state is also produced.

In addition to the identification of electronic states, the laser-induced fluorescence (LIF) technique used in our laboratory can also be employed to determine the nascent rotational and vibrational distribution of the C_2 radicals in these states. Table 1 summarizes the experimental information that has been obtained thus far for the production of C_2 from the photolysis of C_2H at 193 nm. This is qualitative evidence that excitation of the C_2H by a photon with energy of the order of 57,000 cm^{-1} should give a variety of electronic states of C_2 in a multitude of vibrational and rotational levels. It is clear from Table 1 that not only are many electronic states of C_2 formed but also a large number of rotational and vibrational levels within each electronic state are formed. In some of these electronic states, notably the $A^1\Pi_u$ and $B'^1\Sigma_g^+$, the rotational distributions exhibit bimodal Boltzmann temperatures. There is also evidence that when other molecules such as C_2D_2 and CF_3C_2H are used as precursors for C_2H/C_2D, similar bimodal behavior can be observed for the $A^1\Pi_u$. These observations suggest that the bimodal behavior is a function of the electronic state of the C_2H produced and not a property of the precursor used to generate the C_2H radical itself. In the next section, we will discuss the implications of these results for C_2 modeling in comets.

COMETARY IMPLICATIONS

The energy level diagram for all the C_2 electronic states observed in the 193 nm photodissociation of C_2H is given

Paper number 91JE01677.
0148-0227/91/91JE-01677$05.00

TABLE 1. Summary of the Experimental Observations of the Quantum State Distribution of C_2 Formed in the Photolysis of C_2H

State	Observation	Method	References
$A^1\Pi_u$	v=1 to 5	emission	*McDonald et al.* [1978]
			Bauer et al. [1985]
	v=0 to 4	REMPI	*Goodwin and Cool* [1988]
	v=0 to 4	LIF	*Urdahl et al.* [1988]
			R.S. Urdahl et al. (unpublished data, 1991)
	rot. dist.[a]	LIF	*Urdahl et al.* [1989]
$B^1\Delta_g$	v=0 to 2	REMPI	*Goodwin and Cool* [1989]
$B'^1\Sigma_g^+$	v=0 to 2	LIF	*Bao et al.* [1991]
	rot. dist.[b]	LIF	R.S. Urdahl et al. (unpublished data, 1991)
$a^3\Pi_u$	v=0 to 8	LIF	*Urdahl et al.* [1988]
			R.S. Urdahl et al. (unpublished data, 1991)
	rot. dist.[c]	LIF	*Urdahl et al.* [1989]
$b^3\Sigma_g^-$	v=0 to 4	REMPI	*Goodwin and Cool* [1989]
	v=1 to 4	IR emission	M. Zahedi et al. (unpublished data, 1990)

[a] Rotational distribution: bimodal Boltzmann (for v=0, T_1=100 K, T_2=1200 K)

[b] Rotational distribution: bimodal Boltzmann (for v=0, T_1=40 K, T_2=470 K; for v=1, T_1=10 K, T_2=280 K)

[c] Rotational distribution: Boltzmann (for v=0, T=2620 K)

in Figure 1. The highest electronic states so far observed in the singlet and triplet manifolds are the $B'^1\Sigma_g^+$ and $b^3\Sigma_g^-$, respectively. Although we have some unidentified LIF spectra that may be due to the $c^3\Sigma_u^+$ state, the basic points of this paper can be made even if we confine our discussion only to the states that have been positively identified.

In the cometary environment, the time between collisions is long compared to the radiative lifetime for an allowed electronic transition. There are allowed electronic transitions between the $B'^1\Sigma_g^+$ - $A^1\Pi_u$, the $B^1\Delta_g$ - $A^1\Pi_u$, and the $A^1\Pi_u$ - $X^1\Sigma_g^+$ in the singlet manifold, and the $b^3\Sigma_g^-$ - $a^3\Pi_u$ in the triplet manifold. These bands all have transition probabilities on the order of microseconds, which is much faster than the average collision time for the C_2 radical in comets [*Chabalowski et al.*, 1983; *Gredel et al.*, 1989; *Theodorakopoulos et al.*, 1987; *Douay et al.*, 1988]. Since each of the upper electronic states contain vibrationally and rotationally excited levels, it follows that the lowest singlet state ($X^1\Sigma_g^+$) and the lowest triplet state ($a^3\Pi_u$) will also have excited vibrational and rotational levels. C_2 radicals that are formed in these excited ro-vibronic states will have a very small probability for relaxation to the lowest level before being electronically excited by solar radiation, since homonuclear diatomic molecules have a low probability for such transitions. Thus the initial population of excited vibrational levels in these lowest two states will be determined by the initial vibrational populations in the excited electronic states and the Franck-Condon factors for the particular transitions. Similarly, the rotational populations in these states will be determined by the initial rotational populations in the excited electronic states, the Franck-Condon factors, the rotational line strengths, and the ΔJ = 0, ±1 selection rule. The time scale for electronic excitation is about 3 s, which is substantially faster than the emission time scale for ro-vibronic transitions within either the $X^1\Sigma_g^+$ or $a^3\Pi_u$ state.

A comparison of these general ideas with the recent detailed modeling of cometary systems suggests that the excess population in low J levels is consistent with the fact that a large number of low J levels are produced in the $A^1\Pi_u$ and $B'^1\Sigma_g^+$ states. Furthermore, the excess population in the v''=1 level over the predictions of the radiative equilibrium model is also consistent with the laboratory observations at 193 nm, which show that vibrationally excited radicals are produced in the photolysis of C_2H.

The laboratory results have all been obtained at one wavelength, and the question can be raised as to what happens at other wavelengths. While no definitive answer can be made to this question at the present time, some expectations can be discussed. The results suggest that the upper excited state of C_2H will dissociate to yield a variety of electronically excited C_2 radicals with "Boltzmann" type vibrational and rotational distributions. This is generally an indication that the excited molecules partition themselves among the available product states in a statistical manner. Since two photons have to be absorbed to produce the observed C_2 radicals, each photodissociation step should be statistical. The absorption spectrum of acetylene above 180 nm gives clear indications of vibronic band structure. This means that the excited state lives longer than a single vibration, which generally implies that the excited C_2H_2 exists long enough for randomization of the available energy among the excited modes before dissociation. The measurement of the rotational distribution of one of the C_2H states formed in reaction (1) shows that this distribution is statistical, in accordance with the view of energy randomization [*Fletcher and Leone*, 1989]. Our beam studies on the photodissociation of acetylene indicate that the initial rotational energy in the parent acetylene molecule is partially mapped onto the final rotational energy of the C_2 fragment. This suggests that the excited state potential surface governs only part of the observed rotational distribution. If these ideas about statistical dissociations can be quantified into a reasonable model which can predict the distributions observed at other wavelengths, a more accurate description of the initial C_2 ro-vibronic distributions can be calculated at the appropriate solar wavelengths. The resulting ro-vibronic distributions would then provide better input for the models that are used to fit the cometary observations.

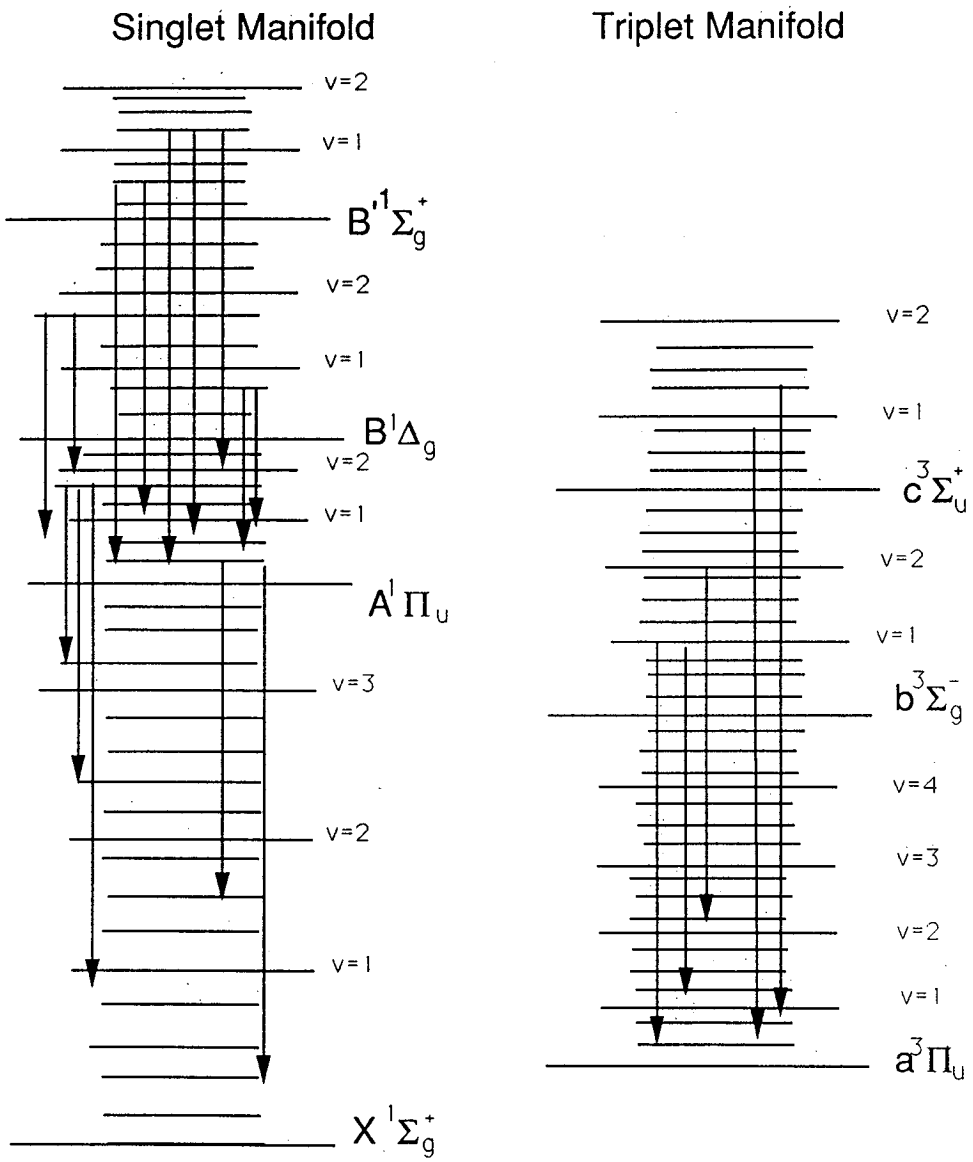

Fig. 1. C_2 energy level diagram. The arrows in the singlet manifold represent the strongest Franck-Condon transitions, while the arrows in the triplet manifold are for illustration purposes only.

CONCLUSIONS

We have shown that the laboratory data from the photolysis of C_2H radicals at 193 nm is qualitatively in accord with the best cometary observations. These laboratory observations show bimodal rotational as well as excited vibrational distributions. The nascent distributions are statistical in character, holding out the distinct possibility that they may be modeled in such a way as to predict their change with photolysis wavelength and thus enable better modeling of the C_2 distributions.

Acknowledgments. The authors gratefully acknowledge the support of NASA under grant NAGW-903 and the National Science Foundation under grant CHE-9008095.

REFERNCES

Balko, B.A., J. Zhang, and Y.T. Lee, 193 nm photodissociation of acetylene, *J. Chem. Phys.*, *94*, 7958-7966, 1991.

Bao, Y., R.S. Urdahl, and W.M. Jackson, Detection of $C_2(B'^1\Sigma_g^+)$ in the multiphoton dissociation of acetylene at 193 nm, *J. Chem. Phys.*, *94*, 808-809, 1991.

Bauer, W., K.H. Becker, C. Hubrich, R. Meuser, and J. Wildt, Radiative lifetime measurements of the $C_2(A^1\Pi_u)$ state, *Astrophys. J.*, *296*, 758-764, 1985.

Chabalowski, C.F., S.D. Peyerimhoff, and R.J. Buenker, The Ballik-Ramsay, Mulliken, Deslandres-d'Azambuja, and Phillips system in C_2: A theoretical study of their electronic transition moments, *Chem. Phys.*, *81*, 51-72, 1983.

Cochran, C.R., C_2 photolytic processes in cometary comae, *Astrophys. J.*, *289*, 388-391, 1985.

Douay, M., R. Nietmann, and P.F. Bernath, The discovery of two new infrared electronic transitions of C_2: $B^1\Delta_g$ - $A^1\Pi_u$ and $B'^1\Sigma_g^+$ - $A^1\Pi_u$, *J. Mol. Spectrosc.*, *131*, 261-271, 1988.

Fletcher, T.R. and S.R. Leone, Photodissociation dynamics of C_2H_2 at 193 nm: Vibrational distributions of the CCH radical and the rotational state distribution of the $A(010)$ state by time-resolved Fourier transform infrared emission, *J. Chem. Phys.*, *90*, 871-879, 1989.

Goodwin, P.M. and T.A. Cool, Resonance ionization spectroscopy of a new $1^1\Delta_u$ <- $A^1\Pi_u$ band system of C_2, *J. Chem. Phys.*, *89*, 6600-6611, 1988.

Goodwin, P.M. and T.A. Cool, Observation of a new $1^1\Delta_u$ <- $B^1\Delta_g$ transition of C_2, *J. Mol. Spectrosc.*, *133*, 230-232, 1989.

Gredel, R., E.F. van Dishoeck, and J.H. Black, Fluorescent vibration-rotation excitation of cometary C_2, *Astrophys. J.*, *338*, 1047-1070, 1989.

Jackson, W.M., The photochemical formation of cometary radicals, *J. Photochem.*, *5*, 107-118, 1976.

Jackson, W.M., J.B. Halpern, and C.S. Lin, Multiphoton ultraviolet photochemistry, *Chem. Phys. Lett.*, *55*, 254-258, 1978.

Lambert, D.L., Y. Sheffer, A.C. Danks, C. Arpigny, and P.Magain, High-resolution spectroscopy of the C_2 Swan 0-0 band from comet P/Halley, *Astrophys. J.*, *353*, 640-653, 1990.

McDonald, J.R., A.P. Baronavski, and V.M. Donnelly, Multiphoton-vacuum-ultraviolet laser photondissociation of acetylene: Emission from electronically excited fragments, *Chem. Phys.*, *33*, 161-170, 1978.

O'Dell, C.R., R.R. Robinson, K.S.K. Swamy, P.J. McCarthy, and H. Spinrad, C_2 in comet Halley: Evidence for its being third generation and resolution of the vibrational population discrepancy, *Astrophys. J.*, *334*, 476-488, 1988.

Theodorakopoulos, G., I.D. Petsalakis, C.A. Nicolaides, and R.J. Buenker, Non-orthonormal basis calculations of the dipole transition moment for the Phillips system ($A^1\Pi_u$ -> $X^1\Sigma_g^+$) in C_2. Theoretical lifetime of the $A^1\Pi_u$ state, *Chem. Phys.*, *112*, 319-324, 1987.

Urdahl, R.S., Y. Bao, and W.M. Jackson, Observation of the LIF spectra of $C_2(a^3\Pi_u)$ and $C_2(A^1\Pi_u)$ from the photolysis of C_2H_2 at 193 nm, *Chem. Phys. Lett.*, *152*, 485-490, 1988.

Urdahl, R.S., Y. Bao, and W.M. Jackson, Laboratory studies of photodissociation processes relevant to the formation of cometary radicals, *NASA Conf. Publ. 3077*, pp.260-264, 1989.

Wodtke, A.M. and Y.T. Lee, Photodissociation of acetylene at 193.3 nm, *J. Phys. Chem.*, *89*, 4744-4751, 1985.

Y. Bao, W.M. Jackson, and R.S. Urdahl, Department of Chemistry, University of California, Davis, CA 95616.

(Received February 14, 1991;
revised May 28, 1991;
accepted June 20, 1991.)

Reprinted from The Journal of Physical Chemistry, 1995, 99.

#116

Time-Resolved IR Chemiluminescence from Reactive Collisions between Hydrogen Atoms and SO_2

Vernon R. Morris,*,† Ke-Li Han,‡ and William M. Jackson§

Department of Chemistry, Howard University, Washington, D.C. 20059, State Key Laboratory of Molecular Reaction Dynamics, Dalian Institute of Chemical Physics, Chinese Academy of Sciences, China, and Department of Chemistry, University of California, Davis, California 95616

Received: April 5, 1994; In Final Form: January 18, 1995⊗

We report the first observation of time-resolved IR emission from the rovibrationally excited OH produced in the H + SO_2 reaction. H atoms were produced via 193 nm photolysis of HBr. Low-resolution emission spectra were collected over the 4000−2800 cm^{-1} spectral region. The high degree of internal excitation deduced from the spectral emission indicates that, unlike similar reactions of this type, the ground state HOSO complex exerts little, if any, influence on the dynamics of this reaction. Quasi-classical trajectory calculations assuming a quasi-triatomic approximation for HSO_2 have also been performed, and these results in conjunction with previous ab initio studies lead to a cohesive model of the reaction dynamics of this tetra-atomic system.

Introduction

The dynamics of elementary atom transfer reactions have long been an area of intense research. Polanyi and his co-workers have been particularly instrumental in determining the relationships between features of the potential energy surface, energy disposal, and consumption in reactions of the type A + BC → AB + C.[1,2] The two most important determinants of the dynamics are the position of the barrier and the relative masses of the atoms involved.[1,2] While the literature on triatomic exchange reactions is exhaustive, relatively few systematic studies of the specificity of energy disposal and reactant energy consumption in atom transfer reactions involving four atoms, A + BCD ↔ AB + CD, have been undertaken. There have been several recent experimental investigations whose results lay the foundation for a richer understanding of the chemical dynamics of tetra-atomic systems. In particular, the class of reactions defined by H + XO_2 → OH + OX have been studied for the first-row atoms X = C, N, and O.[3−12] In each of these instances the nascent internal state distributions of at least one of the products was found to be distinctly nonstatistical.

The reaction between H + CO_2 → OH + CO is endoergic by 24 kcal/mol. Hence, translationally hot hydrogen atoms have been used for the study of the H + CO_2 reaction by several different groups.[3−8] Reviews of the extensive efforts that have gone into the study of the H + CO_2 reaction dynamics have been reported elsewhere,[3−5] but a brief summary of the critical results is in order. Wittig and co-workers have used laser-induced fluorescence to probe the OH product and reported an internal state distribution which was effectively described by a statistical model.[3] Other recent work by Jacobs et al. also supported the existence of a long-lived HOCO intermediate which leads to near-statistical populations in the OH product and the majority of available energy being channeled into relative translation of the products.[6] Baronovski and co-workers have used laser-induced fluorescence (LIF) to probe the internal state distributions of the nascent CO product.[7,8] Their results suggested that the H + CO_2 system exhibits nonstatistical behavior due to incomplete randomization of the available energy and that the well corresponding to HOCO on the ground potential energy surface plays an important role in determining the energy deposition.

The H + NO_2 → OH + NO reaction ($\Delta H° = -30$ kcal/mol) has also been the focus of several experimental investigations.[9−12] The recent studies have employed LIF to probe the nascent internal state distribution of the OH formed in this reaction. Smith and co-workers presented complementary LIF determinations of the complete internal state distribution of the OH and NO produced in the thermal reaction of H atoms and NO_2.[11,12] The OH product was found to be more excited than would be expected on a purely statistical basis. In addition, there was significant excitation observed in NO vibration ($v'' = 3$). Excitation in the "old" bond in this reaction was again indicative of a strong influence of the HONO well on the ground electronic surface exerting a strong influence on the reaction dynamics. The nonstatistical internal state distributions were resolved by invoking a model in which the reaction proceeded through the HONO intermediate on the ground state potential surface but on a time scale short with respect to that required for complete energy randomization.[11,12]

The H + O_3 → OH + O_2 reaction ($\Delta H° = -77$ kcal/mol) has sufficient reaction exothermicity to populate OH up to ($v'' = 9$), and the population distributions have been found to peak at or near the energetic limit.[9,10,13] The nascent rotational distributions resulting from this reaction have also been determined to be non-Boltzmann.[9,10] In general, reactions involving the attack of a light atom on a molecule consisting of considerably heavier atoms leads to preferential deposition of the available energy into relative translational energy of the fragments. Hence, the high degree of selectivity in channeling the excess energy from the hot-atom reaction into the OH product vibration is quite remarkable. The strongly attractive nature of the potential surface involved in this reaction has been attributed to a long-range crossing onto an ionic surface similar to those postulated for alkali metal + halogen atom reactions.[10]

The H + SO_2 reaction represents another member in the class of bimolecular, tetra-atomic gas-phase oxygen atom transfer reactions. In addition to providing another case study for comparing the influence of the barrier on the energy deposition in this class of reactions it provides a system for which the mass combination effect on the dynamics of endoergic reactions may

† Howard University.
‡ Chinese Academy of Sciences.
§ University of California, Davis.
⊗ Abstract published in *Advance ACS Abstracts,* April 15, 1995.

0022-3654/95/2099-10086$09.00/0

be further explored. Aside from its relevance to the fundamental study of inelastic atom−triatomic collisions, the H + SO_2 reaction has potential importance to combustion chemistry as a primary reaction in the SO_2-catalyzed recombination of hydrogen atoms in flames.[14,15]

$$H + SO_2 \rightarrow OH + SO \qquad \Delta H^\circ = +29 \text{ kcal/mol} \qquad (1)$$

$$\rightarrow HSO + O \qquad \Delta H^\circ = +78 \text{ kcal/mol} \qquad (2)$$

$$\rightarrow HOS + O \qquad \Delta H^\circ = +83 \text{ kcal/mol} \qquad (3)$$

$$\rightarrow HS + O_2 \qquad \Delta H^\circ = +53 \text{ kcal/mol} \qquad (4)$$

While there has been some disagreement in the kinetics of channel 1, all investigators have found the H + SO_2 reaction is negligible at temperatures below 500 K. Recently, we reported a theoretical investigation of the H + SO_2 reaction intermediates and product channel energetics.[16] In this paper we present the first experimental evidence of reaction between SO_2 and hydrogen atoms produced in the 193 nm photolysis of HBr. The experimental results have been combined with quasi-classical trajectory calculations in order to obtain the London−Eyring−Polanyi−Sato (LEPS) potentials and gain insights into the dynamics of this reaction system.

Experimental Section

The experiments were performed in a pulsed laser photolysis (PLP) continuous flow system which has been described in detail elsewhere.[17] Briefly, gas mixtures of the precursors and reactants are flowed through an aluminum reaction vessel and irradiated by 193 nm radiation. Pressures were monitored with standard 1 or 10 Torr capacitance manometers. The cell was equipped with gold-coated Welsh collection optics which directed the IR emission onto the entrance slit of a Perkin-Elmer 180 monochromator, and the dispersed radiation was focused onto an InSb photodetector. A laser repetition rate of 28 Hz was employed with typical pulse energies between 50 and 75 mJ. Time decay profiles over the first 200−600 μs after the laser fires were collected for each step in a spectral scan. At each step the rf noise, background radiation, and any other dc offset are subtracted on alternate laser shots which are stored in the computer and averaged. This leads to typical signal-to-noise (S/N) ratios for the individual time decays in excess of 10^2. Shot-to-shot averaging was used to decrease the random noise due to photolysis laser power fluctuations and intrinsic noise in the photodetector.

The small signal size made it necessary to conduct the infrared emission experiments at low spectral resolution, 50−60 cm^{-1}. This resolution is insufficient to resolve individual rotational contours in the OH vibrational bands (B = 18.9 cm^{-1}). However, the OH radical has a large anharmonicity (60 cm^{-1}) and thus, depending on the rotational excitation, individual vibrational bands can be resolved.

In these experiments HBr ($\sigma_{193} = 1.77 \times 10^{-18}$ cm^2) was photolyzed to produce translationally hot H atoms.[18] Working pressures ranged from 10 to 100 mTorr of HBr, 50 to 200 mTorr of SO_2, and 0 to 10 Torr of argon. Previous studies of the 193 nm photolysis of HBr have shown that the H atoms exhibit a bimodal velocity distribution corresponding to the two different types of bromine atoms produced, $Br_{1/2}$ and $Br_{3/2}$.[19] The spread in the H-atom translational energies is thus from 62 to 51 kcal/mol, respectively. The H atoms possess an average effective initial translational energy of 58 kcal/mol based on the branching ratio reported by Lambert et al.[20] The absorption cross section of SO_2 is larger than that for HBr, $\sigma_{193} = 1.1 \times 10^{-17}$ cm^2.[21] Thus, the total reaction system consists of the reactive species H, SO, O, and Br radicals along with the precursors. The side reactions which could lead to OH or HSO were suppressed so that they occurred only to a negligible extent on the time scale of our detection. For example, the O + HBr → OH + Br has a reported rate constant of $k = 4.4 \times 10^{-14}$ cm^3 $molecule^{-1}$ s^{-1} and no reaction has been observed for SO + HBr.[22] The lifetime of the oxygen atoms with respect to the O + HBr reaction for a partial pressure of 100 mTorr HBr is 7 ms. This is well outside of our detection window and thus the effects of this reaction should be negligible. The rate constant of the H + SO reaction has not been reported, but if we assume that this rate is comparable to that for the analogous H + O_2 reaction, then this is also too slow to be observed on the microsecond time scale under our experimental conditions. It is unlikely that any other processes will lead to production of OH or HSO as a result of secondary reactions, but these can also be suppressed by working at low total precursor partial pressures (≤200 mTorr), moderate laser fluences, and pseudo-first-order conditions in SO_2. This ensures that the H atoms produced in the photolysis are consumed primarily via collisions with SO_2 molecules.

A final potential source of spectral interference is the atomic emission from the excited bromine atoms ($Br_{1/2} \rightarrow Br_{3/2}$, $\tau \cong 1$ s) at 3685 cm^{-1}. Background spectra were taken under identical conditions to the reaction system in which only HBr was photolyzed and compared to the emission spectra from the reaction in order to determine the influence of this emission on the entire profile. (See Figure 1) The secondary production of bromine atoms via the H + HBr reaction, $k = 6.3 \times 10^{-12}$ cm^3 $molecule^{-1}$ s^{-1}, was suppressed by using $P(SO_2)/P(HBr) \leq 2$.[23] The atomic emission from the electronically excited bromine atoms is seen as a broadened peak centered at 3685 cm^{-1}. The spin state splitting of the bromine atom is near resonant with the 0 ← 1 vibrational transition of the OH radical. However, due to the low collision frequency and the small cross section for $E \rightarrow V$ relaxation, energy transfer between the product OH and the bromine is expected to be negligible over the first 10 μs after the photolysis pulse. The intensity of this feature persists for over 200 μs under our conditions due to the inefficiency of the possible collision partners in relaxing the spin−orbit states of the bromine atom. It is also unlikely that relaxation due to H atoms or SO radicals are efficient on this time scale under our experimental conditions due to the low collision frequencies and the absence of resonant energy exchange mechanisms. Hence, the 10 μs and earlier time delay emission spectra are assumed to be representative of the nascent vibrational distribution of the product OH.

Results

Typical traces of the low-resolution IR emission between 4000 and 2800 cm^{-1} observed from the H + SO_2 reaction are shown in Figure 1. These spectra show a nearly static distribution growing in over the first 10 μs of the reaction and a partially relaxed distribution which persists through 200 μs. The time delay spectra at earlier times ~5 μs exhibits the same spectral intensity distribution as the 10 μs spectra but with a slightly lower S/N ratio. The persistence of the same spectral intensity distribution over the first 10 μs is a strong indication that the excited vibrational states of the product OH are not being efficiently relaxed and that the observed emission is from a near-nascent vibrational distribution. We note that the rather abrupt falloff of the emission below 2900 cm^{-1} was instrument-limited due to a cold band-pass filter which is installed on the InSb photodetector. Separate experiments were performed with an unfiltered, but less sensitive, InSb photodetector which indicated that the signal from this emission band fell below the

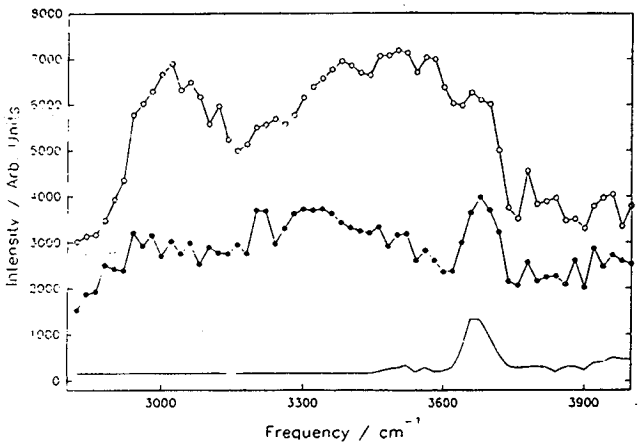

Figure 1. IR emission between 4000 and 2800 cm^{-1} from the H + SO_2 reaction. The experimental resolution of the spectra is 60 cm^{-1} with 55 mTorr of HBr and 100 mTorr of SO_2. The ● and the ○ refer to spectra taken at delay times of 10 and 50 μs, respectively. The lower trace is the 10 μs emission spectra from 193 nm photolysis of 130 mTorr of neat HBr.

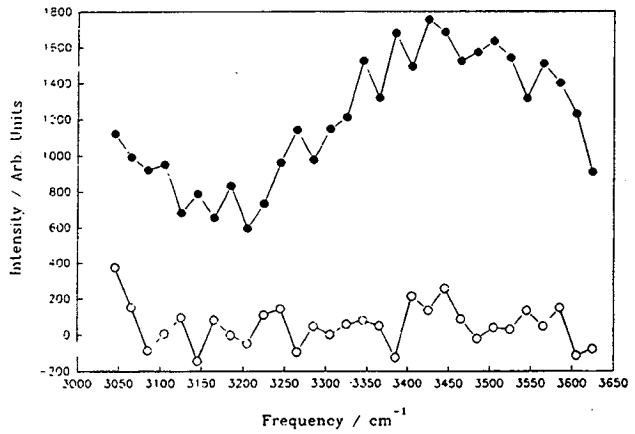

Figure 2. Effect of argon partial pressure on emission from the H + SO_2 reaction with $P(SO_2)$ = 100 mTorr, P(HBr) = 55 mTorr, and 60 cm^{-1} resolution. The ● refer to spectra taken for P(Ar) = 0 mTorr, and the ○ refer to spectra taken for P(Ar) = 1.9 Torr. Both spectra represent 20 μs time delay conditions.

noise level by 2800 cm^{-1}. The lower trace in Figure 1 shows the IR emission from photolysis of pure HBr at a delay time of 10 μs after the laser firing. The presence of the atomic emission from bromine ~3680 cm^{-1} does not adversely influence the entire range of the spectra because the predominant infrared emission occurs to the red of this feature.

The middle trace in Figure 1 shows the 10 μs IR emission from the OH produced in the H + SO_2 reaction. The total pressure in these experiments was 155 mTorr which translates into most of the OH radicals produced having experienced fewer than seven collisions. The only species in the system to quench product OH vibration or rotation are HBr, SO_2, H, Br, and SO, with the majority of collisions occurring between SO_2 and HBr. The HBr and SO_2 vibrational frequencies are not near-resonant with the OH vibrational frequency and, on that basis, are not be expected to be efficient in quenching OH internal excitation. Conversely, the SO_2 molecule is known to form long-lived adducts with OH which may facilitate the relaxation of OH.[24] However, at the total pressures employed in these experiments, the likelihood of this three-body reaction leading to the $HOSO_2$ adduct is small, and the relaxation due to this process is assumed to be negligible.

Figure 2 shows the dramatic effect of increasing the argon partial pressure on the IR emission from the H + SO_2 reaction.

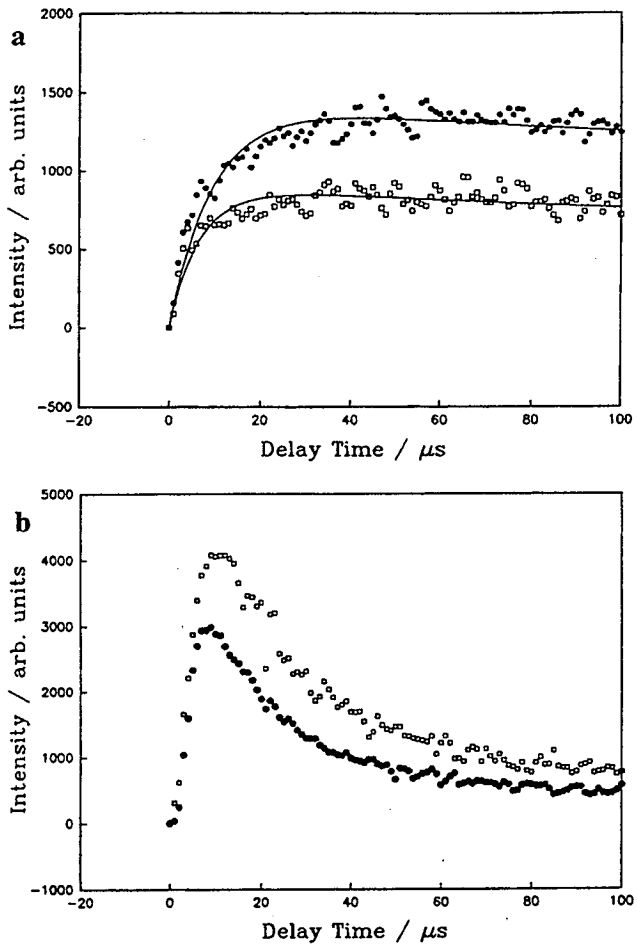

Figure 3. Time decay curves at 3185 and 3085 cm^{-1} are depicted by the ● and the □, respectively. The plots in part a are from experiments without argon, and the plots in part b are from experiments with 1.9 Torr of argon. Both experiments have 130 mTorr of SO_2 and 50 mTorr of HBr.

The addition of higher partial pressures of argon results in a marked increase in hot-H + Ar collisions which may lead to some translational cooling of the H atoms. However, the large mass disparity between these H and Ar these collisions militates against efficient energy transfer. On addition of 800 mTorr of argon and 150 mTorr of SO_2 the fastest H atoms will have experienced more than 10 collisions with argon for every single collision with an SO_2 molecule. In Figure 2 the longwave emission between 3000 and 3700 cm^{-1} is shown under experimental conditions with 0 and 2 Torr of argon. The high partial pressure of argon is effective in reducing the overall signal intensity of the product emission in this spectral region. It also has significant effects on the decay profile of the individual time decays.

The overall intensity of the IR emission throughout the entire spectral range, 3000−4000 cm^{-1}, is seen to decrease significantly. This can be explained if we assume that, although both the translationally hot H atoms and the SO_2 molecules will have suffered many collisions with argon before their mutual encounter, the H-atom collisions will be nearly elastic in nature. The SO_2 molecules will have undergone many inelastic collisions with argon and may thus be quenched to below the reaction barrier by the buffer before encountering an H atom.

Figure 3 shows single time decay curves under conditions of zero and high pressures of argon buffer gas. The experimental scatter in the individual points of the time decay curve are a function of signal averaging and are reproducible for constant experimental conditions. The intensity scales for Figure 3a,b

TABLE 1: Parameters for LEPS Potential Surface

	D_0 (kJ/mol)	B (Å^{-1})	r_o (Å)	S (barrier = 1 eV)	S (barrier = 0.5 eV)
OH	446	1.29	−0.97	0.8	0.1
OS−O	552	1.37	1.43	0.995	0.985
OS−H	377	1.25	1.35	−0.85	−0.7

have not been normalized. We note that the intensity maxima of the time decays for the experiments with argon are larger than those in the experiments without argon. This is due to the more rapid quenching of states into the chosen bandwidth under these conditions. The total time-integrated emission within the bandwidth is significantly less. The time decays at 3185 and 3085 cm^{-1} are chosen to eliminate interference effects of the emission from the atomic bromine and the cutoff filter. All time decays for the neat experiments can be fit with a simple biexponential function of the general form $A_o\{\exp(-k_1t) - \exp(-k_2t)\}$, where k_1 and k_2 are the pseudo-first-order rate constants for OH production and relaxation, respectively. The average rate constant, obtained from the arithmetic mean of each step in the spectral scan, is $k_1 = 3 \times 10^{-11}$ cm^3 molecule^{-1} s^{-1}. We have observed that the same production term, i.e., the rate constant, can be used to obtain reasonable fits of the time decay curves under both experimental conditions.

The physical significance of the value of the rate constant is meaningful only in its relationship to the total cross-section for reaction of the hot H atoms with SO_2 at the average center-of-mass velocity. Thus, we can estimate an effective impact parameter for an average collision energy of 58 kcal/mol of H atoms generated in the 193 nm photolysis of HBr by using the relationship $k_{av} = \sigma v$, where σ is the reaction cross section ($\sigma = \pi b^2$) and v is the average velocity.[20] The maximum impact parameter based on this average rate constant is thus 0.2 Å.

Theoretical Model

We have assumed a quasi-triatomic approximation to simplify a model LEPS potential energy surface for the H + SO_2 → OH + SO reaction. This assumption is supported by recent ab initio calculations which suggest that one of the SO bonds of SO_2 remains nearly adiabatic in the addition reactions between H and SO_2. The generalized LEPS for of the H + SO_2 PES can be constructed as

$$U = \sum Q_i - [(^1/_2)\sum (J_i - J_j)^2]^{1/2} \quad (5)$$

$$Q_i = \{D_i/[4(1 + S_i)]\}E_i[E_i(3 + S_i) - 2(1 + 3S_i)] \quad (6)$$

$$J_i = \{D_i/[4(1 + S_i)]\}E_i[E_i(1 + 3S_i) - 2(3 + S_i)] \quad (7)$$

where Q_i and J_i are the Coulomb and exchange integrals of the ith diatomic molecule (i = 1, 2, and 3 for AB, BC, and AC, respectively).

$$E_i = \exp[-\beta_i(R_i - R_i^\circ)] \quad (8)$$

where R_i, R_i°, D_i, β_i, and S_i are the internuclear distances, Morse parameters, and the Sato adjustable parameters of the ith diatomic or quasi-diatomic molecule. The parameters of the LEPS PES used in our calculations are given in Table 1.

The Sato adjustable parameters, S_i, depend on the energy distributions and the vibrational populations of the reaction products as a function of the assumed collision energy and the excitation function. The initial conditions for all calculations were chosen to correspond to the experimental conditions. The collision energy was assumed to be 58 kcal/mol, and the entrance channel barrier height and amount of vibrational energy in the SO_2 molecule were varied systematically between 0 and

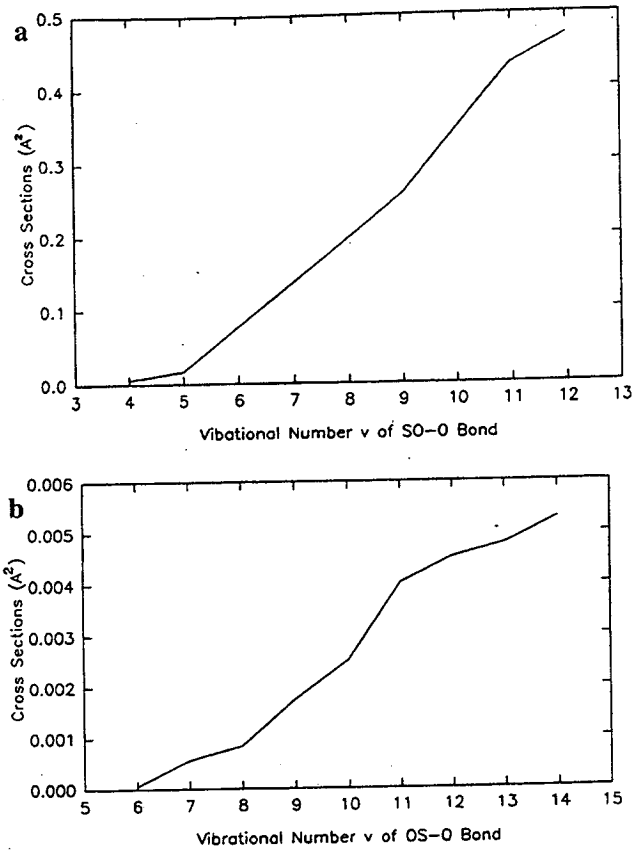

Figure 4. (a) Total reaction cross sections for the H + SO_2 → OH + SO reaction assuming an entrance channel barrier height of 0.5 eV. (b) Total reaction cross sections for the H + SO_2 → OH + SO reaction assuming an entrance channel barrier height of 1.0 eV.

1 eV and from v = 0 to v = 13, respectively. The collision shell radius, ϱ°, was chosen to be 8 Å in order to ensure that interactions between the H atom and the SO_2 molecule would be negligible at the start of each trajectory. The trajectories were integrated with a step size of 2.03×10^{-3} Å, the maximum impact parameter was taken to be 2 Å, and for each set of initial conditions 3000 trajectories were computed. These conditions were selected to ensure the conservation of total energy and angular momentum, computational accuracy to five significant digits, and a mean statistical error smaller than 10%. The total reaction cross sections for barrier heights of 0.5 and 1 eV as a function of the vibrational level of the SO_2 are shown in Figures 4a,b. The vibrational energy threshold for the H + SO_2 reaction is predicted to be v = 3 for an entrance channel barrier of 0.5 eV, but the magnitude of the cross section rises sharply for v > 5 (Figure 4a). We also observe that the cross section for product channels 2 and 3 become significant for higher reagent vibrational excitations, $SO_2(v \geq 10)$. The reaction cross sections predicted under the same initial conditions but with a 1.0 eV barrier height are negligible in comparison (Figure 5). The calculated vibrational distributions of the OH for different vibrational excitation of the SO_2 reactant are shown in Figures 5a−c. These distributions may have as much as 30% error due to the inherent limitations of the model; however, the general form of the distribution is qualitatively correct. The chief observations to be gained from these results are the statistical but non-Boltzmann vibrational distribution, the sharp falloff in populations after the v = 1 state, and the insensitivity of the relative population in the higher v states to increases in the vibrational content of the SO_2. The results of the quasi-classical trajectory calculations can be summarized as follows:

(1) The vibrational excitation in the SO_2 is critical in the reaction with a predicted threshold of v = 3 for the OH product

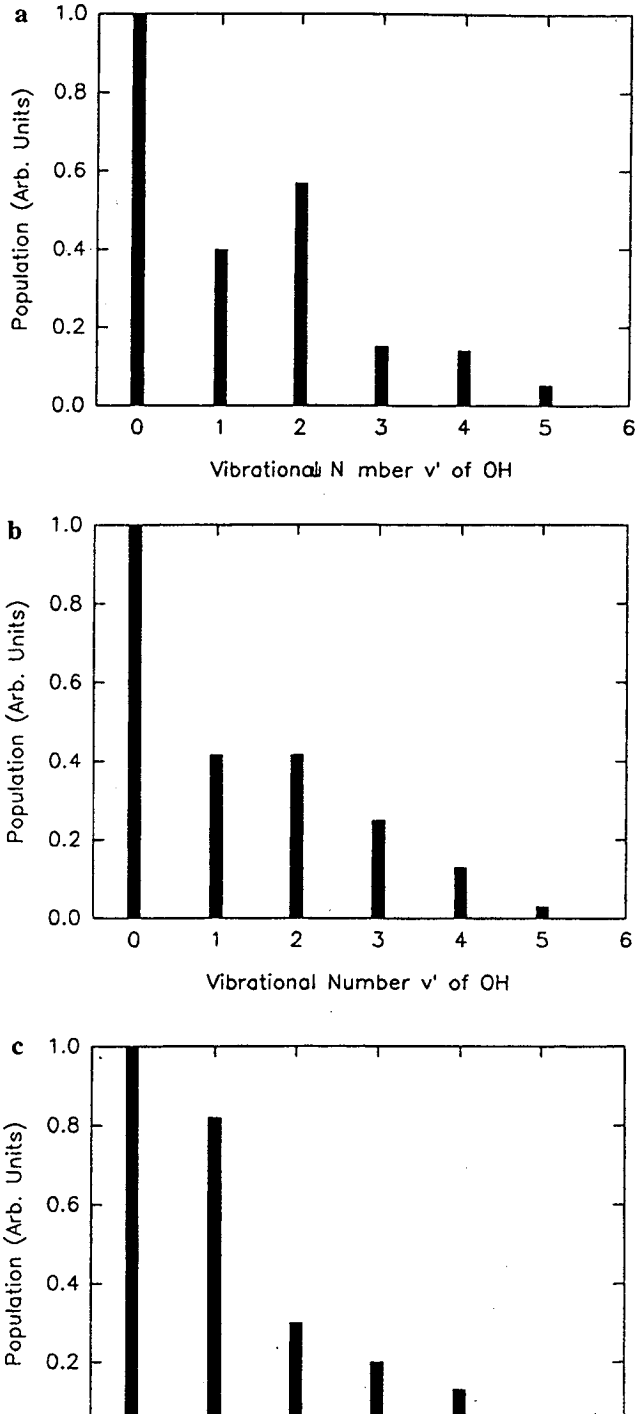

Figure 5. (a) Calculated vibrational distribution for OH produced in the H + $SO_2(v=11)$ reaction assuming a barrier height of 0.5 eV. (b) Calculated vibrational distribution for OH produced in the H + $SO_2(v=12)$ reaction assuming a barrier height of 0.5 eV. (c) Calculated vibrational distribution for OH produced in the H + $SO_2(v=13)$ reaction, assuming a barrier height of 0.5 eV.

channel and at high excitations, $v \geq 10$, can open the HSO and HOS product channels.

(2) The OH product vibrational distribution is cold and relatively insensitive to changes in both barrier height and reagent vibrational excitation.

(3) The reaction cross sections are small even for low entrance channel barriers.

The prediction of a cold vibrational distribution in the product OH is in good agreement with the experimental observations and supports a dynamical model in which very little energy is channeled into the vibrational degrees of freedom and most of the energy is released in relative translation of the separating fragments.

Discussion

Despite the low spectral resolution we can make qualitative interpretations about the distributions due to the large anharmonicity and the rotational constant of the hydroxyl radical. The rotational excitation in the lowest excited vibrational state is relatively small, with $J \leq 7$. This is evident from the fact that the shorter wavelength emission, i.e., the P-branch of the $v = 1$ emission, does not extend beyond 3800 cm^{-1} and from the straightforward calculation of line positions based on the spectroscopic constants of the OH radical ($\omega_e = 3735$ cm^{-1}, $\chi_e\omega_e = 82.8$ cm^{-1}, and $B = 18.9$ cm^{-1}). The reaction dynamics implied by this qualitative limit on the rotational excitation is consistent with the classical picture of light atom abstraction reactions in which little of the available energy is deposited into product rotation. We observed product infrared emission in the 3700−2900 cm^{-1} region in all experiments in which less than 1 Torr of argon was used. The spectral emission near 2900 cm^{-1} would be representative of high ($J \sim 20$) levels in the $v = 2$ state or low J levels in the $v = 3$ state of OH.

Laser-induced fluorescence (LIF) experiments presently underway in our laboratory indicate that collisions between H atoms and vibrationally excited SO_2 may be playing a key role in the OH production in this system.[25] The highly vibrationally excited SO_2 is produced by the absorption of a 193 nm photon to produce electronically excited SO_2 and then subsequent relaxation into the upper vibrational levels in ground state SO_2.

Recent theoretical studies at the MP2/DZP level of theory predict an 49 kcal/mol barrier in the entrance channel of the H + SO_2 reaction to the formation of HOSO.[16] This is well above the total energy of the thermal reactants, but it is below the total energy of the hot H atom + thermal SO_2 reactants employed in these experiments. There is a much lower barrier (~12 kcal/mol) predicted for the formation of the HSO_2 in which the hydrogen is bound to the sulfur atom rather than to one of the oxygen atoms. If the system passes over the lower barrier with enough energy to isomerize or directly inserts into one of the vibrationally excited SO bonds, one would expect the OH product to be rotationally hot but have a relatively small vibrational excitation since the energy release would be late along the reaction coordinate. A barrier of *ca.* 23 kcal/mol has been suggested for the $HSO_2 \rightarrow$ HOSO isomerization on the basis of previous ab initio studies of the HSO_2 species at the PMP4/6-31G*/MP2/3-21G* level of theory.[26] There is enough energy present initially in H-atom translation to surmount both of these barriers, but it is not clear how effective reagent translation is in surmounting the second barrier. Passage over a critical barrier late along the reaction coordinate is generally suggestive of the importance of reagent vibrational excitation, i.e., SO_2 ($v'' > 0$). The time-resolved IR emission experiments do not give any information on the distribution in the ground vibrational state, so we cannot make any quantitative statements about the fractional amount of vibrationally excited product OH. However, the data from these IR chemiluminescence experiments is suggestive of low rotational and vibrational excitation in the OH product.

Recent ab initio calculations have indicated that the "old" SO bond is virtually unaffected by the addition of an H atom to form either the HSO_2 or HOSO adducts.[16] This result is in qualitative agreement with our experimental observation of low

vibrational excitation in the OH product. Combining the theoretical results and the experimental observation of a small reaction cross section and the preliminary evidence for the role of vibrationally excited SO_2 leads us to suggest the following mechanisms. The H atom can attack the SO_2 molecule by the lowest energy path and form the HSO_2 adduct adiabatically while the SO_2 maintains significant vibrational excitation. The vibrational energy is then consumed in the isomerization from the HSO_2 to HOSO which dissociates to products. Alternatively, the H atom may insert directly into one of the SO bonds which is elongated during excited vibrational motion and the resulting collision complex dissociates directly into OH and SO products. The role of vibrationally excited SO_2 in the $H + SO_2$ reaction will be treated explicitly in an upcoming paper.[25]

This paper reports the first observation of IR emission from the OH produced in the reaction between $H + SO_2$. There are strong indications from the experimental results that vibrational excitation in the SO_2 is critical for reaction. We have found that the OH product has a cold vibrational distribution with relatively low rotational excitation in the $v = 1$ and 2 states. The resolution employed in these IR emission studies is low because of the inherently small signal intensity. Thus, it is difficult to quantify the role of translationally hot H atoms from vibrationally hot SO_2 based solely on these experiments. Since both OH and SO are amenable to pump/probe characterization, it would be useful to determine the internal state distributions of both products under experimental conditions in which the vibrational and translational degrees of freedom of the reactants could be independently controlled. Quantitative internal state distributions for the SO and OH products will be reported from LIF experiments presently underway in our laboratory.[25] Future experiments will involve a photolysis laser centered at 212 nm which will lead to photolysis of HBr and considerable absorption by SO_2 without dissociation. Another direction of interest is the use of more energetic H atoms for the investigation of the higher energy HOS and HSO product channels. The HSO radical can also be probed by the LIF technique and both channels, if active, should prove to have quite interesting dynamics. Quasi-classical trajectory calculations have also been performed to complement the IR emission studies using the experimental conditions as initial input. The results are in good qualitative agreement with experiment and lead to a consistent model of the reaction dynamics of the $H + SO_2$ reaction.

Acknowledgment. The authors gratefully acknowledge the support of NASA under grant number NAGW-903, and V.R.M. thanks the University of California Presidential Postdoctoral Program for support. We also thank Dr. Hua Lin for many helpful discussions and comments on this manuscript.

References and Notes

(1) Polanyi, J. C. In *The Chemical Bond*; Zewail, A. H., Ed.; Academic Press, Inc.: San Diego, 1992; Chapter 7 and references therein.
(2) Smith, I. W. M. *Kinetics and Dynamics of Elementary Gas Phase Reactions*; Butterworths: London, 1980; Chapter 3 and references therein.
(3) Hoffman, G.; Oh, D.; Chen, Y.; Engel, Y. M.; Wittig, C. *Isr. J. Chem.* **1990**.
(4) Flynn, G. W. *Science* **1989**, *246*, 1009.
(5) Flynn, G. W.; Weston, R. E., Jr. *J. Phys. Chem.* **1993**, *97*, 8116.
(6) Jacobs, A.; Volpp, H.-R.; Wolfrum, J. *Chem. Phys. Lett.* **1994**, *218*, 51.
(7) Rice, J. K.; Chung, Y. C.; Baronovski, A. P. *Chem. Phys. Lett.* **1990**, *167*, 151.
(8) Rice, J. K.; Baronovski, A. P. *J. Chem. Phys.* **1991**, *94*, 1006.
(9) Polanyi, J. C.; Sloan, J. J. *Int. J. Chem. Kinet.* **1977**, *5*, 1, 51.
(10) Klenerman, D.; Smith, I. W. M. *J. Chem. Soc., Faraday Trans. 2* **1987**, *883*, 229.
(11) Irvine, A. M. L.; Smith, I. W. M.; Tuckett, R. P.; Yang, X. *J. Chem. Phys.* **1990**, *93*, 3177.
(12) Irvine, A. M. L.; Smith, I. W. M.; Tuckett, R. P. *J. Chem. Phys.* **1990**, *93*, 3187.
(13) Cullis, C. F.; Mulcahy, M. F. R. *Combust. Flame* **1971**, *17*, 197.
(14) Zacharia, M. R.; Smith, O. I. *Combust. Flame* **1987**, *69*, 125.
(15) Nelson, D. D., Jr.; Schiffman, A.; Nesbitt, D. J.; Orlando, J. J.; Burkholder, J. B. *J. Chem. Phys.* **1990**, *93*, 7003.
(16) Morris, V. R.; Jackson, W. M. *Chem. Phys. Lett.* **1994**, *223*, 445.
(17) Mohammad, F.; Morris, V. R.; Jackson, W. M. *J. Phys. Chem.* **1993**, *97*, 6974.
(18) Huebert, B. J.; Martin, R. M. *J. Phys. Chem.* **1968**, *72*, 3046.
(19) Magnotta, F.; Nesbitt, D. J.; Leone, S. R. *Chem. Phys. Lett.* **1981**, *83*, 21.
(20) Lambert, H. M.; Carrington, T.; Filseth, S. V.; Sadowski, C. M. *J. Phys. Chem.* **1993**, *97*, 128.
(21) Black, G.; Scharpless, R. L.; Slanger, T. G. *Chem. Phys. Lett.* **1982**, *90*, 55.
(22) Demore, W. B.; Sander, S. P.; Golden, D. M.; Molina, M. J.; Hampson, R. F.; Kurylo, M. J.; Howard, C. J.; Ravishankara, A. R. *JPL Publ.* **1990**, *90* (1).
(23) Talukdar, R. K.; Warren, R. F.; Vaghijianii, G. L.; Ravishankara, A. R. *Int. J. Chem. Kinet.* **1992**, *24*, 973.
(24) Kuo, Y. P., Cheng, B. M., Lee, Y. P. *Chem. Phys. Lett.* **1991**, *177*, 195.
(25) Lin, H.; Han, K.-L.; Morris, V. R.; Jackson, W. M. Manuscript in preparation.
(26) Binns, D.; Marshall, P. *J. Chem. Phys.* **1991**, *95*, 4940.

JP9408443

#118

JOURNAL OF MOLECULAR SPECTROSCOPY **174,** 274–276 (1995)

Revised Molecular Constants for the $D\ ^1\Sigma_u^+$ State of C_2

The visible and UV spectroscopy of the C_2 radical has been extensively investigated for several decades (*1–5*). This has allowed accurate determination of spectroscopic constants for several states, which have been compiled by Huber and Herzberg (*6*) and more recently by Martin (*7*). However, the $D\ ^1\Sigma_u^+$ state is the exception; to the authors' knowledge only one determination of molecular constants has been reported (*5*). The $D\ ^1\Sigma_u^+$ state was first observed in carbon arc emission at $\lambda = 230$ nm by Mulliken (*4*), but the most detailed analysis to date was published by Landsverk in 1939 (*5*). He assigned the band to the $D\ ^1\Sigma_u^+$–$X\ ^1\Sigma_g^+$ electronic transition. The vibrational progressions are headless, i.e., the Q branch is missing, and they are shaded to the right. Only even rotational lines are observed due to nuclear spin statistics.

In this Note, measurements are reported of the Mulliken band of C_2 radicals produced from C_2H_2 by focusing a 193-nm laser beam. C_2 radicals formed in the $X\ ^1\Sigma_g^+$ state have approximately 52 kcal of energy available to them; consequently, much higher vibrational and rotational levels are observed than in carbon arcs. The nascent rotational and vibrational distributions of the $X\ ^1\Sigma_g^+$ state were probed by laser-induced fluorescence (LIF) between 230 and 231 nm in the $\Delta v = 0$ region of the Mulliken band. A portion of the nascent LIF spectrum is shown in Fig. 1. Landsverk data were used to calibrate rotational line positions. Using new molecular constants for the $X\ ^1\Sigma_g^+$ state, obtained by Nietmann *et al.* from high-resolution studies of the Phillips band ($A\ ^1\Pi_u^+$–$X\ ^1\Sigma_g^+$) (*8*), and the requisite equations from Ref. (*5*), the $D\ ^1\Sigma_u^+$ state constants were optimized to give the best fit to experimental line positions to within 0.5 cm^{-1}. Because of the complexity of the spectrum, it was necessary to rotationally quench the radicals with 10 Torr of argon gas. Removal of high rotational excitation resulted in a simplified spectrum that could be easily assigned (see Fig. 2). The ν_0, B_v, and D_v values for $v = 0$, 1, 2, 3, and 4 of the X and D states are shown in Table I.

Previously, the 0–0, 1–1, 2–2, and 3–3 bands were assigned by Landsverk (*4*). Two additional bands, 4–4 and 5–5, are reported. Due to heavy blending, only the 4–4 band could be extracted; the observed line positions are listed in Table II. A few of the lines in the 4–4 band were observed by Landsverk, but no assignments were made. The rotational and centrifugal distortion constants decrease linearly with vibrational quantum number v', except for $v' = 4$, where D_v increases. This may simply be due to insufficient data, or may indicate the onset of perturbations in the D state.

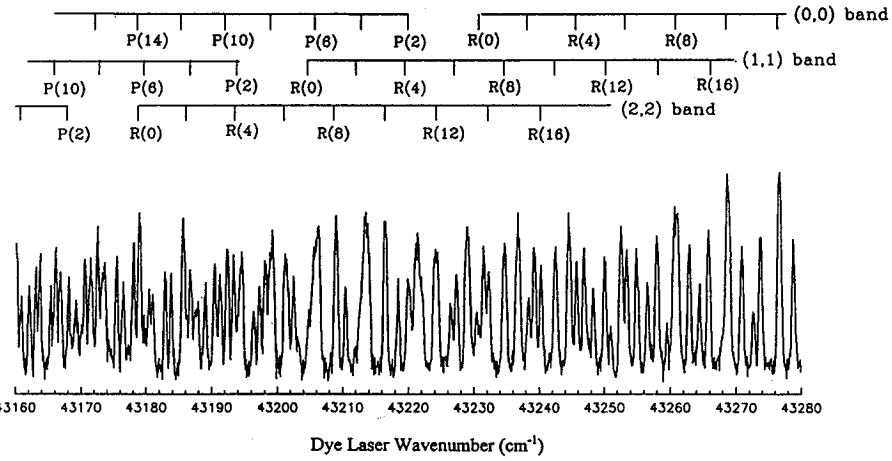

FIG. 1. Nascent distribution of C_2 radicals in the $X\ ^1\Sigma_g^+$ state, probed via the Mulliken band. The delay between the pump and probe laser was 70 nsec.

0022-2852/95 $12.00

TABLE I

Molecular Constants for the $D\ ^1\Sigma_u^+$ State of C_2

Band	ν_0(cm^{-1})	B_v(cm^{-1})	D_v(cm^{-1})
0-0	43227.33(40)[a]	1.82322(15)	7.39(29) x 10^{-6}
	43227.33(02)[b]	1.8232(02)	7.54(05) x 10^{-6}
1-1	43201.39(33)[a]	1.80370(39)	7.29(20) x 10^{-6}
	43201.39(03)[b]	1.8026(05)	6.87(10) x 10^{-6}
2-2	43175.77(23)[a]	1.78390(06)	7.19(30) x 10^{-6}
	43175.77(05)[b]	1.7825(05)	6.15(20) x 10^{-6}
3-3	43151.14(25)[a]	1.76470(50)	7.09(35) x 10^{-6}
	43150.56(20)[b]	1.762(05)	--
4-4	43121.92(15)[a]	1.74724(20)	7.6(20) x 10^{-6}
	--	--	--

[a] Entries in this row are new constants.

[b] Entries in this row were taken from reference 5.

TABLE II

Line Positions of 4–4 Band

R(J)	Wavenumber (cm^{-1})
26	43223.83
28	43231.78
30	43239.99
32	43247.13
34	43256.27
36	43264.25
38	43272.26
40	43281.45
42	43289.46

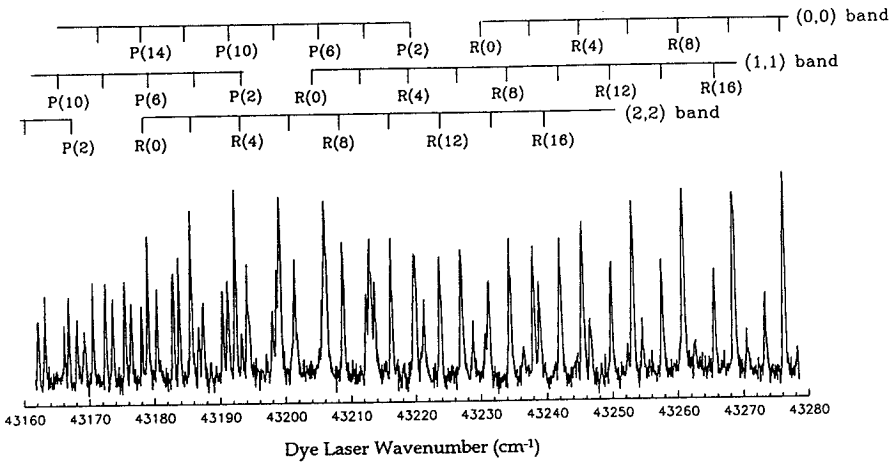

FIG. 2. Cold spectrum of C_2 radicals in the $X\,^1\Sigma_g^+$ state, probed via the Mulliken band. The delay between the pump and probe laser was 2 μsec.

ACKNOWLEDGMENT

The authors gratefully acknowledge the support of NASA under Grant NAGW-903G.

REFERENCES

1. J. G. PHILLIPS, *Astrophys. J.* **108,** 434–452 (1948).
2. J. G. PHILLIPS, *Astrophys. J.* **110,** 73–89 (1949).
3. E. A. BALLIK AND D. A. RAMSAY, *Astrophys. J.* **137,** 61–83 (1963).
4. R. S. MULLIKEN, *Z. Elektrochem.* **36,** 603–605 (1930).
5. O. G. LANDSVERK, *Phys. Rev.* **56,** 769–777 (1939).
6. K. P. HUBER AND G. HERZBERG, "Molecular Spectra and Molecular Structure IV. Constants of Diatomic Molecules," Van Nostrand–Reinhold, New York, 1979.
7. M. MARTIN, *J. Photochem. Photobiol. A: Chem.* **66,** 263–289 (1992).
8. M. DOUAY, R. NIETMAN, AND P. F. BERNATH, *J. Mol. Spectrosc.* **131,** 250–259 (1988).

V. M. BLUNT
H. LIN
O. SORKHABI
W. M. JACKSON

Department of Chemistry
University of California
Davis, California 95616
Received April 12, 1995

NON-ADIABATIC INTERACTIONS IN EXCITED C_2H MOLECULES AND THEIR RELATIONSHIP TO C_2 FORMATION IN COMETS

WILLIAM M. JACKSON, VICTOR BLUNT, HUA LIN, MARTINA GREEN, GREGORY OLIVERA, WILLIAM H. FINK, YIHAN BAO, RANDALL S. URDAHL, FIDA MOHAMMAD and MANSOUR ZAHEDI
Department of Chemistry, University of California, Davis, CA 95616

Abstract. A unified picture of the photodissociation of the C_2H radical has been developed using the results from the latest experimental and theoretical work. This picture shows that a variety of electronic states of C_2 are formed during the photodissociation of the C_2H radical even if photoexcitation accesses only one excited state. This is because the excited states have many avoided crossings and near intersections where two electronic states come very close to one another. At these avoided crossings and near intersections, the excited radical can hop from one electronic state to another and access new final electronic states of the C_2 radical. The complexity of the excited state surfaces also explains the bimodal rotational distributions that are observed in all of the electronic states studied. The excited states that dissociate through a direct path are limited by dynamics to produce C_2 fragments with a modest amount of rotational energy, whereas those that dissociate by a more complex path have a greater chance to access all of phase space and produce fragments with higher rotational excitation. Finally, the theoretical transition moments and potential energy curves have been used to provide a better estimate of the photochemical lifetimes in comets of the different excited states of the C_2H radical. The photochemically active states are the $2^2\Sigma^+$, $2^2\Pi$, $3^2\Pi$, and $3^2\Sigma^+$, with photodissociation rate constants of 1.0×10^{-6}, 4.0×10^{-6}, 0.7×10^{-6}, and 1.3×10^{-6} s^{-1}, respectively. These rate constants lead to a total photochemical lifetime of 1.4×10^5 s.

Introduction

Several years ago we reviewed the status of laboratory work on the photodissociation of the C_2H radical produced during the high intensity photolysis of C_2H_2 at 193 nm [1]. At that time, we pointed out the initial vibrational and rotational distributions of the C_2 radical had to be considered in modeling the corresponding distributions in comets. This is a consequence of the fact that the radical has no permanent dipole moment so that pure vibrational and rotational transitions are dipole forbidden and only electronic transitions will occur with a high probability. Thus, the nascent vibrational and rotational distributions in various electronic states formed during the photochemical step will be mapped upon the rotational and vibrational distributions of the lowest electronic states in the singlet and triplet manifolds, namely the $X^1\Sigma_g^+$ and $a^3\pi_g$, respectively. The nascent rotational distributions in all of the electronic states studied were bimodal in character and each of them showed considerable population in the higher vibrational levels. These results were obtained at only one wavelength so at the time it was not clear how these particular conclusions could be applied to C_2H radicals formed and photodissociated under cometary conditions. Recently, a very important theoretical publication on

Astrophysics and Space Science **236:** 29–47, 1996.

the excited electronic states of C_2H radicals has appeared [2]. This paper along with our new experimental results provide additional insights into the issues raised in the previous paper [1].

In the present paper, a brief review of the problem of C_2 in comets along with a summary of the observational, experimental, and theoretical work that address this problem will be presented. The latest theoretical work will then be used to compute the photochemical lifetime of C_2H at 1 AU. The experimental and theoretical lifetimes associated with the formation of C_2 in comets will then be compared with the lifetimes derived from scale length measurements in comets. Nascent rotational and vibrational distributions obtained for a variety of electronic states of C_2 during the photodissociation of C_2H are presented and the implications of these results to cometary conditions is discussed. Finally, based on the present state of our knowledge, the formation of C_2 in comets will be discussed and the additional laboratory, theoretical, and observational studies that need to be done are outlined.

Review

The basic problem of C_2 formation in comets is that there is no known parent compound that can produce this free radical in one photochemical step [1, 3]. If the radical is formed photochemically it has to be a granddaughter of an unknown parent compound. It has been suggested that C_2H_2 is the parent molecule and that the radical is formed by reactions (1) and (2) and then lost by reaction (3) [1, 3];

$$C_2H_2 + h\nu \rightarrow C_2H + H \tag{1}$$

$$C_2H + h\nu \rightarrow C_2 + H \tag{2}$$

$$C_2 + h\nu \rightarrow C_2^+ + e^-. \tag{3}$$

O'Dell *et al.* have shown using data obtained from Comet Halley that the observed C_2 is a granddaughter species by fitting surface brightness over distances that extend from 250 km out to 63,000 km [4]. From the fits, they obtained scale lengths for reactions (1), (2) and (3) of 2.6×10^4, 1.7×10^4 and 1.4×10^5 km, respectively. These scale lengths can be converted to lifetimes by dividing them by the flow velocity of the gas. If a flow velocity of 0.8 km/s is used, the lifetimes will then be 3.2×10^4, 2.1×10^4 and 1.8×10^5 s, respectively [5]. These are to be compared with the lifetimes for an active sun given by Huebner *et al.* of 5.4×10^4 s for reaction (1) and 4.6×10^5 s for reaction 3 [6]. These two values are in reasonable agreement with the observations since they are within a factor of 2 and 3, respectively. No information is available for the photochemical lifetime of reaction (2) other than a crude estimate made earlier based on a photodissociation threshold, assumed cross sections and the known solar flux [7].

There are other issues which arise from the spectroscopy of the C_2 radicals observed in comets. Earlier, it was pointed out that the cometary C_2 spectra should contain remnants of the initial vibrational and rotational populations produced when this radical is formed [1]. Infrared emission within the $X^1\Sigma_g^+$ and $a^3\pi_g$ states to lower vibrational and rotational levels is dipole forbidden because C_2 is a homonuclear diatomic molecule. It will therefore be much harder for this radical to lose the signatures that are characteristic of its formation process. This subject has also been addressed in the work of O'Dell *et al.* [4] in which they found a vibrational excess in the inner coma. They attributed this to newly formed C_2 molecules being formed with vibrational temperatures much higher than the 5800 K color temperature of the sum. A bimodal rotational distribution has also been observed in the rotationally resolved cometary emission from the C_2 Swan bands [7]. In this paper we will further discuss how this observation can be explained on the basis of ours and others laboratory measurements of the two step photochemical formation of C_2 from acetylene.

Laboratory studies of the UV fluorescence using an unfocused ArF laser at 193 nm showed that this emission could only be explained by a two step mechanism, since one photon could not excite the observed Phillips and Swan band emissions [8, 9]. Laser induced fluorescence studies of the photolysis products at 193 nm have shown that the $B'^1\Sigma^+$, $A^1\Pi$, $B^1\Delta$, and the $a^3\pi_g$ states of C_2 are produced [10, 11, 12]. Photofragment spectroscopy studies have established that the two step mechanism for the formation of C_2 from acetylene does occur in the laboratory [13, 14]. Time resolved infrared spectroscopy studies observed the $B^1\Delta \rightarrow A^1\Pi$ and $b^3\Sigma_g^- \rightarrow a^3\pi_g$ transitions, which further confirms the formation of these upper states [15]. Despite the fact that these observations clearly show that the C_2 radical is formed, there are still many questions that need to be answered. To date, no one has reported whether C_2 is formed in the $X^1\Sigma_g^+$ state, which is the lower level of the Phillips bands in comets. Furthermore, all of the direct evidence for the formation of C_2 from laboratory studies has been accumulated at only one wavelength, and under conditions that are not appropriate for comets. Earlier, we argued that the C_2H radicals that are photolyzed in the laboratory must be vibrationally excited [10, 11]. This is supported by the FTIR studies of Fletcher and Leone that showed at least some of these radicals to be vibrationally excited [16]. In the coma of a comet, any C_2H radicals will all relax via infrared emission to the lowest vibrational and rotational levels of the ground electronic state. Two important questions must then be asked. If these radicals absorb light at shorter wavelengths in comets, will they dissociate in the same manner as the vibrationally hot radicals at 193 nm? Do the nascent distributions observed in the laboratory support the observed vibrational and rotational distributions observed in comets?

Recently, the quantum yield for the formation of H atoms in the photolysis of C_2H_2 at 193 nm was determined to be 0.26 ± 0.04 by Satayapal and Bersohn and 0.30 ± 0.1 by Seki and Okabe [17, 18]. At the same time it is known that the fluorescence quantum yield at 193 nm is very small implying that there must be

metastable C_2H_2 molecules in the system [19]. When these metastable acetylene molecules absorb a second photon, do they produce C_2 and if they do, what are the quantum state distributions of the products?

In addition to the experimental data, the theoretical work of Duflot *et al.* [2] can be used to directly address some of the issues raised by the laboratory work and the cometary observations. Their work is especially relevant because they have calculated the electronic energies of the low lying valence states of the C_2H radical as a function of the $r_{C_2...H}$ internuclear distance and the CCH bond angle. This kind of information can be used to interpret some of the dynamical data taken at 193 nm and hence allow us to qualitatively evaluate how this data provides new insights into the photochemical processes that could in principle produce C_2 and C_2H in comets from C_2H_2. They have also calculated the transition dipole moments from the ground state to the excited states as a function of the $r_{C_2...H}$ bond length. This data may be used to provide a better estimate of the photochemical lifetime for C_2H in comets.

In the present paper, results from the theoretical work will first be used to estimate the photochemical lifetime of C_2H in an effort to see if this value is close to those derived from cometary observations. The vertical excitation energies and symmetries will then be used to construct a correlation diagram, which we will invoke to explain the recent experimental work on the nascent rotational distributions. Finally a discussion will be presented on what remains to be done theoretically, in the laboratory and observationally in order to pin down more precisely the mechanism of C_2 formation in comets.

Photochemical Lifetime of C_2H

The photochemical lifetime, $\tau_{C_2...H}$, is given by the following expression,

$$\tau^{-1}_{C_2...H} = \int I_\lambda \sigma_\lambda \, d\lambda = \Sigma I_\lambda \sigma. \tag{4}$$

The solar flux, I_λ, has been tabulated so one only needs the absorption cross section, σ_λ, to determine the photochemical lifetime [6]. Duflot *et al.* have calculated the transition dipole moments, $D(r_{C_2...H})^2$, from the ground electronic state as a function of the $C - H$ bond length to the individual excited states of C_2H [2]. Thus, if the $C - H$ bond length is known, then their data can be used with the following relationship to determine the absorption cross section.

$$\sigma_\lambda = KD(r_{C_2H})^2 = K|\langle \Psi_f|\mu|\Psi_i\rangle|^2. \tag{5}$$

The K in this equation is the number of allowed transitions namely 4 when a Π state is involved and 1 for Σ states. The wavefunction in this equation involves only electronic degrees of freedom, so that the Franck-Condon factor is not included. Using the curves given by Duflot *et al.* [2] will overestimate the absorption coefficient. This in turn will lead to a lower limit on the photochemical lifetime. The

Table I
Photodissociation rate coefficients for specific transitions in C_2H at 1 AU

Transition	Mean Energy (nm)	Bandwidth nm	Rate Coefficient (s^{-1})
$X^2\Sigma^+ \rightarrow 2^2\Sigma^+$	187.0	15.5	1.0×10^{-6}
$X^2\Sigma^+ \rightarrow 2^2\Pi$	175.4	8.1	4.0×10^{-6}
$X^2\Sigma^+ \rightarrow 3^2\Pi$	154.0	27	0.7×10^{-6}
$X^2\Sigma^+ \rightarrow 3^2\Sigma^+$	151.4	44	1.3×10^{-6}

Total rate constant = 7.0×10^{-6} s^{-1} Total lifetime = $\tau = 1.4 \times 10^5$ s

excitation bandwidth for each of the transitions was estimated by first calculating the zero point energy of the $X^2\Sigma^+$ state of C_2H and then drawing a horizontal line across its potential curve at this energy. Perpendicular lines are drawn from the ground state to the particular excited state under investigation at the extremes of the ground state potential curve. The differences in the vertical distances of these two lines then determines the bandwidth for the excitation of rotationally and vibrationally cold C_2H radicals to the higher state. Because the transition moment given by Duflot *et al.* [2] is available as a function of $r_{C_2...H}$, the integration in Equation 4 is accomplished by mapping the energy difference of the two limbs of the vertical excitation into $r_{C_2...H}$ and then integrating over this range of distance from Duflot *et al.* in Figure 7. The rate coefficients and bandwidths for each of the bands with appreciable oscillator strength are given in Table I. The total photochemical lifetime for C_2H is calculated to be 1.4×10^5 s, which should be compared to the observational lifetime of 2×10^4 s derived from the C_2 scale lengths of O'Dell *et al.* [4]. The theoretical lifetime is an order of magnitude higher than the highest value suggested for the lifetime derived from the longest scale lengths obtained by O'Dell *et al.* [4]. The discrepancy is in fact even larger because our calculations have not included the Franck-Condon factors and are therefore lower limits for the lifetime. It is difficult to see how the observations could be this far off. The large discrepancy suggests that either the theory is wrong or C_2H is not the source of C_2 in comets. There could be a problem in the quantitative details of the theory. Specifically, the wave functions for the excited states which are needed to compute the transition dipole moments were calculated keeping the $C - C$ bond distance in C_2H fixed. Furthermore, the separation of the transition moment for the $X^2\Sigma^+ \rightarrow 2^2\Pi$ and the $X^2\Sigma^+ \rightarrow 3^2\Pi$ absorptions into a transition moment and a Franck-Condon factor is highly suspect, since the computed transition moments are changing too rapidly with internuclear distance. Even though the theoretical studies may not allow us to accurately calculate the photochemical lifetime of C_2H, they should provide a good qualitative picture about the dynamics of the photodissociation, which can then be compared with the laboratory results.

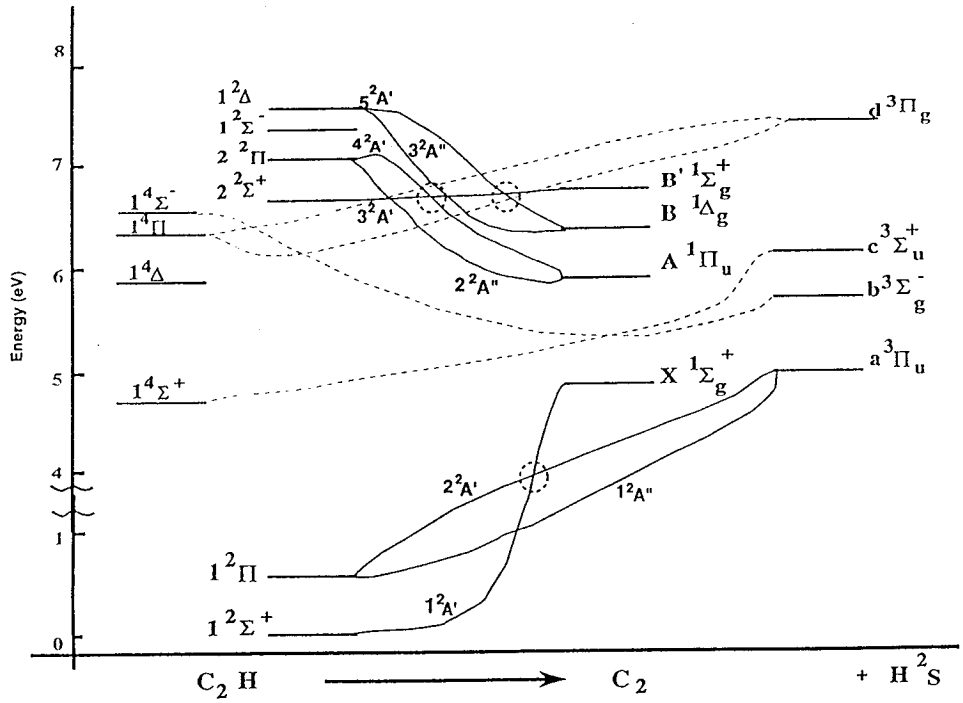

Figure 1. Correlation diagram for the photodissociation of C_2H. The energies on the vertical axis were taken from the work of Duflot *et al.* for linear C_2H [2]. The dissociation coordinate is schematic and corresponds to bending and stretching of the $CC \ldots H$ bond. The dotted circles are also only schematic to indicate the possibility of an avoided crossing.

Correlation Diagram

Figure 1 is a correlation diagram for the dissociation of the C_2H radical which we constructed from the theoretical calculations of the excited state energy levels. Most of the studies on the photodissociation of the C_2H radical have been done by photodissociating C_2H_2 using focused lasers, most of which were at 193 nm. Under these conditions a large percentage of the C_2H_2 molecules are dissociated to produce the C_2H radical. Time resolved IR emission studies with both a FTIR spectrometer and a monochromator have shown that under these circumstances, the C_2H radical is vibrationally excited [15, 16]. Because of this vibrational excitation, large regions of the excited state potential energy curve can be accessed when the radical absorbs a second photon. There is enough vibrational energy in the linear geometry so that both the $2^2\Pi$ and the $2^2\Sigma^+$ excited states can be populated when the radical absorbs a second 193 nm photon. Figure 1 shows that the $2^2\Pi$ state of C_2H correlates to the $A^1\Pi_u$ state of C_2 but avoided crossings arise as the molecule bends, allowing a dissociating molecule to cross over to the $3^2A'$ which correlates to $C_2(B'^1\Sigma_g^+)$. This state should also have an avoided crossing with the $5^2A'$ surface

of C_2H which correlates to $C_2(B^1\Delta_g)$, thus giving the dissociating molecule access to this state. Excitation of the $2^2\Sigma^+$ state can lead to the direct production of the $C_2(B'^1\Sigma_g^+)$, and because of the previously noted avoided crossings, both the $A^1\Pi_u$ and the $B^1\Delta_g$ states are accessible from this level as well.

Three other states of the C_2 radical have been observed in the 193 nm focused photolysis of acetylene. They are the $X^1\Sigma_g^+$, $a^3\pi_u$, and the $b^3\Sigma_g^-$ states, none of which directly correlate to any of the C_2H states that are initially excited or can be reached as result of curve crossings. It is possible for the excited C_2H radicals to hop from one surface to another even if the correlation diagram does not indicate an avoided crossing between the two states. These are diabatic transitions, and the only requirement is that the two surfaces come sufficiently close to each other so that the probability for the transition is high. Figure 2 shows 3-D diagrams of the $3^2A'$ and the $2^2A'$ states plotted using the results of the theoretical calculations, and illustrates these two states do come close to each other at large $r_{C_2...H}$ distances as the correlation diagram suggests. The ripple ridge feature in the foreground of the $3^2A'$ surface with a maximum at about 4.5 bohr can be associated with the curve crossings identified in Figure 1. Since the $2^2A'$ state correlates directly to the $a^3\pi_u$ state of C_2, this is a reasonable explanation about how this state is formed. Similar curves for the $2^2A'$ and the $1^2A'$ states are shown in Figure 3. The proximity of these two surfaces over the entire range of variables implies the nuclear vibrational motion of the states will be so intermixed as to make them indistinguishable from each other. Hopping between these surfaces should be easy. A dissociating molecule on the $2^2A'$ surface can easily transfer to the $1^2A'$ which then correlates with $C_2(X^1\Sigma_g^+)$, and explains why it is observed. The $C_2(b^3\Sigma_g^-)$ state does not correlate to any of the doublet states C_2H but rather to a quartet state, so that its formation can only be explained by surface hopping in the exit channel or by the decomposition of some other molecular species in the system. Surface hopping between two states with different multiplicities should be a process with a very low probability, so it is likely that this species arises from the decomposition of some other molecular species in the system. One possibility is the formation of C_2H in the quartet state from the decomposition of an excited C_2H_2 molecule in the triplet state. Several pieces of laboratory data will be discussed later in support of this hypothesis.

Dynamics of the Photodissociation Process

The laboratory experiments also provide information about the nascent vibrational and rotational energy of the products in addition to their electronic states. The correlation diagram gives a qualitative explanation of the observed rotational distribution of the C_2 radicals formed during the photodissociation of C_2H. Since the ejected H atom is much lighter than the C_2 fragment, in the sudden approximation (where all of the excess energy is released into the recoiling fragments) the con-

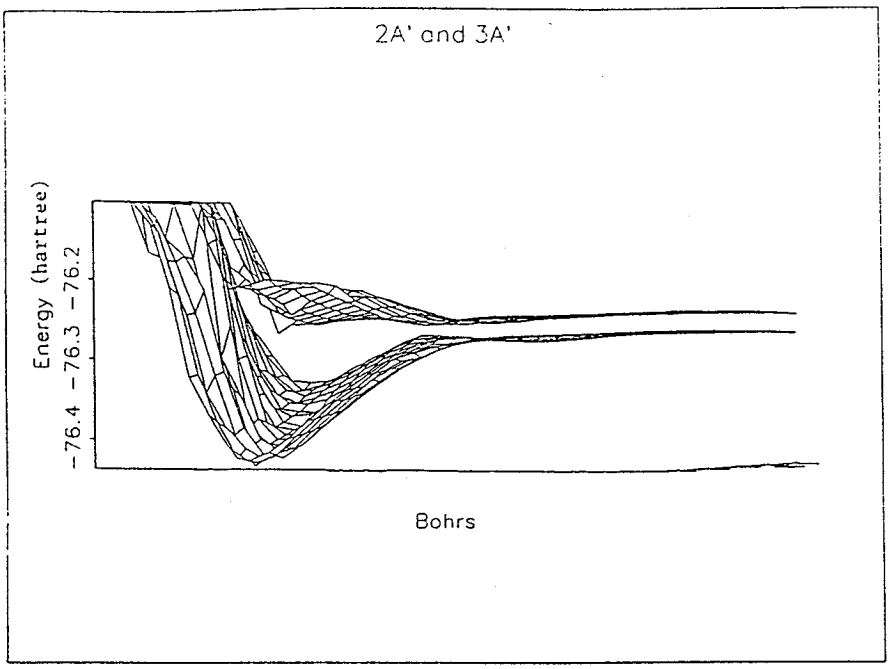

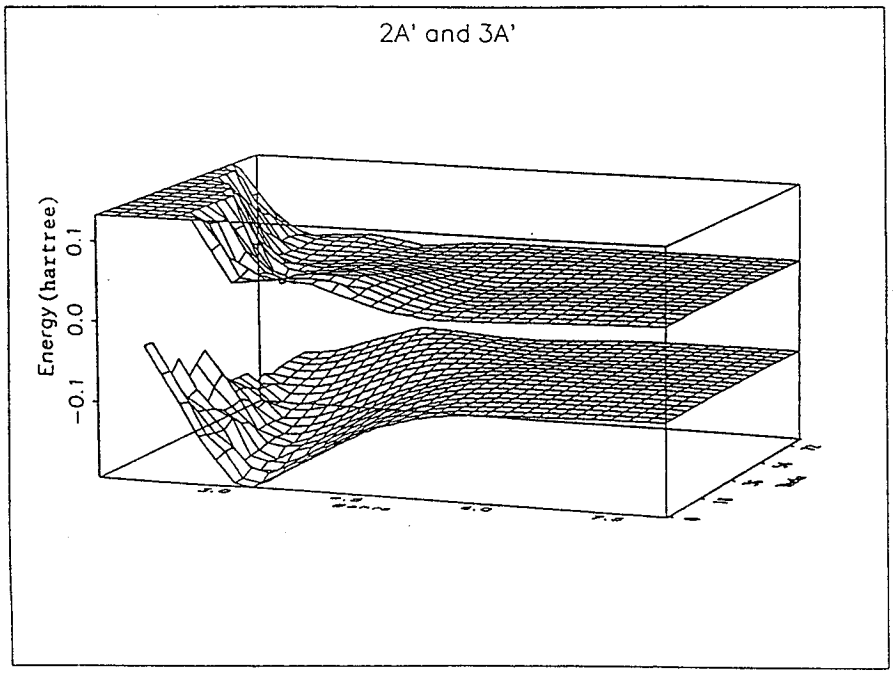

Figure 2. Two different perspective views of the $CC\ldots H$ distance and CCH angle degrees of freedom of the $3^2A'$ and the $2^2A'$ potential energy surfaces of the C_2H. The data was digitized from the curves presented in reference 2. The upper view is from a perspective point chosen to display the separation between the two surfaces. The lower view has changed the vertical axes of the surfaces by adding 76.15 ($2^2A'$) and 76.30 ($3^2A'$) hartrees added to the values reported in reference 2. This addition artificially enhances the gap between the surfaces by 0.15 hartree so the internal features of the surface may be seen. The point of closest approach of the two surfaces occurs at 5 bohr just outside the ripple ridge evident in the $3^2A'$.

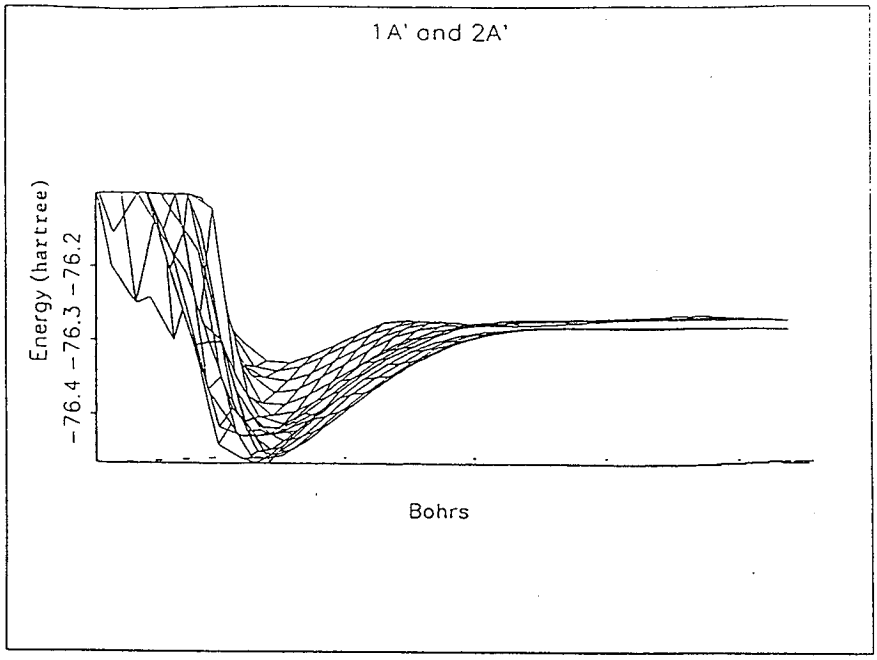

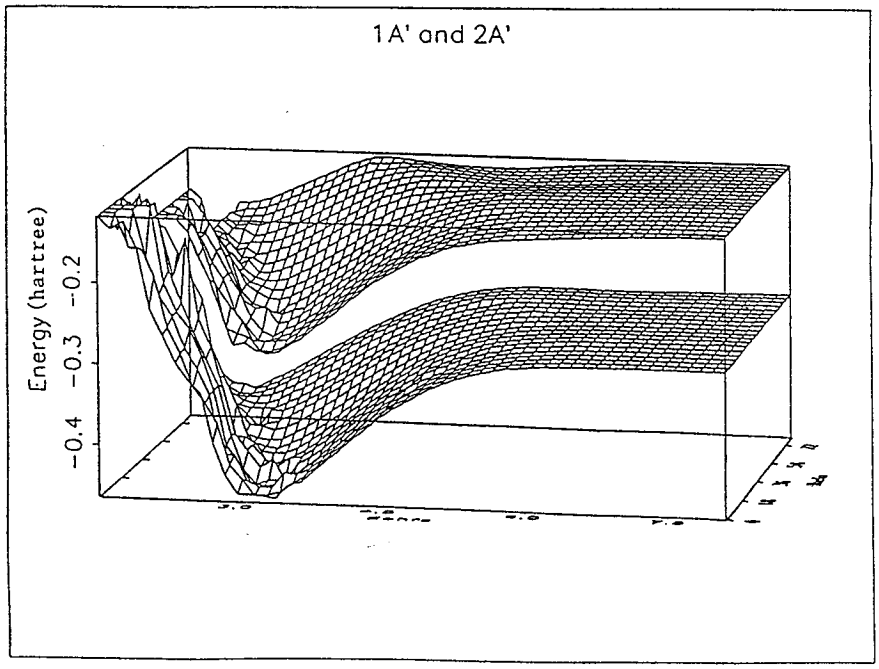

Figure 3. The two different perspectives of the $CC\ldots H$ distance and CCH angle degrees of freedom of the $2^2A'$ and the $1^2A'$ potential energy surfaces of C_2H. The data was digitized from the curves presented in reference 2. The perspective was chosen as for Figure 2, but the vertical axes have had 76.0 ($1^2A'$) and 76.15 ($2^2A'$) hartree added to the values of reference 2. This artificially enhances the intersurface gap by 0.15 hartree. The glove like fit of these two surfaces is particularly evident in the upper view.

Table II
Rotational energy disposal in the C_2 in various electronic states

State	E (avail) (cm^{-1})	J_{max} (impulse)	J_{max} (energetic)	J_{max} (observed)
$X^1\Sigma_g^+$				
$v'' = 0$	18.361	20	100	≈ 78
$v'' = 1$	16,537	18	94	≈ 66
$v'' = 2$	14,566	18	90	≈ 58
$v'' = 3$	12,963	16	84	≈ 58
$v'' = 4$	11,216	14	78	n.d.
$v'' = 5$	9.497	14	72	n.d.
$v'' = 6$	7,806	12	64	n.d.
$A^1\Pi_u$				
$v'' = 0$	10,093	14	78	n.d.
$v'' = 1$	8,509	14	72	n.d.
$v'' = 2$	6,949	12	64	n.d.
$B'^1\Sigma_g^+$				
$v'' = 0$	3,165	8	46	n.d.
$v'' = 1$	1,746	6	34	34
$v'' = 2$	332	2	14	14

n.d. stands for not determined.

servation equations will limit the amount of rotational energy available to C_2. In this model, the amount of angular momentum that appears in the C_2 fragment is determined by the ratio of the masses, the angle, θ, between the H atom and C_2, and the available energy, E_{avail}, released in the process. The maximum amount of rotational energy $E(\text{rot})_{max}$, that can appear in the C_2 fragment can be calculated using the following relationship;

$$E(\text{rot})_{max} = E_{avail}\{m_H m_C \sin^2\theta/(m_H m_C \sin^2\theta + m_C(m_{C_2\ldots H}))\} \tag{6}$$

$$E(\text{rot})_{max} = \{1/26\}E_{avail}. \tag{7}$$

Table II summarizes the results of a variety of experiments that have been carried out in our laboratory, and it shows that in all of the cases where the rotational distribution for a particular vibrational level of a given electronic state has been measured, the maximum observed rotational energy is much higher than an impulse model would predict. This suggests that an additional dynamical process must be occurring during photodissociation, other than the immediate rupture of the $C-H$ bond, if the observed experimental rotational distributions are to be explained.

The phase space model is the antithesis of a sudden approximation where all of the available energy suddenly appears in the bond between the recoiling fragments. In this model, the molecule lives "long enough" on a particular excited

state potential energy surface that it has a chance to access all of the available phase space, leading to energy equilibration among all of the internal modes of the excited molecule [20]. Examples of the application of this model to the $B'^1\Sigma_g^+$ and the $A^1\Pi_u$ of C_2 are shown in Figures 4 and 5, respectively [22, 23]. In each of these cases, the phase space model provides a reasonable fit to most of the J values, but there is excess population in the lower rotational levels. The phase space and the sudden model both predict the maximum rotational energy in the heavy fragment increases with available energy, which as Table II shows, is in agreement with the experimental observations.

The correlation diagram and the three dimensional curves not only explain how the different electronic states of C_2 are produced but also give a qualitative explanation of how the rotational levels of each one of these states are formed. The three dimensional curves show that there are clear pathways to the final products on the $2^2A'$ and $3^2A'$ surfaces. If the initial trajectory of the H atom recoiling from C_2 is along one of these clear pathways, then the conservation laws will limit the amount of rotational energy in this fragment. If on the other hand, the initial trajectory is in the direction of an avoided crossings, a near intersection, such as the ripple ridge with a maximum at about 4.0 Bohr which is evident on the $3A'$ surface in Figure 2, or toward the repulsive barrier, a variety of other things may happen. As the system approaches an avoided crossing or a near intersection, there is a possibility for a transfer or hop to another electronic state. When the H atom moves toward the repulsive barrier it will rebound from this barrier and have another chance to either exit cleanly, cross, or hop over to another electronic state. Any time the H atom can cleanly exit the excited potential energy surface, the classical conservation laws will limit the amount of rotational energy in the C_2 fragment. This could lead to excess population in the lower rotational levels similar to the observations. If the hydrogen atom does not cleanly exit the potential energy surface, it can access more of the available potential energy surface and thus produce the C_2 fragments that are observed with larger amounts of rotational energy. A more quantitative comparison of theory with experiments requires a classical or semi-classical trajectory calculation on these ab-initio potential energy surfaces.

The bimodal rotational distributions that are observed in the laboratory are in accord with the bimodal rotational distributions observed in the C_2 Swan system from Comet P/Halley by Lambert *et al.* [7]. They suggest C_2 radicals are produced with an excess population in the lowest J levels and considerable population in the upper rotational levels. Electronic pumping by the sun will tend to distribute this population according to the color temperature of the sun when the system is in radiative equilibrium. Monte-Carlo calculations have shown that a longer period of time will be required to reach radiative equilibrium when the radicals are initially excited as compared to when they all start out in the lowest J levels [21]. Furthermore, since the different electronic states are produced with different amounts of vibrational and rotational excitation, they all will be approaching this

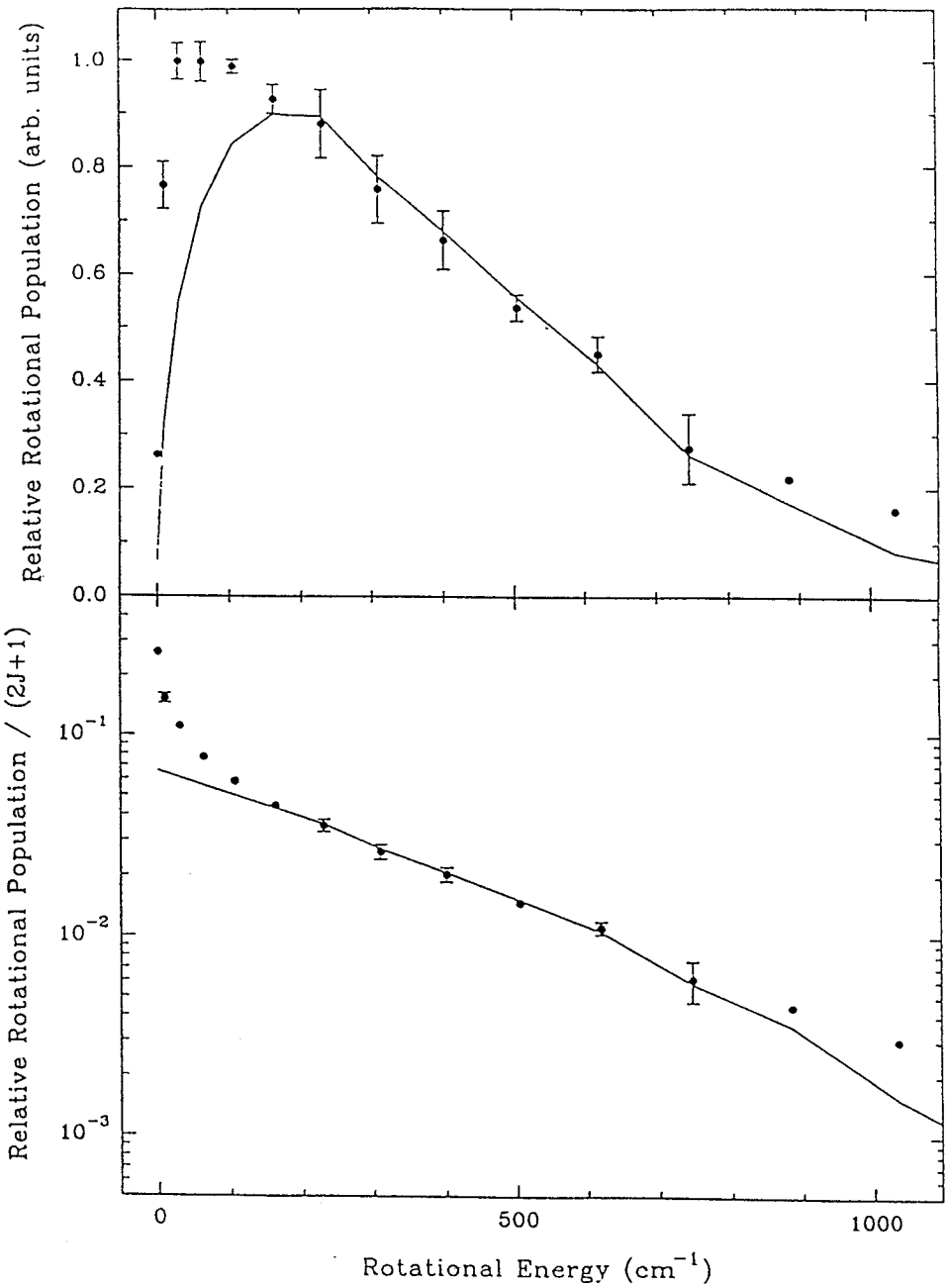

Figure 4. Rotational distribution of $C_2(B'^1\Sigma_g^+)$ produced in the focused 193 nm photolysis of a supersonic beam of C_2H_2. The solid line is the distribution expected using a phase space model. The upper curve is the plotted on a linear Y axis and the lower curve is presented as a Boltzmann plot. The error bars are 1σ error bars and if none are shown the error was smaller than the size of the points. The experimental points can also be fitted with a sum of two Boltzmann curves with temperatures of 440 K and 40 K.

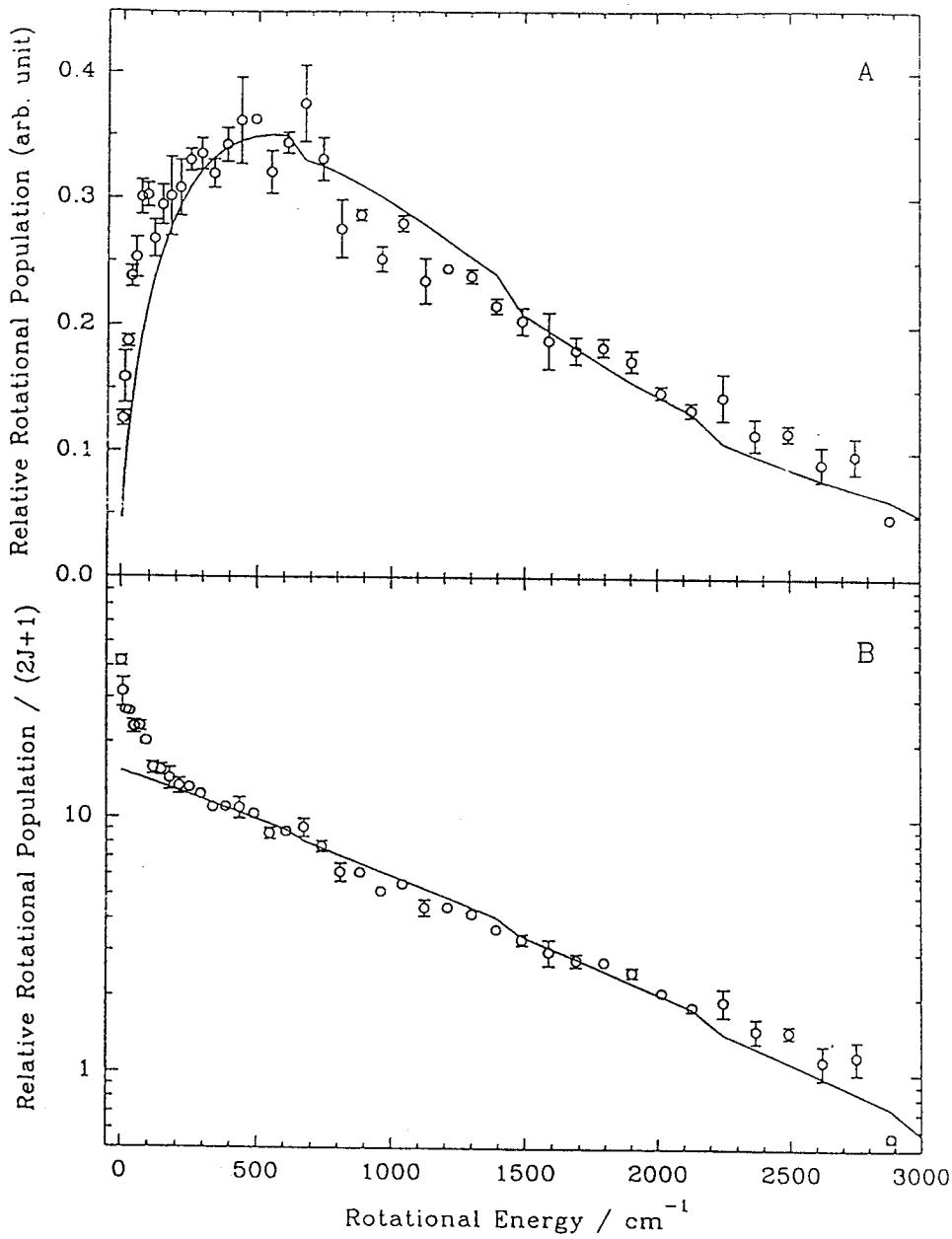

Figure 5. Rotational distribution of $C_2(A^1\Pi_u)$ produced in the focused 193 nm photolysis of a supersonic beam of C_2H_2. The solid line is the distribution expected using a phase space model. The upper curve is the plotted on a linear Y axis and the lower curve is presented as a Boltzmann plot. The error bars are 1σ error bars and if none are shown the error was smaller than the size of the points. The experimental points can also be fitted with a sum of two Boltzmann curves with temperatures of 1250 K and 54 K.

equilibrium at different rates. Our latest laboratory results indicate the $X^1\Sigma_g^+$, $A^1\Pi_u$ and $B'^1\Sigma_g^+$ have significantly different bimodal rotational distributions. The $v'' = 0$ and 1 levels of $X^1\Sigma_g^+$ state have bimodal distributions that cannot be characterized by Boltzmann temperatures. The $v' = 0$, 1, and 2 levels of the $A^1\Pi_u$ state have rotational temperatures of 1250 K and 54 K; 960 K and 150 K; and 640 K and 58 K, respectively [22]. Whereas, the $v' = 0$ and 1 levels of the $B'^1\Sigma_g^+$ state have rotational temperatures of 440 K and 40 K; and 290 K and 30 K, respectively [23].

The vibrational populations of the C_2 radicals in the various electronic states are not directly addressed by the theoretical work since the calculations were done for a fixed carbon-carbon bond distance in C_2H. The vibrational excitation must arise as a result of a stretching motion in this carbon-carbon bond during the dissociation process. This undoubtedly leads to even more complicated excited potential surfaces, which in turn can increase the lifetime of the excited molecules before they dissociate. The fact that the phase space model can be used to explain the formation of C_2 radicals in higher rotational levels implies the excited C_2H radicals live long enough for energy redistribution to occur. As this happens, some of the C_2 radicals will also be produced vibrationally excited. All of the vibrational distributions that have been determined can be described by a Boltzmann "temperature". The vibrational temperature for the $A^1\Pi_u$ state is 2500 K based upon the measured populations of the $v'' = 0$, 1, and 2 levels [22]. No temperature was derived for the $B'^1\Sigma_g^+$ or the $X^1\Sigma_g^+$ states because in the former case, only two states were observed when the signal was linear with the probe laser intensity, and in the latter case the populations of the vibrational levels have not been extracted from the six vibrational bands that have been observed. Nevertheless, the populations of the upper vibrational levels are much higher than one would expect for a frozen $C - C$ bond distance in C_2H.

There is one electronic state which has been observed in the laboratory, namely the $b^3\Sigma_g^-$ state, which is not explained on the basis of the theoretical calculations for the photodissociation of C_2H. The correlation diagram shows that this state correlates to a quartet state, and surface hopping from a doublet state of C_2H should be very slow because it requires a spin flip, which for light molecules is not very probable. Figure 6, shows the infrared emission from this state obtained in our laboratory when a focused UV laser is used to photolyze C_2H_2 [24]. The size of the signal is large, suggesting this emission is not weak, so it is unlikely to be explained by such an improbable process. A more reasonable explanation of this observation is that this fragment is produced by the photodissociation of triplet acetylene, which produces the C_2H radical in a quartet state along with an H atom in the ^2S state. Infrared emission spectra in Figure 7 obtained using a FTIR spectrometer and an unfocused ArF laser show that there are emissions that have not been identified. One of these has been tentatively identified as the 6_0^2 transition of $C_2H_2(a^3B_2)$. The other unidentified features could be due to emission from the

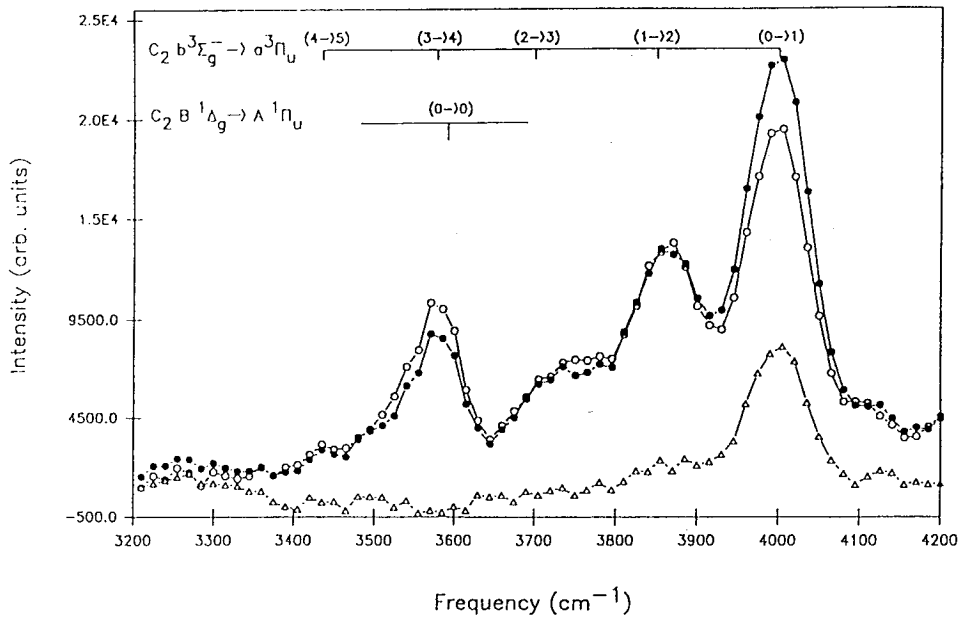

Figure 6. The time resolved $C_2b^3\Sigma_g^- \rightarrow a^3\pi_g$ infrared emission spectrum formed in the focused 193 nm photolysis of C_2H_2. The spectrum were taken at 2 Torr argon pressure and do not represent a nascent rotatioal distribution.

lowest triplet state of C_2H_2, or C_2H in a quartet state. More work needs to be done with this system to positively identify these emissions.

Quantum Yields

The laboratory quantum yields that have been measured for the photodissociation of acetylene at 193 nm by Satayapal and Bersohn, and Seki and Okabe of 0.26 ± 0.04 and 0.30 ± 0.1, respectively, show that under their conditions not all of the excited molecules dissociate [17, 18]. The alternatives to molecular dissociation following excitation are radiative decay back to the ground state, intersystem crossing to an electronic manifold of different multiplicity, collisional quenching, or internal conversion to an upper vibrational level of a lower electronic state with the same multiplicity. The question that needs to be answered is whether the low quantum yields found in the laboratory are to be expected under cometary conditions. In a typical water ice comet at 1 AU with a radius of 5 km, the mean free path between collisions of water with C_2H is 4,900 km at the O'Dell *et al.* [4] scale length for the production of C_2H of 26,000 km. Therefore, the time between collisions is of the order of 6,000 s, so within this time period, any excited molecule has ample time to radiate even via a dipole forbidden transition. During this period, it is also possible for excited molecules that have undergone an intersystem crossing

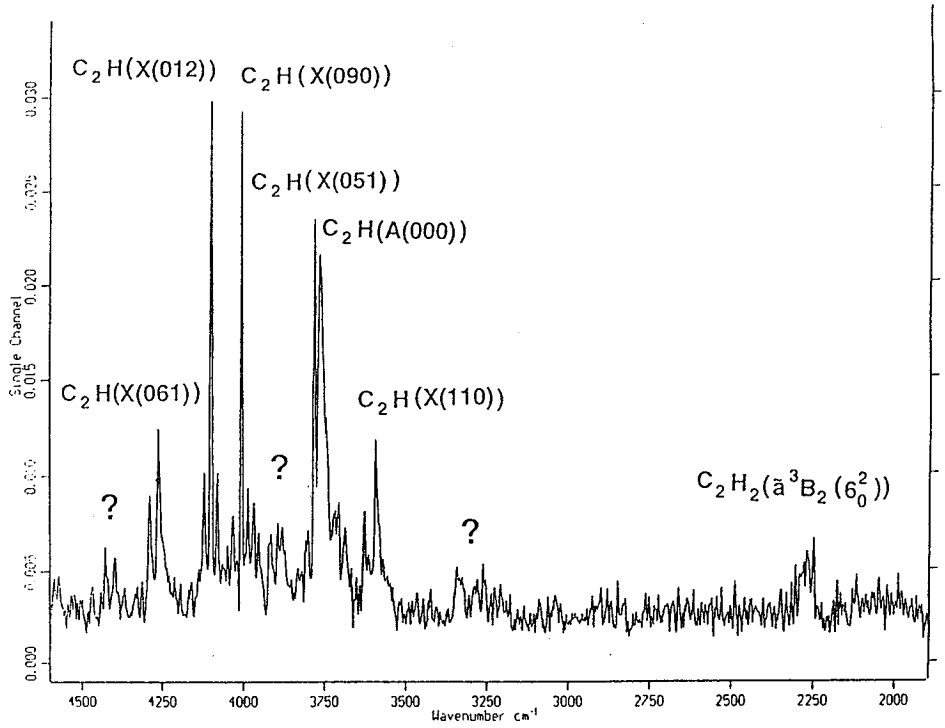

Figure 7. Time resolved Fourier transform infrared spectrum taken during the unfocused 193 nm photolysis of C_2H_2. The laser energy was 45 $\sim$ 51 mJ/pulse, time delay 5 μs, $P_{C_2H_2} = 160$ mT, $P_{Ar} = 2$ T, $\Delta\omega = 4$ cm^{-1}. The unidentified emissions can be due to triplet acetylene C_2H_2 or quartet C_2H.

or internal conversion to undergo the reverse transition, so that they can repopulate the dissociative state from which they were originally formed. If anything other than radiation occurs, the net effect will be that more of the excited molecules will be dissociated in comets than one would predict based upon the measured laboratory quantum yield.

Compare this now with the situation that occurs in the laboratory. The lowest pressures at which the quantum yields were measured under laboratory conditions were 10 mTorr. At these pressures the time between collisions is $\sim$ 14 μs, which allows plenty of time for any metastable C_2H_2 molecules formed in reaction (1) to react by colliding with a ground state molecule or be quenched at the walls of the vessel. This is unlike the case in comets or under the laboratory conditions where high laser intensities lead to C_2 formation. In the latter case, a significant number of metastable molecules can absorb a second photon within the $\sim$ 20 to 30 ns pulse duration of the laser. Results from molecular beam experiments also support this interpretation of our LIF measurements since there is no evidence for the formation of C_2 via a direct photochemical step [13, 14]. All of the C_2 formed

in these experiments comes from secondary photolysis of C_2H, and these experiments should be able to probe any metastable states which dissociate with lifetimes of a few microseconds. The metastable molecules could have lifetimes longer than this, but it is unlikely that they will be long enough to collide with another cometary molecule. The more likely scenarios in comets will be radiative decay, dissociation from the triplet state or a high lying vibrational level of the ground state. Measurements of the fluorescence from excited C_2H_2 molecules in a molecular beam indicate that the fluorescence was undetectable at wavelengths below 215.8 nm and remained so out to the limits of the measurement at 209.6 nm[19]. It is therefore unlikely that the quantum yield for dissociation due to radiation loss of the excited state population negligible.

A more likely possibility is that some of the molecules excited in reaction 1 undergo the following,

$$C_2H_2^*(A^1A_u) \rightarrow C_2H_2^{\#}(b^3B_u) \text{ or } C_2H_2^{\#}(a^3B_2). \tag{8}$$

Of the two products, the a^3B_2 should have the highest probability of formation because it will have the highest density of states, which increases the probability of intersystem crossing. The results in Figure 7 support this channel through the tentative identification of the 6_0^2 transition of $C_2H_2(a^3B_2)$. In the laboratory, this state could either react with the ambient acetylene or absorb a second 193 nm photon under high intensity conditions and dissociate to produce $C_2(b^3\Sigma_g^-)$:

$$C_2H_2^{\#}(a^3B_2) + h\nu \rightarrow C_2(b^3\Sigma_g^-) + 2H. \tag{9}$$

If this sequence of reactions are occurring, one has to wonder why Satayapal and Bersohn did not see an increase in their quantum yields at higher laser intensities [17]. It may be because the highest laser fluences they used in their work was only 110 mJ/cm^2, whereas the fluences used in the studies where $C_2(b^3\Sigma_g^-)$ was observed were on the order of 600 to 2000 mJ/cm^2. In comets, it is likely that the triplet state of acetylene will fall apart before it can collide or be further excited by a solar photon. If it does dissociate, it may produce $C_2 + H_2$ or C_2H in a quartet state plus an H atom. Quartet radicals can open entirely new channels for photodissociation if they live long enough.

Conclusions

The most recent high quality theoretical results on the excited electronic states of the C_2H radical have been used to examine the latest laboratory data and to develop a uniform model for the dissociation of this radical. The results of this examination suggest that the details of the excited potential energy surfaces can explain why C_2 radicals are formed in a variety of electronic states with bimodal rotational distributions. The laboratory results at 193 nm are consistent with the view that when an intermediate radical is produced vibrationally excited,

the photodissociation process accesses a large range of the excited state surfaces. It is thus believed the general features of the dissociation process will be similar for cold C_2H radicals when they are photolyzed in the VUV region at 187.0 and 175.4 nm which are more appropriate to cometary conditions.

Bimodal rotational distributions that are observed in the laboratory and in comets have been attributed to the different manner in which excited C_2H radicals dissociate on the excited surfaces. The low rotational temperatures arise from those radicals that dissociate in one vibration via a direct dissociation pathway to the final products. The higher rotational temperature comes about when the excited molecule spends a much longer time on this excited surface and has a chance to sample a large part of the phase space. The geometry of the excited state surface has only been investigated as a function of the $r_{C_2...H}$ bond length and the $C-C-H$ bond angle θ, so it can not provide information about the vibrational excitation that is observed in the C_2 radical. Nevertheless, vibrational excitation should be a consequence of the randomization of energy in the excited molecules during the dissociation process.

A theoretical photodissociation lifetime has been calculated for cold C_2H radicals in comets which is at least an order of magnitude higher than one would predict from the observed scale lengths. In light of the evidence that a large body of facts are predicted using the theoretical potential energy surface, we suggest that this discrepancy arises because the transition moments are not properly described when the r_{C--CH} is fixed at the equilibrium distance, and the conventional formalism used in the theoretical estimation of the lifetime is inadequate for the $X^2\Sigma^+ \rightarrow 2^2\Pi$ transition.

It has been argued that the laboratory quantum yields are too low for comets because of the longer time scales that are available in comets. It has been suggested that triplet acetylene molecules can be formed and dissociate to produce $C_2 + H_2$ or C_2H in a quartet state plus an H atom.

Despite the many answers that have already been obtained on the photodissociation of C_2H, a variety of theoretical and experimental questions remain. For example, the dynamics and cross sections need to be measured in the laboratory for cold C_2H radicals in the laboratory in the VUV region. These studies should be done as a function of wavelength so that they can be compared directly with observations. The theoretical calculations should be repeated to determine how the transition moments vary with $r_{C...CH}$ distance, and in particular, we need to know if they become larger when this distance is increased.

Acknowledgements

Martina Green gratefully acknowledges the support of NASA under grant number 4016 and the University of California UERG grant and the CALSPACE under grant number CS-48-93. William M. Jackson, Yihan Bao, and R.S. Urdahl gratefully acknowledge the support of NASA under grant number 1144, and 903 G.

Greg Olivera gratefully acknowledges the support of NSF under the Minority Undergraduate Research Participation in the Mathematical and Physical Sciences (MURPPS) grant number NSF CHE 93-07622 and Victor M. Blunt and Lin Hua gratefully acknowledge the support of the NSF Chemistry division under grants NSF CHE 93-08183.

References

1. Jackson, W.M., Bao, Y. and Urdahl, R.S.: 1991, *J. Geophys. Res.* **96**, 17, 569–17, 572.
2. Duflot, D., Robbe, J.-M. and Flament, J.P.: 1994, *J. Chem. Phys.* **100**, 1236–1246.
3. Jackson, W.M.: 1976, *J. Photochem.* **5**, 107–118.
4. O'Dell, C.R., Robinson, R.R., Krishna Swamy, K.S., McMarthy, P.J. and Spinard, Hyron: 1988, *Astrophys. J.* **334**, 476–488.
5. Crifo, J.F.: 1991, in: R.L. Newburn, Jr., M. Neugebauer and J. Rahe (eds.), *Comets in the Post-Halley Era*, Kluwer, Dordrecht, 2, 937–989.
6. Huebner, W.F., Keady, J.J. and Lyon, S.P.: 1992, *Solar Photo Rates for Planetary Atmospheres and Atmospheric Pollutants*, Kluwer, Dordrecht, p. 61 & p. 178.
7. Lambert, D.L., Sheffer, Y., Danks, A.C., Arpigny, C. and Magain, P.: 1990, *Astrophys. J.* **353**, 640–653.
8. Jackson, W.M., Halpern, J.B. and Lin, C.S.: 1978, *Chem. Phys. Letters* **55**, 254–258.
9. McDonald, J.R., Baronavski, A.P. and Donelly, V.M.: 1978, *Chem. Phys.* **33**, 161–170.
10. Bao, Y., Urdahl, R.S. and Jackson, W.M.: 1991, *J. Chem. Phys.* **94**, 808–809.
11. Urdahl, R.S., Bao, Y. and Jackson, W.M.: 1988, *Chem. Phys. Letters* **152**, 485–490.
12. Goodwin, P.M. and Cool, T.A.: 1989, *J. Mol. Spectrsc.* **133**, 230–232.
13. Wodtke, A.M. and Lee, Y.T.: 1985, *J. Phys. Chem.* **89**, 4744–4751.
14. Balko, B.A., Zhang, J. and Lee, Y.T.: 1991, *J. Chem. Phys.* **94**, 7958–7966.
15. Mohammad, F., Bao, Y., Urdahl, R.S., Zahedi, M. and Jackson, W.M.: 1994, in: W.M. Jackson and B.J. Evans (eds.), *Henry C. McBay: A Chemical Festschrift*, MIT Press, Cambridge, Mass., 101–122.
16. Fletcher, T.R. and Leone, S.R.: 1988, *J. Chem. Phys.* **89**, 6600–6611.
17. Satyapal, S. and Bersohn, R.: 1991, *J. Phys. Chem.* **95**, 8004–8006.
18. Seki, K. and Okabe, H.: 1993, *J. Phys. Chem.* **97**, 5284–5290.
19. Haijima, A., Fujii, M. and Ito, M.: 1990, *J. Chem. Phys.* **92**, 959–968.
20. Pechukas, P., Light, J.C. and Rankin, C.: 1966, *J. Chem. Phys.* **44**, 794.
21. Rousselot, P., Goidet-Devel, B., Clairemidi, J. and Moreels, G.: 1994, in: I. Nenner (ed.), *Molecules and Grains in Space*, AIP Conference Proceedings 312, AIP Press, New York, 255.
22. Bao, Y.: 1992, *The photodissociation dynamics of C_2H_2 and C_2H: Detection of the C_2 fragment using laser induced fluorescence*, Ph.D. Dissertation, University of California, Davis.

SPATIAL EXTENT OF DUST IN THE INNER COMA

The radial profiles presented in Fig. 1 may be completed with a bi-dimensional representation of the scattered intensity inside the field of view scanned by the spectrometer. A composite image of this type, which depicts the intensity at 482 nm is given in Fig. 2a,b. Two jets appear in this monochromatic image: a weaker one, on the left, in the direction of the Sun and a stronger one, in a perpendicular direction. As a result, the distribution of dust at distances of 10000 to 40000 km from the nucleus appears as strongly anisotropic. As shown in Fig. 1, the intensity inside the jets is two times more intense than inside the valley (between the jets).

PRODUCTION OF AN EXTENDED SOURCE BY DUST JETS

The spatial distribution of dust particles may be visualized at different wavelengths, in the near-UV at 377 nm and the red at 607 nm. A pixel-to-pixel ratio of the images at $\lambda_1 = 377$ and $\lambda_2 = 482$ nm is presented in Fig. 2c,d. A slight excess of blue coloration, of the order of 25% in intensity, is apparent in the 10000-25000 km region, closely correlated with the presence of jets. This coloration is interpreted as being due to the existence of a population of sub-micronic grains located in the vicinity of the jets. The calculation of the ratio of the quantum efficiencies at two wavelengths, $Q_{sca}(\lambda_1) / Q_{sca}(\lambda_2)$ based upon Mie theory shows that a small excess of tiny grains with $a < 0.8$ μm can produce a slight coloration of the scattered radiation. In present case, we calculated that the observed coloration may be reproduced if one assumes that a fraction of 10^{-7}-10^{-6} of the dust particles present at 20000 km undergoes fragmentation and produces small grains of mass 10^{-15}-10^{-13} g. This results from the fact that the optical scattering efficiency of a given mass of dust particles is roughly inversely proportional to the average radius of the particles.

In an attempt to explain the dust-scattered radiation measurements in the inner coma, it is necessary to introduce a fragmentation mechanism which produces sub-micronic particles. The existence of dust jets and the slight coloration observed in the vicinity of the jets give serious arguments supporting the following process : dust jets originating from fissures at the nucleus surface and extending to several 10000 km. A small fraction of the dust particles would suffer fragmentation after having been heated for several hours starting from their ejection from the nucleus. During this process, they would release gas components such as the CO molecules which were found to form, during the Giotto encounter (Eberhardt et al., 1987), an extended source around 10000 km.

CONCLUSION

The spatial distribution of dust-scattered intensity in the inner coma shows the existence of two well-contrasted dust jets inside the field of view of the spectrometer. A model based on Mie theory and the particle measurements of Mazets et al., (1987) shows that the slight coloration observed in the jets between 10000 and 25000 km may be explained by a population of sub-micronic particles of mass 10^{-15}-10^{-13} g. It is proposed that this population of very small grains results from the fragmentation of the dust particles inside the jet and that the gas released during this process constitutes the diffuse source measured in CO in comet Halley and in H_2CO in comet Levy.

REFERENCES

A'Hearn M.F., Hoban S., Birch P.V. et al. (1986) Cyanogen jets in comet Halley Nature, 324, 649-651.
Clairemidi J.et al.. (1990a) Spectro-imagery of P/Halley'sinner coma Astron. Astrphys., 231, 235-240.
Clairemidi J.et al.(1990b) Gaseous CN, C_2 and C_3 jets in the inner coma of comet P/Halley Icarus, 86, 115-128.
Cosmovici C.B. et al.(1988) Gas and dust jets in the inner coma of comet Halley Nature, 332, 705-709.
Crovisier J. (1991) Radio spectroscopy of comets : recent results and future prospects ACM 91, Abstract p. 45.
Eaton N. (1984) Comet dust - Applications of Mie scattering Vistas in Astronomy, 27, 111-129.
Eberhardt P.. et al. (1987) The CO and N_2 abundance in comet P/Halley Astron. Astrophys., 187, 481-484.
Keller H.U. et al. (1986) First Halley Multicolour Camera imaging results from Giotto Nature, 321, 320-326.
Massone L. (1985) Coma morphology and dust emission pattern of comet Halley Adv. Space Res., 5, 12, 187-196.
Mazets E.P. et al. (1987) Dust in comet P/Halley from Vega observations Astron. Astrophys., 187, 699-706.
Mukai T et al.(1987) Complex refractive index ...deduced of comet P/Halley Astron. Astrophys., 187, 650-652.
Sagdeev R.Z. et al. (1986) Television observations of comet Halley from Vega spacecraft Nature, 321, 262-266.
Schloerb H.P.et al. (1991) Sub-millimeter molecular line observations of comet Levy ACM 91, Abstract p. 187
Suzuki B.et al.(1991) C_2 jets in recent comets ACM 91, Abstract p. 212.

Asteroids, Comets, Meteors 1991, pp. 249–252
Lunar and Planetary Institute, Houston, 1992

Formation of Ions and Radicals From Icy Grains in Comets

William M. Jackson
Department of Chemistry
University of California
Davis, California 95616

ABSTRACT

Two theoretical models for the formation of radicals from ice grains are examined to determine if this can explain the jets in comets It is shown that the production rates for these radicals by the photolysis of molecules in the icy grains are not high enough to explain the jets. A new mechanism is proposed involving the release of cations and anions in the gas phase as the icy mantle surrounding the grains is evaporated. Solar visible radiation can then form radicals by photodetachment of the electrons from these anions. The production rate of radicals formed in this manner is in accord with the production rates of the observed radicals.

Introduction

Recent observations of jet-type CN and C_2 structures with diameters of 24,000 km in Halley's comet by A'Hearn et. al. [1986] have prompted their group as well as others [Clairemidi et al., 1990a, 1990b] to suggest that radicals might be produced directly from the photodissociation of molecules in the grains. In this paper, this idea will be investigated along with the possibility of producing radicals via photodetachment of electrons from negative ions that might already be present in the grains.

Photochemical Production of Radicals from Grains

Combi [1987] attempted to model the photochemical production of radicals from grains by assuming they were produced by photosputtering of radicals and atoms from the grains. In this model, the photodissociation rate was assumed to be the same as it was in the gas phase. The photodissociation rate in the grains will depend, however, on the photodissociation mechanisms of the individual molecules. Those molecules which dissociate in one molecular vibration, i. e., direct dissociation, after they are electronically excited will be less affected by the presence of the solid than those molecules that only dissociate after many molecular vibrations, i.e., predissociate. The former process will occur in times of the order of 0.01 to 0.1 ps while the latter process will take place in times of the order of 1 to 100 ps. Photodissociation in the grains will compete with quenching of the excited state energy into the phonon modes of the solid, which will occur on a time scale of 0.1 to a few ps. A further complication is the "cage effect", which is the enhanced recombination of the fragments because of the surrounding solid matrix [Schriever, et al.,1991]. Thus, bulky or slow fragments are not able to escape the surrounding cage before they collide with each other and recombine to form the original molecule. Hydrogen atoms and other first row atoms escape more effectively from the cage than heavier atoms or fragments because they are smaller and recoil with a higher velocity. These ideas are incorporated in the following equations describing the total yield, Y, for free radical production from one icy grain in a Halley type comet at 1 AU;

$$Y(r_g) = \{\Sigma_\lambda \Phi(\lambda)\, I_\lambda 2\pi r_g^2 [1-\exp(-\sigma_\lambda \rho 2r_g)]\}\tau \qquad (1)$$

In Eq. 1, the radius of the grain is r_g, the intensity at a given wavelength (λ) of the solar radiation at 1 AU is I_λ, the number density of the molecules in the grain is ρ, the absorption cross-section of the molecule, σ_λ, and τ is the lifetime of the grain, which is taken to be 10^5 s. The quantum yield, $\Phi(\lambda)$, for dissociation is equal to $[k_d/(k_d + k_q)]$, where k_d and k_q are the rate constants for

dissociation and quenching, respectively. Both of these rate constants can vary with wavelength, and they are unknown quantities that can drastically reduce the yield of the free radicals. For simplicity, the quantum yield is assumed to be one. Equation 1 was used in Eq. 2 to compute the production rate of the radical R, Q(R), by multiplying it by the flux at a particular r_g, $F(r_g)$, and then summing over all r_g:

$$Q(R) = S_{r_g} Y(r_g)F(r_g) \qquad (2)$$

The grain fluxes were taken from the in-situ measurements of Giotto [McDonnell, et al.,1987]. The Q(R) for OH is 1.8×10^{25} s^{-1}, which is four orders of magnitude less than the observed rate [Feldman, 1991]. Clearly, this mechanism does not explain any OH jets in the comets because the contrast between the OH produced by gas phase photolysis will be too small. The calculated Q(R)'s for CN from HCN and C_2N_2 are 8.4×10^{24} and 3.2×10^{25} s^{-1}, respectively. This is closer calculated rates are based upon very optimistic assumptions. The calculated rates assume that the quantum yield is one and independent of wavelength. Both HCN and C_2N_2 are known to predissociate, so the true rates will be much smaller than those that were calculated. The calculated rates also assume the radicals formed on the interior of the grain eventually arrive in the gas phase. This can only be true if the grains completely evaporate and if the radicals do not recombine before evaporation. Thus it can be concluded that the photochemical production of gas phase radicals from grains can not be used to explain the jets in comets.

Free Radicals from the Photodetachment of Negative Ions

Blakely et al. [1980] have shown that ions can be generated in the gas phase without the use of an external ionizer, if ice particles containing anions and cations are evaporated. When this happens, the positive and negative ions that were trapped inside of the ice particle are released. This mechanism does not require charged ice particles because overall neutrality is maintained, since the charges on the anions and cations balance. If the icy grains in comets contain both cations and anions, then the radicals in the coma might be formed by photodetachment of electrons from the gas phase anions in the coma.

All of the models of comets suggest they were originally formed 10^9 to 10^{10} years ago in the primordial solar nebula or in the nearby interstellar medium [Swamy, 1986]. It is thought that this occurred by agglomeration of ice particles and mineral grains. Ions in the grains could be formed by cosmic radiation, radioactive decay and photoionization before the ice particles agglomerate to form the comet nucleus. Photoionization is the most efficient mechanism for forming ions in a small ice particle. The photoionization threshold for a single H_2O molecule is at 12.6 eV [Lide,1990], however, when the molecule dimerizes and forms clusters the following type of reactions will lower this threshold [Nishi et al., 1984]:

$$(H_2O)_2 + h\nu \rightarrow (H_2O)_2^+ + e^- \quad \text{I.P.} = 11.2 \text{ eV} \qquad (3)$$

$$(H_2O)_2 + h\nu \rightarrow H_3O^+ + OH + e^- \quad \text{I.P.} = 11.7 \text{ eV} \qquad (4)$$

This will decrease the photoionization lifetime by a factor of five due to the increase in the photon flux [Huebner and Carpenter, 1979]. In Eqn. 2, a free radical and an ion are both produced by a single photon. This is a result of the added stability of the protonated ion, which not only lowers the ionization potential of the cluster relative to water, but also leads to a lower dissociation energy for the radical and the ion. Similar mechanisms should be possible for other hydrated molecules [Nishi et al.,1986, and Castleman et al. 1986].

The wavelength distribution of the UV radiation present during comet formation should be similar to the UV distribution in H II regions around young stars. Greenberg and Hage [1990] have shown that it only takes 10^4 years to completely process the mantle of a grain. This is a very short time compared to the 10^8 to 10^9 years available for this purpose, so it is likely that the

outer mantel has been processed many times before the grains agglomerate to form the cometary nucleus. The shortest wavelength of VUV radiation in the H II region is at 13.6 eV, which is low enough to ionize most of the possible cometary molecules except CO and CO_2 [Duley and Williams, 1984]. The electrons that are formed during the photoionization process can attach themselves to atoms and radicals with a high electron affinity, E.A. The E. A. of the most common cometary ions such as CH, OH, CN, C_2, and C_3 are 1.24, 1.82, 3.82, 3.39, and 1.98 eV, respectively [Lide, 1990]. Thus, some of the most stable negative ions can be formed from cometary radicals. The charge on the negative ions formed from these radicals can be counter-balanced by the positive charges on stable species such as H_3O^+, and H_2CO^+. Both CO and CO_2 could be bound up in CO_3^-, which could be formed by the reaction of O_2^- and O^- with them in the icy grains. If these grains are shielded from visible radiation inside the nucleus and are kept cold, then these cations and anions will be stable for long periods of time. When these negative ions are later released from the grain into the gas phase they will quickly form free radicals, since the photodetachment lifetimes are only of the order of a few seconds. These arguments suggest that it is not unreasonable to believe that the VUV radiation in a HII region could have formed cations and anions in the mantles of icy grains that later form the nucleus of a comet.

An estimate of the production rate of radicals that can be produced via the release of anions that are trapped in the icy grains can be made by calculating the number of molecules in the mantle, $N(r_g)$, as a function of the grain radius. The thickness of the mantle is independent of the grain size, and can be approximated from the optical depth of water ice in the VUV spectral region. This is 0.03 mm for ice grains with a density of 1 gm/cc and a mean absorption cross section of 1×10^{-17} cm^2. The production rate, $Q^-(R)$, is then calculated using Eqn. 5 by multiplying $N(r_g)$ by the flux of grains with a given radius, the fraction, ξ, of the mantle that contains the radical anion precursor, and then summing over all grain radii:

$$Q^-(R) = \Sigma_{r_g} N(r_g) F(r_g) \xi \qquad (5)$$

The result of this calculation is that the $Q^-(R)$ for all of the mantle molecules is 2.4×10^{29} s^{-1}. The ratios of the production rate of OH to the production rates of C_2, C_3, and CN are 250, 6700, and 770, respectively [Fink, et al., 1991]. The production of OH in Halley at 1 AU was 4×10^{29} s^{-1} [Feldman, 1991], thus only tenths to hundredths of a percent of the escaping molecules must be anions to explain the observation of jet structures in comets. There is no physical reason why this cannot be the case, since stable solids such as ionic crystals can be made with 100 % ions.

Conclusions

Theoretical calculations have shown that even with the most optimistic assumptions, the yield of free radicals from the photochemical destruction of grains is much to low too explain the observed jets in comets. An alternate mechanism for the production of free radicals and ions in the gas phase from cometary ice grains has been proposed. This mechanism involves the direct evaporation of trapped anions and cations in the icy grain. Radicals are then produced by photodetachement of the electrons on the anions by solar radiation.

Acknowledgements: William M. Jackson gratefully acknowledges the support of NASA under grant NAGW-1144.

References

A'Hearn M. F., Hoban S., Birch P. V., Bowers C., Martin R., and Klinglesmith III D. A., (1986) Cyanogen jets in comet Halley, Nature, 324, 649-651.

Blakely C. R., Carmondy J. J., and Vestal M. L., (1980) A new soft ionization technique for mass spectrometry of complex molecules, J. Am. Chem. Soc., 102, 5931-5933.

Castleman Jr. A. W., Albertoni C. R., Marti Kurt, Hunton D. E., and Keese R. G., (1986) Photodissociation of negative ions and their clusters, Faraday Discuss. Chem. Soc., 82, 261-273.

Clairemidi J., Moreels G., and Krasnopolsky V. A. , (1990a) Spectro-imagery of P/Halley's inner coma in the OH and NH ultraviolet bands, Astron. Astrophys., 231, 235-240.

Clairemidi J., Moreels G., and Krasnopolsky V. A. , (1990b) Gaseous CN, C_2, and C_3 Jets in the Inner Coma of Comet P/Halley Observed from the Vega 2 Spacecraft, Icarus, 86, 115-128.

Combi M. R. (1987) Sources of Cometary Radicals and Their Jets: Gasses or Grains, Icarus, 71, 178-191.

Duley W. W., and Williams D. A. (1984) Interstellar Chemistry, Academic Press, London, p.72.

Feldman P. D., (1991) Ultraviolet spectroscopy of Cometary Comae. In comets in the Post-Halley Era, Vol. 1, (R. L. Newburn, Jr., M. Neugebauer, and J. Rahe, eds.), pp139-148, Kluwer Academic Publishers, Dordrecht..

Fink Uwe, Combi Michael R., and DiSanti Michael A.,(1991) P/Halley: Spatial distributions and scale lengths for C_2, CN, NH_2, and H_2O, Submitted Ap. J.

Greenberg Mayo J., and Hage J. I., (1990) From Interstellar Dust to Comets: A Unification of Observational Constraints, Ap. J., 361, 260-274.

Heubner W. F., and Carpenter C. W. (1979) Solar Photo Rate Coefficients, LA-8085-MS, Los Alamos Scientific Laboratory, pp 10.

Lide David R. ed.(1990) CRC Handbook of Chemistry and Physics, 71st ed., CRC Press, Boca Raton FL.

McDonnell J. A. M., Alexander W. M., Burton W. M., Bussoletti E., Evans G. C., Evans S. T., Firth J. G., Grard R. J. L., Green S. F., Grun E., Hanner M. S., Hughes D. W., Igenbergs E., Kissel J., Kuczera H., Lindblad B. A., Langevin Y., Mandeville J. C., Nappo S., Pankiewicz G. S. A., Perry C. H., Schwehm G. H., Sekanina Z., Stevenson T. J., Turner R. F., Weishaupt U., Wallis M. K., and Zarnecki J. C. (1987) The dust distributions within the inner coma of comet P/Halley 1982i: encounter by Giotto's impact detectors, Astron. Astrophys., 187, 719-741.

Nishi N., Shinohara H., and Okuyama T. (1984) Photodetachment, photodissociation and photochemistry of surface molecules of icy solids containing NH_3 and pure H_2O ices, J. Chem. Phys., 80, 3898-3910.

Nishi N., Shinohara H., Yamoto K., Nagashima U., and Washida N., (1986) Fragmentation of Hydrogen-bonded Molecular Clusters on Photoionization, Faraday Discuss. Chem. Soc., 82, 359-370.

Schriever R., Chergui M., and Schwenter N., (1991) Cage Effect on the Photodissociation of H_2O in Xe Matrices, J. Phys. Chem., 95, 6124-6128.

Swamy K. S. Krishna, (1986) Physics of Comets, World Scientific Pub. Co., Philadelphia PA.

Asteroids, Comets, Meteors 1991, pp. 253–256
Lunar and Planetary Institute, Houston, 1992

Cometary Implications of Recent Laboratory Experiments on the Photochemistry of the C_2H and C_3H_2 Radicals

William M. Jackson, Yihan Bao, Randall S. Urdahl, Xueyu Song, Jai Gosine and Chi Lu
Department of Chemistry
University of California
Davis, California 95616

Abstract

Recent laboratory results on the photodissociation of the C_2H and C_3H_2 radicals are described. These studies show that the C_2 and C_3 radicals are produced by the 193 nm photolysis of the C_2H and C_3H_2 radicals, respectively. The quantum state distributions that were determined for the C_2 radicals put certain constraints on the initial conditions for any models of the observed C_2 cometary spectra. Experimental observations of C_2 formed by the 212.8 nm photolysis of C_2H are used to calculate a range of photochemical lifetimes for the C_2H radical.

Introduction

The formation of C_2 and C_3 in comets has been an intriguing problem in cometary astrophysics [Jackson, 1976]. Numerous laboratory studies suggest that these radicals cannot be produced as a daughter product by photolyzing a parent molecule. Rather, it has been postulated that they are formed as granddaughters via the following reaction scheme [Jackson, 1976]:

$$\text{parent} \rightarrow \text{daughter} \rightarrow \text{granddaughter} \qquad (1)$$

Cometary observations of the spatial profiles of C_2 and C_3 radicals have generally supported the idea that these are granddaughter species [Cochran, 1985 and O'Dell, 1988]. Alternate explanations are that these radicals result from ion-molecule reactions in the coma or some type of direct volatilization from grains and the cometary nuclei. These explanations are certainly more complicated than the photochemical formation of granddaughter species. It is important to test this proposed mechanism to determine what limitations must be placed on using it to explain cometary observations. In this paper, we will describe some recent laboratory experiments that do put restrictions on the use of this postulate to explain cometary observations.

C_2

The laser-induced fluorescence (LIF), visible emission, time-resolved Fourier transform infrared emission spectroscopy, and photofragment time-of-flight techniques have all been used to establish that the mechanism for the primary and secondary photolysis of acetylene at 193 nm can be summarized by the following two reactions:

$$C_2H_2 + h\nu_{193} \rightarrow C_2H^* + H \qquad (2)$$

$$C_2H^* + h\nu_{193} \rightarrow C_2(E_{el}, E_v, E_r) + H \qquad (3)$$

Fletcher and Leone have observed that the C_2H radical formed in reaction (2) is vibrationally excited with several quanta of energy in the bending mode [Fletcher and Leone, 1989]. Earlier it

had been argued that this must be the case, since the C_2H radical has enough internal energy such that a 193 nm photon can be used to excite it to the second excited state in the linear configuration, i.e., the $B^2\Sigma^+$ state [Urdahl,et al., 1988]. Ab-initio theoretical calculations have shown the energies of this and the third excited state decrease when the C_2H radical bends away from the linear configuration of the ground state [Shih et al., 1979]. The energies of these excited states are still not accurately known, but recent experiments in our laboratory suggest that the $B^2\Sigma^+$, which becomes the $3^2A'$ in the bent configuration, must be at about 47,200 ± 700 cm^{-1} above the ground state. This number was derived from the observation of $C_2(a^3\Pi_u)$ radicals with the LIF technique when C_2H_2 was photolyzed at 212.8 nm. The error bars arise because the C_2H radical intermediate could have as many as 2 quanta of vibrational energy in the ν_2 bending mode. In comets, all of the C_2H radicals will be in the lowest vibrational and rotational levels of the ground electronic state. Thus one needs to add 700 cm^{-1} to the above figure to compensate for the vibrational energy that was present in the laboratory experiments. A correction also needs to be made for the fact that the energy of the C_2H excited state is higher when it is linear than when it is bent. The ab-initio theoretical calculations suggest that this correction could be as high as 8100 cm^{-1} [Shih et al., 1979]. The experimental observations and the theoretical calculations imply that photons with energies between 47,200 and 55,300 cm^{-1} will be able to dissociate cold C_2H radicals in comets.

Maximum photochemical lifetimes can be calculated, with a few assumptions, using the above information and the data on the solar flux reported by Heubner and Carpenter, [1979]. First, it is assumed that the absorption cross section for solar radiation can be replaced by an averaged absorption cross section, $\langle\sigma\rangle$. This averaged absorption cross section is then combined with the solar radiation for a variety of different absorption bandwidths. The largest absorption bandwidth corresponds to a long wavelength absorption limit of 210.5 nm, while the smallest absorption bandwidth corresponds to an upper wavelength limit of 180.2 nm. Table 1 shows that the estimated photochemical lifetime can vary from 329 s to 3.8 x 10^5 s depending on the absorption coefficient and bandwidth. The absorption bandwidth could be limited further if errors could be put on the ab-initio calculations, however the range of lifetimes are certainly within the range of lifetimes required by cometary observations [Fink et al., 1991].

The C_2 products formed in reaction (3) have been observed to contain electronic, vibrational, and rotational energy. In comets, these radicals will also be excited since they will arise from the same excited electronic state of the C_2H radical. Once the C_2 radicals are formed in comets, they will emit radiation in the singlet and the triplet manifolds and populate the various vibrational and rotational levels of the $X\ ^1\Sigma_g^+$ and the $a^3\Pi_u$ states, respectively [Jackson, et al., 1991]. In the singlet manifold, the laboratory studies have shown that the $A^1\Pi_u$, $B^1\Delta_g$, and the $B'\ ^1\Sigma_g^+$ states are produced. Radiation from these excited singlet states could produce at least three different rotational and vibrational distributions in the $X^1\Sigma_g^+$state. Similarly, the laboratory

studies have also shown that C_2 is formed in the $a^3\Pi_u$ and $b^3\Sigma_g^+$ states, so two distributions of vibrational and rotational levels could be present in the C_2 ($a^3\Pi_u$) in comets. Once the radicals reach their lowest electronic states in the singlet and triplet manifolds, they cannot relax further via infrared emission because the C_2 radical has no permanent electric dipole moment. This argument suggests that the C_2 radical in comets will be formed with two initial vibrational and rotational distributions in the $a^3\Pi_u$ state, and at least three initial vibrational and rotational distributions in the $X\ ^1\Sigma_g^+$ state. Modeling of the Swan and the Phillips systems in comets should take into account these initial distributions[Gredel et al., 1989].

$\underline{C_3}$

Laboratory studies on allene (CH_2CCH_2), and propyne (CH_3C_2H), using the photofragment time-of-flight and laser-induced fluorescence techniques have shown that the C_3 radical is produced by the following sequence of photochemical reactions at 193 nm:

$$CH_2CCH_2 + h\nu_{193} \rightarrow C_3H_2^* + H_2 \quad (4)$$

$$CH_3C_2H + h\nu_{193} \rightarrow C_3H_2^* + H_2 \quad (5)$$

$$C_3H_2^* + h\nu_{193} \rightarrow C_3(X^1\Sigma_g^+) + H_2 \quad (6)$$

LIF spectra taken during the photolysis of allene and propyne at 193 nm show that the rotational distributions of the C_3 ($X^1\Sigma_g^+$) radicals are identical, even though the spectrum obtained using propyne is considerably weaker than it is with allene [Gosine et al., 1991]. Theoretical calculations using RRKM theory suggest that the excited propyne molecules must first isomerize to excited allene before undergoing dissociation. For comets, the importance of this result is that it suggests that the C_3H_2 radical, which is known to be one of the most abundant interstellar molecules, can be photolyzed to form C_3. It also suggests that the C_3H_2 radical can be produced from a number of different parent molecules.

Conclusions

Laboratory studies on photochemical sources for the daughter radicals that can dissociate to produce the C_2 and C_3 radicals have revealed certain constraints on their formation in comets. The acetylene studies suggest that an initial bimodal distribution of vibrational and rotational levels should be used in any modeling of the Swan system in comets. Limits have been placed on the energy of the upper electronic state of C_2H that may be involved in the production of C_2 radicals in comets. A range of photochemical lifetimes have been calculated for the C_2H radical, and the results are consistent with cometary observations. Any molecule that can dissociate to produce the intermediate daughter radicals C_2H and C_3H_2 will probably lead to the formation of the C_2 and C_3 cometary radicals.

Acknowledgements

The authors gratefully acknowledge the support of this work by NASA under grant number NAGW-903.

Table 1

Calculated C_2H Photochemical Lifetime at 1 AU

Long Wavelength Absorption Edge (nm)	Averaged Absorption Cross Section $\langle\sigma\rangle(cm^2)$		
	1×10^{-16}	1×10^{-17}	1×10^{-18}
	LIFETIME, τ, (s)		
210.5	329	3290	32900
200.0	844	8440	84400
190.5	1683	16830	168300
180.2	3786	37860	378600

References

Cochran C.R. (1985) C_2 Photolytic Processes in Cometary Comae, Astrophys. J., 289, 388-391.

Fink Uwe, Combi Michael R., and DiSanti Michael A. (1991) P/Halley: Spatial distributions and scale lengths for C_2, CN, NH_2, and H_2O, Submitted Ap. J.

Fletcher T.R. and Leone S.R. (1989) Photodissociation dynamics of C_2H_2 at 193 nm: Vibrational distributions of the CCH radical and the rotational state distribution of the A(010) state by time-resolved Fourier transform infrared emission, J. Chem. Phys., 90, 871-879.

Gosine Jaimini N., Song Xueyu, Bao Yihan, Urdahl Randall S., and Jackson William M. (1991) The 193 nm multiphoton dissociation of allene and propyne; Evidence for photoisomerization, in preparation.

Gredel R., van Dishoeck E.F., and Black J.H. (1989) Fluorescent vibration-rotation excitation of cometary C_2, Astrophys. J., 338, 1047-1070.

Heubner W. F., and Carpenter C. W. (1979) Solar Photo Rate Coefficients, LA-8085- MS, Los Alamos Scientific Laboratory, pp 10.

Jackson W.M. (1976) The photochemical formation of cometary radicals, J. Photochem., 5, 107-118.

Jackson William M., Bao Yihan, and Urdahl Randall S. (1991) Implications of C_2H photochemistry on the modeling of C_2 distributions in comets., J. Geophys. Research, 96(E2),17,569-17,572.

O'Dell C.R., Robinson R.R., Swamy K.S.K., McCarthy P.J.,and Spinrad H. (1988) C_2 in comet Halley: Evidence for its being third generation and resolution of the vibrational population discrepancy, Ap. J., 334, 476-488.

Shih, Shing-Kuo, Peyerimhoff Sigrid D., and Buenker Robert J. (1979) Calculated Potential Surfaces for the description of the emission spectrum of the C_2H radical, J. Mol. Spectrosc., 74, 124-135.

Urdahl R.S., Bao Y., and Jackson W. M. (1988) Observation of the LIF spectra of $C_2(a\ ^3\Pi_u)$ and $C_2(A\ ^1\Pi_u)$ from the photolysis of C_2H_2 at 193 nm, Chem. Phys. Lett., 152, 485-490.